UNIVERSITÀ
DEGLI STUDI
DI MILANO

Micro- and nanoplastic:

Fate in the freshwater ecosystem, formation through the use of plastic water bottles, and a model for human health risk evaluation

by

Anna Sophie Winkler

XXXIV Cycle

Tutor: Prof. Diego Rubolini

Co-tutor: Prof. Paolo Tremolada

This thesis was submitted in January 2022

for the degree of Doctor of Philosophy

Contents

Abstract

Although the degradation of plastics is desirable, the degradation products of plastic materials, micro- and nanoplastics, are of increasing concern. These plastic particles are now emerging pollutants in the environment and are considered potentially hazardous to organisms and humans. This thesis had the scope of giving further insights into the understanding of these pollutants by addressing fate, generation, detection and effects on human health.

In detail, the following questions were posed: How do microplastics distribute in a river ecosystem and does the biotic microplastic pollution reflect that of the abiotic matrices? Can the use of plastic packaging generate plastic particles? How are nanoplastic particles chemically modified during secondary formation, and through which analytical approach can they be identified and quantified? What are the human health effects of inhaled microplastics, and is the 3D structured human airway organoid model suitable for human risk assessment of atmospheric plastic particles?

For investigating the occurrence and fate of microplastic in a freshwater ecosystem, two projects were conducted on the Ticino River (North Italy); one on microplastics extracted from multiple matrices (water, sediment, fish and macroinvertebrates) simultaneously sampled along the river and one on microplastic isolated from pellets of an avian freshwater species. The results demonstrated a high complexity of the distribution of microplastics along the river, evidenced by the absence of correlation of concentration between the matrices and along the river, and that a single matrix alone cannot accurately represent the microplastic pollution level of a river ecosystem. Moreover, the spatial variability and the opposing microplastic concentrations in water and sediment further indicates a strong role of the pronounced hydrodynamic conditions of the Ticino River, where microplastics can be deposited, retained and resuspended. Furthermore, using regurgitated pellets and a tied use of different analytical techniques, here μ-FTIR and SEM-EDS, were proven to be a suitable approach for identifying (micro)plastics for avian plastic ingestion studies.

The formation of plastic particles from packaging was investigated in two further projects focusing on the release of micro- and nanoplastic particles from drinking water plastic bottles (single-use) under simulated use. The results demonstrate that the bottle lid (made of high-density polyethylene) was the source of the formation of plastic particles, which were also detected on bottlenecks and, therefore, available for human exposure via ingestion. In this context, the modifications of the physical-chemical characteristics of secondary nanoplastic particles were detected and described. High resolution SEM, XPS, SPES and μ-Raman analysis, in combination with concentration steps proved to be suitable for quantifying and identifying nanoplastics in simple matrices like drinking water.

The last project was dedicated to an innovative model for the risk evaluation of inhaled and deposited atmospheric micro- and nanoparticles on humans. In this work, 3D human airway organoids were characterised and exposed to synthetic microplastic fibres released by drying textiles in a tumble dryer. The result shows that the presence of nonbiodegradable fibers during the repair phase of a damaged lung epithelium may lead to their inclusion in the repaired tissue with unknown effects on long term perspective. Concluding that human airway organoids are suitable for testing airborne micro-and nanoplastics to determine the potential

risks of atmospheric particles in developing adverse pulmonary effects, this thesis contributes to the development of urgently needed human models for assessing the impact of particulate matter pollutants.

Covering different aspects of micro- and nanoplastic pollution, this thesis contributed to understanding the complexity of this pollutant and to the optimisation of future micro- and nanoplastic research regarding the evaluation of environmental concentrations, human exposure of plastic particles from packaging and human risk evaluation of atmospheric particulate matter. Also, with a perspective on the future of plastic materials (here packaging and textiles), the results of this work should stimulate and be taken into consideration for the re-design of plastic materials.

Acknowledgements

First and foremost, I would like to thank Prof. Diego Rubolini, without whose tutorship my PhD candidature would not have been possible. I would also like to express my sincere gratitude to my co-supervisor Prof. Paolo Tremolada for his continuous support during my PhD and creating opportunities that led to some of the projects. I felt very welcome in his research team and enjoyed the collaboration very much. Thank you for passing on your knowledge and believing in me.

I would like to extend my thanks to Dr. Renato Bacchetta and Dr. Nadia Santo, with whom I had the best working experiences in our research team, for their kind support and analytical instrument training.

My appreciation goes out to my parents and my sister for their encouragement and infinite support in the past few years, as well as to my grandmother (and late grandfather) and my aunt – I am very grateful for your support throughout my academic career. My thanks also go to my dear friends who have always been there for me when I needed them.

CHAPTER I – General Introduction

1.1 Micro- and nanoplastics

With the consistent production and consumption of plastics, emissions of plastic are increasing and will continue to do so even in the most optimistic future scenarios for plastic waste reduction.[1,2] Stimulated by reports of plastic waste in the marine environment[3,4] and adverse impacts for animals (e.g. entanglement),[5] the discussion about environmental pollution by plastic has gained public interest in recent years. Conventional plastics are synthetic polymers mainly derived from petroleum-based raw materials and can contain a wide range of low molecular weight additives to improve their processability, properties, and performance.[6] Plastics may be toxicologically relevant when the chemicals, including these additives (e.g. plasticisers, stabilisers, flame retardants) and other molecules present in plastics, leach from the material.[6] Micro and nano-size ranged plastic particles, so-called micro- and nanoplastics, are part of the overall plastic pollution problem and have been considered a potential threat to humans.[7–9] It is therefore not surprising that the scientific community has contributed substantially to the research of these emerging contaminants in recent years. By now, it is well known that microplastics are ubiquitous in the environment due to their small size[10] and slow degradation, which depends on the polymer properties and environmental conditions.[11] Less information is available for nanoplastics because they have not yet been extensively measured in the environment. However, there is growing concern that this size fraction of plastics may be more prevalent and hazardous than larger particles.[12]

1.1.1 Microplastics in freshwater

Although there is still no agreement on the upper and lower size limits to microplastics, the following proposed definition by Frias and Nash (2019)[13] goes in line with the most used definitions: "*Microplastics are any synthetic solid particle or polymeric matrix, with regular or irregular shape and with size ranging from 1 μm to 5 mm, of either primary or secondary manufacturing origin, which are insoluble in water*".

This elaborate description already indicates that microplastics is a collective term for a heterogeneous group of diverse and complex contaminants[14] with shapes ranging from fibre, film, fragment, foam to spheres.[6] Microplastic particles can be produced as such and added to products to improve their functionality (e.g. printing ink, lubricants) or as a major component (e.g. paints, cosmetics) and are defined as primary microplastics.[15] Recently, the European Chemical Agency (ECHA) proposed a restriction of primary microplastics under the REACH regulation.[16] The majority of microplastics in the environment, however, are secondary microplastics deriving from the fragmentation and degradation of plastic litter via biological, physical, and chemical processes. Moreover, they can be generated when using a plastic product, for example, the release of microplastic fibers from wearing or laundering synthetic clothes,[17] particles from tyre wear[18] or packaging material.[19]

Once in the environment, microplastics can be transported through the atmosphere, reaching very remote areas such as glaciers,[20] the Arctic region,[21,22] Antarctica,[23,24] and even the highest mountain on earth.[25] In the marine environment, the presence of microplastic has been studied extensively.[26,27] Also, there has been a surge of interest in studying microplastic pollution in freshwater ecosystems. The presence of microplastic has been detected in surface water[28–30] and sediment[31–33] of rivers and lakes worldwide. Microplastics have also been

observed in organisms, such as fish[34,35] and invertebrates,[36,37] and in traces of organisms (e.g. mammal faeces),[38] indicating the ubiquity of microplastics in aquatic ecosystems. The levels of microplastic vary greatly. According to a recent review,[39] the reported microplastic concentrations span eight orders of magnitude in freshwater (1.2×10^{-3} to 5.4×10^{5} particles m^{-3}) and six orders of magnitude in sediments (8.1×10^{-1} to 9.5×10^{5} particles kg^{-1}). Higher microplastic concentrations are often associated with areas of high industrial activity,[29] which might be explained by the main input pathways of microplastic to rivers that are known to be effluents from wastewater treatment plants,[40] surface runoff from roads and agriculture,[41] and atmospheric fallout.[42] Interestingly, the plastic consumption by polymer type, which lists polyethylene types (PEs), such as high-density polyethylene (HDPE) and low-density polyethylene (LDPE), polypropylene (PP), polystyrene (PS) and its expanded version (EPS), polyvinylchloride (PVC) and Poly(ethylene terephthalate) (PET) as plastics of highest demand,[43] is also reflected in the order of globally detected polymers in freshwater and drinking water studies: PE ≈ PP > PS > PVC > PET.[44]

For the chemical identification of the microplastics, spectroscopic methods are most often used: Fourier-transform infrared (FTIR) and Raman spectroscopy coupled to a microscope (μ-FTIR, μ-Raman), and scanning electron microscopy combined with energy dispersive X-ray spectroscopy (SEM/EDS). Also, pyrolysis gas chromatography/mass spectrometry (Pyr-GC/MS) for providing the mass of microplastics is commonly used.[39] It has been rigorously highlighted that there is an urgent need to establish standardised and harmonised protocols for sampling, sample processing, analysis and reporting of microplastics from various environmental matrices due to the rapid increase in microplastic pollution studies.[39,45,46] Particularly challenging is the chemical identification of microplastics, especially those of a few micrometre size.

Plastic particles are considered an environmental risk due to their chemical and physical properties. Potentially negative impacts of microplastics on biota are associated with the leaching of monomers and additives, of which some have been proven to have endocrine-disruptive, toxic, or carcinogenic effects.[47–49] Additionally, microplastics can serve as a carrier for other toxic pollutants that are already in the environment, including persistent organic pollutants[50,51] and heavy metals[52,53] sorbed to the surface of microplastics. Microplastics can also have physical impacts such as injuries caused by internal scratches and obstructions in the digestive tract or deprived nutrient availability via gut blockage, false satiety sensation.[54,55] However, the reported effects of microplastic on the biota, which depended on species, size, shape, chemical composition and concentration, are highly contradictory. The impacts ranged from negative (including lethal) through no impacts up to detoxification (when the initial concentration of pollutants in organisms was higher than in the ingested microplastics).[56,57] Furthermore, many toxicity studies were implemented with microplastic concentrations exceeding those measured in the environment by far.[56] The ambiguity of these results and the shortcoming in sampling and detection have cast doubt on the relevance of microplastic studies in freshwater systems.[57] The environmental risk of larger microplastics for freshwater biota has been suggested to be rather low, while a higher risk remains for small microplastics (few micrometres) and nanoplastics.[57]

1.1.2 Nanoplastics

The further weathering of macro- and microplastics can lead to a substantial load of nanoplastics in various ecosystems.[12] Nanoplastics differ from microplastics due to their size

and their size-dependent properties. Contributing to the on-going debate on size definitions for micro- and nanoplastics, Gigault et al.[58] defined nanoplastics as "*particles resulting from the degradation of plastic objects"* and that *"nanoplastics exhibit a colloidal behaviour within size ranging from 1 nm to 1 μm*", which in turn is consistent with Frias and Nash's[13] lower size limit to microplastics (1 μm).

The size-dependent properties of nanoplastics have consequences for transport, interactions with colloids, bioavailability, potential toxicity and leaching times for additives.[59] Due to these properties, nanoplastics are even considered to be more extensively distributed and damaging than microplastics.[12,60] Previous research has shown that nanoplastics can permeate through biological membranes due to their small size.[61]

However, unlike microplastics, nanoplastics have rarely been measured in the environment due to methodological challenges.[62] The technical development and feasibility for the analysis of particles below certain sizes are still limited. Chemical identification techniques relying on laser spot sizes such as μ-Raman or transmitted/reflected μ-FTIR microscopy are popular in microplastics analysis as physical and chemical information can be obtained with a single instrument; however, they have a resolution limit.[59] Although the nanoplastic research benefits from existing studies on engineered nanomaterials, whose analytical methods are now being adapted and improved for the quantification and identification of nano-scales plastics,[59] understanding the formation and detection of nanoplastics is in its infancies. To overcome the limits of single instruments, it has become practical to couple different techniques to obtain the necessary information on the chemical character, shape, size discrimination, and concentration, including field flow fractionation, mass spectrometry, and light scattering.[56,58]

Moreover, scientific evidence about their interactions with organism is rare and inconclusive; depending on the measurement metric used (numerical, mass-based or volumetric concentration) and the nanoplastic model characteristics,[59,63,64] toxicity experiments can lead to varying outcomes.[65] The recent perspective by Mitrano et al.[12] reports that there is insufficient information to conduct an adequate risk assessment of nanoplastics leaving key knowledge gaps that still must be filled in terms of both nanoplastic hazard and nanoplastic exposure. To fill this research gap, the physical-chemical properties of secondary nanoplastic debris needs to be better understood.

1.1.3 Human health

With growing studies on plastic particles in the environment and animal and cell-based experiments in the laboratory producing inconsistent results,[65,66] the question emerged how plastic particles affect humans; through which pathways do we take up micro- and nanoplastics, and, most importantly, do they have harmful effects on our health?

The presence of microplastics in food and beverages has been demonstrated before[19,67,68], and their oral ingestion has been proven recently.[69] The oral uptake of micro- and nanoplastics via direct exposure from consumer goods is therefore undisputed. For drinking water, the World Health Organization reports that there are currently no or low health concerns regarding the consumption of microplastics and associated chemicals.[70] Yet, increasing concentrations in our food may have unknown consequences in the future and particularly for nanoscale particles, reliable information is lacking. Moreover, science has just begun to look more closely at the plastic food packaging itself as a source of micro- and nanoplastic particles for human exposure. The release of plastic particles by food packaging under thermal stress

was observed by a study analysing the water after steeping a plastic teabag.[71] Plastic food containers and plastic cups were also recently identified as potential ingestion sources.[72] Considering the role that plastic food packaging plays in our daily lives, understanding their contribution as unintentional sources of secondary micro- and nanoplastics and the level of human exposure is important. In this context, it is particularly important to determine the physical-chemical properties of secondary nano-scale particles that might occur during the use of a plastic product.

Other pathways of micro- and nanoplastic intake by humans are the inhalation of atmospheric particles, which has already been demonstrated *in vivo* for microplastic fibres.[73,74] The main sources of microplastics in the air are industrial emissions, traffic, materials in building, waste incineration and, considered as the major source, synthetic textiles from, for example, clothes and house furniture.[42,75] The latter explains also, why the largest portion of microplastics in the atmosphere consists of microplastic fibres.[42] Reports on the concentration of microplastic in the air are still few.[76–78] Those comparing indoor with outdoor airborne microplastic concentration observed higher concentration in indoor environments,[77] with levels ranging from 1–60 particles m^{-3} day^{-1}.[79] The estimated atmospheric microplastics that a person could inhale was calculated to be 26–130 airborne microplastics a day.[75]

Commonly, the human health effects of these emerging contaminants are deduced from *in vivo* exposure tests in animal models, i.e., mammalian or nonmammalian models such as mice,[80] rats,[81] *Xenopus laevis*,[82] and zebrafish,[83] and from *in vitro* models such as human cell cultures.[57,84] After exposure, i.e. inhalation or ingestion, micro- and nanoplastics may pass through biological barriers, leading to translocation in the body tissue, which, however, is size-dependent.[85] To date, the most common *in vitro* models used to evaluate the biological effects associated with micro- and nanoplastic exposure are human two-dimensional (2D) cell cultures with a variety of human cell lines, including epidermal cells,[57] lung epithelial cells,[84,86,87] endothelial cells,[88] and intestinal cells.[89,90] However, it is known that these 2D systems have limitations, such as an inaccurate representation of the *in vivo* tissue,[91] or, usually being monocultures, allow the study of only one cell type,[92] and are therefore increasingly being seen as inefficient model.[93] Recently, three-dimensional (3D) cellular structures called organoids generated from induced pluripotent stem cells, embryonic stem cells, or adult tissue-resident stem cells have been shown to be a powerful tool to overcome the limits of 2D cultures.[91,94]

1.2 Thesis objective

The overall quest of this doctoral thesis was to give further insights into the understanding of the emerging pollutant micro- and nanoplastic, particularly the occurrence and fate of microplastic in the freshwater environment (Paper 1 and 2), formation of plastic particles from plastic packaging and detection methodologies for nanoscale particles (Paper 3 and 4), and consequences for human health (Paper 5).

The first specific objective of the thesis was inspired by the increasing interest in microplastics in freshwater ecosystems. Yet, the simultaneous sampling of multiple matrices and analysis of how the microplastic concentration in these matrices varies along a river course is rare. For this reason, the objective was to provide additional insight into the microplastic contamination of specific matrices, their variation along a river system both spatially and in between the matrices to analyse potential correlations among the matrices and driving factors such as environmental features and potential sources. Sampled matrixes were abiotic and biotic samples; surface water, subtidal sediment, gastrointestinal tract of fish (wels catfish, *Silurus glanis*), and macroinvertebrates (caddisfly, Hydropsychidae from the order Trichoptera) collected along the length of the Ticino River in Northern Italy (Paper 1). Additionally, since very little information on avian plastic ingestion of freshwater bird species is available, the microplastic ingestion of the common kingfisher (*Alcedo atthis*) from the Ticino River was studied by examining its regurgitated pellets. Moreover, the aim was to evaluate the kingfisher as monitoring species for avian microplastic pollution. In this context, the differences, advantages and disadvantages for identifying microplastics of the selected analytical methods, SEM and μ-FTIR, were also discussed (Paper 2).

The second specific objective of the thesis was dedicated to the presence of microplastic in drinking water from plastic bottles and on the possible formation of plastic particles from these water bottles. This investigation was motivated by the suspicion that mineral water from plastic bottles could contain microplastics and that mechanical stress to which the bottles are subjected by their use could release more plastic particles to which humans are exposed when drinking from these bottles. To test this, water bottles made of PET (body) and HDPE (lid) were opened and closed several times and subjected to a squeezing mechanism (to simulate use). The aim was to quantify PET and HDPE particles in the micro-size range both in the water itself and on the surfaces of the plastic materials of the bottle (Paper 3). However, the decreasing size of plastic particles challenges their detection and identification, which is why there is little information on secondary nanoplastics in the environment and their exposure to humans. Therefore, a further aim of this thesis was to provide an analytical approach to quantitatively and qualitatively detect the release of nanoplastics in the water matrix and to measure the direct exposure of consumers by the simulated use of plastic water bottles (Paper 4). In this context, the work aimed to identify and discuss the modification of the physical-chemical properties of nanoplastics that occur during their formation and their impact on identification and quantification. Since there is growing concern that nano-sized plastic particles may be more hazardous than larger particles due to the small size,[12] the need for reliable nanoplastic exposure studies is crucial.

After demonstrating the occurrence and fate of microplastic in a freshwater ecosystem and analysing the formation of plastic particles from packaging material, the third specific objective of this work addressed the impact on human health, particularly testing an innovative

exposure model to study the effects of this emerging contaminant. As atmospheric microplastic pollution is one of the main sources of microplastic uptake in humans, the lungs are potentially the most affected human organ. As such, innovative 3D structured human airway organoids offer a promising model, even though still being in the development phase. Since this model has not yet been used to study the effects of inhaled plastic particles, the objective of this thesis was to describe the model and test its application for human exposure tests for micro- and nanoplastic and other inhalable particulate contaminants (Paper 5). The test contaminant used was polyester fibres emitted from the drying process of synthetic clothes and fabrics. This took into account that the largest portion of microplastics in the atmosphere consists of microplastic fibres deriving from synthetic fabrics.[42] The overall aim was, therefore, to contribute to the understanding of human exposure risk and consequences of microplastic fibre exposure, which still remain unclear due to rare and insufficient information providing evidence of the negative human health effects of inhaled microplastic fibres.[10,75]

CHAPTER II – Papers

PAPER 1 – Following the fate of microplastic in four abiotic and biotic matrices along the Ticino River (North Italy)

Anna Winkler, Diego Antonioli, Andrea Masseroni, Riccardo Chiarcos, Michele Laus, Paolo Tremolada

Science of the Total Environment 2022

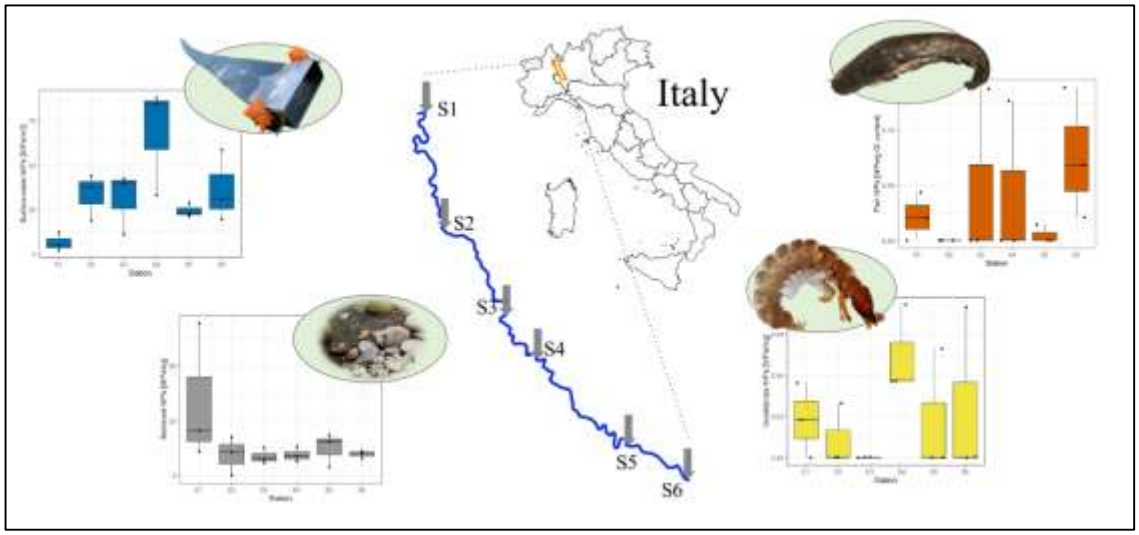

Science of the Total Environment 823 (2022) 153638

Contents lists available at ScienceDirect

Science of the Total Environment

journal homepage: www.elsevier.com/locate/scitotenv

Following the fate of microplastic in four abiotic and biotic matrices along the Ticino River (North Italy)

Anna Winkler [a,*], Diego Antonioli [b], Andrea Masseroni [a], Riccardo Chiarcos [b], Michele Laus [b], Paolo Tremolada [a]

[a] Department of Environmental Science and Policy, University of Milan, Via Celoria 26, 20133 Milan, Italy
[b] Department of Science and Innovation Technology (DISIT), University of Eastern Piedmont, Via T. Michel 11, 15121 Alessandria, Italy

HIGHLIGHTS

- Abiotic MP levels were 33 items m^{-3} in surface water and 11 items kg^{-1} in sediment.
- Biotic MP levels were 0.032 items g^{-1} in fish and 0.030 items mg^{-1} in macroinvertebrates.
- MP levels of biota did not correlate with MP levels of abiotic matrices.
- No increasing trend of MP concentrations with the length of the river.

GRAPHICAL ABSTRACT

ARTICLE INFO

Article history:
Received 8 September 2021
Received in revised form 12 January 2022
Accepted 29 January 2022
Available online 4 February 2022

Editor: Damia Barcelo

Keywords:
Microplastic
Freshwater ecosystem
Sediment
Surface water
Fish
Macroinvertebrates

ABSTRACT

Microplastics (MPs) are emerging contaminants in freshwater systems that have already attracted much scientific interest, but little attention has been paid to a multi-matrix analysis of MP occurrences along the length of a river. The present research provides the first record of MP contamination of four abiotic and biotic matrices from a river ecosystem simultaneously analysed. MPs were isolated and identified by micro-Fourier Transform Infrared (μ-FTIR) spectroscopy from samples collected along the Ticino River in North Italy during spring 2019. Abiotic samples were surface water (n = 18, 33 MPs m^{-3}) and sediment (n = 18, 11 MPs kg^{-1}), while biological samples consisted of stomach and gut content of fish (n = 18, wels catfish, *Silurus glanis*, 0.032 MPs g^{-1}) and macroinvertebrates (n = 90, caddisfly larvae, Hydropsychidae, 0.03 MPs mg^{-1}). MPs were found in biota from all stations; 44% of fish and 61% of macroinvertebrate samples contained MPs. The calculated unit-consistent concentration ratios indicate that both *S. glanis* and Hydropsychidae larvae had a consistent higher amount of MPs than their respective medium (sediment and water), strongly suggesting an efficient uptake pathway into organisms. MP levels in surface water, sediment, fish and macroinvertebrates were not correlated and did not increase with the river's length. From our mass balance calculations, the Ticino River transports a consistent amount of MP (yearly load of $3.40 \times 10^{11} \pm 1.1 \times 10^{11}$ MPs) to the Po River. This MP load was almost half than an estimated MP load from wastewater treatment plants (WWTPs). On that basis and supported by the finding that MP concentration in sediment was mostly opposed to that in surface water but was on average 750-fold higher compared to the water matrix, we surmise that the complex hydrological network of the Ticino River retains a consistent amount of MPs which might build up over time.

1. Introduction

The interest in studying the pollution of microplastic (MP, synthetic polymers <5 mm) in freshwater ecosystems is increasing continuously. Previous studies have already reported the presence of MP in surface water

* Corresponding author.
E-mail address: anna.winkler@unimi.it (A. Winkler).

http://dx.doi.org/10.1016/j.scitotenv.2022.153638

(Mani et al., 2016; Dris et al., 2018a; Mintenig et al., 2020), sediment (Rodrigues et al., 2018; Klein et al., 2015; Horton et al., 2017), fish (Roch et al., 2019; Wang et al., 2020), mammals (Smiroldo et al., 2019) and invertebrates (Xu et al., 2020; Sfriso et al., 2020), indicating the ubiquity of MPs in aquatic ecosystems. In rivers, MPs enter through various sources, such as effluents from wastewater treatment plants (WWTPs) (Schmidt et al., 2020), surface runoff from roads and agriculture (Xia et al., 2020), atmospheric fallout (Dris et al., 2016), and degradation of larger plastic waste items. These input pathways might explain why higher concentrations of MP are often associated with areas of high industrial activity (Dris et al., 2018a). Rivers are conduits for MP to the sea, yet, not all MPs entering the river are directly transported toward the marine environments. MPs can be retained, stored and deposited for a long time in sediments (Nizzetto et al., 2016; Horton and Dixon, 2018), increasing the exposure to organisms and the retention potential of the inland hydrological network.

Although the ingestion of MPs by biota from diverse trophic levels is gaining attention, the intake and effects remain poorly understood (Hermsen et al., 2018). Furthermore, in-situ investigation of MP loads in river insect species is still rare (Nel et al., 2018). The ingestion of MP by organisms depends on the particle size, among other factors (Phuong et al., 2018). Once ingested, the potential adverse effects on the aquatic life can be of a physical nature (blockage and disruption of digestion) or have chemical impacts such as pollutant transfer due to their properties as vector and leaching of plastic additives (Kukkola et al., 2021). The incorporation of MPs into the benthic food web might also rely on the river flow dynamic, given that many benthic organisms feed on particulate matter settling on the sediment. The investigation of MP concentrations in benthic organisms as potential indicators of MP pollution of the freshwater environment has been discussed before (Nel et al., 2018).

To date, only one study investigated MP levels in different species and abiotic matrices simultaneously; however, it addressed the marine ecosystem (Karlsson et al., 2017). Comprehensive studies of multi-matrices covering more abiotic and biotic samples are still rare, especially with accompanying analyses of how MP concentration in these matrices varies along a river course. In the present study, we analyse surface water, subtidal sediment, gastrointestinal tract of fish (wels catfish, *Silurus glanis*), and macroinvertebrates (larval hydropsychid caddisfly, Hydropsychidae:Trichoptera) sampled along the length of a river (Ticino River in Northern Italy). This study aims to provide additional insight in MP contamination of the specific matrices, variation along a river system both spatially and in between the matrices to analyse potential correlations among matrices and driving factors such as environmental features and potential sources. By analysing MP in different environmental matrices, we can better estimate relative concentration ratios in biotic vs. abiotic matrices. Based on observations from previous studies, we hypothesise that the concentration of MP in surface water increases with the increasing length of the river and that MP concentrations of biotic matrices reflect those of abiotic matrices.

2. Material and methods

2.1. Research area and sample collection

The Ticino River [7228 km^2 total catchment area; 350 $m^3 s^{-1}$ mean discharge (Cushing et al., 2006)] is a 248 km long river located in Southern Switzerland and Northern Italy and is a main tributary of the Po River. The Ticino was selected as it represents one of Italy's most natural rivers yet flows through the urbanized and industrialised Po Plain. Moreover, MPs were already found in the ecosystem of the Ticino River, i.e. in pellets from the kingfisher (Winkler et al., 2020) and in faeces of otter (Smiroldo et al., 2019). Six sampling stations (S1–S6) were chosen based on spatial proximity to potential main MP input sources (drainage canal outflows, WWTPs) and accessibility, covering a transect of 80 km (1189 km^2 catchment area) of the Italian part of the Ticino River (Fig. 1). Sampling of surface water, sediment and macroinvertebrates took place in shallow banks of the river. Stations S1, S3 and S4 were located in outer bands of the meandering river, while S2, S5 and S6 were located in inner bands.

Surface water, sediment and macroinvertebrates sampling was implemented on three subsequent days in July 2019, while fish were sampled from February to July 2019 for logistical reasons. For surface water sampling, we used an in-house manufactured Neuston trawl (60 μm mesh size of nylon net, 3 m length, steel frame 0.2 m deep and 0.5 m wide). Sampling was implemented by two persons standing in the current and holding the trawl in position with ropes. Flow velocity was measured with a flowmeter and was 0.44 ± 0.11 m s^{-1} on average (Table S1). Filtered water volume was estimated by multiplying the area of the trawl opening through which the water passed with the flow velocity and the duration of sampling. The mean ± SD filtered water volume was 10.88 ± 2.60 m^3 (see Table S1 for details). Water was filtered three times for 10 min for each position. Sample material in the net was rinsed with river water from the outside to the inside into the cod end of the trawl. The collected material was then rinsed into a glass jar and frozen until extraction.

Subtidal sediment was collected from three spots located 1 m from the shoreline at approximately 5 m intervals. Subtidal sediment in the littoral zone was selected based on proximity to macroinvertebrate sampling site to allow comparison of MP data. Where necessary, the layer of larger stones was put aside before removing the first 3 cm of river sediment from an area of approximately 100 cm^2 with a metal shovel. We chose a shovel as the sampling method for cost-effectiveness and simplicity as suggested by previous literature (Wang et al., 2017; Wen et al., 2018; Peng et al., 2018). Sample material was transported in aluminum trays closed with aluminum foil and stored at −20 °C.

The fish species selected was the wels catfish (*Silurus glanis*), for two main reasons: it is one of the top predators of the river and is therefore at the top of the food chain (potential accumulation of MPs), and it is an invasive species and as such was being caught anyhow by a local containment campaign. The fish were caught via electrofishing during a containment campaign performed in the Action C7 (Active defence of *Acipenser naccarii* spawning sites) of the "Ticino Biosource" LIFE project (Parco del Ticino, 2021). They were killed according to the ethical statement of the project and according to the DGR n.8/6308, 21/12/2007 of the Lombardy Region: "Management of *A. naccarii*, of reproductive sites and of fishing", approved to guarantee long-term survival of the species. For these reasons, sampling took place over 5 months (February–July). Whether there were temporal effects on the MP concentration was statistically calculated (see S1.5). Among those fish caught for containment purposes, three were selected having similar size in each sampling station. Thus, $n = 3$ fish per station were sampled. The fish had a mean (± SD) length and weight of 84.1 ± 11.2 cm and 4.5 ± 1.9 kg, respectively. Since the gastrointestinal tract (GIT; oesophagus to vent) for the MP extraction was targeted, GITs were immediately removed in the laboratory and stored at −20 °C until further processing.

For macroinvertebrate samples, the larvae of hydropsychid caddisflies (Hydrospsychidae:Trichoptera) was selected due to their numerical abundance. Preliminary sampling of the macroinvertebrate communities of the river continuum revealed that Hydropsychidae was the only insect family present in sufficient individual numbers at each station. Larval Hydropsychidae typically colonize hard bottom substrates of different types and particle sizes and are categorised as filter-feeders/collectors and processors of suspended organic materials (Ficsór and Csabai, 2021). To facilitate their filter-feeding, they build retreats consisting of silk and substrate material to which catch-nets of a specific mesh sized are attached (Ficsór and Csabai, 2021). At each sampling station, 15 individuals were collected by hand-picking the individuals from rocks and larger stones (Chessman, 1995). The individuals were identified in the field, placed in glass jars and immediately fixed in 70% ethanol.

2.2. Isolation of MP

For the isolation of MP from the matrix, it was necessary to process the samples before digesting them chemically in a purification step and separate the MP from the solution via density separation. Surface water samples ($n = 18$) contained relatively large volumes of suspended organic matter

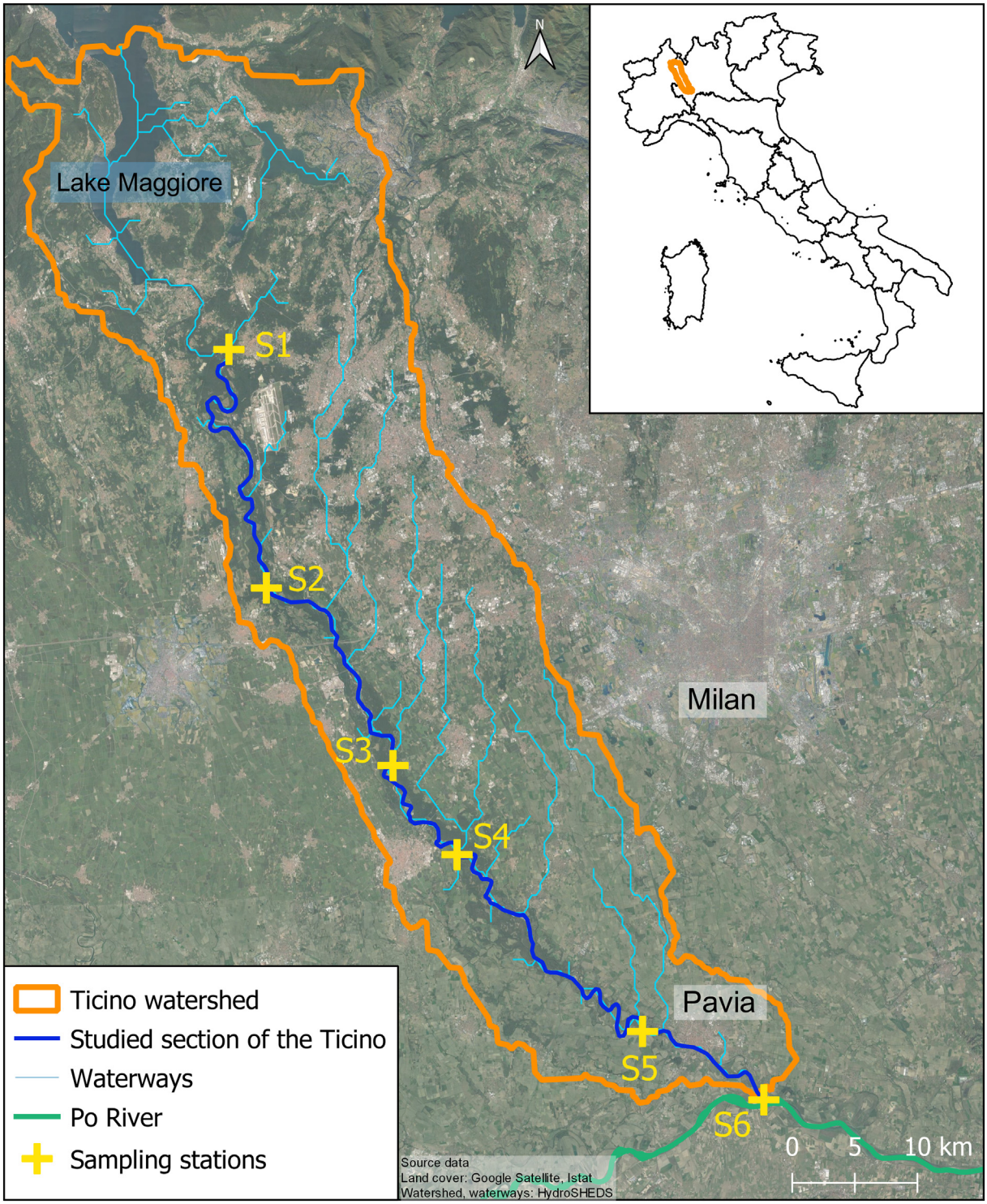

Fig. 1. Overview map of the study area showing the watershed of the Ticino River and its waterways. Sampling stations are located along the 80 km long stretch of the studied section of the Ticino River, with S1 upstream near the Lake Maggiore and S6 downstream at the confluence of Ticino and Po River.

and algae due to the small pore size of the net. Therefore, we filtered the sample matrix over a stacked arrangement of sieves following the protocol by NOAA (Masura and Baker, 2015). Sample material was poured and rinsed over a stainless steel sieve (2 mm mesh size) into an aluminum-framed nylon net (60 μm mesh size), thereby reducing also the water volume. Retained material on the 2 mm-sieve was visually inspected for any MPs < 5 mm and discarded. Sieved material on the nylon net was rinsed carefully into a clean beaker.

Collected sediment (n = 18) varied between stations, but the numbers of MPs per sediment sample were normalised to 1 kg. To report MP concentrations in kg of dry weight (MPs kg^{-1}), sediment samples were oven-dried at 50 °C until constant weight (up to 10 days). The drying at higher temperatures to speed up the process was prevented as temperatures >50 °C might influence the integrity of MPs inside the sample (Pfeiffer and Fischer, 2020). Mean (± SD) sample dry weight (dw) was 0.634 ± 0.064 kg (see Table S2 for values for each station). Each dry weight amount was used

to normalize MP concentrations in kg of dry weight of sediment (MPs kg^{-1}). Throughout the course of the river, the grain size distribution of sediments changed, resulting in differing sample compositions. Therefore, the grain size classes of each sample were determined by fractioning the grains in three size categories: < 2 mm (clay, silt, sand), fine gravel (2–4.75 mm) and medium gravel (> 4.75 mm) using a stacked arrangement of stainless steel sieves (see Table S2 for grain size ratios). Relationships between grain size class distribution of each sample and MP concentrations were evaluated.

As the entire GIT of catfish (n = 18) was too large, we released the content into a glass beaker using filtered Milli-Q water to rinse the residues in the tract. When ingested fish or crab parts or entire bodies were found, they were rinsed off over the beaker and discarded. Mean (± SD) GIT content wet weight (ww) was 46 ± 34 g (Table S3).

Hydropsychidae macroinvertebrate samples were rinsed with filtered distilled water to remove any exterior MPs, placed in glass beakers covered with pierced aluminum foil and then freeze-dried under vacuum to determine biomass (mg dw). Five individuals were pooled together to provide composite samples (n = 18) with a mean (± SD) weight of 33.6 ± 6.5 mg. Subsequently, samples were homogenised with a mortar and pestle and placed in beakers.

To digest the organic material chemically, surface water and sediment samples were treated with hydrogen peroxide with iron as catalyst (H_2O_2 + Fe^{II}), and biota samples with potassium hydroxide (KOH). Additionally, density separation with a saturated salt solution (NaCl) was performed on water, sediment and fish samples. All solutions were then filtered on cellulose membrane for the visual identification under the stereo microscope to isolate putative MP items. The details of these steps are elaborated in the SI of this work (S1.2).

2.3. μ-FTIR analysis

To verify our visual identification accuracy and identify the polymeric origin of MPs, micro-Fourier Transform Infrared Spectroscopy (μ-FTIR, Thermo Scientific Nicolet iN10 MX) was used. For water surface samples, 40 ± 23% (mean ± SD) of items on each filter were randomly selected for validation. For sediment samples, 67 ± 22% (mean ± SD) of items on each filter were randomly selected. For fish and macroinvertebrate samples, we conducted an 82 ± 28% and 82 ± 19% FTIR validation of visually identified MPs, respectively (Table S4). Particle image, final FTIR spectrum and the best match with the library were recorded for each analysed particle and marked by the univocal code of the particle. The spectra matching with a quality index between 60 and 70% were accepted and labelled as "synthetic polymer", while spectra with a quality index higher than 70% were recorded with the name of the polymer type. Final MPs concentrations in water, sediment, fish and macroinvertebrate samples were adjusted by the percentage of FTIR-confirmed plastics in each category, deducting the verified non-plastics. For details of μ-FTIR analysis, see S1.3.

2.4. Quality control

All glass ware and metal cutleries were cleaned with washing detergent and rinsed with Milli-Q water, previously filtered through a mixed cellulose ester membrane (0.45 μm). Laboratory surfaces were wiped with ethanol and paper tissue. All persons wore cotton lab coats or non-synthetic clothes and washed their hands after each procedure. The NaCl, the H_2O_2, the Fe and the KOH solution applied in this study were all filtered using 0.45 μm pore size cellulose membranes.

We included six lab blanks for water samples and three blanks each for sediment, fish and macroinvertebrate matrix to cover the different sample handling, chemical digestion steps and used reagents, with a total of 15 blanks. Blanks underwent the same post sampling process simultaneously with the respective field samples. In blanks, water, sediment and fish material were replaced by 100 mL filtered Milli-Q water, macroinvertebrates by 5 mL. Only fibres were detected in the procedural blanks, never fragments, spheres or foils. The fibre contamination was low and stable; in all water blanks, 1 MP fibre (PAN) was found, fish blanks had 1 MP fibre (PET), no MPs were found in blanks for sediment and invertebrates. The MP abundances in environment samples of each matrix reported for this study were blank-corrected (subtracted by the mean level of blanks, listed in Table S5).

To evaluate the efficiency of the applied MP extraction technique, we implemented a mass recovery test with positive control samples. The samples consisted of PS standard pellets (INEOS Styrolution PS 124 N/L, Frankfurt am Main, Germany) and PET water bottles, representing low and high-density polymers. The material was cryomilled and sieved to a 60 μm – 2000 μm fraction. The control samples underwent the same MP extraction procedure (preparation, chemical digestion, density separation and filtration) as surface water and fish samples, representing the chemical digestion step with Fenton's Reagent and KOH, respectively. For details of the mass recovery test, see S1.4, Table S6. SEM images of the recovered plastic particles indicated that the chemical digestion had little-to-no impact on the integrity of the material. The mean (± SD) recovery rate for PS fragments was 98.2 ± 1.0% and 97.1 ± 2.4% for the extraction following the extraction procedure for water/sediment and biota, respectively. For PET fragments, the recovery rate was 47.1 ± 28.7% following the procedure for water/sediment and 41.0 ± 16.8% following the procedure for biota (Table S6).

2.5. Data analysis

The performed statistical analyses are elaborated in the SI of this work along with the calculations of unit-consistent ratios between the matrices and estimated MP load from the Ticino River and from WWTPs (S1.5).

3. Results

3.1. MP validation and composition

We deliberately refrain from mentioning all calculated data in this section. Further details can be found in S2. A total of 772 items from all samples were analysed via μ-FTIR, and 582 (75.3%) were identified as MPs from 28 different polymer types (Table S9). The validation rate of visual identification (validated MPs out of all selected items including natural polymers, minerals etc.) varied between the sample matrices. For example, the success rate for water surface sample was 91 ± 18% (mean ± SD), while for macroinvertebrates, only 33 ± 37% (mean ± SD) of all selected items turned out to be plastic (Table S10). The average MP concentrations for all matrices are summarised in Table 1. The mean (± SD) MP concentration and the shape composition of MP for each matrix and single station are listed in Table S11–S14. Examples of detected MP items on silver membranes for each matrix can be seen in Fig. S3. The number of MPs per replicate can be retrieved from Tables S15–S18. In the following, mean MP concentration, polymer type and shape are reported for each matrix.

Surface water samples had an average MP concentration of 33 (± 20) items m^{-3} (n = 18; ± SD). Total surface water samples contained 26

Table 1
Mean (± SD) concentration of MP for all matrices.

Matrix	Total number of samples (n)	Mean (± SD) MP concentration
Surface water	18	33.336 (± 20.363) [items m^{-3}]
Sediment, subtidal	18	11.016 (± 7.769) [items kg^{-1}]
Fish (catfish, *Silurus glanis*, gastrointestnial tract (GIT))	18	0.032 (± 0.029) [items g^{-1} GIT content] 1.404 (± 1.309) [items $individual^{-1}$]
Macroinvertebrates (caddisfly, Hydropsychidae, whole specimen)	18 (5 individuals pooled as 1 sample)	0.030 (± 0.025) [items mg^{-1}] 0.207 (± 0.184) [items $individual^{-1}$]

different polymer types, of which LDPE (19.3%), PET (18.2%) and PP (17.5%) were in the majority. Considering the shape of detected MPs, water samples were dominated by irregular particles (59.3%) followed by fibres (36.5%), while film, foam and spheres contributed less than 2% each.

The concentration of MPs in sediments was on average 750-fold higher compared to surface water concentration (when referring to the same volume, S2.2, Table S19). Subtidal sediment samples contained an average MP concentration of 11 (± 8) items kg^{-1} (n = 18; ± SD). Of 11 detected plastic polymer types, EVA (39.2%) was the most predominant polymer, followed by PP (15.2%) and PET (8.9%). Most of the detected MPs were irregular particles (83.5%), followed by fibres (12.7%) and spheres (3.8%).

We found plastics in the digestive tracts of 8 of 18 catfish (44.44%). Each fish GIT contained an average of 1.4 (± 1.3) items of ingested MP per fish (max 7), corresponding to 0.032 (± 0.029) MPs g^{-1} ww. We identified 6 different polymer types in all fish samples, of which LDPE (39.1%) and nylon (13%) was prevalent. In the average composition of MP shapes in fish samples, irregular particles (70.8%) dominated over film (16.7%), fibres (8.3%) and spheres (4.2%). The MP quantity per fish was not significantly correlated to the weight of analysed GIT content and the sampling period did not have a significant effect on MP content (Kruskal-Wallis Test, p = 0.213). For logistical reasons, the fish were not sampled solely in the time frame in which the other matrices were sampled. The fish sampling was tied to the containment campaign for this species, over which we had no control. However, the electrofishing from the boat was carried out beyond flooding conditions and can therefore be considered as an approximation of the ideal sampling campaign, which would have been truly simultaneous to the other matrices. Possible misleading findings resulting from this approximation have been taken into account in the statistical evaluation, supporting the assumption that our fish sampling extended for a longer time compared to the other matrices can be considered the best experimental surrogate for truly simultaneous fish sampling.

Sixty-one percent (61%) of all Hydropsychidae samples contained MPs. Overall, Hydropsychidae incorporated 0.21 ± 0.18 (mean ± SD) MP items per individual, corresponding to a mean value of 0.030 (± 0.025) MP items mg^{-1} dw (n = 90 individuals; ± SD). The MP composition in macroinvertebrates was dominated by PS (26.7%) and PET (26.7%). However, the majority of suspected MPs in macroinvertebrates were found to be cellulose. In 11 out of 18 samples, 29 cellulose items (76% fibres, 24% irregular particles) were detected. A contamination from the used cellulose membrane can be excluded since the isolated cellulose fibres were all of a different colour (Fig. S3D). Considering the shape of detected MPs in macroinvertebrates, most detected MP were irregular particles (60%), the rest were all fibres (40%).

In terms of size distribution, we can observe a general trend for all matrices. Grouping the amount in size categories (Fig. 2), it becomes apparent that the number of MPs < 1000 μm increases with decreasing size. The smallest sizes are impeded by the sampling method (60 μm mesh size of our applied Neuston trawl) and the identification limit of visual isolation and μ-FTIR. The smallest MP isolated by visual identification was 19 μm, and the chemical identification by μ-FTIR loses accuracy when the target particles are smaller than 20 μm. For surface water samples, the frequency of MPs below 300 μm, which is the mesh size of commonly used mantra trawls, was 21%, highlighting the importance of applying sampling nets of smaller mesh sizes. Only 0.2% of MPs were < 60 μm. The highest number of MP in water surface samples were in the class of 1000–2000 μm (21.8%, min = 48 μm). Sediments had the highest number of MP smaller than 100 μm (27.8%, min = 19 μm). Fish ingested most particles in the size range of 1000–3000 μm (41.7%, min = 96 μm). For macroinvertebrates, half of the items were smaller than 200 μm (26.7% ≤ 100 μm, 26.7% between 100 and 200 μm, min = 38 μm) (Fig. 2). The chi-square test revealed no selectivity of Hydropsychidae larvae with respect to MP size compared to MPs in their host sediment (smaller: < 100 μm, larger: ≥ 100 μm; χ^2 = 0.009, DF = 1, p = 0.925).

3.2. Fate along the river

For surface water samples, the station had a significant effect on the MP concentration (DF = 5, F-value = 3.979, p = 0.023), however, except for S1 and S4 (p_{adj} = 0.010), the MP concentration did not significantly differ from each other. Located at the first sampling site along the river, the surface water of S1 had the lowest MP concentration. However, following the river course, we did not observe a general trend of increasing (or decreasing) MP concentration. Instead, we observed a correlation of surface water flow velocity and MP concentrations in water (see S2.3 for details, Fig. S4). Due to the possible interfering effect of the different flow rate on the MP concentrations in water samples, differences among stations were tested by GLM using "flow rate" as a covariate; in this case MPs concentrations in water did not vary significantly among the stations (F4;12 = 2.1; p = 0.14), confirming that the low MP concentration at the first station could be due to the low flow velocity at that station.

Notably, the two stations with the lowest MP concentrations in surface water samples (S1 and S5) had the highest concentrations in sediment samples (Fig. 3B + C). Station S1 was located on the shallow bank in the outer band of the river just before a dam for hydroelectric power generation. Therefore, the local hydrodynamic conditions probably explain the opposing concentrations; particles can sink from the water surface to the sediment. However, considering the density of detected polymer types in water and sediment samples, both water and sediment samples had a higher amount of lighter (< 1.1 g cm^{-3}) than heavier density MPs (χ^2 = 4.9, DF = 1, p = 0.026, Table S9). Comparing the MP properties of the water and sediment samples, we noted a significant association between the matrices and the particle size (χ^2 = 38.9, DF = 1, p = 4.4 × 10^{-10}).

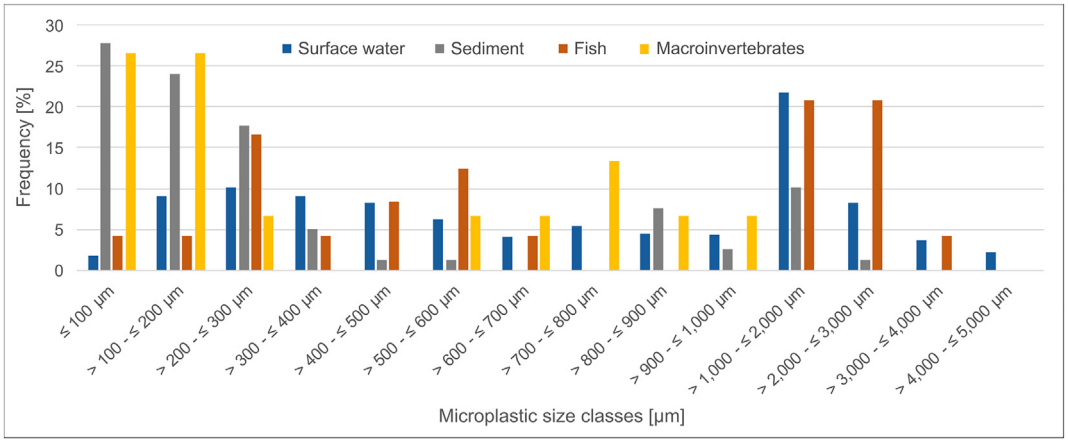

Fig. 2. MP size distribution for all matrices. Items below 1,000 μm in size are grouped in 100 μm size classes, while items between 1,000 μm and 5,000 μm are grouped in classes of 1,000 μm.

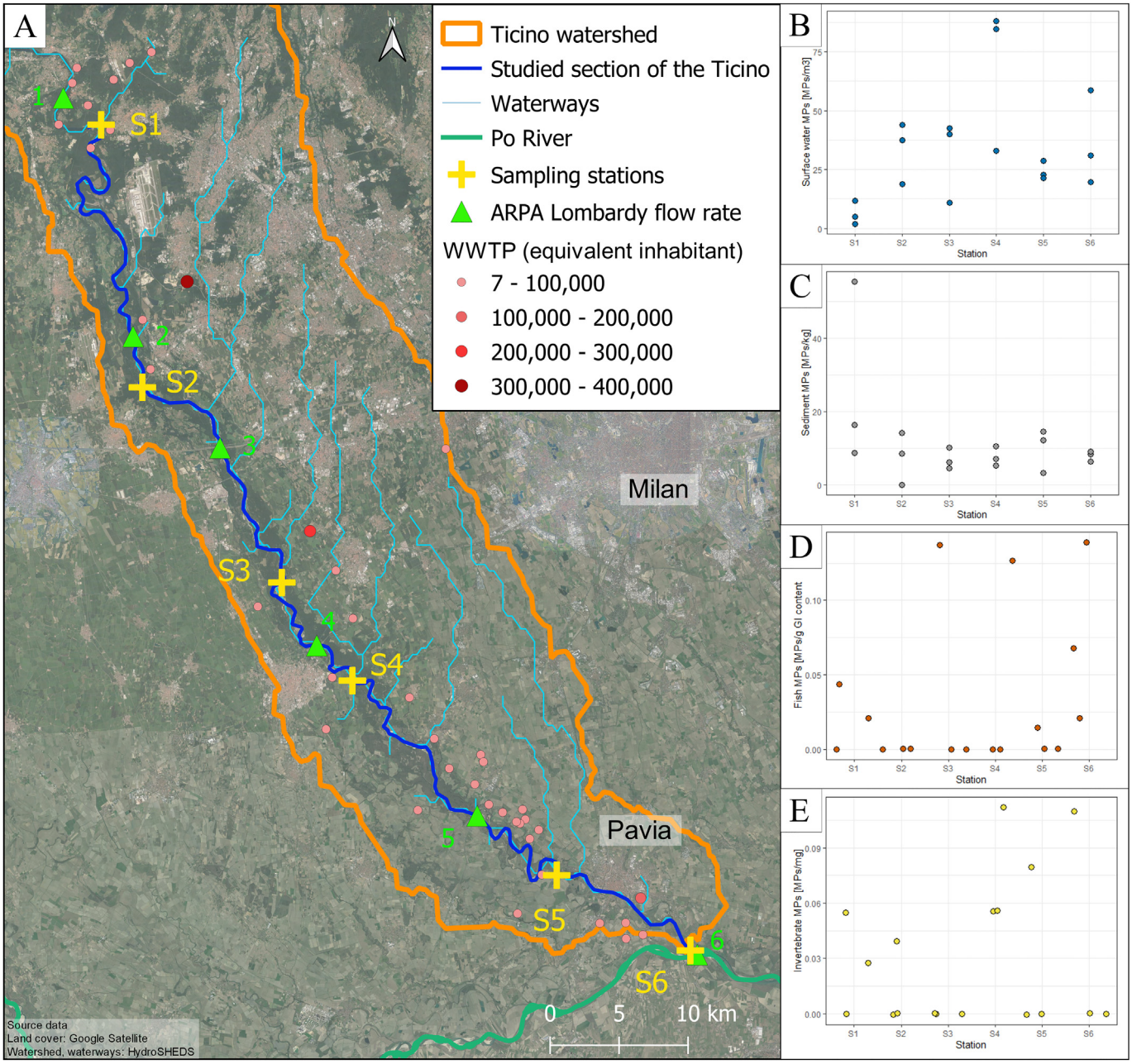

Fig. 3. (A) Overview map with sampling stations at the Ticino River and point of measurements of yearly mean flow rates (green triangle) performed by Regional Agency for the Environmental Protection (ARPA Lombardy). (B–E) MP concentrations of surface water, subtidal sediment, catfish (*Silurus glanis*) and macroinvertebrates (Hydropsychidae larvae), respectively, from the different stations.

Sediment samples contained a significantly greater proportion of smaller MPs (< 500 μm) than water samples which contained more larger MPs. While the majority of MPs collected in both matrices were irregular particles, the proportion of irregular particles from sediment samples (83%) compared to water samples (59%) was significantly greater ($\chi^2 = 23$, DF = 4, $p = 0.0001$). A comparison of MP sizes between water and sediment samples along the river (differences in sampling sites, Fig. S2) confirms that sediment had a higher abundance of smaller MP particles than water at each station. It is also evident that where MP concentrations were highest in sediment and lowest in surface water (S1 at the dam, Fig. 3B + C), the abundance of smaller particles in sediment was highest (Fig. S2). The particle size composition in the sediment at S1 differed most from the other stations, while the particle size distribution in the water samples did not show any prominent differences along the river.

The MP concentration for surface water and macroinvertebrates was both highest at station S4 (Fig. 3B + E). However, significant relationships of MP concentrations between all the matrices could not be detected (Spearman's correlations, $p > 0.05$). For sediment, fish and invertebrate samples, the MP concentrations of the 6 stations did not differ significantly from each other, nor did they reveal any trend (e.g. increasing concentration) with the length of the river. The grain size ratio of the sediment samples varied strongly; from 62% sand and 16% gravel in the upper station to almost 100% sand in the lowest station. Nevertheless, MP concentration in sediments was not significantly correlated to grain size ratio. The MP load carried by the Ticino River at the confluence with the Po River was $3.40 \times 10^{11} \pm 1.1 \times 10^{11}$ MP items year^{-1} (see S2.4, Table S20 for details), calculated by multiplying the mean measured MP concentrations of surface water in each station (item m^{-3}) with the yearly mean flow rate

Table 2
MP concentration for surface water and sediment of selected previous studies compared to this study. All sediment sampling studies used NaCl for density separation.

	Surface water (items m^{-3})	Sediment (items kg^{-1})	Sampling methods	Literature
Ticino River, Italy	33 ± 20	11 ± 8	Neuston net (60 μm) / metal shovel	This study
Rhône and Têt Rivers, France	12–42		Manta net (333 μm)	Constant et al. (2020)
Seine River, France	108		Plankton net (80 μm)	Dris et al. (2018b)
Pearl River, China	379–7924	80–9597	Bulk sampler and mesh membrane filter (20 μm) / Van Veen grab	Lin et al. (2018)
Antua River, Portugal	58–1265	18–629	Pump with mesh net (55 μm) / Van Veen grab	Rodrigues et al. (2018)
Ebro River, Spain	3.5 ± 1.4	2052 ± 746	Neuston net (5 μm) / Van Veen grab	Simon-Sánchez et al. (2019)
Ofanto River, Italy	0.9–13		Stainless steel sieve (300 μm)	Campanale et al. (2019)
Ombrone River, Italy		45–1069	Manual bucket	Guerranti et al. (2017)

of the Ticino River (m^3 $year^{-1}$) at that station reported by ARPA Lombardy (2021) (Fig. 3A).

4. Discussion

4.1. MPs in abiotic matrices

The first objective of the present study was to assess the MP pollution in four different matrices. We found MP in all matrices from all stations. MPs in river ecosystems have attracted global attention in the past decade due to their high concentration in sediment and water samples. A comparison with previous studies on MP contamination of river surface water and sediment is challenging due to variation in the methodology and reported units (Kumar et al., 2021). For example, the smallest detectable MP particle, and thus the number of MP items, can be influences by the pore size of the nets used and the detection limit of the chemical identification instrument. Intercalibration experiments and reference materials are not yet diffused but would be of great interest and highly recommended in the future. An inter-laboratory comparison study on PET microparticle determination in water organized by the European Commission JRC and BAM highlighted that different methodologies applied by different laboratories on a homogeneous sample can give very different results spanning several orders of magnitude (European Commission, 2021). Considering even more complex matrices such as river water, sediment or biota samples, differences deriving from the varying analytical methodologies can be even higher. However, at the present state of the art, comparisons with MP concentration data from other research papers are recommended to establish large differences such as those concerning the order of magnitude of the MP contamination. It is implicit that those differences could be partially due to differences in analytical methodologies. This is one of the reasons of the importance and the scientific relevance of the present results which reports methodologically-consistent data in four matrices in six stations along the Ticino River. Overall, the values we measured are in their entirety within the larger range reported worldwide for surface water and sediments.

Table 2 lists selected previous studies and their measured MP concentrations for surface water and sediment for comparison with our study. In detail, the surface water MP concentration measured in this study (33 ± 20 items m^{-3}, Neuston net 60 μm) are similar to those found in Rhône and Têt Rivers in France (Constant et al., 2020), while they were lower compared to, e.g. the Seine River in France (Dris et al., 2018b), the Pearl River in China (Lin et al., 2018) and the Antua River in Portugal (Rodrigues et al., 2018). Our measured values are higher than those measured in, e.g. the Ebro River in Spain (Simon-Sánchez et al., 2019) and in the Ofanto River in South Italy (Campanale et al., 2019). For further comparison, the reader is referred to a recent review (Kumar et al., 2021). LDPE (branched version of PE), PET and PP were the most common polymer types in our water samples which were also the predominant polymer types detected by many previous studies of MPs in freshwaters (in the order PE ≈ PP > PS > PVC > PET; Koelmans et al., 2019).

Regarding the MP concentration in sediment samples (11 ± 8 items kg^{-1}), our values are lower than reported by most studies (Table 2, Kumar et al., 2021). MP was reported with higher concentrations in sediment of the Pearl River in China (Lin et al., 2018), of the Antua River in Portugal (Rodrigues et al., 2018), and of the Ebro River in Spain (Simon-Sánchez et al., 2019). Also in Italy, documented MP concentrations in riverine sediments of Ombrone River (Central West Italy) varied greatly, but were higher than our reported values (Guerranti et al., 2017). Next to the actual occurrence of MP, the main driving factor for differences in reported values for sediment samples is the used salt for the density separation. However, the studies mentioned above all used NaCl for the density separation, as does the present study. Our sediment samples showed a less diverse polymer distribution than our water samples, but the most common polymer types (EVA, PP and PET) were similar to those in water. With the exception of EVA, the detected polymer types were also most frequently observed in previous studies on MP in sediment (Yang et al., 2021). EVA, on the other hand, is very common for footwear and packaging material (Maiti et al., 2012; Sonia and Priya Dasan, 2013), was detected less frequently but nonetheless consistently in previous sediment MP studies (Fu and Wang, 2019; Ferreira et al., 2020).

Generally, the most prevalent polymer types in our samples were LDPE, PET, EVA, PP, nylon and PS (Table S7). Despite the use of saturated NaCl solution for the density separation of MP from residual non-polymeric solids, which has a lower density compared to other solutions (e.g. $ZnCl_2$), we found denser polymers such as PVC in sediment samples. Nevertheless, the recovery test performed with irregular PET particles for the extraction of MP in sediment samples showed that denser particles in our samples were underestimated (recovery rate was 48% for PET particles, Table S6). Indeed, the chi-square test resulted that both water and sediment samples contained a higher proportion of light-density (< 1.1 g cm^{-3}) polymer types. Thus, the number and occurrence of different denser polymers (of irregular shape) could be much higher (for PET by approx. 50%). Despite these limitations, the presented results indicate that the methodology used is capable of extracting and revealing the concentration of lighter polymers quite accurately, but also the contamination of heavier plastic polymers even if underestimated. The choice of not to correct the concentrations of polymers with a low recovery (e.g. PET) is consistent with a prudential approach in which underestimations are preferred to possible overestimations.

4.2. MPs in biotic matrices

Together with MP evaluation in abiotic matrices, MP detection in biota is an essential for assessing MP bioavailability which relates to MP intake, exposure and potential adverse effects. The effects of MP exposure on aquatic organisms are inconsistent across studies, which challenges the evaluation of the overall potential impact of MP pollution. The meta-analysis of published literature by Foley et al. (2018) detected only a few generalizable trends consistent across taxonomic grouping or shape of plastic, with a reduction in consumption being the most consistent negative effect. The strongest effects were observed on lower trophic level organisms. In this study, MP particles were identified at every site in fish and macroinvertebrates. MP amounts per individual found in both fish GIT and macroinvertebrates were generally low and generally consistent with previous studies. MP occurrences of catfish reported in this study (1.40 ± 1.31 MP items $individual^{-1}$, Table 1) are similar to those reported for other species retrieved in the vicinity of our sampling area. The Eurasian perch (*Perca*

fluviatilis) from the Lake Maggiore, through which the Ticino River flows, had a mean MP content per individual of 1.73 ± 1.83 (Galafassi et al., 2021). The study followed a similar protocol but excluded fibres from the analysis, suggesting that detected concentrations might have been underestimated. An overview of MP concentration in freshwater fish samples from previous literature was performed by Galafassi et al. (2021) and Collard et al. (2019). Taking the summarised values reported therein and calculating an overall mean value for MP concentration per individual, we obtain a value of 3.03 ± 4.39 MP items individual^{-1} (ranges were excluded). Compared to this overall mean value (although it may be very restrictive and not representative), catfish of the Ticino River contained around half as many MPs, but fall within the range of other measured concentrations. The sampled catfish species, *Silurus glanis*, has only been subjected to MP analysis once before. The study by Garcia et al. (2021) found 0.23 ± 1.31 MP items individual^{-1} (n = 13) and thus reported lower values than the present study. Also the composition of MPs found in this research is comparable to that reported in previous studies. The most frequently detected polymer types in our catfish samples were PE (including LDPE), nylon, PET and PP, and were also prevalently present in fish from other studies on freshwater fish contamination (Wagner et al., 2019; Galafassi et al., 2021; Yuan et al., 2019; Cera et al., 2020). With the exception of nylon, PE and its branched version LDPE, PET and PP were also the predominant polymer type of surface water detected in this study and in many previous studies of MPs in freshwaters (Koelmans et al., 2019).

Research providing evidence of in-situ MP ingestion by riverine macroinvertebrates is still rare although being considered as suitable indicators for assessing MP pollution, both in the water column and in the benthic zone (Akindele et al., 2020). Pan et al. (2021) analysed the MP occurrence on 11 different invertebrate taxa sampled in the Dommel River in the Netherlands and demonstrated that the MP uptake of benthic invertebrates was taxon-specific. They found that the MP number concentration was higher in Tubificidae (Clitellata), Chironomidae (Insecta), and Asellidae (Malacostraca) compared to the remaining taxa. For example, Asellidae had the highest MP number concentration (19 MP items mg^{-1}), followed by Chironomidae (5.5 MP items mg^{-1}). In contrast, Gammaridae (Malacostraca) had very low levels of MP (0–0.034 MP items mg^{-1}). Hydropsychidae (our targeted insect family of the Insecta taxa) were not included in this study, however, our measured MP concentrations (0.03 ± 0.03 MP items mg^{-1}) lie within the lower range of MP levels in macroinvertebrates reported by Pan et al. (2021). MP ingestion by Hydropsychidae has been found only once before. Windsor et al. (2019) found 50% of all macroinvertebrates (Hydropsychidae, Beatidae, Heptageniidae) contaminated with MP and reported a maximum of 0.140 MP items per mg tissue (yet failing to report single mean data for solely hydropsychids), which is almost double of our measured maximum concentration (0.075 MP items mg^{-1}, Table S14). Nonetheless, the presence of MP in 61% of our macroinvertebrate samples is of concern considering the potential effects of a trophic transfer along the food web associated with MP, i.e. adhered pollutants (Huang et al., 2021) or additives leaching into the body (Wang et al., 2018). Macroinvertebrates were mainly affected by PET and PS, which was also frequent polymer type both in sampled sediment and water and was also observed by Cera et al. (2020) having reviewed 8 studies with macroinvertebrates.

Larval Hydropsychidae are categorised as filter-feeders/collectors (Ficsór and Csabai, 2021) feeding on algae, plant and animal detritus as well as on other organism such as early stages of other macroinvertebrates or zooplankton (Hilsenhoff, 2001). Scherer et al. (2017) found out that filter feeders appear to be specifically susceptible to MPs ingestion. The ingestion of MP by hydropsychids is of course subject to physical limits due to the size of the organism and the morphology of the mouthparts (Windsor et al., 2019). The largest MP recorded was a fibre with a length of 945 μm, but it is known that even fibres with a length of several millimetres can be easily ingested by small organisms such as the larvae of *Xenopus laevis* due to their very small diameter (Bacchetta et al., 2021). Although the size of ingested MP increased with decreasing size, our results suggest that Hydropsychidae larvae showed no selection preference for small MP (< 100 μm) or large MP (≥ 100 μm) over those in the sediment. MP can be taken up by hydropsychid larvae directly from the medium (collected or filtered with their catch nets), where they can be mistaken for the larvae's natural prey or accidently ingested during normal feeding behaviour, or indirectly via ingestion of contaminated prey. Although MPs are readily ingested by, for example, zooplankton (Botterell et al., 2019), the evidence of indirect ingestion of contaminated prey via filter feeding or collection is limited. Moreover, organisms potentially preyed by Hydropsychidae larvae are small and MP taken up by the prey hence even smaller, reducing the likelihood of being detected (detection limit of our visual identification and μ-FTIR analysis was around 20 μm). Once ingested by Hydropsychidae larvae, MP can have potential adverse effects related to the chemical nature of MP as mentioned above or the physical characteristics such as shape and size of particles leading to internal damages as observed for other freshwater species' larvae (Bacchetta et al., 2021) or blockage of the digestive tract (Kukkola et al., 2021). However, results of MP effects on freshwater organism vary greatly and often lack realistic environmental conditions.

Furthermore, the dominance of cellulose fibres found in macroinvertebrate samples raises questions about the relative risk that non-MP anthropogenic items pose for lower trophic level organisms. High quantities of textile fibres, including natural polymers such as wool and cotton, have been found in the environment before, but their impacts are unknown (Collard et al., 2019; Zhao et al., 2016; Barrows et al., 2018). It was assumed that natural fibres pose similar environmental concerns as synthetic fibres because both have been associated with chemicals, such as dyes, additives and substances adsorbed from the environment, which could be bioavailable and cause adverse health effects after being ingested by organisms (Zhao et al., 2016). The high amounts of cellulose fibres found in our environmental biota samples highlight the need to include natural fibres as a reference treatment in ecotoxicological studies.

The size distribution analysis highlighted that the number of reported MPs increased with decreasing size. The high number of detected MP items in surface water (n = 464, Table S9) forms a strong data basis for the performed size analysis. The results confirm that the use of small mesh size is indispensable for avoiding underestimations of the concentrations in the biologically relevant size class. Moreover, with 26.7% of the MPs being <100 μm found in macroinvertebrates and 8.4% in fish, we report MPs in a class of biological relevancy, although the most toxic and bioavailable class of MPs (< 10 μm) (Beiras and Schönemann, 2020), were not detectable with our methods. It is recorded that with decreasing size of MPs, the ecological risk to organisms increases (higher bioavailability, translocation and toxicity) (Beiras and Schönemann, 2020).

As observed for abiotic matrices (surface water and sediment), which were highly variable even at the same station and at the same time, the two biotic matrices (macroinvertebrates and fish GIT) showed even greater variability, ranging from no detection of MP to multiple items found even at the same location and time. Once more, these results strongly suggest that MP contamination is characterised by a large variability and underline that at least three samples should be taken from the same site to reduce it. It should be noted that in addition to this variability in sampling, a large temporal variability during the year can be expected, but this aspect has not been considered in the experimental design, which focused exclusively on multi-matrix sampling and large-scale spatial variability along the river. Analytical difficulties in analysing MP in biotic matrices are well known in the literature and should be taken into account when considering MP data. Nevertheless, these data are of great interest for the assessment of uptake and exposure to MP, even if the reliability of the data is currently low. For the same reason, an attempt can be made to determine the relationship between biotic and abiotic concentrations (see below in Section 4.3) without establishing an exact and reliable value, but with the aim of showing the main tendency and suggesting research for further confirmation. The present work is suitable for a direct comparison of MP concentration data in representative biotic and abiotic matrices of river ecosystems, as it provides spatially, temporally and methodologically comparable data.

4.3. Inter-matrix MP concentration correlations

The second objective of this work was to detect potential correlations between MP concentrations of abiotic and biotic samples. The parallel analysis of water and sediment samples from the same site, as performed in this study, could indicate whether MP ingested by biota reflects the environmental contamination, previously suggested by (Iannilli et al., 2019) for amphipods and by Nel et al. (2018) for chironomids. Also fish were suggested as biomarkers of environmental contamination after having found a higher abundance of MP in fish GIT when samples near urbanized areas (Silva-Cavalcanti et al., 2017). This is not the case for our data since we did not detect a significant correlation between biota (*S. glanis* and Hydropsychidae) and their environment (water and sediment). In our case, it should be taken into account that both water and sediment did not vary significantly between the six stations and thus there were no major differences in MP contamination levels. Without significant differences in contamination levels, the possibility to test the indicator potential of a species is only indirect (similar levels in biota vs. similar levels in abiotic matrices). In the case of macrobenthos and sediment, another reason for the lack of correlation could be that the family Hydropsychidae might not be an ideal indicator of sediment contamination, since they feed on particles in the near-bed water column (water-sediment interface) and not from the sediment itself (Maguire et al., 2020). Interestingly, previous studies have shown that the silk structures of populations of caddisfly larvea are arranged to maximize interception of flow, suggesting that changes to near-bed hydraulics induced by these insects, which have been demonstrated, may influence ecological processes such as food delivery rates (Maguire et al., 2020; Georgian and Wallace, 1981; Cardinale et al., 2002), and, thus, the filtering of MPs. Considering this aspect, the Hydropsychide family could be not the optimum as indicator of the sediment contamination but of the water sediment interface and they could maximize the MPs detection for their effective MP intake, as demonstrated by the high macroinvertebrate/sediment ratio (see below). Instead of Trichoptera, Nel et al. (2018) and Akindele et al. (2020) suggested Diptera, i.e. the deposit feeder *Chironomus* sp. as a suitable bioindicator for MP pollution of sediments, but in our case we were obliged to sacrifice the optimum indicator group for maximize the sample comparability, as explained in materials and methods section.

Having calculated the unit-consistent ratios to test the tendency of MP uptake by the biota in relation to their living medium (MP pollution in fish can be assigned to that in water and pollution in macroinvertebrates to that in sediment, Table S19), we observed that both macroinvertebrates and fish had a consistent higher amount of MPs than their respective medium (sediment and water), around three orders of magnitude more, strongly suggesting an efficient uptake pathway into organisms. The comparison between the two organisms is not easy due to differences in the analysed portion (the whole organism and the GIT for macroinvertebrates and fish, respectively). Nevertheless, these data demonstrated that benthic macroinvertebrates, being in same food chain as fish but in a lower trophic level, are highly exposed to MP contamination.

4.4. Environmental features affecting MP concentrations

The third objective of this study was to report changes of MP concentrations along the river course, with the assumption of an increasing concentration trend along the river due to the cumulative effect of the different MP inputs, i.e. such as those coming from WWTPs. Urbanisation is known to strongly correlate with MPs loads in surface waters (de Carvalho et al., 2021). Increasing urbanisation implies an increasing number of sizes of WWTPs, which are still classified as the major input source of MP to the aquatic environment, although these systems can eliminate more than 84% of MPs from the water (Magni et al., 2019; Gies et al., 2018). The present study highlights the potential contamination role of WWTP effluents along the river because MP loads at each station calculated from measured MP concentrations of river surface water are correlated with the estimated load of MPs from WWTPs (see S2.5, Fig. S5 for details). Yet, these do not significantly increase with the river's length, although potential MP sources, such as WWTP effluents, are distributed along the whole watercourse (Fig. 3A, Table S21) and, therefore, their loads should cumulate along the river. The absence of this evidence suggests a strong role of MP retention by the hydrological network of the river, which is able to protect the downstream water bodies, but raising concern about the MP accumulation in the riverine environment over a period of time. While some studies reported that the concentration of MPs in surface water increased with the increasing length of the river (Stanton et al., 2020), this study cannot support these findings. Since station S4 had the highest MP concentration for both water and macroinvertebrate samples, we can locate a strong input source between S3 and S4, probably carrying the MPs from urban and agricultural runoff as well as from WWTP effluents (Fig. 3A, Table S22). The reasons why we could not observe a continuous increase of MP concentrations in the course of the river are manifold. Firstly, the hydrological conditions in the Ticino vary greatly. Accumulation zones in the sediment due to low flow velocity, such as upstream of the dam at station S1, could explain the increased concentration in sediment samples due to the sinking of particles. Secondly, temporal differences, which can lead to significant variations in freshwater MP concentrations (Stanton et al., 2020), were not investigated in this study. Nevertheless, they should not be neglected, as particles can be resuspended from the sediment into the water after rain falls with subsequent higher flow velocities. The conditions of our sampling (intermediate state of the river, far from typical flood or drought periods) represent the typical hydrological condition of the river and thus the most representative state in term of MP contamination. Our data can therefore be considered sufficiently representative of the general condition of the river, and by this, they allow to extrapolate general conclusions, even if more detailed seasonal analyses are obviously suggested. Our sampling was a snapshot and not a continuum, so we cannot exhaustively explain the complex MP behaviour in the Ticino River environment. Further research specifically addressed to temporal variability may support the presented data, furnishing further confirmations and more precise estimations.

Data of this work indicated that, generally, when concentrations in surface water were high, those in sediment were low and the opposite. This seems to be contradictory considering the principle of the partition equilibrium between water and sediment (high concentration in water will give high concentration in sediment) such as for traditional contaminants, but it is not if we consider the particulate nature of MPs and therefore deposition and transport phenomena governed by flow velocity and flow amount as generally described by the Hjulström curve (Worrall et al., 2018). MPs are physical entities which are expected to respond to physical river dynamics, such as those governed by the flow velocity and the flood erosion potential. For example, high velocity would favour resuspension and transport of MPs and thus higher concentration in surface water, while low velocity would favour deposition and retention phenomena in sediment. According to this, a significant relationship was found between MP concentrations in water and the flow velocity in each sampling site. This is consistent with the Hjulström curve and with the particulate nature of MPs and supports the high spatial heterogeneity of the MPs contamination in relation to the four-dimensional gradient of the flow velocity in the river. This hypothesis should be tested by more experimental data but seems to be supported by data of this work and theoretically robust.

Another aspect related to the physical behaviour of MPs in water is linked to the different size and density of the different polymers. By physical laws, heavier polymer and bigger particles should be preferentially retained in the sediments, while lighter and smaller particles are preferentially transported within the water compartment and have more chances to upwell to surface waters. We tested the heavier/lighter polymer ratio and the smaller/larger particle one between surface water and sediment compartments, considering polymers with a density < 1.1 g cm^{-3} as lighter polymers and ≥ 1.1 g cm^{-3} as heavier ones and < 500 μm and ≥ 500 μm as the smaller and larger particles. Interestingly, the chi-square test revealed that both matrices contained larger proportions of lighter polymers, thus, no differences between water and sediment samples regarding the density. This may be due to a generally higher load of lighter polymers in

the river or due to the higher mobility of the lighter polymers, which preferentially enter the main stream of the river from their sources (e.g. WWTP effluents). Although we cannot further test and discuss the two hypotheses, it is interesting to report this result. Moreover, sediment contained a higher proportion of smaller particles compared to water. However, the proportion of fibres in the water samples was in general significantly higher than in the sediment samples. This difference was compensated by the higher proportion of irregular particles in the sediment samples compared to the water samples. This distribution was observed also by previous studies (Watkins et al., 2019). For this observation, it is also important to mention the relationship between surface size of MP particles, biofilm growth and sedimentation rate. Existing studies have already found that biofouling increases MP deposition (Kalčíková and Bundschuh, 2021; Miao et al., 2021; Kaiser et al., 2017). The formation of a biofilm is enhanced by a larger relative surface area and surface roughness (Van Melkebeke et al., 2020; Rummel et al., 2017). This would explain both the observation of increased amounts of irregular and smaller particles in the sediment compared to the surface water. However, the phenomenon of biofilm as a driver of MP behaviour in the resuspension/settling dynamics is complex and research at best limited (Kalčíková and Bundschuh, 2021).

4.5. MP fluxes along the river

Data of this work and from the literature (Hoellein et al., 2019) suggest that MPs are subject to a deposition and resuspension cycles as they travel along the river, depending on their properties (e.g. size, density, biofilm) and on environmental conditions such as flow velocity and flood events. Rivers can thus act both as conduits and accumulators of MPs. Our data (sediments were 750 times more contaminated than surface water, Table S19) and previous studies finding higher abundance of MP in benthic sediments compared to the water column suggest that sediments can be a sink for MPs (Hoellein et al., 2017, 2019; Nel et al., 2018). We experimentally found the absence of an increasing concentration trend along the river and a direct relationship between the concentration in water and flow velocity. Moreover, MPs concentrations in water were mainly opposed to those in sediment. While the MP size distribution in water samples showed little variance along the river, the one in sediment samples varied stronger (Fig. S2): the highest abundance of small-sized MPs in sediment samples were found at the station where MP concentration in sediment were highest and lowest in water samples (station S1, Fig. 3 B + C). All these findings are consistent with the assumed deposition and resuspension cycles between water and sediment, which would lead to a high spatial and temporal heterogeneity expected in the hydrological network of the river. In the riverside plains, many lentic ecosystems such as oxbow lakes and ponds may act as predominant retention areas, while the mainstream of the river (mostly lotic conditions) may act as prevailing transport pathway. As MPs are highly persistent to degradation, they can be temporally retained in the sediment or in the riverside banks, especially during droughts, while during flood events they are remobilized and efficiently transported downstream following the sediment transport.

Finally, considering the mean MP concentration found in water at the confluence with the Po River, a yearly load of $3.40 \times 10^{11} \pm 1.1 \times 10^{11}$ MPs from the Ticino River can be obtained. Even if the calculated load of the Ticino River into the Po River is only an estimation, this data element is essential for understanding the overall MPs contamination of the freshwater environments in relation to the final receptor. However, the data suggest that the whole hydrological network is likely to be involved in the possible retention of MPs and so is the river itself.

5. Conclusions

This work is a comprehensive study of the MP contamination of a freshwater ecosystem, reporting for the first time the incidence of MP in all four abiotic and biotic simultaneously sampled matrices for direct comparison. Having identified 582 MPs in total under the same conditions, the present data have a strong basis for all analyses and calculations. MP concentration in sediments were on average 750-fold higher than in surface water, and both benthic macroinvertebrates (Hydropsychidae larvae) and fish (*S. glanis*) had a consistent higher amount of MPs than their respective medium (sediment and water), strongly suggesting an efficient uptake pathway into organisms. Finding 61% of macroinvertebrates samples to contain MP indicates a potential trophic transfer of MPs along the food web and a threat to food chain since these insects are lower trophic level organisms. However, MP ingestion by the sampled biota did not strictly reflect the environment (absence of correlation of concentration in the biota to that in water and sediment).

We show that the MP contaminations of the water surface varied across space and correlated with the flow velocity and the presence of WWTPs (estimated loads). All MP concentrations of the analysed matrices, do not show an increasing trend with the length of the river, contrary to what is suggested by other work from the literature and the principle of the cumulative effect of the loads along the river. This observation indicates a strong role of the pronounced hydrological network of the Ticino River and the hydrodynamic conditions leading to deposition, retention and resuspension, which is supported by the findings that MP concentrations were mostly opposing for water and sediment samples. In addition, the observed differences in MP from sediment and water samples in regard to size and shape indicate a considerable influence of other environmental factors such as e.g. biofouling in driving the environmental fate of MPs. By comparison with work from other literature, we may conclude that the Ticino River is moderately polluted despite the fairly well preserved naturalness of the habitats. Riverine ecosystems may act as an effective retention system preserving downstream water bodies, but are potentially able of releasing their MP load during floods as well as accumulating them in lateral lentic ecosystem potentially threatening their fauna.

CRediT authorship contribution statement

Anna Winkler: Conceptualization, Methodology, Data curation, Formal analysis, Visualization, Writing – original draft. **Diego Antonioli:** Investigation. **Andrea Masseroni:** Formal analysis, Investigation. **Riccardo Chiarcos:** Investigation. **Michele Laus:** Resources. **Paolo Tremolada:** Supervision, Resources, Validation, Writing – review & editing.

Declaration of competing interest

The authors declare that they have no known competing financial interests or personal relationships that could have appeared to influence the work reported in this paper.

Acknowledgements

We would like to thank Andrea Casoni and Mauro Bardazzi from GRAIA srl for providing us with catfish caught via electrofishing, and Stefano Camazzola and Stefano Gazzotti from the Department of Chemistry of the University Milan for providing us with cryo-milled polymer particles. We thank Sigrid Algosaibi and Udo Krupka for proofreading the manuscript. After the third revision, improved by constructive criticism, we are very grateful to all six reviewers for their substantial contribution to the present manuscript.

Funding

This research did not receive any specific grant from funding agencies in the public, commercial, or not-for-profit sectors.

Appendix A. Supplementary data

Supplementary data to this article can be found online at https://doi.org/10.1016/j.scitotenv.2022.153638.

References

Akindele, E.O., Ehlers, S.M., Koop, J.H.E., 2020. Freshwater insects of different feeding guilds ingest microplastics in two gulf of Guinea tributaries in Nigeria. Environ. Sci. Pollut. Res. 27, 33373–33379. https://doi.org/10.1007/s11356-020-08763-8.

ARPA Lombardy, 2021. Agenzia Regionale per la Protezione dell'Ambiente Lombardia, Portale Idrologico Geografico. https://idro.arpalombardia.it/ last access: 26 August.

Bacchetta, R., Winkler, A., Santo, N., Tremolada, P., 2021. The toxicity of polyester fibers in xenopuslaevis. Water 13, 3446. https://doi.org/10.3390/w13233446.

Barrows, A.P.W., Cathey, S.E., Petersen, C.W., 2018. Marine environment microfiber contamination: global patterns and the diversity of microparticle origins. Environ. Pollut. 237, 275–284. https://doi.org/10.1016/j.envpol.2018.02.062.

Beiras, R., Schönemann, A.M., 2020. Currently monitored microplastics pose negligible ecological risk to the global ocean. Sci. Rep. 10, 22281. https://doi.org/10.1038/s41598-020-79304-z.

Botterell, Z.L.R., Beaumont, N., Dorrington, T., Steinke, M., Thompson, R.C., Lindeque, P.K., 2019. Bioavailability and effects of microplastics on marine zooplankton: a review. Environ. Pollut. 245, 98–110. https://doi.org/10.1016/j.envpol.2018.10.065.

Campanale, C., Stock, F., Massarelli, C., Kochleus, C., Bagnuolo, G., Reifferscheid, G., Uricchio, V.F., 2019. Microplastics and their possible sources: the example of ofanto river in Southeast Italy. Environ. Pollut. 113284. https://doi.org/10.1016/j.envpol.2019.113284.

Cardinale, B.J., Palmer, M.A., Collins, S.L., 2002. Species diversity enhances ecosystem functioning through interspecific facilitation. Nature 415, 426–429. https://doi.org/10.1038/415426a.

de Carvalho, A.R., Garcia, F., Riem-Galliano, L., Tudesque, L., Albignac, M., ter Halle, A., Cucherousset, J., 2021. Urbanization and hydrological conditions drive the spatial and temporal variability of microplastic pollution in the Garonne River. Sci. Total Environ. 769, 144479. https://doi.org/10.1016/j.scitotenv.2020.144479.

Cera, A., Cesarini, G., Scalici, M., 2020. Microplastics in freshwater: what is the news from the world? Diversity 12, 276. https://doi.org/10.3390/d12070276.

Chessman, B.C., 1995. Rapid assessment of rivers using macroinvertebrates: a procedure based on habitat-specific sampling, family level identification and a biotic index. Austral Ecol. 20, 122–129. https://doi.org/10.1111/j.1442-9993.1995.tb00526.x.

Collard, F., Gasperi, J., Gabrielsen, G.W., Tassin, B., 2019. Plastic particle ingestion by wild freshwater fish: a critical review. Environ. Sci. Technol. 53, 12974–12988. https://doi.org/10.1021/acs.est.9b03083.

Constant, M., Ludwig, W., Kerhervé, P., Sola, J., Charrière, B., Sanchez-Vidal, A., Canals, M., Heussner, S., 2020. Microplastic fluxes in a large and a small Mediterranean river catchments: the Têt and the Rhône, northwestern Mediterranean Sea. Sci. Total Environ. 716, 136984. https://doi.org/10.1016/j.scitotenv.2020.136984.

Cushing, C.E., Cummins, K.W., Minshall, G.W., 2006. River and Stream Ecosystems of the World. 1st pbk. ed. University of California Press, Berkeley. 817 pp.

Dris, R., Gasperi, J., Saad, M., Mirande, C., Tassin, B., 2016. Synthetic fibers in atmospheric fallout: a source of microplastics in the environment? Mar. Pollut. Bull. 104, 290–293. https://doi.org/10.1016/j.marpolbul.2016.01.006.

Dris, R., Gasperi, J., Tassin, B., 2018a. Sources and fate of microplastics in urban areas: a focus on paris megacity. In: Wagner, M., Lambert, S. (Eds.), Freshwater Microplastics. vol. 58. Springer International Publishing, Cham, pp. 69–83. https://doi.org/10.1007/978-3-319-61615-5_4.

Dris, R., Gasperi, J., Rocher, V., Tassin, B., 2018b. Synthetic and non-synthetic anthropogenic fibers in a river under the impact of Paris megacity: sampling methodological aspects and flux estimations. Sci. Total Environ. 618, 157–164. https://doi.org/10.1016/j.scitotenv.2017.11.009.

European Commission, 2021. Current Status of the Quantification of Microplastics in Water : Results of a JRC/BAM Interlaboratory Comparison Study on PET in Water. Publications Office, LU.

Ferreira, M., Thompson, J., Paris, A., Rohindra, D., Rico, C., 2020. Presence of microplastics in water, sediments and fish species in an urban coastal environment of Fiji, a Pacific small island developing state. Mar. Pollut. Bull. 153, 110991. https://doi.org/10.1016/j.marpolbul.2020.110991.

Ficsór, M., Csabai, Z., 2021. Longitudinal zonation of larval hydropsyche (Trichoptera: Hydropsychidae): abiotic environmental factors and biotic interactions behind the downstream sequence of central european species. Hydrobiologia 848, 3371–3388. https://doi.org/10.1007/s10750-021-04602-0.

Foley, C.J., Feiner, Z.S., Malinich, T.D., Höök, T.O., 2018. A meta-analysis of the effects of exposure to microplastics on fish and aquatic invertebrates. Sci. Total Environ. 631–632, 550–559. https://doi.org/10.1016/j.scitotenv.2018.03.046.

Fu, Z., Wang, J., 2019. Current practices and future perspectives of microplastic pollution in freshwater ecosystems in China. Sci. Total Environ. 691, 697–712. https://doi.org/10.1016/j.scitotenv.2019.07.167.

Galafassi, S., Sighicelli, M., Pusceddu, A., Bettinetti, R., Cau, A., Temperini, M.E., Gillibert, R., Ortolani, M., Pietrelli, L., Zaupa, S., Volta, P., 2021. Microplastic pollution in perch (Perca fluviatilis, linnaeus 1758) from italian south-alpine lakes. Environ. Pollut. 288, 117782. https://doi.org/10.1016/j.envpol.2021.117782.

Garcia, F., de Carvalho, A.R., Riem-Galliano, L., Tudesque, L., Albignac, M., ter Halle, A., Cucherousset, J., 2021. Stable isotope insights into microplastic contamination within freshwater food webs. Environ. Sci. Technol. 55, 1024–1035. https://doi.org/10.1021/acs.est.0c06221.

Georgian, T.J., Wallace, J.B., 1981. A model of seston capture by net-spinning caddisflies. Oikos 36, 147–157. https://doi.org/10.2307/3544439.

Gies, E.A., LeNoble, J.L., Noël, M., Etemadifar, A., Bishay, F., Hall, E.R., Ross, P.S., 2018. Retention of microplastics in a major secondary wastewater treatment plant in Vancouver, Canada. Mar. Pollut. Bull. 133, 553–561. https://doi.org/10.1016/j.marpolbul.2018.06.006.

Guerranti, C., Cannas, S., Scopetani, C., Fastelli, P., Cincinelli, A., Renzi, M., 2017. Plastic litter in aquatic environments of maremma Regional Park (Tyrrhenian Sea, Italy): contribution by the ombrone river and levels in marine sediments. Mar. Pollut. Bull. 117, 366–370. https://doi.org/10.1016/j.marpolbul.2017.02.021.

Hermsen, E., Mintenig, S.M., Besseling, E., Koelmans, A.A., 2018. Quality criteria for the analysis of microplastic in biota samples: a critical review. Environ. Sci. Technol. 52, 10230–10240. https://doi.org/10.1021/acs.est.8b01611.

Hilsenhoff, W.L., 2001. Diversity and classification of insects and collembola. Much of the material on Collembola was contributed by Barbara L. Peckarsky, Department of Entomology, Cornell University. The author and editors greatly appreciate her generous contribution of this material. In: Thorp, J.H., Covich, A.P. (Eds.), Ecology and Classification of North American Freshwater Invertebrates, Second edition Academic Press, San Diego, pp. 661–731 https://doi.org/10.1016/B978-012690647-9/50018-1.

Hoellein, T.J., McCormick, A.R., Hittie, J., London, M.G., Scott, J.W., Kelly, J.J., 2017. Longitudinal patterns of microplastic concentration and bacterial assemblages in surface and benthic habitats of an urban river. Freshw. Sci. 36, 491–507. https://doi.org/10.1086/693012.

Hoellein, T.J., Shogren, A.J., Tank, J.L., Risteca, P., Kelly, J.J., 2019. Microplastic deposition velocity in streams follows patterns for naturally occurring allochthonous particles. Sci. Rep. 9, 3740. https://doi.org/10.1038/s41598-019-40126-3.

Horton, A.A., Dixon, S.J., 2018. Microplastics: an introduction to environmental transport processes. WIREs Water 5, e1268. https://doi.org/10.1002/wat2.1268.

Horton, A.A., Svendsen, C., Williams, R.J., Spurgeon, D.J., Lahive, E., 2017. Large microplastic particles in sediments of tributaries of the river Thames, UK – abundance, sources and methods for effective quantification. Mar. Pollut. Bull. 114, 218–226. https://doi.org/10.1016/j.marpolbul.2016.09.004.

Huang, W., Song, B., Liang, J., Niu, Q., Zeng, G., Shen, M., Deng, J., Luo, Y., Wen, X., Zhang, Y., 2021. Microplastics and associated contaminants in the aquatic environment: a review on their ecotoxicological effects, trophic transfer, and potential impacts to human health. J. Hazard. Mater. 405, 124187. https://doi.org/10.1016/j.jhazmat.2020.124187.

Iannilli, V., Pasquali, V., Setini, A., Corami, F., 2019. First evidence of microplastics ingestion in benthic amphipods from Svalbard. Environ. Res. 179, 108811. https://doi.org/10.1016/j.envres.2019.108811.

Kaiser, D., Kowalski, N., Waniek, J.J., 2017. Effects of biofouling on the sinking behavior of microplastics. Environ. Res. Lett. 12, 124003. https://doi.org/10.1088/1748-9326/aa8e8b.

Kalčíková, G., Bundschuh, M., 2021. Aquatic biofilms—sink or source of microplastics? A critical reflection on current knowledge. Environ. Toxicol. Chem. https://doi.org/10.1002/etc.5195.

Karlsson, T.M., Vethaak, A.D., Almroth, B.C., Ariese, F., van Velzen, M., Hassellöv, M., Leslie, H.A., 2017. Screening for microplastics in sediment, water, marine invertebrates and fish: method development and microplastic accumulation. Mar. Pollut. Bull. 122, 403–408. https://doi.org/10.1016/j.marpolbul.2017.06.081.

Klein, S., Worch, E., Knepper, T.P., 2015. Occurrence and spatial distribution of microplastics in river shore sediments of the Rhine-Main area in Germany. Environ. Sci. Technol. 49, 6070–6076. https://doi.org/10.1021/acs.est.5b00492.

Koelmans, A.A., Mohamed Nor, N.H., Hermsen, E., Kooi, M., Mintenig, S.M., De France, J., 2019. Microplastics in freshwaters and drinking water: critical review and assessment of data quality. Water Res. 155, 410–422. https://doi.org/10.1016/j.watres.2019.02.054.

Kukkola, A., Krause, S., Lynch, I., Sambrook Smith, G.H., Nel, H., 2021. Nano and microplastic interactions with freshwater biota – current knowledge, challenges and future solutions. Environ. Int. 152, 106504. https://doi.org/10.1016/j.envint.2021.106504.

Kumar, R., Sharma, P., Manna, C., Jain, M., 2021. Abundance, interaction, ingestion, ecological concerns, and mitigation policies of microplastic pollution in riverine ecosystem: a review. Sci. Total Environ. 782, 146695. https://doi.org/10.1016/j.scitotenv.2021.146695.

Lin, L., Zuo, L.-Z., Peng, J.-P., Cai, L.-Q., Fok, L., Yan, Y., Li, H.-X., Xu, X.-R., 2018. Occurrence and distribution of microplastics in an urban river: a case study in the Pearl River along Guangzhou City, China. Sci. Total Environ. 644, 375–381. https://doi.org/10.1016/j.scitotenv.2018.06.327.

Magni, S., Binelli, A., Pittura, L., Avio, C.G., Della Torre, C., Parenti, C.C., Gorbi, S., Regoli, F., 2019. The fate of microplastics in an italian wastewater treatment plant. Sci. Total Environ. 652, 602–610. https://doi.org/10.1016/j.scitotenv.2018.10.269.

Maguire, Z., Tumolo, B.B., Albertson, L.K., 2020. Retreat but no surrender: net-spinning caddisfly (Hydropsychidae) silk has enduring effects on stream channel hydraulics. Hydrobiologia 847, 1539–1551. https://doi.org/10.1007/s10750-020-04210-4.

Maiti, M., Jasra, R.V., Kusum, S.K., Chaki, T.K., 2012. Microcellular foam from ethylene vinyl Acetate/Polybutadiene rubber (EVA/BR) based thermoplastic elastomers for footwear applications. Ind. Eng. Chem. Res. 51, 10607–10612. https://doi.org/10.1021/ie300396m.

Mani, T., Hauk, A., Walter, U., Burkhardt-Holm, P., 2016. Microplastics profile along the Rhine River. Sci. Rep. 5. https://doi.org/10.1038/srep17988.

Masura, J., Baker, J.E., 2015. 1959-, Foster, G. D. (Gregory D., Arthur, C., and Herring, C.: Laboratory Methods for the Analysis of Microplastics in the Marine Environment : Recommendations for Quantifying Synthetic Particles in Waters and Sediments.

Miao, L., Gao, Y., Adyel, T.M., Huo, Z., Liu, Z., Wu, J., Hou, J., 2021. Effects of biofilm colonization on the sinking of microplastics in three freshwater environments. J. Hazard. Mater. 413, 125370. https://doi.org/10.1016/j.jhazmat.2021.125370.

Mintenig, S.M., Kooi, M., Erich, M.W., Primpke, S., Redondo- Hasselerharm, P.E., Dekker, S.C., Koelmans, A.A., van Wezel, A.P., 2020. A systems approach to understand microplastic occurrence and variability in dutch riverine surface waters. Water Res. 176, 115723. https://doi.org/10.1016/j.watres.2020.115723.

Nel, H.A., Dalu, T., Wasserman, R.J., 2018. Sinks and sources: assessing microplastic abundance in river sediment and deposit feeders in an austral temperate urban river system. Sci. Total Environ. 612, 950–956. https://doi.org/10.1016/j.scitotenv.2017.08.298.

Nizzetto, L., Bussi, G., Futter, M.N., Butterfield, D., Whitehead, P.G., 2016. A theoretical assessment of microplastic transport in river catchments and their retention by soils and river sediments. Environ Sci Process Impacts 18, 1050–1059. https://doi.org/10.1039/C6EM00206D.

Pan, C.-G., Mintenig, S.M., Redondo-Hasselerharm, P.E., Neijenhuis, P.H.M.W., Yu, K.-F., Wang, Y.-H., Koelmans, A.A., 2021. Automated μFTIR imaging demonstrates taxon-specific and selective uptake of microplastic by freshwater invertebrates. Environ. Sci. Technol. 55, 9916–9925. https://doi.org/10.1021/acs.est.1c03119.

Peng, G., Xu, P., Zhu, B., Bai, M., Li, D., 2018. Microplastics in freshwater river sediments in Shanghai, China: a case study of risk assessment in mega-cities. Environ. Pollut. 234, 448–456. https://doi.org/10.1016/j.envpol.2017.11.034.

Pfeiffer, F., Fischer, E.K., 2020. Various digestion protocols within microplastic sample processing—evaluating the resistance of different synthetic polymers and the efficiency of biogenic organic matter destruction. Front. Environ. Sci. 8, 263. https://doi.org/10.3389/fenvs.2020.572424.

Phuong, N.N., Poirier, L., Lagarde, F., Kamari, A., Zalouk-Vergnoux, A., 2018. Microplastic abundance and characteristics in french Atlantic coastal sediments using a new extraction method. Environ. Pollut. 243, 228–237. https://doi.org/10.1016/j.envpol.2018.08.032.

Roch, S., Walter, T., Ittner, L.D., Friedrich, C., Brinker, A., 2019. A systematic study of the microplastic burden in freshwater fishes of South-Western Germany - are we searching at the right scale? Sci. Total Environ. 689, 1001–1011. https://doi.org/10.1016/j.scitotenv.2019.06.404.

Rodrigues, M.O., Abrantes, N., Gonçalves, F.J.M., Nogueira, H., Marques, J.C., Gonçalves, A.M.M., 2018. Spatial and temporal distribution of microplastics in water and sediments of a freshwater system (Antuã River, Portugal). Sci. Total Environ. 633, 1549–1559. https://doi.org/10.1016/j.scitotenv.2018.03.233.

Rummel, C.D., Jahnke, A., Gorokhova, E., Kühnel, D., Schmitt-Jansen, M., 2017. Impacts of biofilm formation on the fate and potential effects of microplastic in the aquatic environment. Environ. Sci. Technol. Lett. 4, 258–267. https://doi.org/10.1021/acs.estlett.7b00164.

Scherer, C., Brennholt, N., Reifferscheid, G., Wagner, M., 2017. Feeding type and development drive the ingestion of microplastics by freshwater invertebrates. Sci. Rep. 7, 17006. https://doi.org/10.1038/s41598-017-17191-7.

Schmidt, C., Kumar, R., Yang, S., Büttner, O., 2020. Microplastic particle emission from wastewater treatment plant effluents into river networks in Germany: loads, spatial patterns of concentrations and potential toxicity. Sci. Total Environ. 737, 139544. https://doi.org/10.1016/j.scitotenv.2020.139544.

Sfriso, A.A., Tomio, Y., Rosso, B., Gambaro, A., Sfriso, A., Corami, F., Rastelli, E., Corinaldesi, C., Mistri, M., Munari, C., 2020. Microplastic accumulation in benthic invertebrates in Terra Nova Bay (Ross Sea, Antarctica). Environ. Int. 137, 105587. https://doi.org/10.1016/j.envint.2020.105587.

Silva-Cavalcanti, J.S., Silva, J.D.B., de França, E.J., de Araújo, M.C.B., Gusmão, F., 2017. Microplastics ingestion by a common tropical freshwater fishing resource. Environ. Pollut. 221, 218–226. https://doi.org/10.1016/j.envpol.2016.11.068.

Simon-Sánchez, L., Grelaud, M., Garcia-Orellana, J., Ziveri, P., 2019. River deltas as hotspots of microplastic accumulation: the case study of the Ebro River (NW Mediterranean). Sci. Total Environ. 687, 1186–1196. https://doi.org/10.1016/j.scitotenv.2019.06.168.

Smiroldo, G., Balestrieri, A., Pini, E., Tremolada, P., 2019. Anthropogenically altered trophic webs: alien catfish and microplastics in the diet of eurasian otters. Mammal Res. 64, 165–174. https://doi.org/10.1007/s13364-018-00412-3.

Sonia, A., Priya Dasan, K., 2013. Celluloses microfibers (CMF)/poly (ethylene-co-vinyl acetate) (EVA) composites for food packaging applications: a study based on barrier and biodegradation behavior. J. Food Eng. 118, 78–89. https://doi.org/10.1016/j.jfoodeng.2013.03.020.

Stanton, T., Johnson, M., Nathanail, P., MacNaughtan, W., Gomes, R.L., 2020. Freshwater microplastic concentrations vary through both space and time. Environ. Pollut. 263, 114481. https://doi.org/10.1016/j.envpol.2020.114481.

del Ticino, Parco, 2021. Life Ticino Biosource – Incrementiamo la Biodiversità Attraverso il Progetto Life del Parco del Ticino, LIFE15 NAT/IT/0000989. http://ticinobiosource.it/en/home-eng/. last access: 26 August.

Van Melkebeke, M., Janssen, C., De Meester, S., 2020. Characteristics and sinking behavior of typical microplastics including the potential effect of biofouling: implications for remediation. Environ. Sci. Technol. 54, 8668–8680. https://doi.org/10.1021/acs.est.9b07378.

Wagner, J., Wang, Z.-M., Ghosal, S., Murphy, M., Wall, S., Cook, A.-M., Robberson, W., Allen, H., 2019. Nondestructive extraction and identification of microplastics from freshwater sport fish stomachs. Environ. Sci. Technol. 53, 14496–14506. https://doi.org/10.1021/acs.est.9b05072.

Wang, J., Peng, J., Tan, Z., Gao, Y., Zhan, Z., Chen, Q., Cai, L., 2017. Microplastics in the surface sediments from the Beijiang River littoral zone: composition, abundance, surface textures and interaction with heavy metals. Chemosphere 171, 248–258. https://doi.org/10.1016/j.chemosphere.2016.12.074.

Wang, F., Wang, F., Zeng, E.Y., 2018. Chapter 7 - sorption of toxic chemicals on microplastics. In: Zeng, E.Y. (Ed.), Microplastic Contamination in Aquatic Environments. Elsevier, pp. 225–247. https://doi.org/10.1016/B978-0-12-813747-5.00007-2.

Wang, S., Zhang, C., Pan, Z., Sun, D., Zhou, A., Xie, S., Wang, J., Zou, J., 2020. Microplastics in wild freshwater fish of different feeding habits from beijiang and Pearl River Delta regions, South China. Chemosphere 258, 127345. https://doi.org/10.1016/j.chemosphere.2020.127345.

Watkins, L., McGrattan, S., Sullivan, P.J., Walter, M.T., 2019. The effect of dams on river transport of microplastic pollution. Sci. Total Environ. 664, 834–840. https://doi.org/10.1016/j.scitotenv.2019.02.028.

Wen, X., Du, C., Xu, P., Zeng, G., Huang, D., Yin, L., Yin, Q., Hu, L., Wan, J., Zhang, J., Tan, S., Deng, R., 2018. Microplastic pollution in surface sediments of urban water areas in Changsha, China: abundance, composition, surface textures. Mar. Pollut. Bull. 136, 414–423. https://doi.org/10.1016/j.marpolbul.2018.09.043.

Windsor, F.M., Tilley, R.M., Tyler, C.R., Ormerod, S.J., 2019. Microplastic ingestion by riverine macroinvertebrates. Sci. Total Environ. 646, 68–74. https://doi.org/10.1016/j.scitotenv.2018.07.271.

Winkler, A., Nessi, A., Antonioli, D., Laus, M., Santo, N., Parolini, M., Tremolada, P., 2020. Occurrence of microplastics in pellets from the common kingfisher (Alcedo atthis) along the Ticino River, North Italy. Environ. Sci. Pollut. Res. 27, 41731–41739. https://doi.org/10.1007/s11356-020-10163-x.

Worrall, F., Burt, T.P., Howden, N.J.K., Hancock, G.R., Wainwright, J., 2018. The fate of suspended sediment and particulate organic carbon in transit through the channels of a river catchment. Hydrol. Process. 32, 146–159. https://doi.org/10.1002/hyp.11413.

Xia, W., Rao, Q., Deng, X., Chen, J., Xie, P., 2020. Rainfall is a significant environmental factor of microplastic pollution in inland waters. Sci. Total Environ. 732, 139065. https://doi.org/10.1016/j.scitotenv.2020.139065.

Xu, X., Wong, C.Y., Tam, N.F.Y., Lo, H.-S., Cheung, S.-G., 2020. Microplastics in invertebrates on soft shores in Hong Kong: influence of habitat, taxa and feeding mode. Sci. Total Environ. 715, 136999. https://doi.org/10.1016/j.scitotenv.2020.136999.

Yang, L., Zhang, Y., Kang, S., Wang, Z., Wu, C., 2021. Microplastics in freshwater sediment: a review on methods, occurrence, and sources. Sci. Total Environ. 754, 141948. https://doi.org/10.1016/j.scitotenv.2020.141948.

Yuan, W., Liu, X., Wang, W., Di, M., Wang, J., 2019. Microplastic abundance, distribution and composition in water, sediments, and wild fish from poyang Lake, China. Ecotoxicol. Environ. Saf. 170, 180–187. https://doi.org/10.1016/j.ecoenv.2018.11.126.

Zhao, S., Zhu, L., Li, D., 2016. Microscopic anthropogenic litter in terrestrial birds from Shanghai, China: not only plastics but also natural fibers. Sci. Total Environ. 550, 1110–1115. https://doi.org/10.1016/j.scitotenv.2016.01.112.

Supporting Information

"Following the fate of microplastic in four abiotic and biotic matrices along the Ticino River (North Italy)"

Data tables: Table S1 – S22

Graphics: Figure S1 – S5

S1 Supplementary Materials and methods

S1.1 Background information on collected samples

Table S1. Measured flow velocity of the sampling stations.

Sampling station	Sampled water volume [m^3]	Flow velocity [$m\ s^{-1}$]
S1	7.14	0.29
S2	13.06	0.53
S3	9.59	0.39
S4	12.852	0.53
S5	9.18	0.38
S6	13.464	0.55
Mean (± SD)	10.88 (± 2.60)	0.44 (± 0.11)

Table S2. Mean grain size ratio, dry weight (dw), volume and density of sediment samples per station.

Sampling station	Fraction of grain size [%]			Mean dw [kg]	Volume [mL]	Density [$g\ cm^{-3}$]
	< 2 mm	2 – 5 mm	> 5 mm			
S1	62.0	22.5	15.5	0.614	300	2.047
S2	51.9	27.3	20.5	0.707	300	2.358
S3	55.6	27.7	16.7	0.655	300	2.183
S4	52.8	28.4	18.9	0.572	300	1.908
S5	98.5	0.9	0.5	0.619	300	2.062
S6	99.7	0.3	0.1	0.638	300	2.127

Table S3. Mean and standard deviation of wet weight (ww) of GIT content from fish samples (catfish, *Silurus glanis*) per station.

Sampling station	Ww GIT content [g]	
	Mean	SD
S1	81.0	47.6
S2	36.7	22.9
S3	35.0	25.2
S4	29.0	13.9
S5	46.3	30.0
S6	48.0	49.7

S1.2 MP extraction

Environmental samples from different matrices require specific solutions and conditions to digest organic material (purification) chemically. An additional step is the separation of the plastic items from the matrix by density separation, where the MPs float in a high-density solution due to their properties. The order of application of these steps varied with the different matrices; while for water surface and fish samples, the purification step was performed before the density separation, for sediment samples, purification was applied after density separation owing to the main mineral composition and the large size of sediment samples. No density separation was performed on macroinvertebrate samples due to the small sample size.

Chemical digestion

Hydrogen peroxide with iron as catalyst ($H_2O_2 + Fe^{II}$) was verified as suitable reagent to digest plant material, while potassium hydroxide (KOH) was more appropriate for animal tissue (Prata et al., 2019). Thus, water surface samples, rich in organic matter (algae, plankton), and sediments were treated with 30% $H_2O_2 + Fe^{II}$ for 1 h at 50 °C and overnight at RT. The iron solution (0.05 M) was prepared by dissolving 1.39 g ferrous sulphate granules ($FeSO_4 \cdot 7H2O$) per 100 mL filtered Milli-Q water and adding 0.6 mL of concentrated sulfuric acid (H_2SO_4). Samples were subjected to the solutions following the protocol by NOAA (Masura et al., 2015); 20 mL of the catalyst solution followed by 20 mL of hydrogen peroxide. Additional 20 mL of H_2O_2 was added until the solution stopped foaming. The beaker was placed on a heating plate with a stirring magnet made out of glass for 1 h at 50 °C and then left overnight at RT.

For the chemical digestion of the fish GIT tissue and macroinvertebrate samples, a solution of 10% (w/v) KOH (1.8 M) was prepared by dissolving 10 g KOH pellets per 100 mL filtered Milli-Q water. The solution was added to the beaker containing the samples in a proportion of 1:3 (w/v 33%) (Foekema et al., 2013; Rochman et al., 2015). The beaker was placed in an oven for 1 h at 50 °C without stirring, as suggested by Dehaut et al. (2016) and Prata et al. (2019).

Density separation

Density separation with saturated chloride solution (NaCl) was performed following the protocol by NOAA (Masura et al., 2015); 6 g of NaCl per 20 mL of sample was added to the beaker and heated to 75 °C to obtain a density of 1.2 g cm^{-3}. The solution was poured into a 500 mL glass funnel, and the beaker was rinsed into the funnel with the saturated salt solution. The solids in the sample were allowed to settle overnight before the separation process was repeated for 5 h with the settled material. The supernatant was drained in a beaker, and the funnel was rinsed carefully with filtered Milli-Q water.

The solution with extracted MP items in the beaker was filtered on a gridded cellulose membrane (0.45 µm pore size) with a glass filtration apparatus. We chose cellulose membranes as they were successfully applied in previous studies for different matrices (Bakir et al., 2020; Bour et al., 2018; Wiggin and Holland, 2019; Han et al., 2020). Moreover, the lines of the gridded membrane facilitated the visual analysis. Both beaker and reservoir flask of the filter were rinsed with filtered Milli-Q. Filters were placed in a glass Petri dish with a closed lid and left in a desiccator for 48 h to dry before they were observed under the stereomicroscope for the identification and isolation of putative MPs.

Visual identification

The filtered material on the cellulose membrane was observed using a Leica EZ 4D Stereo microscope equipped with a digital camera. Items identified as putative plastics by their properties (Hidalgo-Ruz et al., 2012) were transferred onto a silver membrane filter (13 mm diameter, 0.8 µm pore size) with a metal needle. Photos were taken of the MPs on the silver filters to record size, shape and abundance of the items. MPs were categorised into five shapes: fibre, film, fragment, foam and sphere (Hartmann et al., 2019). The size (maximum Feret diameter) was measured using the image process program ImageJ. Fibres were measured using the freehand line tool from start to end. The silver filters were stored and transported in glass Petri dishes until µ-FTIR validation.

S1.3 µ-FTIR analysis

FTIR microscopy was performed using a Thermo Scientific Nicolet iN10 MX Infrared Imaging Microscope. The silver membrane filters were placed onto the specimen holder of the instrument. Measurement of all particles was carried out in reflection mode in a wavenumber range of 4,000–650 cm^{-1} controlled by OMNIC Picta software. A total of 256 scans were taken for each spectrum, with a spectral resolution of 4 cm^{-1}. The IR absorbance was compared with spectra in the software database.

Table S4. Mean and standard deviation of the ratio [%] of items on the filters verified via µ-FTIR for each matrix.

	Surface water	Sediment	Fish	Macroinvertebrates
Mean [%]	40	67	82	82
SD [%]	23	22	19	28

S1.4 Quality control

Blanks

Table S5. Mean and standard deviation of detected MPs in blanks for each matrix.

Matrix	Mean	SD
Surface water	0.3	0.7
Sediment	0	0
Fish	0.3	0.6
Macroinvertebrates	0	0

Mass recovery test

The weight of positive control material (n = 3 for each polymer and extraction procedure) was measured before and after the process (Table S6). To analyse the integrity of the material, here for PET, scanning electron microscope (SEM) images were taken from the cryomilled particles (fragments) before and after the extraction steps by a Zeiss LEO 1430 SEM. Samples were fixed on adhesive tape on aluminum sample holders and sputtered with an Au nanolayer. The images are shown in Figure S1. SEM images indicated that the chemical digestion had little-to-no impact on the integrity of the material. Only in 250 X images of KOH treated samples, finest fissures can be seen on the surface of the particles.

Table S6. Weight (mass recovery) of positive control material before and after the extraction process.

Positive control polymer	Chemical digestion solution	Original mass [mg]	Mass recovery [%]
PET from food packaging, milled amorphous particles (0.06-2 mm)	H_2O_2+Fe	Rep 1: 23.0 Rep 2: 22.1 Rep 3: 23.0	Rep 1: 18.8 (4.2 mg) Rep 2: 75.6 (16.7 mg) Rep 3: 47.2 (11.6 mg) **Mean: 47.7 ± 28.7**

PET from food packaging, milled amorphous particles (various size < 2 mm)	KOH	Rep 1: 22.2 Rep 2: 23.1 Rep 3: 24.6	Rep 1: 45 (10 mg) Rep 2: 55.4 (14.9 mg) Rep 3: 22.6 (5.2 mg) **Mean: 41.0 ± 16.8**
PS, Styrolution 124N/L from INEOS, milled amorphous particles (0.06-0.5 mm)	H_2O_2+Fe	Rep 1: 456.3 Rep 2: 451.6 Rep 3: 463.9	Rep 1: 97.1 (443.08 mg) Rep 2: 98.9 (446.52 mg) Rep 3: 98.6 (514.6 mg) **Mean: 98.2 ± 1.0**
PS, Styrolution 124N/L from INEOS, milled amorphous particles (various sizes < 0.5 mm)	KOH	Rep 1: 42.9 Rep 2: 42.6 Rep 3: 42.9	Rep 1: 99.3 (42.6 mg) Rep 2: 94.6 (40.3 mg) Rep 3: 97.4 (41.8 mg) **Mean: 97.1 ± 2.4**

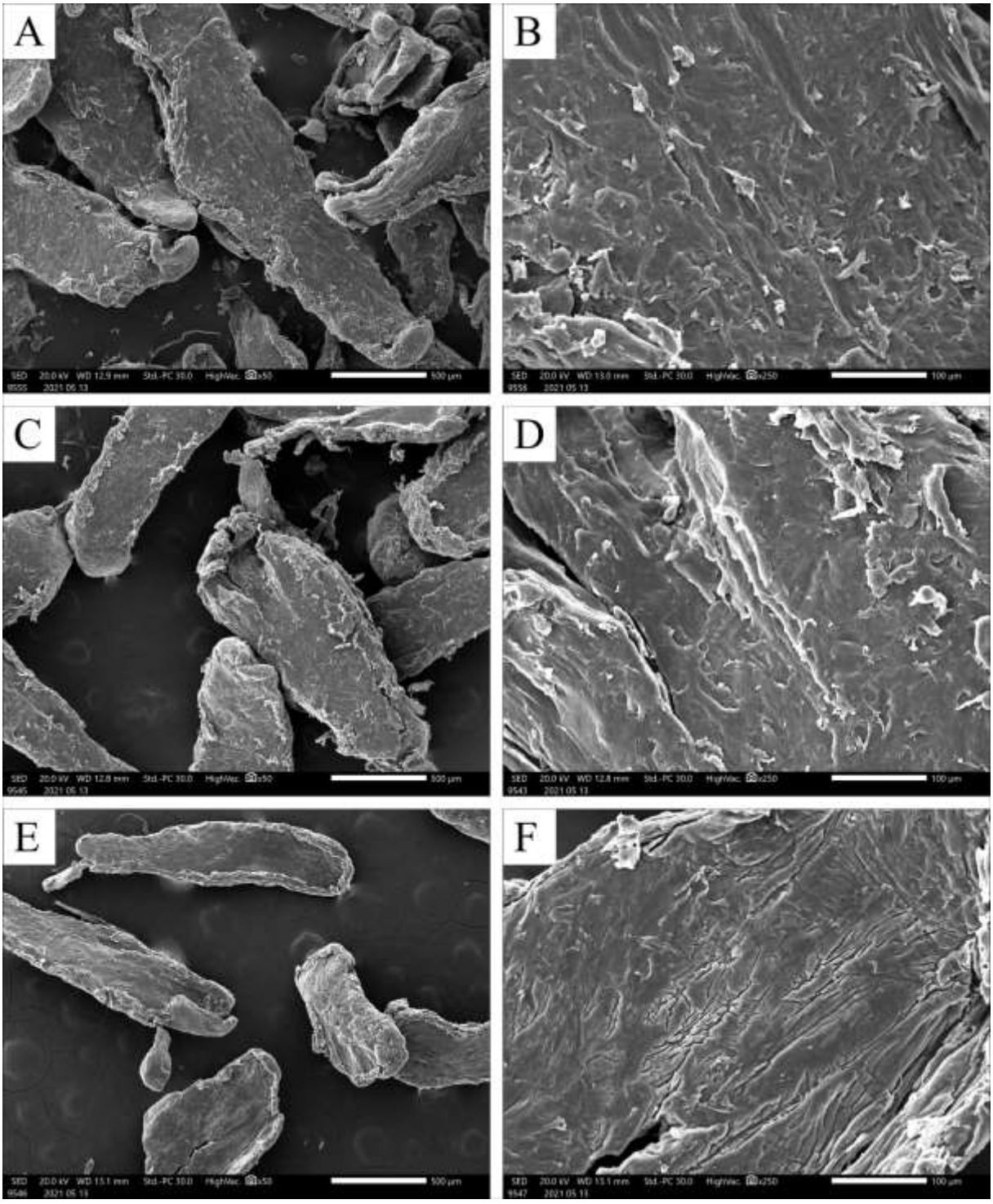

Figure S1. Scanning electron microscope images of cryomilled PET fragments used for the mass recovery test: (A – B) before the extraction procedure, (C – D) after extraction involving the digestion with Fenton's Reagent, (E – F) after extraction involving KOH digestion.

S1.5 Data analysis

Statistical analysis

The normality of each variable was determined using the Shapiro-Wilk normality test. To test for differences in the MP concentrations from surface water samples between locations, one-way ANOVA followed by Tukey-Kramer post hoc test for multiple comparisons were applied. A simple linear regression and Pearson rank correlation analysis was performed to test if the flow velocity for each station was correlated to the MP concentration of surface water (MPs m^{-3}). Differences in MP concentration among stations were tested by GLM using "flow rate" as a covariate. Since the data for sediment, fish and invertebrates were not normally distributed, Kruskal-Wallis Test was used to test for significant differences among the different stations for each matrix. Kruskal-Wallis Test was also applied to determine whether there was an effect of the different timing of fish sampling on the MP concentration in fish. Simple linear regression and Pearson rank correlation analysis was performed to test if the MP quantity per fish was correlated to the weight of the analysed GIT content.

Chi-square tests were used to determine if collected MPs from surface water and sediment differed by size category (smaller, larger), density of the polymer type (lighter, higher) or shape. MPs below 500 µm in size were considered as "smaller", above 500 µm as "larger MPs". A polymer type was attributed to the category "lighter" when the density was < 1.1 g cm^{-3}, and to "higher" when density was ≥ 1.1 g cm^{-3}. The relationships of MP concentration between the different matrices and MP concentration and grain size ratio of sediment samples were determined using Spearman rank correlations (since all variables except surface water were not normally distributed). The average of three replicates per station for all variables was used to make the correlation analysis.

Differences in the size of collected MPs between Hydropsychidae larvae and the host sediment were examined. The chi-square test was used to examine the selectivity of macroinvertebrates with respect to MP size (smaller: < 100 µm, larger: ≥ 100 µm).

For all tests, a significance level of 0.05 was chosen. Microsoft Excel 2016 and RStudio were used for data analysis. Map data was generated using QGIS 3.6.1-Noosa. Microsoft Excel 2016 and Inkscape were used for exporting data graphs.

Unit-consistent ratio between matrices

The unit-consistent ratios between the MP concentrations of sediment and water for each station were calculated (C_{sed}/C_{water}) to determine if sediment concentrations (v/v) were higher than water concentrations or *vice versa*. The ratios were calculated by dividing the mean MP concentration of sediment by the mean concentration in water, both in MPs m^{-3}. The unit conversion of sediment concentration from MP kg^{-1} to MPs m^{-3} for each station was calculated by multiplying the mean sediment concentrations (MPs kg^{-1}, Table S12) by the density of sediment (kg m^{-3}, Table S2). The MP concentrations of biotic and abiotic matrices were used to estimate the unit-consistent ratios between them for each station. The ratios (mean ± SE, $C_{fish/water}$ and $C_{macro/sed}$) in each station were calculated by dividing the mean MP concentration in biota (in MPs kg^{-3}) by the mean concentration in the host medium (water and sediment for fish and macroinvertebrates, respectively), both in MPs m^{-3}. The uncertainty was evaluated from the SE of the MP concentrations in biota and the medium in each station using the propagation of error formula (Brooke and Crookes, 2014). The overall mean ratio was obtained

by the geometric mean of the ratio values for each station and its uncertainty regarding the SE of the means.

Calculation of the MP load of the Ticino River

The MP load per year (MPs $year^{-1}$) was extrapolated from the measured MP concentrations of this work. The measured mean MP concentration in surface water for each monitored station was multiplied with the yearly mean flow rates of the Ticino River at that station provided by the Regional Agency for the Environmental Protection (ARPA Lombardy, 2021, referred to the interval 2001–2015 and 6 stations along the river) (Figure 3A). The ARPA measurement site located upstream of each sampling station in this work was selected as representative of the flow rate at the sampling point.

Calculations of MP load from WWTPs

To estimate the MP load from wastewater treatment plants (WWTPs) of the Ticino River into the Po River, we grouped the following information according to the six sampling stations: municipalities and number of inhabitants within the catchment area of the Ticino (Table S7), and WWTPs connected to the Ticino River with details such as respective equivalent inhabitant, outlet flow rates and treatment evaluation (Table S8). Municipalities and WWTPs located upstream of a sampling station were grouped. This classification allowed for a characterization of sampling stations by their surface area, inhabitants and WWTPs discharging their effluents in the Ticino River. From the WWTP effluent flow rates (m^3 $year^{-1}$) above each sampling station and the mean MP concentration in WWTP effluents (MPs m^{-3}) obtained from a literature overview (Schmidt et al. 2020), the hypothetical MP load (MPs $year^{-1}$) was derived (estimated value).

Table S7. Number of inhabitants, surface and inhabitant density of the municipalities included in the watershed above each sampling station (Parco Ticino, 2021; Parco Naturale del Ticino, 2021).

Sampling station	Municipality	Inhabitants	Surface area (km^2)	Density (inhabitants km^{-2})
S1	Sesto Calende	11,160	25.04	446
	Castelletto Sopra Ticino	7,946	14.61	544
	Golasecca	2,626	7.44	353
S2	Vergiate	8,649	21.78	397
	Somma Lombardo	17,482	30.51	573
	Arsago Seprio	4,765	10.51	453
	Besnate	5,420	7.48	725
	Varallo Pombia	4,878	13.58	359
	Pombia	2,176	11.96	182
	Cardano al Campo	14,443	9.42	1,533
	Casorate Sempione	5,632	6.91	815
	Gallarate	54,008	20.98	2,574
	Vizzola Ticino	565	7.61	74
	Ferno	6,698	8.66	773
	Samarate	16,035	16.01	1,002
	Marano Ticino	1,615	7.84	206
	Lonate Pozzolo	11,365	29.24	389
	Vanzaghello	5,233	5.56	941
	Oleggio	11,317	37.8	299
	Bellinzago Novarese	9,451	39.36	240
	Nosate	641	4.88	131
	Castano Primo	10,937	19.17	571
S3	Cameri	10,994	39.65	277
	Galliate	13,346	29.54	452
	Buscate	4,540	7.83	580
	Turbigo	7,043	8.52	827
	Robecchetto con Induno	4,738	13.93	340
	Cuggiono	8,163	14.93	547
	Romentino	5,626	17.69	318
	Bernate Ticino	3,023	12.16	249
	Boffalora Sopra Ticino	4,099	7.65	536
	Trecate	18,028	38.36	470
	Magenta	23,918	21.99	1,088
	Cerano	7,084	32.10	221
	Robecco sul Naviglio	6,757	19.79	341
	Cassinetta di Lugagnano	1,829	3.32	551
S4	Abbiategrasso	32,473	47.78	680
	Cassolnovo	6,920	31.74	218
	Ozzero	1,417	10.97	129
	Morimondo	1,025	26.00	39
	Vigevano	62,064	81.37	763
S5	Besate	2,036	12.74	160
	Motta Visconti	8,037	10.51	765
	Gambolò	9,910	51.70	192
	Borgo San Siro	954	17.64	54
	Bereguardo	2,641	17.86	148
	Garlasco	9,716	39.18	248
	Zerbolò	1,753	37.19	47
	Torre d'Isola	2,427	16.44	148

S6	Groppello Cairoli	4,429	26.22	169
	Villanova d'Ardenghi	772	6.61	117
	Carbonara al Ticino	1,446	14.78	98
	Pavia	71,006	62.86	1,130
	San Martino Siccomario	6,443	14.29	451
	Valle Salimbene	1,469	7.16	205
	Travacò Siccomario	4,385	17.05	257

Table S8. Wastewater Treatment Plants (WWTP), number of equivalent inhabitants, flow rate, treatment evaluation (high, medium and low performance) and inland water receptors in the watershed above each sampling station (Vailati and Trovò, 2003).

Sampling station	**WWTP**	**Equivalent inhabitants**	**Flow rate (m^3 day^{-1})**	**Treatment evaluation**	**Inland water receptor**
S1	Dormelletto	45,000	8,496	Medium	Rio Arlasca, Maggiore Lake
	Sesto Calende	10,000	1,680	Medium	River Ticino
	Sesto Calende San'Anna	190	33	Medium	River Ticino
	Golasecca Presualdo	1,300	525	Medium	River Ticino
	Golasecca Bizzorra	1,500	350	Medium	River Ticino
	Somma Lombardo Coarezza	700	168	Medium	River Ticino
S2	Somma Lombardo	15,497	5,760	Medium	River Ticino
	Somma L. Maddalena	10,000	3,840		Industrial Canal, River Ticino
	Daverio	3,500	1,250	Medium	Strona creek, River Ticino
	Mornago	6,840	1,634	Medium	Strona creek, River Ticino
	Vergiate	5,000	1,863	Low	Strona creek, River Ticino
	Lonate Pozzolo	360,000	95,000	Medium	Marinone canal, River Ticino
	Nosate	1,000	137	High	Industrial Canal, River Ticino
	Varallo Pombia	3,500	683	Low	Rio Linosa, River Ticino
	Pombia				Rio Riale, River Ticino
	Bellinzago Novarese	25,000	9,504	Low	River Ticino
	Bellinzago N. Cavagliano	400	48		Fontana Milanesi, River Ticino
S3	Robecco sul Naviglio	195,000	9,1507	Medium	River Ticino
	Turbigo	30,000	6,720	Medium	Dead Branch, River Ticino
	Bareggio	46,000	15,068	Low	Scolmatore Canal, River Ticino
S4	Abbiategrasso	25,000	11,507	Medium	Roggia Rile, River Ticino

	Ozzero	2,000	356	Low	Roggia Rile, River Ticino
	Cassolnovo	5,000	4,234	Low	Fosso Vegetato, River Ticino
	Cerano	60,000	27,168	Medium	Ramo dei Prati, River Ticino
	Vigevano	50,000	21,120	Low	River Ticino
S5	Besate	7,000	408	Low	Mezzabarba canal, River Ticino
	Motta Visconti	5,000	986	Low	Canalino canal, River Ticino
	Bereguardo	2,014	403	Medium	Fontanoni Canal, River Ticino
	Bereguardo La Zelata	200		Low	Talentina Canal, River Ticino
	Bereguardo Frutteto	41	3	Low	Re Canal, River Ticino
	Torre d'Isola	100	14	Low	irrigation canal, River Ticino
	Torre d'Isola Casottole	300	43	Low	Roggia Vecchia, River Ticino
	Torre d'Isola Carpana	100	14	Low	irrigation canal, River Ticino
	Torre d'Isola San Varese	500	58	Low	Roggia Vecchia, River Ticino
	Torre d'Isola Ca' de Vecchi	100	14	Low	Roggia Vecchia, River Ticino
	Torre d'Isola Villaggio Pioppi	100	14	Low	Roggia Bergonzola, River Ticino
	Torre d'Isola Villaggio Camp.	100	29	Low	Roggia Bergonzola, River Ticino
	Torre d'Isola Pesca Sportiva	100	14	Low	Roggia Vecchia, River Ticino
	Zerbolò	700		Low	Roggia Martina, River Ticino
	Zerbolò Parasacco	300		Lo	Roggia Castellana, River Ticino
S6	Pavia	145,000	4,399	Medium	Naviglio Pavese, River Ticino
	Groppello Cairoli	4,828	1,536	Medium	Cavo Gipponi, River Ticino
	Carbonara Ticino	1,241	605	Low	Colatore Quaglio, River Ticino
	Travacò Siccomario Rotta	7,241	1,920	Low	Gravellone Canal, River Ticino
	Travacò Siccomario Chiavica	259	15	Low	Gravellone Canal, River Ticino
	Travacò Siccomario Boschi	130	15	Low	Gravellone Canal, River Ticino

	Travacò Siccomario Battella	149	28	Low	Gravellone Canal, River Ticino
	Travacò Siccomario Valbona	119	10	Low	Gravellone Canal, River Ticino
	Travacò Siccomario Scotti	57	3.6	Low	Gravellone Canal, River Ticino

S2 Supplementary Results and Discussion

S2.1 MP in abiotic and biotic matrices

Table S9. Identified plastic polymer types [%] and their densities for all matrices and number of MP items identified via µ-FTIR. The density class of the polymer types was formed according to the following principle: lighter < 1.1 g cm^{-3}, heavier ≥ 1.1 g cm^{-3}.

Polymer type	Surface water [%], n = 464 items	Sediment [%], n = 79 items	Fish [%], n = 24 items	Macro-invertebrates [%], n = 15 items	Density g cm^{-3}	Density class
ABS	0.2				1.07	lighter
Acrylate polymer		1.3			1.05	lighter
Acrylonitrile copolymer	0.2				0.8	lighter
EEA	0.2				0.93	lighter
EPDM	0.2				0.9	lighter
Ethyl acrylate	0.2				0.9	lighter
EVA	3.1	39.2			0.95	lighter
HDPE	2.0				0.95	lighter
LDPE	19.3	5.1	39.1		0.92	lighter
Nylon	1.8		13.0		1.0-1.1	lighter
PA	0.4	2.5			1.02-1.42	lighter
PAM	0.2				1.3	heavier
PAN	10.5			6.7	1.184	heavier
PC-ABS	0.2				1.1	lighter
PE	6.1	7.6	4.3	6.7	0.854	lighter
PET	18.2	8.9	8.7	26.7	1.333	heavier
Phenoxy resin		2.5			1.18	heavier
PMMA	0.2			6.7	1.2	heavier
Polyvinyl propionate:acrylate	0.2				1.12	heavier
PP	17.5	15.2	8.7		0.861	lighter
PS	5.3	5.1		26.7	1.052	lighter
PUR	1.3				0.03-0.5	lighter
PVA	3.9	6.3	4.3		1.19	heavier
PVC	0.4	5.1			1.388	heavier
SAN	1.3				1.08	lighter
SBR	0.2				0.935	lighter
Synthetic polymer	6.8	1.3	21.7	26.7	-	-

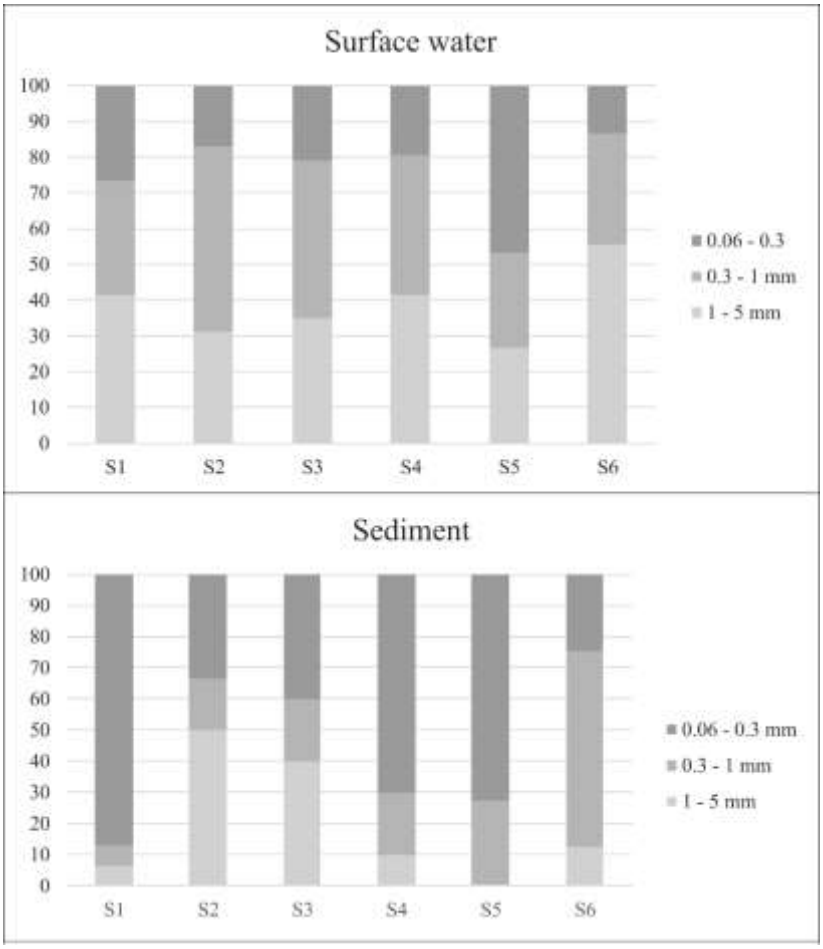

Figure S2. Size distribution of MPs in surface water and sediment samples along the river. For comparability reason, only particles with a size of 0.060–5 mm were included in the size distribution analysis (leaving out < 0.06 mm MPs from the sediments).

Table S10. Mean and standard deviation of the validation ratio [%] of visual identification with regard to natural particles/non-plastic items.

	Surface water	**Sediment**	**Fish**	**Macroinvertebrates**
Mean [%]	91	80.9	19.5	33
SD [%]	18	19.0	25.4	37

Table S11. MP mean concentration and shape composition for all surface water samples and sample stations.

Station	Percentage [%] MP shape (for all replicates)					Amount MPs station^{-1}		Items m^{-3}	
	Fibre	Irregular particle	Foam	Sphere	Film	Mean	SD	Mean	SD
S1	19	62	17	0	2	44.5	36.4	6.239	5.101
S2	44	56	1	1	1	435.5	171.2	33.360	13.111
S3	43	50	0	2	4	298.7	169.0	31.155	17.631
S4	46	55	0	0	0	881.5	396.1	68.588	30.817
S5	23	71	0	3	3	222.7	36.3	24.256	3.954
S6	6	86	0	6	0	489.5	269.9	36.358	20.046

Table S12. MP mean concentration and shape composition for all subtidal sediment samples and sample stations.

Station	Percentage [%] MP shape (for all replicates)					Amount MPs station^{-1}		Weight, dw [kg]	Items Kg^{-1}	
	Fibre	Irregular particle	Foam	Sphere	Film	Mean	SD		Mean	SD
S1	0	100	0	0	0	16.4	15.4	0.61	26.782	25.051
S2	43	43	0	14	0	5.3	5.0	0.71	7.540	7.116
S3	9	73	0	18	0	4.6	1.9	0.66	6.955	2.894
S4	50	50	0	0	0	4.3	1.5	0.57	7.571	2.669
S5	0	100	0	0	0	5.8	4.3	0.62	9.429	6.874
S6	30	70	0	0	0	5.0	0.9	0.64	7.818	1.390

Table S13. MP mean concentration and shape composition for all fish (catfish, *Silurus glanis*) samples and sample stations.

Station	Percentage [%] MP shape (for all replicates)					Amount MPs station^{-1}		Weight of GIT content, ww [g]	Items g^{-1}		Items individual^{-1}	
	Fibre	Irregular particle	Foam	Sphere	Film	Mean	SD		Mean	SD	Mean	SD
S1	0	40	0	0	60	1.73	1.76	81.000	0.021	0.022	1.730	1.763
S2	0	0	0	0	0	0.00	0.00	36.667	0.000	0.000	0.000	0.000
S3	0	50	0	0	50	1.60	2.78	35.000	0.046	0.079	1.603	2.777
S4	0	100	0	0	0	1.22	2.12	29.000	0.042	0.073	1.222	2.117
S5	100	0	0	0	0	0.22	0.38	46.333	0.005	0.008	0.222	0.385
S6	0	91	0	9	0	3.64	2.85	48.000	0.076	0.059	3.644	2.852

Table S14. MP mean concentration and shape composition for all macroinvertebrate (Hydropsychidae) samples and sample stations.

Station	Percentage [%] MP shape (for all replicates)					Amount MPs station^{-1}		Weight, dw [mg]	Items mg^{-1}		Items individual^{-1}	
	Fibre	Irregular particle	Foam	Sphere	Film	Mean	SD		Mean	SD	Mean	SD
S1	33.3	66.7	0	0	0	1.0	1.0	36.500	0.027	0.027	0.200	0.200
S2	0	100	0	0	0	0.3	0.6	25.617	0.013	0.023	0.067	0.115
S3	37.5	62.5	0	0	0	0.0	0.0	31.833	0.000	0.000	0.000	0.000
S4	0	0	0	0	0	2.7	1.2	35.793	0.075	0.032	0.533	0.231
S5	0.0	100	0	0	0	1.1	1.9	41.203	0.027	0.046	0.219	0.379
S6	100	0	0	0	0	1.1	1.9	30.413	0.037	0.063	0.222	0.385

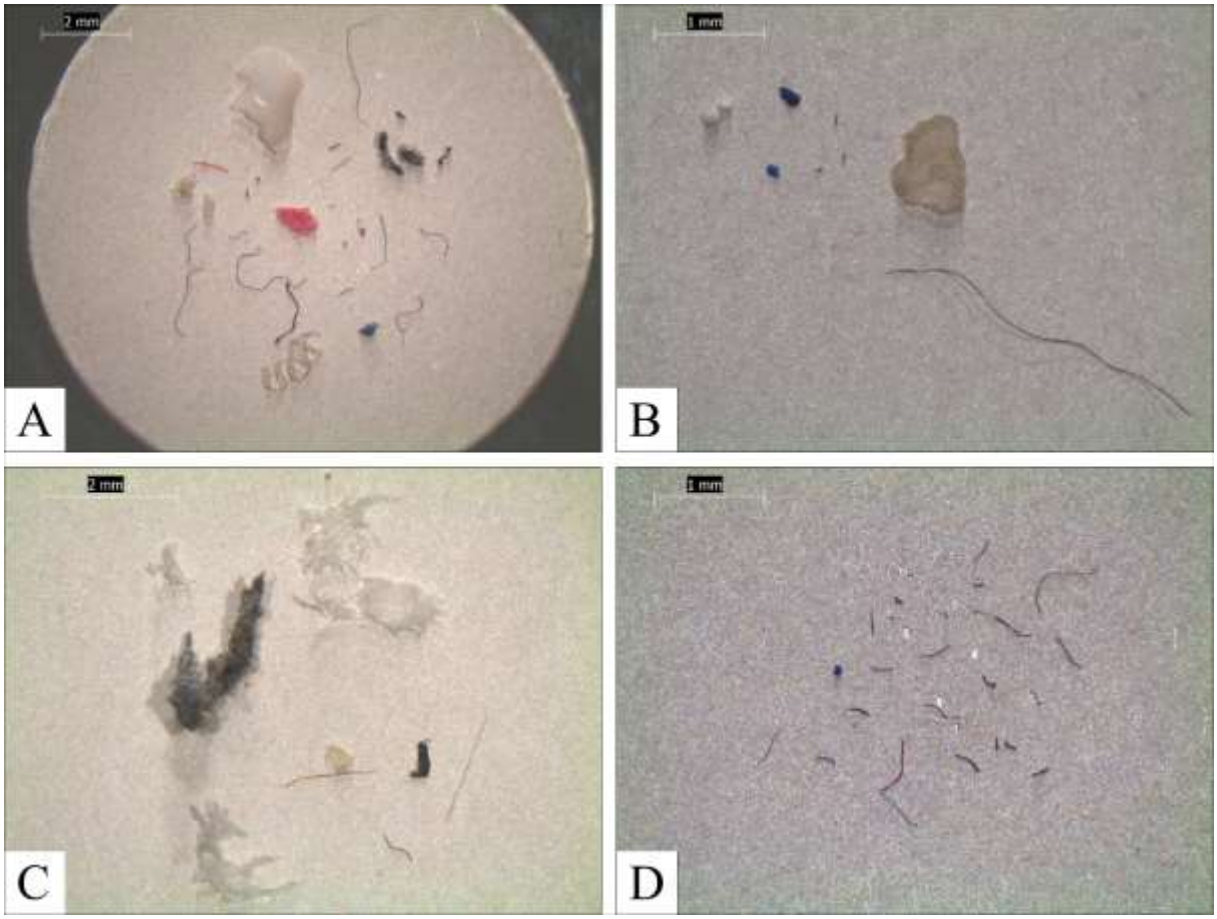

Figure S3. Items detected in samples from (A) surface water, (B) subtidal sediment, (C) fish, and (D) macroinvertebrates isolated on silver membranes for MP verification with μ-FTIR.

Table S15. MP number per replicate for all surface water samples.

Station - Sample	Total MP number	Blank corrected MP number	Volume [m^3]	Items m^{-3}
S1 - 1	14.00	13.70	7.14	1.92
S1 - 2	35.50	35.20	7.14	4.93
S1 - 3	85.01	84.71	7.14	11.87
S2 - 1	244.58	244.28	13.06	18.71
S2 - 2	488.25	487.95	13.06	37.38
S2 - 3	574.64	574.34	13.06	43.99
S3 - 1	408.00	408.00	9.59	42.56
S3 - 2	104.00	104.00	9.59	10.85
S3 - 3	384.00	384.00	9.59	40.06
S4 - 1	1089.61	1087.81	12.85	84.64
S4 - 2	426.67	424.87	12.85	33.06
S4 - 3	1133.60	1131.80	12.85	88.06
S5 - 1	208.00	208.00	9.18	22.66
S5 - 2	264.00	264.00	9.18	28.76
S5 - 3	196.00	196.00	9.18	21.35

S6 - 1	416.00	416.00	13.46	30.90
S6 - 2	264.00	264.00	13.46	19.61
S6 - 3	788.57	788.57	13.46	58.57

Table S16. MP number per replicate for all sediment samples.

Station Sample	Total MP number	Blank corrected MP number	Weight [kg]	Items kg^{-1}
S1 - 1	34.00	34.00	0.61	55.37
S1 - 2	10.00	10.00	0.61	16.29
S1 - 3	5.33	5.33	0.61	8.69
S2 - 1	0.00	0.00	0.71	0.00
S2 - 2	6.00	6.00	0.71	8.48
S2 - 3	10.00	10.00	0.71	14.14
S3 - 1	3.00	3.00	0.66	4.58
S3 - 2	4.00	4.00	0.66	6.11
S3 - 3	6.67	6.67	0.66	10.18
S4 - 1	4.00	4.00	0.57	6.99
S4 - 2	3.00	3.00	0.57	5.24
S4 - 3	6.00	6.00	0.57	10.48
S5 - 1	7.50	7.50	0.62	12.12
S5 - 2	9.00	9.00	0.62	14.55
S5 - 3	1.00	1.00	0.62	1.62
S6 - 1	5.25	5.25	0.64	8.23
S6 - 2	5.71	5.71	0.64	8.96
S6 - 3	4.00	4.00	0.64	6.27

Table S17. MP number per replicate for all fish samples.

Station - Sample	Total MP number	Blank corrected MP number	Weight of GI content [g]	Items g^{-1}
S1 - 1	2.00	1.67	81.00	0.02
S1 - 2	3.86	3.52	81.00	0.04
S1 - 3	0.00	0.00	81.00	0.00
S2 - 1	0.00	0.00	36.67	0.00
S2 - 2	0.00	0.00	36.67	0.00
S2 - 3	0.00	0.00	36.67	0.00
S3 - 1	0.00	0.00	35.00	0.00
S3 - 2	0.00	0.00	35.00	0.00
S3 - 3	5.14	4.81	35.00	0.14
S4 - 1	4.00	3.67	29.00	0.13
S4 - 2	0.00	0.00	29.00	0.00
S4 - 3	0.00	0.00	29.00	0.00
S5 - 1	0.00	0.00	46.33	0.00
S5 - 2	1.00	0.67	46.33	0.01
S5 - 3	0.00	0.00	46.33	0.00
S6 - 1	3.60	3.27	48.00	0.07
S6 - 2	1.33	1.00	48.00	0.02
S6 - 3	7.00	6.67	48.00	0.14

Table S18. MP number per replicate for all macroinvertebrate samples.

Station - Sample	Total MP number	Blank corrected MP number	Weight [mg]	Items mg^{-1}
S1 - 1	1.00	1.00	36.50	0.03
S1 - 2	2.00	2.00	36.50	0.05
S1 - 3	0.00	0.00	36.50	0.00
S2 - 1	0.00	0.00	25.62	0.00
S2 - 2	1.00	1.00	25.62	0.04
S2 - 3	0.00	0.00	25.62	0.00
S3 - 1	0.00	0.00	31.83	0.00
S3 - 2	0.00	0.00	31.83	0.00
S3 - 3	0.00	0.00	31.83	0.00
S4 - 1	2.00	2.00	35.79	0.06
S4 - 2	4.00	4.00	35.79	0.11
S4 - 3	2.00	2.00	35.79	0.06
S5 - 1	0.00	0.00	41.20	0.00
S5 - 2	3.29	3.29	41.20	0.08
S5 - 3	0.00	0.00	41.20	0.00
S6 - 1	0.00	0.00	30.41	0.00
S6 - 2	0.00	0.00	30.41	0.00
S6 - 3	3.33	3.33	30.41	0.11

S2.2 Unit-consistent ratios between matrices

This work provides a consistent set of concentration data in six stations along the same river and in four different matrices for which sampling modalities and analytical procedures were fully comparable within and among stations regarding space and time variables. The data are therefore suitable for calculating the unit-consistent concentration ratios. The purpose of calculating the unit-consistent ratios was to determine which of the abiotic matrices (water and sediment) was higher contaminated (C_{sed}/C_{water}) and to analyse the tendency of MP uptake by the biota in relation to their living medium; MP pollution in fish can be assigned to that in water ($C_{fish/water}$) and pollution in macroinvertebrates to that in sediment ($C_{macro/sed}$).

The results are presented in Table S19. The overall mean ± SE (n = 6) ratio of MP concentration in sediment to that in water (C_{sed}/C_{water}) was 750 ± 660, implying that the sediment concentration was 750-fold higher compared to the water matrix. Both fish GIT and macroinvertebrates showed high ratios in all analysed stations ranging from 210 – 3,400 for $C_{fish/water}$ (overall mean ratio ± SE of 1,100 ± 310; n = 5), and 500 – 5200 for $C_{macro/sed}$ (overall mean ratio ± SE of 1,400 ± 450; n = 5). The high variability found within each station and among the different stations revealed that MP distribution is characterised by an intrinsic high fluctuation and that individual values should be considered not reliable. However, the overall consistency of the order of magnitude of the values calculated in six independent stations support the validity of the proposed approach. Only the overall mean of the ratios calculated at the six station should be used as reference value. To avoid overestimation of calculated values, the geometric mean was used as the best estimate, reflecting the general tendency of MP uptake from the living medium with sufficient reliability. Summing and subtracting the respective SE values to the overall means, the following intervals were obtained for $C_{sed/Cwater}$, $C_{fish/water}$ and $C_{macro/sed}$: 100–1,400, 800–1,400 and 1,000–1,900, respectively.

Both macroinvertebrates and fish GIT presented overall mean ratios of about 1,000, highlighting a similar strong tendency of MP to be ingested by the biota.

Table 19. Unit-consistent ratios ± SE for sediment/water, fish (*S. glanis*'s GIT) and macroinvertebrates (Hydropsychidae family) for each sampling station and as mean of all stations.

Sampling station	C_{sed}/C_{water}	$C_{fish/water}$	$C_{macro/sed}$
S1	8,800 ± 8,900	3,400 ± 3,600	490 ± 550
S2	530 ± 410	–	730 ± 1,200
S3	490 ±280	1,500 ± 2,000	–
S4	210 ± 98	610 ± 770	5,200 ± 2,300
S5	800 ± 410	210 ± 210	1,400 ± 2,000
S6	460 ± 190	2,100 ± 1,600	2,200 ± 2,400
Geometric mean	750 ± 660	1,100 ± 310	1,400 ± 450

The calculated values, especially considering the overall mean values, should overcome discrepancies deriving from the intrinsic variability of MP contamination, as observed in this work among replicates for each station. In fact, six different stations were analysed with three replicates each allowing to calculate mean values for each station and mean values among

stations. The concentration ratio summarizes the intake directly from the medium and that of the food chain. Here, however, the two processes cannot be distinguished. Although calculated unit-consistent ratios reflect the MPs transfer from direct intake from the medium as well as potential indirect transfer of contaminated prey, these two organisms live in different habitats of the river, and thus they must be compared with the background MP contamination of their medium. The similar ranges of the mean concentration ratios of fish GIT and macroinvertebrates (800–1400 and 1000–1900, respectively) strongly suggests an effective transfer of MPs inside the organism's digestive system in relation to their medium. A direct comparison between the two organisms is not possible in this work, because, for analytical reasons, the MP contamination was calculated considering the whole body for macroinvertebrate and only the GIT for fish.

S2.3 Correlation flow-velocity *vs.* MP concentration in water

The MP concentration in surface water concentration was measured in each station during water samplings. The correlation coefficient between MP concentration in water and flow velocity was 0.587 ($p = 0.010$), suggesting that the flow velocity had a significant effect on the MP concentration (MP m^{-3}) in surface water (Figure S4).

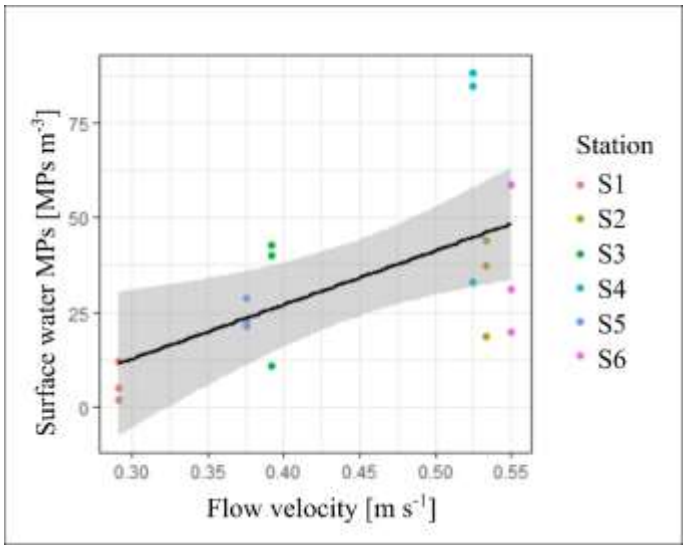

Figure S4. Scatter plot showing the correlation between MP concentration in surface water samples and the measured flow velocity in all six stations.

S2.4 Calculations of MP load from the Ticino River

Multiplying the mean measured MP concentrations of surface water in each station (item m^{-3}) with the yearly mean flow rate of the Ticino River (m^3 $year^{-1}$) at that station reported by ARPA Lombardy (Figure 3A), we extrapolated the yearly MP load carried by the river at each station and a total MP load at the confluence with the Po River of $3.40 \times 10^{11} \pm 1.1 \times 10^{11}$ MP items $year^{-1}$ (Table S20).

Table S20. Measured mean MP concentration in each sampling station (± SE; *n* =3), yearly mean flow rates of the Ticino River measured in ARPA stations (Figure 3A, ARPA Lombardy, 2021) and calculated MP load based on the measured concentrations and the reported flow rates of the Ticino River for each sampling station (± SE was calculated by the propagation error formula).

Sampling station	Measured MP conc. (items m^{-3})	Ticino River flow rates (m^3 $year^{-1}$)	Calculated MPs load (items $year^{-1}$)
S1	6.2 ± 2.9	8.64×10^9	$5.39 \times 10^{10} \pm 2.5 \times 10^{10}$
S2	33 ± 7.6	4.80×10^9	$1.60 \times 10^{11} \pm 3.6 \times 10^{10}$
S3	31 ± 10	6.03×10^9	$1.88 \times 10^{11} \pm 6.1 \times 10^{10}$
S4	69 ± 18	7.79×10^9	$5.35 \times 10^{11} \pm 1.4 \times 10^{11}$
S5	24 ± 2.3	8.93×10^9	$2.17 \times 10^{11} \pm 2.0 \times 10^{10}$
S6	36 ± 12	9.34×10^9	$3.40 \times 10^{11} \pm 1.1 \times 10^{11}$
Total		9.34×10^9	$3.40 \times 10^{11} \pm 1.1 \times 10^{11}$

S2.5 Calculations of MP load from WWTPs

In the attempt to evaluate the role of WWTPs in the MP contamination of the river, we calculated the expected MP load from the local WWTPs that discharge their effluent into the Ticino watershed. The Ticino River presents only two urban sites located directly on the river; one in the North at the outlet of Lake Maggiore (Sesto Calende, 11,160 inhabitants, Table S7), and the second at the end of the river course near the confluence with the Po River (Pavia, 71,006 inhabitants, Table S7). The remaining riverine valley is dominated by natural riparian strips and agriculture, up to 10 km wide. Despite the naturalness of the Ticino area, a high number of people live in its watershed (around half a million people, Table S7 and S21).

Table S21. Number of inhabitants, surface, inhabitant density (Parco Ticino, 2021; Parco Naturale del Ticino, 2021) above each sampling station and number of WWTPs, equivalent inhabitants and total flow rate above each sampling station (Vailati and Trovò, 2003).

Sampling station	Inhabitants	Surface area (km^2)	Density (inhab. Km^{-2})	WWTP (number)	WWTP (e.i.)	Flow rate (m^3 day^{-1})
S1	21,732	47.09	461	6	58,690	11,252
S2	191,310	309.26	619	11	430,737	119,719
S3	119,188	267.46	446	3	271,000	113,295
S4	103,899	197.86	525	5	142,000	64,385
S5	37,474	203.26	184	15	16,655	2,000
S6	89,950	148.97	604	9	159,024	8,532
Total	563,553	1173.9	480	49	1,078,106	319,183

The northern part of the basin is more densely populated, while the southern part is much less so except for the city of Pavia near the confluence with the Po River. Many WWTPs treat domestic effluents as well as from industrial and commercial activities. Out of the 49 WWTPs having the Ticino River as a final receptor (Table S8, Vailati and Trovò (2003)), only 3 exceeded 100,000 equivalent inhabitants (Figure 3A), and 10 were between 10,000 and 100,000 equivalent inhabitants. The depuration efficiency of the small WWTPs was low, while

that of medium and high dimension WWTPs was medium. None of the listed WWTPs had an optimum depuration efficiency, implying also that the efficiency in removing MPs was limited.

Having no direct measure of the MPs concentrations in the WWTPs outlets, we consider a representative MP concentration level at the WWTP outlet and refer to the median of 6,400 items m^{-3} indicated by Schmidt et al. (2020), who recently reviewed available data on MP concentrations in WWTP effluents. With that, the indicative MP loads from WWTPs can be derived upstream of each station, considering the WWTPs discharging their effluents upstream that station (Table S21). Finally, the total MP load at the confluence with the Po River of 7.46×10^{11} MP items $year^{-1}$ was calculated as sum of the contribution of all WWTPs discharging their effluents into the river (Table S22). The total flow rate from WWTPs (1.17×10^{8} m^3 $year^{-1}$) is around 1% of the yearly mean flow rates of the Ticino River at the confluence (9.34×10^{9} m^3 $year^{-1}$).

Table S22. WWTP flow rates (sum of WWTPs flow rates upstream of each sampling station based on values in Table S9), calculated MP loads for WWTPs based on the median MP concentration in WWTPs effluents reported by Schmidt et al. (2020), and cumulative MP loads for WWTPs along the river.

Station	WWTPs flow rate (m^3 $year^{-1}$)	MP loads by WWTPs (items $year^{-1}$)
S1	4.11×10^{6}	2.63×10^{10}
S2	4.37×10^{7}	2.80×10^{11}
S3	4.14×10^{7}	2.65×10^{11}
S4	2.35×10^{7}	1.50×10^{11}
S5	7.30×10^{5}	4.67×10^{9}
S6	3.11×10^{6}	1.99×10^{10}
Total	1.17×10^{8}	7.46×10^{11}

The MP load estimated from WWTP effluents is nearly double than the MP load of the Ticino River (Table S20) obtained from measured MP concentrations, suggesting that a consistent amount (mathematically the difference 4.06×10^{11} MP items $year^{-1}$) is retained by the hydrological network of the Ticino watershed, considering only MP loads from WWTPs. Obviously, the calculated values should be considered as rough estimates of the actual amount released by the WWTPs in the watershed, as they were calculated assuming that they discharge a number of MP equal to the median indicated by Schmidt et al. (2020). However, no best estimation was possible because no data on MPs in WWTP effluents in the area were available, therefore, the proposed MP mean concentration can be accepted as the best available estimate based on the current literature knowledge. The estimations proposed here suggest that WWTPs represent a consistent source of MPs to the river and that the hydrological network can retain a consistent MP load from putative sources. This is consistent with the obtained ratios between sediment and water MP concentrations.

Figure S5 depicts the relationship between MP flows (Log_{10} MP items $year^{-1}$) calculated from measured MP concentration and the cumulative MP loads by WWTPs (Log_{10} MP items $year^{-1}$) calculated from WWTPs effluent flow rates and the median MP concentration in WWTP effluents indicated by Schmidt et al. (2020). Independently from the best interpolation model, the linear regression ($n = 6$; $R^2 = 0.80$; $F = 16.14$; $p = 0.02$) was proposed as statistical

evaluation relationship. The six points derived by data of this work did not allow a more precise evaluation of the type of the relationship (linear or asymptotic); the purpose of this elaboration was to test the role of the WWTPs in determining MP contamination in water.

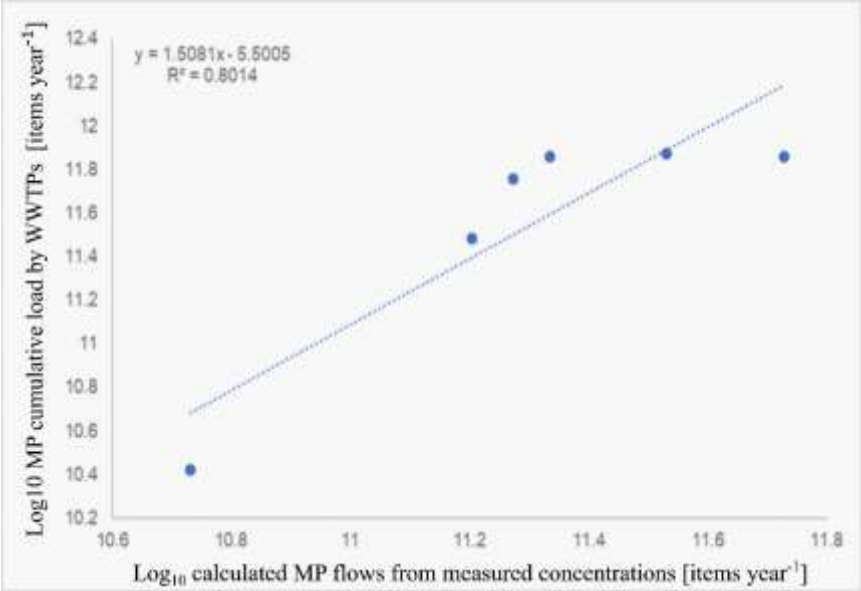

Figure S5. Correlation between MP flows (Log_{10} MP items $year^{-1}$) and the cumulative MP loads by WWTPs (Log_{10} MP items $year^{-1}$).

S3 Supplementary References

ARPA Lombardy, Agenzia Regionale per la Protezione dell'Ambiente Lombardia, Portale Idrologico Geografico: https://idro.arpalombardia.it/, last access: 26 August 2021.

Bakir, A., Desender, M., Wilkinson, T., Van Hoytema, N., Amos, R., Airahui, S., Graham, J., and Maes, T.: Occurrence and abundance of meso and microplastics in sediment, surface waters, and marine biota from the South Pacific region, Mar. Pollut. Bull., 160, 111572, https://doi.org/10.1016/j.marpolbul.2020.111572, 2020.

Bour, A., Avio, C. G., Gorbi, S., Regoli, F., and Hylland, K.: Presence of microplastics in benthic and epibenthic organisms: Influence of habitat, feeding mode and trophic level, Environ. Pollut., 243, 1217–1225, https://doi.org/10.1016/j.envpol.2018.09.115, 2018.

Brooke, D. and Crookes, M. J.: Bioaccumulation of chemicals in fish: investigation of the dependence of depuration rate constant on lipid content of fish, Environment Agency, Bristol, Great Britain, 2014.

Dehaut, A., Cassone, A.-L., Frère, L., Hermabessiere, L., Himber, C., Rinnert, E., Rivière, G., Lambert, C., Soudant, P., Huvet, A., Duflos, G., and Paul-Pont, I.: Microplastics in seafood: Benchmark protocol for their extraction and characterization, Environ. Pollut., 215, 223–233, https://doi.org/10.1016/j.envpol.2016.05.018, 2016.

Foekema, E. M., De Gruijter, C., Mergia, M. T., van Franeker, J. A., Murk, A. J., and Koelmans, A. A.: Plastic in North Sea Fish, Environ. Sci. Technol., 47, 8818–8824, https://doi.org/10.1021/es400931b, 2013.

Han, M., Niu, X., Tang, M., Zhang, B.-T., Wang, G., Yue, W., Kong, X., and Zhu, J.: Distribution of microplastics in surface water of the lower Yellow River near estuary, Sci. Total Environ., 707, 135601, https://doi.org/10.1016/j.scitotenv.2019.135601, 2020.

Hartmann, N. B., Hüffer, T., Thompson, R. C., Hassellöv, M., Verschoor, A., Daugaard, A. E., Rist, S., Karlsson, T., Brennholt, N., Cole, M., Herrling, M. P., Hess, M. C., Ivleva, N. P., Lusher, A. L., and Wagner, M.: Are We Speaking the Same Language? Recommendations for a Definition and Categorization Framework for Plastic Debris, Environ. Sci. Technol., https://doi.org/10.1021/acs.est.8b05297, 2019.

Hidalgo-Ruz, V., Gutow, L., Thompson, R. C., and Thiel, M.: Microplastics in the Marine Environment: A Review of the Methods Used for Identification and Quantification, Environ. Sci. Technol., 3060–3075, https://doi.org/10.1021/es2031505, 2012.

Masura, J., Baker, J. E., 1959-, Foster, G. D. (Gregory D., Arthur, C., and Herring, C.: Laboratory methods for the analysis of microplastics in the marine environment : recommendations for quantifying synthetic particles in waters and sediments, 2015.

Parco Naturale del Ticino: https://www.parcoticinolagomaggiore.com/it-it/aree-protette/servizi/parco-naturale-del-ticino, last access: 18 June 2021.

Parco Ticino: https://ente.parcoticino.it/il-parco/lamministrazione-del-parco/gli-enti-aderenti/, last access: 18 June 2021.

Prata, J. C., da Costa, J. P., Girão, A. V., Lopes, I., Duarte, A. C., and Rocha-Santos, T.: Identifying a quick and efficient method of removing organic matter without damaging microplastic samples, Sci. Total Environ., 686, 131–139, https://doi.org/10.1016/j.scitotenv.2019.05.456, 2019.

Rochman, C. M., Tahir, A., Williams, S. L., Baxa, D. V., Lam, R., Miller, J. T., Teh, F.-C., Werorilangi, S., and Teh, S. J.: Anthropogenic debris in seafood: Plastic debris and fibers from textiles in fish and bivalves sold for human consumption, Sci. Rep., 5, https://doi.org/10.1038/srep14340, 2015.

Schmidt, C., Kumar, R., Yang, S., and Büttner, O.: Microplastic particle emission from wastewater treatment plant effluents into river networks in Germany: Loads, spatial patterns of concentrations and potential toxicity, Sci. Total Environ., 737, 139544, https://doi.org/10.1016/j.scitotenv.2020.139544, 2020.

Vailati, A. M. and Trovò, P.: La depurazione delle acque reflue nei Parchi del Ticino: censimento degli impianti di depurazione civili ed industriali, Parco Ticino Lombardo e Parco Naturale della Valle del Ticino, Corbetta (Milano), Italy, 154 pp., 2003

Wiggin, K. J. and Holland, E. B.: Validation and application of cost and time effective methods for the detection of 3–500 μm sized microplastics in the urban marine and estuarine environments surrounding Long Beach, California, Mar. Pollut. Bull., 143, 152–162, https://doi.org/10.1016/j.marpolbul.2019.03.060, 2019.

PAPER 2 – Occurrence of microplastic in pellets from the common Kingfisher (*Alcedo atthis*) along the Ticino River, North Italy

Anna Winkler, Alessandro Nessi, Diego Antonioli, Michele Laus, Nadia Santo, Marco Parolini, Paolo Tremolada

Environmental Science and Pollution Research 2020

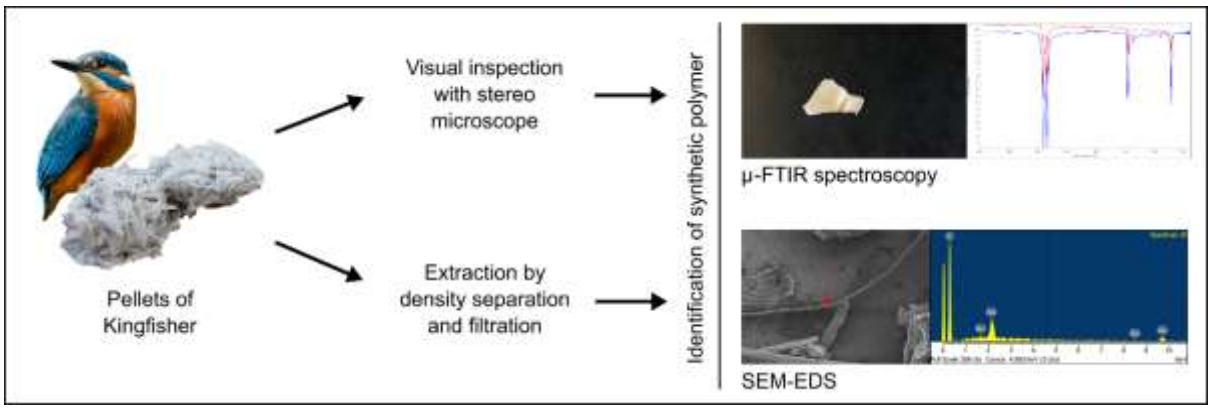

Environmental Science and Pollution Research
https://doi.org/10.1007/s11356-020-10163-x

RESEARCH ARTICLE

Occurrence of microplastics in pellets from the common kingfisher (*Alcedo atthis*) along the Ticino River, North Italy

Anna Winkler[1] · Alessandro Nessi[1] · Diego Antonioli[2] · Michele Laus[2] · Nadia Santo[3] · Marco Parolini[1] · Paolo Tremolada[1]

Received: 25 February 2020 / Accepted: 16 July 2020

Abstract

Previous research has reported avian plastic ingestion in marine bird species. Yet, while research attention on plastic pollution is shifting from marine to freshwater ecosystems, very few information on plastic ingestion is available for freshwater birds. Here, we examined the presence of microplastic in regurgitated pellets of the common kingfisher (*Alcedo atthis*) collected along the Ticino River (North Italy). In total, 133 kingfisher's pellets were examined between March and October 2019 from 54 transects along the river. Plastic elements were detected and identified by visual inspection followed by μ-FTIR and SEM-EDS. Overall, we found 12 (micro)plastics from at least three different polymers in 7.5% of the pellets. This study provides the first report of plastic uptake of this bird species. It highlights the importance of spectroscopic techniques in plastic monitoring studies in order to avoid misidentification of items found. Documenting the presence of plastic ingestion by top carnivores such as fish-eating birds is necessary to understand the pervasiveness and impact of (micro)plastic pollution in food webs of freshwater ecosystems.

Keywords Microplastic · Common kingfisher · Freshwater ecosystem · μ-FTIR · SEM-EDS · Plastic ingestion · Ticino River

Abbreviations

EDS	Energy-dispersive X-ray spectroscopy
μ-FTIR	Micro-Fourier transform infrared spectroscopy
PE	Polyethylene
PET	Polyethylene terephthalate
PP	Polypropylene
PS	Polystyrene
PVC	Polyvinyl chloride
SEM	Scanning electron microscopy

Responsible Editor: Christian Gagnon

✉ Anna Winkler
anna.winkler@unimi.it

[1] Department of Environmental Science and Policy, University of Milan, Via Celoria 26, 20133 Milan, Italy

[2] University of Piemonte Orientale, DISIT, Via T. Michel 11, 15121 Alessandria, Italy

[3] Unitech NOLIMITS, Imaging facility, University of Milan, Via Golgi 19, 20133 Milan, Italy

Introduction

The interest in the study of microplastics (synthetic polymers < 5 mm in size; Arthur et al. 2009) in freshwater ecosystems is increasing continuously. The presence of microplastic in freshwater has been reported worldwide (Dris et al. 2018; Lahens et al. 2018; Mani et al. 2016, amongst others) and recently also in Italy (Campanale et al. 2019). Thus, it is not surprising that research attention is shifting towards the entire freshwater ecosystem and its food web, including fish-eating birds which are on the top level of this food web (Gochfeld et al. 1999). Several studies have investigated avian plastic ingestion in a wide array of marine species from offshore and coastal waters (e.g., Acampora et al. 2016; Avery-Gomm et al. 2013; Franco et al. 2019). However, information about (micro)plastic ingestion by continental birds is still scarce (Blettler et al. 2018; Reynolds and Ryan 2018). A recent study has pointed out the necessity of exploring the presence of (micro)plastics in waterbirds because this might represent a potential problem for continental freshwater bird conservation (Gil-Delgado et al. 2017).

Monitoring of plastic ingested by birds is mainly obtained by stomach analyses of dead birds (Acampora et al. 2014; Avery-Gomm et al. 2013; van Franeker et al. 2011).

Published online: 21 July 2020

Methods for monitoring macro- and microplastics in living birds, however, are a suitable alternative for determining plastic contamination in the absence of finding dead animals. For bird species that do not accumulate plastic in their digestive tracts which can then be analysed in their faeces (Acampora et al. 2017a), the analysis of regurgitated pellets (indigestible residues of food composed of fish bones and teeth, scales, exoskeletons of insects, and other organic material) provides the information on the incidence of litter in the diet. One of the freshwater birds regurgitating pellets is the common kingfisher (*Alcedo atthis*, hereafter kingfisher). The species is distributed throughout most of Europe, Africa, and Asia and feeds on pelagic and benthic fish species and aquatic invertebrates (Čech and Čech 2015; Vilches et al. 2012). Their prey, mostly pelagic fish, is caught by a harpooning maneuvre of the kingfisher as he dives into the water, up to 25-cm deep (Fry et al. 2010). Plastic litter in regurgitates was analysed earlier in pellets from the great cormorant (Acampora et al. 2017a), in regurgitates from chicks of the black-legged kittiwake, northern fulmar, and great cormorant (Acampora et al. 2017b) in Ireland, and in pellets from Great Skua from the Farøe Islands (Hammer et al. 2016). However, these pellets were collected from marine species. There are currently no published data on plastic in pellets from freshwater birds, such as the kingfisher.

Therefore, the aim of this study was to assess the ingestion of (micro)plastic items by the kingfisher by analysing its regurgitated pellets collected along the Ticino River (North Italy). Hereby, we used an integrated approach relying on a preliminary visual inspection and the further application of two different analytical techniques, namely micro-Fourier transform infrared spectroscopy (μ-FTIR) and scanning electron microscopy coupled with energy-dispersive X-ray spectroscopy (SEM-EDS). Previous studies already stressed the importance of spectroscopic techniques in plastic monitoring studies as they are critical in avoiding misidentification of natural items for synthetic polymers (Nicastro et al. 2018; Wesch et al. 2016). In particular, when analysing small plastic items such as microplastic fibres which can be easily mistaken for cotton fibre and vice versa, thus, the objectives of the present study were (i) to provide information on the presence of plastic in pellets from a freshwater, fish-predatory bird; (ii) to highlight the necessity of using analytical methods for plastic identification and especially high-resolution techniques; and (iii) to investigate the spatial variation of pellets containing microplastics along the length of the Ticino River.

Material and methods

Sample collection

The sampling of a total of 133 kingfisher's pellets was implemented between March and October 2019 from 15 out of 54 examined transects along the Ticino River (North Italy). The sampling transects were located along the main course and tributaries of the river with an average length of 551 ± 364 m from the Lake Maggiore down to the confluence into the Po River. The transects were examined for pellets under potential resting points of the kingfisher two times at a minimum (up to six times once pellets were detected in a transect). Visual observation of the kingfisher or response to a bird whistle indicated that the species was distributed along the whole watercourse, confirming previous findings of its high occurrence in the Ticino valley (Casale 2015). A map of the study area with the locations of pellets is shown in the result section.

Sample preparation and microplastic extraction

In the laboratory, pellets were placed in glass petri dishes and visually inspected for the presence of potential plastic items (e.g., fragments, particles, fibres) under a stereo microscope (Wild M3B Heerbrugg Switzerland, 6.4 X – 40 X) with a detection and selection limit of 40 μm for particles and fragments. Most fibres had a thickness < 40 μm but were detected due to their length. Images were taken with the camera of the stereo microscope to measure the size of detected items using the imaging software Fiji. The putative plastic items were transferred into small glass vials with metal tweezers or needle and stored until analysis of their polymeric composition by μ-FTIR. The detection and identification limit with regard to particle size for the applied μ-FTIR instrument was 10 μm. Considering the detection and selection limit of the visual identification with the stereo microscope and the resolution limit of the μ-FTIR instrument, the application of an additional extraction method followed by an analytical high-resolution technique, which is the advantage of SEM-EDS (identification limit of 3 μm), was necessary in order to determine the occurrence of even smaller plastic items.

Therefore, after visual inspection and removal of the items for μ-FTIR analysis, the remaining pellet material was further processed for density separation extraction and SEM-EDS analysis. Out of all pellet material, we chose ten pellets from different transects representing the northern and southern areas of the Ticino River (five each). The material was placed in a beaker and underwent a density separation in 100 mL of a saturated sodium chloride solution (NaCl, 0.0616 M) for 24 h to settle parts of the prey such as bones and to float MP items. Subsequently, the supernatant was filtered with an in-house manufactured glass filtration apparatus on silver membrane filters (Sterlitech, 0.8-μm pore size, 13-mm diameter, filtration area of 19.6 mm^2). The filters were dried for 48 h in a glass desiccator and stored until analysis with SEM-EDS.

Quality control precautions

In order to assess potential sample contamination by atmospheric deposition of microplastic, we included procedural blanks into our analysis. In the field, an aluminium foil was placed next to a detected pellet and remained open for the duration of pellet collection, then closed, transported, and stored in the same way as the pellet samples. The blanks were taken for each sampling date and transect where a pellet was found. In the event that more than ten pellets were found in one transect of the same date, one blank per ten pellets was taken. In total, 29 blanks were sampled in the field. These field blanks were then further used to include potential airborne contamination of microplastic in the laboratory. For the duration of the visual analysis of pellets under the stereo microscope, field blank samples were opened and placed next to the microscope. All field blanks were then examined under the stereo microscope to search for potential deposited microplastics.

Additionally, for the extraction procedure as preparation for the SEM-EDS analysis, two blank samples deriving from the northern and southern project areas were processed and analysed in the same way as the pellet samples. All glassware were cleaned with washing detergent and rinsed with ultrapure Milli-Q water, which was previously filtered through cellulose membrane (0.45 μm). All the laboratory procedures were implemented on pre-cleaned surfaces, and executive persons wore cotton lab coats and washed their hands regularly.

Sample analysis

FTIR microscopy was performed using a Thermo Scientific Nicolet iN10 MX Infrared Imaging Microscope. Items identified as putative plastics during the preliminary visual inspection by the stereo microscope were transferred individually on a silver membrane filter and placed onto the specimen holder of the instrument. Measurement of all particles was carried out in reflection mode in a wavenumber range of 4000–650 cm^{-1} controlled by OMNIC Picta software. A total of 256 scans were taken for each spectrum, with a spectral resolution of 4 cm^{-1}. A detected polymer was considered as such when the match to the respective polymer in the library was > 70%.

For SEM-EDS analysis, high-resolution images of the filtrated sample material on the silver filter were taken. Polymer particles or fibres were identified by their elemental composition signatures. After blank and sample filters were attached to standard SEM stubs and coated with a thin film of evaporated gold, they were placed in a Zeiss LEO 1430 SEM coupled with an Oxford detector for EDS analysis. The analysed area/filter area ratio of the silver membrane filter was 11.46% (25 fields vertically, 20 fields horizontally, magnification × 500, total analysed area 2.25 mm^2). Particles and fibres detected in the cross-shaped transect were analysed by EDS using the Oxford Instruments INCA ver. 4.04 software (Abingdon, UK). The smallest particle size/fibre thickness analysed was 3 μm (identification limit of the EDS). Operating conditions were the following: accelerating voltage 20 kV, probe current 80 μA, and working distance 15.0 mm. The expected elemental composition of polymers corresponds to their composition stoichiometry. For example, for polyethylene terephthalate (PET – $(C_{10}H_8O_4)_n$), the stoichiometric C:O ratio is 73:27, given that hydrogen does not provide a detectable peak in the EDS spectrum. Preoperational EDS tests on pure PET material confirmed the elemental ratio (with a gold trace of gold ~ 1%), with 5% variability for each element. A particle found on the filter was identified as PET when EDS spectra revealed the same elemental composition and when measured peaks matched those of spectra from the preoperational test. Elemental composition of 100% carbon indicated polyolefin composition, such as polyethylene (PE), polypropylene (PP), or polystyrene (PS), but could not be further specified since these polymers consist of no other elements besides carbon and hydrogen to distinguish them from each other. After the cross-shaped transect was analysed, the entire filter surface was scanned (× 30) looking for fibres and particles and inspected for their elemental composition. Potential confusion of synthetic fibres with natural textile fibres or fibres from drying paper tissue was prevented by measuring elemental composition of wool, cotton, and paper resulting in a mean ratio of C:O:N:S = 62:19:17:2, C:O = 61:39, and C:O = 66:34, respectively.

Results

Overall, 12 plastic items were detected in 10 out of 133 regurgitated pellets from the kingfisher along the Ticino River. Micro-FTIR analysis of items detected under the stereo microscope determined three plastic elements in three different pellets (one from the northern, two from the southern project area). The identified polymers were a fragment of polyethylene (Fig. 1a), a polyurethane fibre (Fig. 1b), and polypropylene fibre (Fig. 1c). Elemental analysis by SEM-EDS performed on a subset from the pellet material (five pellets from the North and South, respectively) revealed five fibres with a C:O ratio corresponding to that of PET (Fig. 2a) and four fibres with the elemental composition of 100% carbon indicating polyolefin composition (Fig. 2b) from, in total seven different pellets (three from the North and four from the South). The detected microplastics were mainly fibres of very small size with a mean length of 1.16 ± 1.22-mm standard deviation, ranging from a length of 63 μm to 3.09 mm.

While the presence of the kingfisher was confirmed throughout the whole watercourse of the river (visual observations and response to bird whistle), most pellets (82%) were found in the southern area of the river. Considering the geographical distribution of pellets which included plastic items,

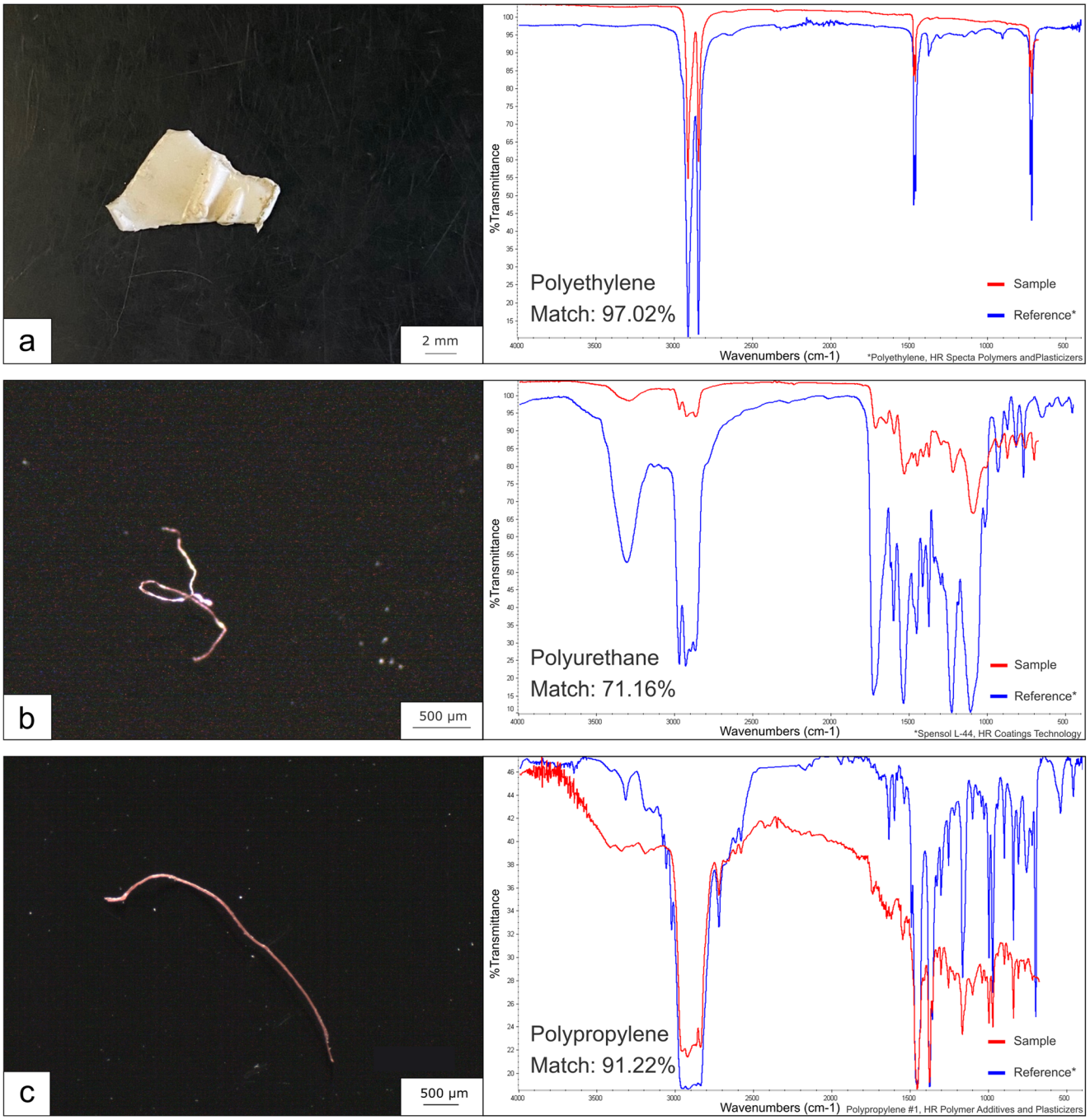

Fig. 1 Microscope images of visually identified microplastics in pellets of the kingfisher and respective µ-FTIR spectra (red) with matches (%) to reference polymer from the library (blue). **a** Polyethylene fragment with a match of 97.02%. **b** Polyurethane fibre with a match of 71.16%. **c** Polypropylene fibre with a match of 91.22%

no strong spatial variation (for example, an increase of microplastics in pellets over the length of the Ticino River) could be detected (Fig. 3). No plastics were detected in pellets in the top northern part of the study area. Following the watercourse, the first occurrence of plastic items in pellets was discovered downstream of a potential primary input source: a large wastewater treatment plant (WWTP) with a population equivalent > 300,000 that discards its effluent into the Ticino River (black dot in map of Fig. 3). The other transects, in which pellets with microplastic were found, were located in the southern part of the study area, where the river crosses the city of Pavia (~ 70,000 inhabitants). The urban area next to the riverside represents a large (micro)plastic source by means of water runoff or atmospheric deposition.

Procedural field blanks were examined under the stereo microscope, but no putative microplastics were found that

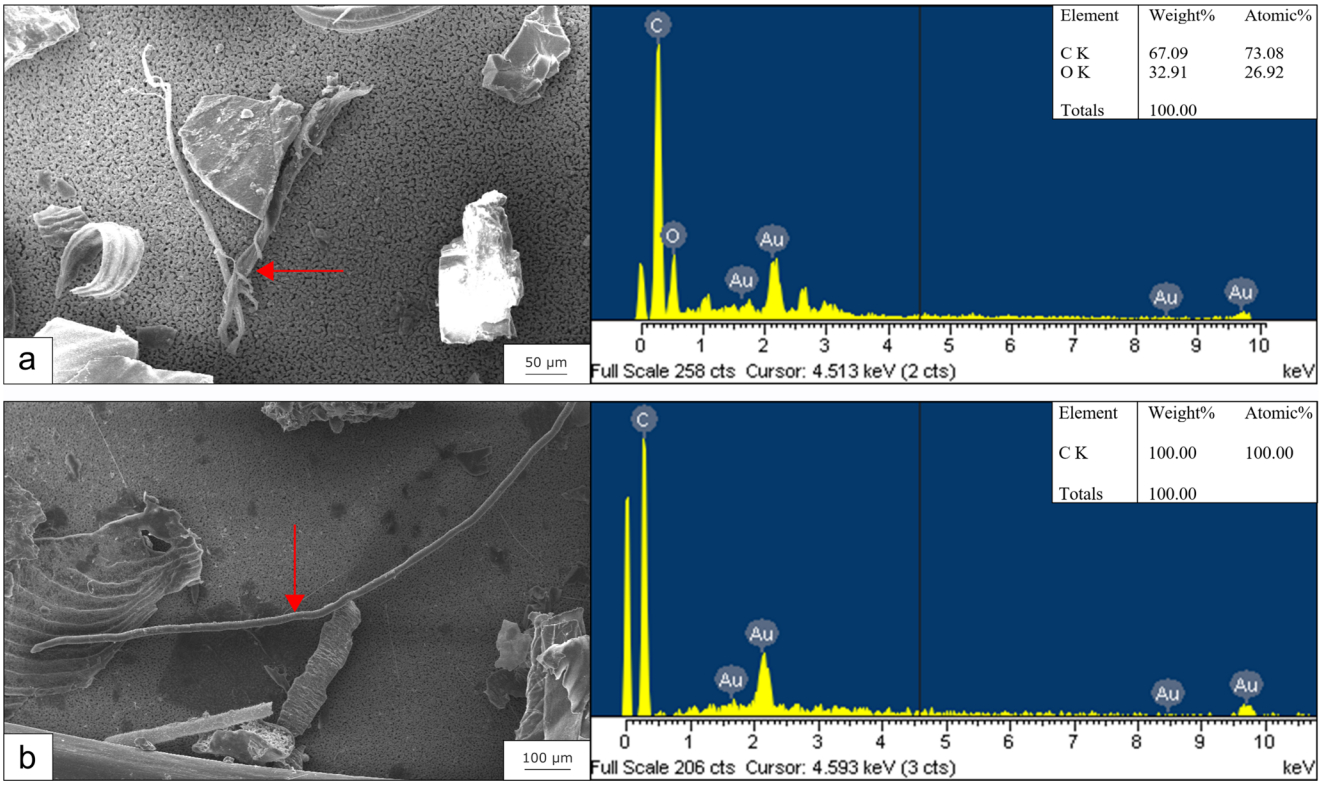

Fig. 2 SEM images and respective EDS spectra with elemental quantitative data of analysed fibres from filtered extracts of pellets of the kingfisher. **a** Microplastic fibre on silver filter with specific elemental composition and C:O ratio corresponding to PET. **b** Microplastic fibre on silver filter with specific elemental composition of C = 100% indicating polymeric origin. Gold (Au) was removed from the output listing as it derived from the gold-coating

could have been analysed by µ-FTIR. Moreover, no microplastic fibres were detected in the two procedural blanks analysed by SEM-EDS; hence, airborne contamination during sampling in the field and analysis in the lab was efficiently minimised.

Discussion

In this study, 7.5% of pellets (10 out of 133) were contaminated by microplastics. Out of the 12 detected microplastics, 11 were fibres. Fibres are often reported as the most abundant microplastic items in water (Campanale et al. 2019; Kay et al. 2018; Mani et al. 2016, amongst others) but also in fish (Collard et al. 2015). Dris et al. (2018) reported that fibres often represent the most common microplastics in surface water of rivers, mainly when sampling of water with a mesh size lower than 300 µm was applied. A key source of fibres is from the breakdown of textiles in washing machines entering the river through the effluent of wastewater treatment plants (Kay et al. 2018). Consequently, it is not surprising that fibres were the predominant form of microplastic found in digestive tracts of fish, such as chubs (*Squalius* spp.) (Collard et al. 2015), which is one of the main genus (in juvenile stage) composing the diet of the kingfisher from the Ticino River (Nessi 2020). In general, juvenile stages of the predominant fish species in the diet of the Kingfisher, such as chubs and barbels (*Barbus* spp.), are exposed to fibres, as they inhabit shallow areas close to the water surface where fibres are floating. However, McGoran et al. (2017) found microplastic fibres also in benthic fish species, indicating that not only fish from shallow habitats ingest fibres. Microplastic fibres in the Ticino River were already detected before, in faeces from otters, a mammal top predator who also feeds on chubs and barbels (Smiroldo et al. 2019). As shown in Fig. 3, the Ticino River receives the effluents of several WWTPs, canals, and smaller rivers, draining also residential, commercial, and industrial areas to the west of the city of Milan. All these discharges are potential input sources of microplastics to the river. Thus, it can be assumed that the microplastic load of the river water increases with its length, as also proven in other studies (Eerkes-Medrano et al. 2015; Mani et al. 2016). The amount of microplastic in pellets from the kingfisher did not reflect this presumed spatial variation; however, it can be related to specific sources as reported in the "Results" section.

Sources of microplastic to the kingfisher

Unlike birds which feed at the water surface, diving birds such as the kingfisher are less prone to directly ingest floating

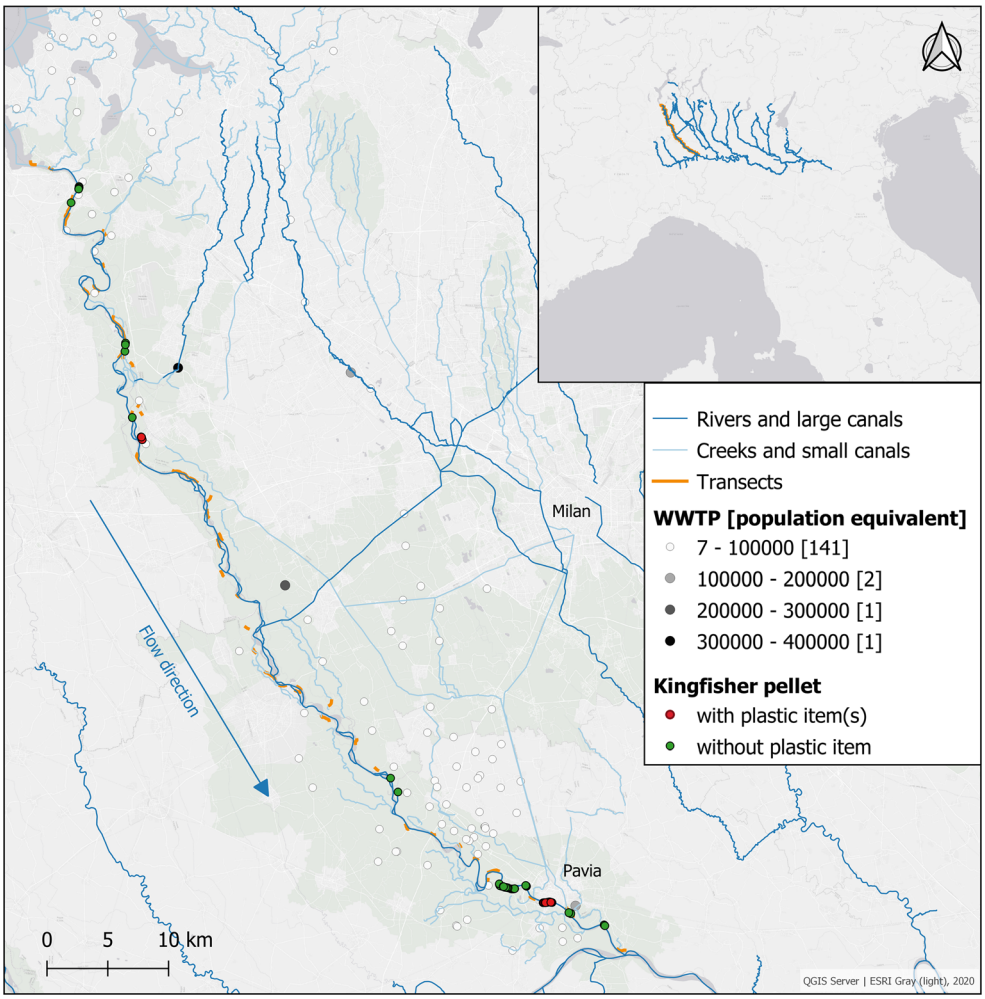

Fig. 3 Map of the Ticino River with transects (orange lines) where the search for kingfisher pellets took place. Green spots represent pellets in which no plastic item could be identified by visual inspection and μ-FTIR analysis. Red spots represent pellets in which plastic items were determined by visual inspection and μ-FTIR or SEM-EDS analysis. Grey-scaled dots are wastewater treatment plants (WWTP) for different population equivalents

plastic material from the water due to the buoyant nature of most plastic items. Considering that diving birds take up plastics more likely through their prey by secondary ingestion, as reported by Acampora and co-authors (2017a), also, the largest detected fragment in the present study (polyethylene of 12.1 mm on its longest side, Fig. 1a) could also be ingested secondarily. Although microplastics can be accidentally ingested from water during fish predation, the possibility that fish already ingested microplastics is high. Therefore, we can speculate that particles and fibres found in kingfisher pellets derive from the diet, and that microplastic was transferred through the food web. Since the regurgitation of pellets presents an effective method of ejecting plastic items, the physical effects are considered to be lower than for non-regurgitating bird species. However, the toxicological consequences of plastic ingestion by birds caused by related chemicals such as additives and micropollutants attached to their surface are poorly studied. Toxins leaching from the plastics upon ingestion are considered to induce adverse health effects in birds, including endocrine disruption and reduced reproduction (Giesy et al. 2003; Roman et al. 2019).

Comparison with other freshwater birds

Only few previous studies showed the ingestion of plastics by freshwater birds. Plastic (mainly fragments) was detected in 9% (n = 148; English et al. 2015) and 11% (n = 350; Holland et al. 2016) of digestive tracts of ducks and geese in Canada. In South Africa, 5% of analysed faeces (n = 283) from different ducks and goose species were found to contain microplastic in the form of fibres (Reynolds and Ryan 2018). Although our findings (7.5% of analysed pellets contained microplastic, n = 133) fall into the range of these previous results, a comparison of our findings with the results of the studies mentioned above is difficult, as they investigated big-sized, mainly herbivorous bird species. For these species, microplastic ingestion derives most likely from sediment particles and water than from their food, although it is not proven. On the contrary, here, we prove microplastic ingestion from a top predator of river ecosystems, for which the ingestion more likely derived from their food rather than from abiotic elements (sediment and water). Moreover, these previous studies did not apply spectroscopic or elemental techniques

for identification of smaller microplastics, which was the purpose of the present work.

Methodological novelties and issues

This study is the first to investigate microplastic load in pellets of a freshwater bird. The kingfisher regurgitates a pellet a few times per day (Fry et al. 2010). Therefore, the sampled pellets may represent only the last ingested meal(s) consumed throughout the same day. Hence, the amount of plastic in the pellets reflects the ingestion over a short-time period, as items could have been previously expelled. Although regurgitated pellets are easily collected, we are aware that the samples may show varying levels of digestion depending on the duration between prey ingestion and final pellet ejection. This aspect might also influence instrumental plastic detection.

Apart from these considerations, another crucial element should be pointed out: unlike the studies mentioned above, in this work, two complementary techniques were applied, μ-FTIR and SEM-EDS. In fact, out of the 12 detected microplastics, three were identified by stereo microscope inspection and μ-FTIR analysis and nine by an additional density separation extraction and high-resolution SEM-EDS analysis. The confirmation by analytical techniques is essential, as natural fibres from wool or cotton can be mistaken for synthetic ones. In fact, from our visual analysis under the stereomicroscope, a high number of items were selected as possible microplastics, of which only three were confirmed as such by μ-FTIR. During the SEM-EDS analysis, many particles with fibre and non-fibre shapes were analysed, yet only nine fibres were confirmed as microplastics. In the case of non-fibre particles, some of them were compatible with the elemental composition of plastic polymers, but particles with similar shape and elemental composition were found in blanks (even if in lower abundance) so that we decided to not consider non-fibre small particles as potential microplastics in the pellet samples. As stated before, polymer identification by SEM-EDS is limited to polymers which consist of other elements besides carbon and hydrogen, such as oxygen in polyethylene terephthalate (PET) and chlorine in polyvinyl chloride (PVC). Thus, SEM-EDS is complementary rather than a substituting technique for other analytical methods such as μ-FTIR.

Regarding the instrumental confirmation of the microplastic detection of this study and the precaution criteria used for determining their presence, the reported findings can underestimate the real number of microplastics in the kingfisher diet. Especially considering that all the pellets were inspected visually under the stereo microscope for analysis by μ-FTIR, only a subset of samples was analysed by density separation and SEM-EDS analysis for smaller particle detection. This part of the research was added mainly for comparative methodological purpose.

Conclusions

This study is the first assessment of the abundance of (micro)plastics in pellets of the common kingfisher. All (micro)plastics were fibres except one larger fragment. Rivers flowing through highly urbanised regions, like the Ticino River, are particularly vulnerable to plastic input, primarily through the effluent of wastewater treatment plants. Indeed, although the Ticino River is included amongst the global biosphere reserve network and is protected by two regional parks, it is subject to considerable plastic contamination. The present findings of plastics in kingfisher pellets confirmed this condition, although plastic contamination of pellets does not reflect assumed increased microplastic load over the length of the river. The kingfisher, being a top-level predator, takes up plastic particles and fibres most likely through secondary ingestion. It seems that the regurgitation of indigestible material is an effective method for the ejection of the ingested plastic particles. Thus, the kingfisher has an advantage over those species which accumulate plastic in their stomach.

The use of regurgitated pellets and the analysis with μ-FTIR and SEM-EDS proved to be a suitable method to assess plastic exposure for freshwater birds like the kingfisher. The limits of SEM-EDS polymer identification to only polymers consisting of other elements than just carbon make this rather a complementary technique than a substitute for μ-FTIR. Nevertheless, by applying high-resolution imaging by SEM-EDS, we confirmed the prevalence of ingested fibres that are not easily detectable under stereo or binocular microscopes. Thus, the results of this work indicate a strong underestimation of microplastic pollution in freshwater birds when only visual inspection under the stereo microscope is applied. Therefore, we suggest the tied use of different analytical techniques for identifying (micro)plastics in pellets and, more general, in future avian plastic ingestion studies, as we observed fibres by SEM-EDS that we did not detect earlier via visual inspection under the stereo microscope.

This study on microplastic in regurgitated pellets presents a baseline for future studies that should be carried out to further assess microplastic ingestion rates for freshwater birds. Plastic presence/absence studies through the collection of pellets are minimally invasive and provide insights into the plastic exposure of freshwater birds that are alive. Several features make the kingfisher an excellent monitoring species: it is widely distributed, site-loyal, and obtains all its food from aquatic systems at a high feeding rate. Moreover, its small size can be considered as a peculiar characteristic making it more suitable for small size microplastic monitoring than bigger birds. Reporting plastic ingestion by top carnivores such as fish-eating birds is necessary to understand the pervasiveness and impacts of microplastic pollution in food webs of freshwater ecosystems. However, we highlight that the application of

spectroscopic analytic techniques is crucial to allow for discrimination between plastic and natural items.

Acknowledgements Open access funding provided by Università degli Studi di Milano within the CRUI-CARE Agreement. The authors wish to thank the Endangered Landscape Program (ELP) of the Cambridge Conservation Initiative (Cambridge, UK) for supporting the interdisciplinary group of experts of the project "Restoring the Ticino River Basin Landscape. One River – Many Systems – One Landscape", which provided useful suggestions for the research. The authors further wish to thank Adriano Bellani and Valentina Parco from the Ticino Natural Park for supporting the research.

Data transparency This manuscript has not been previously published and the paper is currently not under consideration by another journal. All authors have approved of and have agreed to submit the manuscript to this journal.

Author contribution Anna Winkler: writing - original draft preparation, methodology, investigation; Alessandro Nessi: methodology, investigation; Diego Antonioli: methodology; Michele Laus: resources; Nadia Santo: methodology; Marco Parolini: validation, writing- reviewing and editing; Paolo Tremolada: conceptualization, methodology, resources, supervision.

Compliance with ethical standards

Conflict of interest The authors declare that they have no conflict of interest.

References

Acampora H, Schuyler QA, Townsend KA, Hardesty BD (2014) Comparing plastic ingestion in juvenile and adult stranded short-tailed shearwaters (*Puffinus tenuirostris*) in eastern Australia. Mar Pollut Bull 78(1–2):63–68. https://doi.org/10.1016/j.marpolbul.2013.11.009

Acampora H, Lyashevska O, Van Franeker JA, O'Connor I (2016) The use of beached bird surveys for marine plastic litter monitoring in Ireland. Mar Environ Res 120:122–129. https://doi.org/10.1016/j.marenvres.2016.08.002

Acampora H, Berrow S, Newton S, O'Connor I (2017a) Presence of plastic litter in pellets from great cormorant (*Phalacrocorax carbo*) in Ireland. Mar Pollut Bull 117(1–2):512–514. https://doi.org/10.1016/j.marpolbul.2017.02.015

Acampora H, Newton S, O'Connor I (2017b) Opportunistic sampling to quantify plastics in the diet of unfledged black legged kittiwakes (*Rissa tridactyla*), Northern Fulmars (*Fulmarus glacialis*) and great cormorants (*Phalacrocorax carbo*). Mar Pollut Bull 119(2):171–174. https://doi.org/10.1016/j.marpolbul.2017.04.016

Arthur C, Baker J, Bamford H (2009) Proceedings of the international research workshop on the occurrence, effects, and fate of microplastic marine debris, 9-11 September 2008. NOAA Technical Memorandum NOS-OR&R30. https://repository.library.noaa.gov/view/noaa/2509. Accessed 20 January 2020

Avery-Gomm S, Provencher JF, Morgan KH, Bertram DF (2013) Plastic ingestion in marine-associated bird species from the eastern North Pacific. Mar Pollut Bull 72(1):257–259. https://doi.org/10.1016/j.marpolbul.2013.04.021

Blettler MCM, Abrial E, Khan FR, Sivri N, Espinola LA (2018) Freshwater plastic pollution: recognizing research biases and identifying knowledge gaps. Water Res 143:416–424. https://doi.org/10.1016/j.watres.2018.06.015

Campanale C, Stock F, Massarelli C, Kochleus C, Bagnuolo G, Reifferscheid G, Uricchio VF (2019) Microplastics and their possible sources: the example of Ofanto river in Southeast Italy. Environ Pollut 113284:113284. https://doi.org/10.1016/j.envpol.2019.113284

Casale F (2015) Atlante degli uccelli del Parco Lombardo della Valle del Ticino, Parco Lombardo della Valle del Ticino e Fondazione Lombardia per l'Ambiente. https://ente.parcoticino.it/wp-content/uploads/2016/12/Atlante_Uccelli_Ticino.pdf. Accessed 06 June 2020

Čech M, Čech P (2015) Non-fish prey in the diet of an exclusive fish-eater: the common kingfisher *Alcedo atthis*. Bird Study 62(4):457–465. https://doi.org/10.1080/00063657.2015.1073679

Collard F, Gilbert B, Eppe G, Parmentier E, Das K (2015) Detection of anthropogenic particles in fish stomachs: an isolation method adapted to identification by Raman spectroscopy. Arch Environ Contam Toxicol 69(3):331–339. https://doi.org/10.1007/s00244-015-0221-0

Dris R, Gasperi J, Tassin B (2018) Sources and fate of microplastics in urban areas: a focus on Paris megacity. In: Wagner M, Lambert S (ed) Freshwater microplastics. Springer International Publishing, Cham 58:69–83. https://doi.org/10.1007/978-3-319-61615-5_4

Eerkes-Medrano D, Thompson RC, Aldridge DC (2015) Microplastics in freshwater systems: a review of the emerging threats, identification of knowledge gaps and prioritisation of research needs. Water Res 75:63–82. https://doi.org/10.1016/j.watres.2015.02.012

English MD, Robertson GJ, Avery-Gomm S, Pirie-Hay D, Roul S, Ryan PC, Wilhelm SI, Mallory ML (2015) Plastic and metal ingestion in three species of coastal waterfowl wintering in Atlantic Canada. Mar Pollut Bull 98(1–2):349–353. https://doi.org/10.1016/j.marpolbul.2015.05.063

Franco J, Fort J, García-Barón I, Loubat P, Louzao M, del Puerto O, Zorita I (2019) Incidence of plastic ingestion in seabirds from the Bay of Biscay (southwestern Europe). Mar Pollut Bull 146:387–392. https://doi.org/10.1016/j.marpolbul.2019.06.077

van Franeker JA, Blaize C, Danielsen J, Fairclough K, Gollan J, Guse N, Hansen PL, Heubeck M, Jensen JK, Le Guillou G, Olsen B, Olsen KO, Pedersen J, Stienen EWM, Turner DM (2011) Monitoring plastic ingestion by the northern fulmar Fulmarus glacialis in the North Sea. Environ Pollut 159(10):2609–2615. https://doi.org/10.1016/j.envpol.2011.06.008

Fry CH, Fry K, Harris A (2010) Kingfishers, bee-eaters and rollers. Bloomsbury Publishing. http://qut.eblib.com.au/patron/FullRecord.aspx?p=624022. Accessed 20 January 2020

Gil-Delgado JA, Guijarro D, Gosálvez RU, López-Iborra GM, Ponz A, Velasco A (2017) Presence of plastic particles in waterbirds faeces collected in Spanish lakes. Environ Pollut 220:732–736. https://doi.org/10.1016/j.envpol.2016.09.054

Giesy JP, Feyk LA, Jones PD, Kannan K, Sanderson T (2003) Review of the effects of endocrine-disrupting chemicals in birds. Pure Appl

Chem 75(11–12):2287–2303. https://doi.org/10.1351/pac200375112287

Gochfeld M, Gochfeld DJ, Minton D, Murray BG, Pyle P, Seto N, Smith D, Burger J (1999) Metals in feathers of bonin petrel, Christmas shearwater, wedge-tailed shearwater, and red-tailed tropicbird in the Hawaian Islands, Northern Pacific. Environ Monit Assess 59(3):343–358. https://doi.org/10.1023/A:1006134125236

Hammer S, Nager RG, Johnson PCD, Furness RW, Provencher JF (2016) Plastic debris in great skua (*Stercorarius skua*) pellets corresponds to seabird prey species. Mar Pollut Bull 103(1–2):206–210. https://doi.org/10.1016/j.marpolbul.2015.12.018

Holland ER, Mallory ML, Shutler D (2016) Plastics and other anthropogenic debris in freshwater birds from Canada. Sci Total Environ 571:251–258. https://doi.org/10.1016/j.scitotenv.2016.07.158

Kay P, Hiscoe R, Moberley I, Bajic L, McKenna N (2018) Wastewater treatment plants as a source of microplastics in river catchments. Environ Sci Pollut Res 25(20):20264–20267. https://doi.org/10.1007/s11356-018-2070-7

Lahens L, Strady E, Kieu-Le TC, Dris R, Boukerma K, Rinnert E, Gasperi J, Tassin B (2018) Macroplastic and microplastic contamination assessment of a tropical river (Saigon River, Vietnam) transversed by a developing megacity. Environ Pollut 236:661–671. https://doi.org/10.1016/j.envpol.2018.02.005

Mani T, Hauk A, Walter U, Burkhardt-Holm P (2016) Microplastics profile along the Rhine River. Sci Rep 5(1):17988–17968. https://doi.org/10.1038/srep17988

McGoran AR, Clark PF, Morritt D (2017) Presence of microplastic in the digestive tracts of European flounder, *Platichthys flesus*, and European smelt, *Osmerus eperlanus*, from the River Thames. Environ Pollut 220:744–751. https://doi.org/10.1016/j.envpol.2016.09.078

Nessi A (2020) Analisi della dieta e presenza di microplastiche in borre di martin pescatore (*Alcedo atthis*) nella valle del Ticino. University of Milan, Master thesis

Nicastro KR, Lo Savio R, McQuaid CD, Madeira P, Valbusa U, Azevedo F, Casero M, Lourenço C, Zardi GI (2018) Plastic ingestion in aquatic-associated bird species in southern Portugal. Mar Pollut Bull 126:413–418. https://doi.org/10.1016/j.marpolbul.2017.11.050

Reynolds C, Ryan PG (2018) Micro-plastic ingestion by waterbirds from contaminated wetlands in South Africa. Mar Pollut Bull 126:330–333. https://doi.org/10.1016/j.marpolbul.2017.11.021

Roman L, Lowenstine L, Parsley LM, Wilcox C, Hardesty BD, Gilardi K, Hindell M (2019) Is plastic ingestion in birds as toxic as we think? Insights from a plastic feeding experiment. Sci Total Environ 665:660–667. https://doi.org/10.1016/j.scitotenv.2019.02.184

Smiroldo G, Balestrieri A, Pini E, Tremolada P (2019) Anthropogenically altered trophic webs: alien catfish and microplastics in the diet of Eurasian otters. Mammal Res 64(2):165–174. https://doi.org/10.1007/s13364-018-00412-3

Vilches A, Miranda R, Arizaga J (2012) Fish prey selection by the common kingfisher *Alcedo atthis* in Northern Iberia. Acta Ornithol 47(2):169–177. https://doi.org/10.3161/000164512X662278

Wesch C, Bredimus K, Paulus M, Klein R (2016) Towards the suitable monitoring of ingestion of microplastics by marine biota: a review. Environ Pollut 218:1200–1208. https://doi.org/10.1016/j.envpol.2016.08.076

PAPER 3 – Does mechanical stress cause microplastic release from plastic water bottles?

Anna Winkler, Nadia Santo, Marco Aldo Ortenzi, Elisa Bolzoni, Renato Bacchetta, Paolo Tremolada

Water Research 2019

Water Research 166 (2019) 115082

Contents lists available at ScienceDirect

Water Research

journal homepage: www.elsevier.com/locate/watres

Does mechanical stress cause microplastic release from plastic water bottles?

Anna Winkler [a], Nadia Santo [b], Marco Aldo Ortenzi [c], Elisa Bolzoni [a], Renato Bacchetta [a, *], Paolo Tremolada [a]

[a] Department of Environmental Science and Policy, University of Milan, Via Celoria 26, 20133, Milan, Italy
[b] Unitech NOLIMITS, Imaging facility, University of Milan, Via Golgi 19, 20133, Milan, Italy
[c] CRC Materiali Polimerici (LaMPo), Department of Chemistry, University of Milan, Via Golgi 19, 20133, Milan, Italy

ARTICLE INFO

Article history:
Received 24 June 2019
Received in revised form
9 September 2019
Accepted 11 September 2019
Available online 13 September 2019

Keywords:
Microplastic sources
Drinking water
Scanning electron microscopy
Water bottles
Plastic degradation

ABSTRACT

Plastic particle ingestion has become of concern as a possible threat to human health. Previous works have already explored the presence of microplastic (MP) in bottled drinking water as a source of MP intake. Here, we consider the release of MP particles from single-use PET mineral water bottles upon exposure to mechanical stress utilizing SEM plus EDS, which allows the implementation of morphological and elemental analysis of the plastic material surface and quantification of particle concentrations in sample water. The aim of this study was to better evaluate the sources of MP intake from plastic bottles, especially considering the effect of daily use on these bottles such as the abrasion of the plastic material. For that, we analysed MP release of PET bottlenecks and HDPE caps on their surfaces after a series of bottle openings/closings (1 x, 10 x, 100 x). Furthermore, we investigated, if the inner surface of the PET bottles released MPs, counted particle increase of the water and identified MPs in the PET bottled water after exposing the bottles to mechanical stress (squeezing treatment; none, 1 min, 10 min). The results showed a considerable increase of MP particle occurrence on the surface of PET and HDPE material (bottlenecks and caps) after opening and closing the bottles. After 100 times the effect was impressive, especially on caps. Moreover, great differences exist in cap abrasion between brands which uncovers a discrepancy in plastic behavior of brands. Interestingly, particle concentrations in the bottled mineral water did not significantly increase after exposure to mechanical stress (squeezing treatment). The morphological analysis of the inner wall surface of the bottles supported this observation, as no stress cracks could be detected after the treatment, implying that the bottles itself are not a consistent source of MP particles after this extent of mechanical stress. However, chances of MP ingestion by humans increase with frequent use of the same single-use plastic bottle, though only from the bottleneck-cap system.

1. Introduction

Microplastic (MP) contamination of food and drinking water is a topical area of plastic pollution investigations. Triggered by the numerous studies on MP occurrence in our environment, and reinforced by the detection of MPs in human stool (Liebmann et al., 2018), plastic pollution has become of concern as potential threat to human health, too. Sources of MP ingestion by humans have already been discussed in several studies (Bouwmeester et al., 2015; Galloway, 2015; Lehner et al., 2019; Schirinzi et al., 2017; Wright and Kelly, 2017). Moreover, the recent studies by (Mason et al., 2018; Ossmann et al., 2018; Schymanski et al., 2018; Zuccarello et al., 2019), attracted the attention of researchers and the general public as they confirmed the presence of MPs in bottled drinking water. Reported particle concentrations differ substantially among these studies due to the application of different methods of sampling, isolating, purifying and identifying MPs, which vary greatly among studies. Moreover, (Koelmans et al., 2019) questions the quality of occurrence studies and highlights

Abbreviations: EDS, Energy dispersive X-ray spectroscopy; HDPE, High density polyethylene; LDPE, Low density polyethylene; PE, Polyethylene; PET, Poly(ethylene terephthalate); PP, Polypropylene; PS, Polystyrene; PVC, Poly(vinyl chloride); SEM, Scanning electron microscopy.

* Corresponding author.
E-mail address: renato.bacchetta@unimi.it (R. Bacchetta).

https://doi.org/10.1016/j.watres.2019.115082
0043-1354/

the need for a standardization of MP analysis improvement of quality assurance.

The most produced types of plastic worldwide are used for packaging and they are polyethylene (PE) - mainly in its low-density form (LDPE; bin bags, plastic wraps, shopping bags) and high-density form (HDPE; shopping bags, bottle caps, detergent bottles), polypropylene (PP; yoghurt packaging, straws, semi-rigid containers), polystyrene (PS; foamed food containers, plastic cutlery), polyvinyl chloride (PVC, toys, pipes) and polyethylene terephthalate (PET; bottles, food trays). The essential compounds of plastics are chains of monomers, mostly deriving from non-renewable fossil fuel, which are molecules capable of combining to form a polymer (UNEP, 2016). To alter the physico-chemical properties of the polymers (such as flame resistance, colour, plasticity/viscosity and lubricity) other chemicals (e. g. bisphenol A, phthalate, fatty acids) can be added to the polymer itself (Hammer et al., 2012). Some of the chemical additives, as well as some monomers used for the synthesis of polymers, are classified as hazardous to human health and the environment. In fact, when released through use and degradation of plastic products, they can be mutagenic and/or carcinogenic, or act as endocrine disruptors (Lithner et al., 2011). However, very little information is available on the toxic potential of MPs and their additives, which strongly depends on size and shape of the plastic particles and dose of the released chemical additives (Waring et al., 2018).

Considering the potential harmful effects of MPs, there is a significant need to better understand possible sources of MP intake to assess quantities and risks related to their properties. Indeed, reports focusing on MPs in bottled mineral water are very scarce, and the reported works have explored solely the presence of MPs in the bottled water. Here, we considered also the release of MP particles (wear particles and fragments from breakage) of single-use water bottles upon exposure to mechanical stress, utilizing scanning electron microscopy (SEM) in conjunction with energy-dispersive X-ray spectroscopy (EDS). While EDS provided spectra revealing the elemental compositions of particles, SEM images were used to quantify detected particles and to morphologically examine all the bottle components. Furthermore, we implemented an additive analysis on HDPE caps of the three brands by gas chromatography/mass spectrometry to determine the lubricant substances and their corresponding concentrations. The final goal of the present study was to better evaluate single-use plastic bottles as one of proven sources of MP intake by humans, especially considering the effects of daily use on these bottles such as the abrasion of the plastic material. For that, we (1) analysed MP release of PET bottlenecks and HDPE caps on their surfaces after a series of bottle openings/closings, (2) performed a morphological analysis of the PET bottle inner wall surface after a squeezing/crushing treatment, and (3) subsequently counted particle increase and identified MPs in the PET bottled water.

2. Material and methods

2.1. Sample material and preparation

For the analysis of particle release from bottle material upon exposure to mechanical stress, three different mineral water bottles (0.5 L) were chosen based on the bottle texture (plastic thickness and, hence, bottle weight). Generally, sparkling and not-sparkling water are associated with heavier and lighter bottles respectively, with thickness/weight differences among brands. We selected three brands representative for light, medium and heavy bottles, to test their reaction to mechanical stress. Mineral water bottles of the selected brands were purchased in Italian supermarkets, in a set of 6 in order to have replicates within the same lot of bottles. All samples were single-use bottles made of PET with screw caps made of HDPE. The water types and bottle net-weights (without cap and label) were: natural water in 9.61 g bottles (Brand 1), sparkling water in 12.03 g bottles (Brand 2), and sparkling water in 16.03 g bottles (Brand 3). Cap weights of respective brands were: 1.15 g, 1.27 g and 1.78 g for Brand 1, 2, 3, respectively. By including different bottle and cap net-weights, the effect of flexibility of PET and HDPE material could be taken into consideration. A complete scheme of the experimental plan, which includes bottleneck and cap analyses (section 2.1.1), bottle water and bottle-inner-wall-surface analyses (section 2.1.2) is shown in Fig. 1. Images of the bottles of the three brands after mechanical stress are presented in Supporting Information S1.

2.1.1. Bottlenecks and caps

MP particle release from bottleneck and cap material from the three brands was studied after an opening and closing procedure. Three treatments were implemented; for the first one, bottles were opened only once in order to analyse bottleneck and cap from the inside, for the second treatment bottles were opened/closed 10 times and, for the third one, 100 times (with 1-min pause every 20 times). The treatments were applied on a second set of bottles from each brand to obtain a true replicate for each treatment and bottle brand, while the same treatment on bottles of different brands represented pseudo-replicates for the applied treatment. Particular emphasis was laid on using the same pressure (same operators) and pressure point when turning the caps. This section (marked before procedure) was then analysed by SEM for all brands and treatments in order to have consistent analyses among samples. Bottlenecks and caps were removed closed from the bottle by a scalpel and stored until analysis in order to avoid post-treatment contaminations. Precautions to avoid post-treatment contaminations are described later, because they were taken also for the analysis of the inner surface of the plastic bottle and for water filtrates.

2.1.2. Bottle water and bottle inner wall surface

To identify a potential MP release from bottle inner wall surface upon mechanical stress, bottles of the three brands were treated the following; no treatment at all, 1 min and 10 min of rolling the bottles on a smooth surface under a vessel having a weight of 5 kg at the speed of one complete bottle round per second. This treatment was performed to mimic the squeezing/crushing effects that plastic bottles are subjected to during handling and use, particularly when re-using the bottles. In order to carry out the treatment, it was necessary to beforehand remove 250 mL water from the initial volume of each bottle. Therefore, the sample volume in each bottle was 250 mL.

Each water sample was filtered via vacuum using an in-house manufactured glass filtration apparatus that allows filtering up to four samples simultaneously (three samples and a blank) but can individually regulate the vacuum (Supporting Information S2). Samples were filtered in blocks of samples of the same brand. For that, sample water was poured into the respective reservoir flasks and covered with aluminium foil. To prevent filtering air, vacuum was turned off subsequent to water addition. The filters (specified below) were carefully removed and attached onto standard SEM stubs immediately after filtration. Then, they were placed within a glass container and dried for 48 h in a glass desiccator.

In order to identify a potential MP source from the bottle inner wall, a piece of bottle wall was taken from the same area of each bottle after the water filtration (Supporting Information S1). The plastic piece was cut out of the bottle with a scalpel, avoiding abrasions, and the inner surface mounted on standard aluminium stubs and kept within a glass container until SEM analysis. Bottle

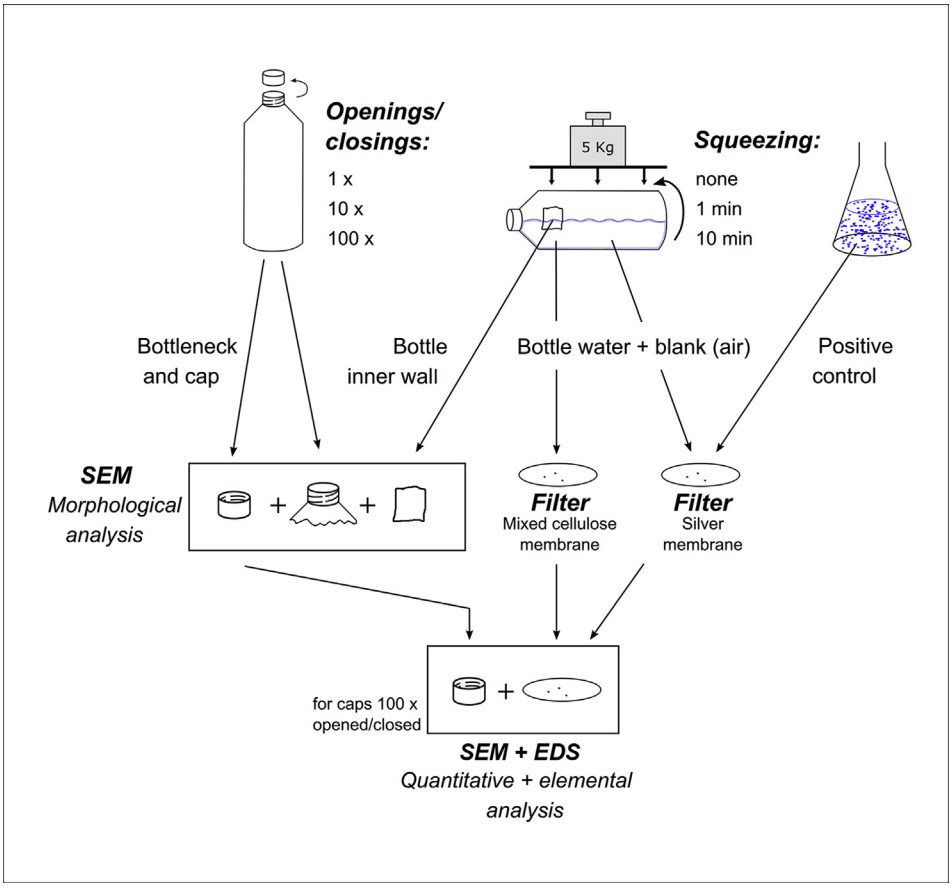

Fig. 1. Experimental draw of all processes performed in this study including sample preparation, sample processing and analysis.

water and bottle-inner-wall-surface analyses were repeated twice for three bottles. However, in the second replicate of the filtered bottle water, we decided to change the filters in order to obtain a better ratio between the SEM analysed area and the filtered one. The analysed area could not be increased, unless loosing minimum-size detection; therefore, lowering the filtering area was the only feasible solution for raising the analysed/filtered area ratio (details are reported in section 2.4).

2.2. Blanks and positive control

To assess sample contamination during the procedure in the lab (particle deposit), we included procedural air blank samples using the same filter used for water analyses. Air blank samples underwent the same procedure as the water sample (experimental set up, filtration, transport, storage, preparation for analysis, analysis itself).

Furthermore, three positive control samples of standard MP in 250 mL Milli-Q filtered water served as a functionality control for the full-applied methodology. For this purpose, a MP solution was prepared by suspending 6.23 µL of a standard polystyrene solution (50 g/L, dark blue, calibrated particle size: 2.91 µm, density: 1.51 g/cm^3, Sigma-Adlrich Chemie GmbH, Steinheim, Germany) in 1 L ultrapure Milli-Q water (filtered three times through glass fibre membrane, pore size: 0.7 µm), resulting in a concentration of ~16,000,000 particles/L (p/L). Dilution by 1:10 and 1:100 provided the following concentrations: ~1,600,000 p/L and ~160,000 p/L. Subsequently, 250 mL of each MP solution (containing ~4,000,000, ~400,000 and ~40,000 particles) were filtered as described in section 2.1.2 on silver membrane filters and quantitatively analysed by SEM (Supporting Information S3). MP bead numbers were counted in 10 randomly selected fields, and the mean counted numbers for the three dilutions were extrapolated to the total filtered particles, based on the analysed/filtered area ratio. The filtration process was considered as applicable when counted and extrapolated concentration of MP beads matched the expected MP concentration of the control sample. For the first control solution, a mean of 52.2 ± 4.9 standard deviation (SD) MP beads were counted, corresponding to a total extrapolated number of 3,866,000 ± 362,900 (4,000,000 expected). In the second control, a mean of 90.5 ± 15.6 (SD) MP beads were counted, corresponding to an extrapolated number of 606,000 ± 104,500 (400,000 expected), and the third control showed a mean of 8.7 ± 3.5 (SD) MP beads, corresponding to an extrapolated number of 58,300 ± 23,500 (40,000 expected). The analysis of SEM images of the positive control samples revealed acceptable matches of expected and actually counted MP beads in the three control solutions, even if precision and accuracy decreased when lowering the concentration.

It is worth mentioning that applied glass fibre filters, which were used to prepare Milli-Q water for the control solution, released glass fibres into our stock solution. Hence, the stock solution contained glass fibres which were filtered amongst the MP beads (Supporting Information S3), highlighting the problem of a safe use of such filters and of particles released by the filters in general.

2.3. Precautions to reduce contamination and loss of sample material

To minimise background contamination during the analysis, samples were placed in closed glass containers whenever

transported or stored. Preparation of the water samples was performed in a laminar flow box, which was previously cleaned with ethanol. All glassware (such as the filtration apparatus) was first cleaned and then rinsed with deionized water. Executive persons wore cotton lab coats and washed their hands regularly.

2.4. SEM imaging and EDS analyses

The combination of SEM and EDS provides high resolution imaging of material surface structures as well as elemental composition signatures in order to confirm the nature of particles. After samples were attached onto standard SEM stubs and coated with a thin film of evaporated gold, they were placed in a Zeiss LEO 1430 SEM coupled with an Oxford detector for EDS analysis.

For the morphological analysis of the inner surface of bottle material samples (bottleneck, cap and bottle inner wall), SEM images were taken from different areas of a sample with varying magnifications (15-1000 X). The areas were chosen consistently (applying a consistent pattern) within a sample kind. Operating conditions were: accelerating voltage 10−20 kV, probe current 80 μA, and working distance varying from 10.0 to 15.0 mm. SEM images of caps (from bottles opened/closed 100 x) were further processed to count particles on the sample material. For that, particles within a vertical line of the sample (from the top to the bottom edge of the inner cap surface, magnification 750 X, consistent over all samples) were counted and their area measured automatically with the image process program ImageJ (Supporting Information S4). To account for irregularities of the detected particles, reported sizes refer to the diameter of a spherical particle of the same area as the detected, irregular particle. To give indications about MP particle densities on caps, counted particle numbers in analysed areas were reported as MP particles/mm^2 (MPs/mm^2) inner surface of cap.

Subsequently, HDPE cap material from bottles that were opened and closed 100 times was inspected for elemental analysis with EDS. For that, individual candidate microplastic particles on bottle cap samples were analysed using the Oxford Instruments INCA ver. 4.04 software (Abingdon, UK). The smallest particle size analysed was 3 μm. Preoperational EDS tests on pure HDPE cap and PET bottle material resulted in an elemental composition of 100% carbon for HDPE with trace of gold (1%) deriving from the coating procedure and for PET in an elemental composition ratio of C:O = 73:27 (always with a gold trace), with 5% variability for each element and no significant differences between the three brands. The measured elemental composition corresponds to the composition stoichiometry of C:O ratio in PET ($(C_{10}H_8O_4)_n$) and PE ($(C_2H_4)_n$), giving that hydrogen doesn't give a detectable peak in the EDS spectrum. A particle found on bottle cap sample was identified as PET or HDPE when EDS spectra revealed the same elemental composition and when measured peaks matched those of spectra from the preoperational test.

Filtered particles from bottle water were analysed for elemental composition by EDS. All elemental signatures were documented. Particles on filters were identified as PET when measured peaks matched those from spectra in the preoperational tests and when analysed C:O ratio lied within the variability range of preoperational measured elemental composition. An elemental composition of 100% carbon indicated polymeric origin, such as PE (HDPE or LDPE), PP or PS, but could not be further specified since these polymers consist of no other elements besides carbon and hydrogen to distinguish them from each other. SEM images of analysed areas were taken and area and shape of all detected particles were measured with the image process program ImageJ (Schneider et al., 2012). Again, to account for irregularities of the detected particles, reported sizes refer to the diameter of a spherical particle of the same area as the one detected. As reported in section 2.1.2, in order to obtain a better ratio between the SEM analysed area and the filtered one, the second set of water samples was filtered on different filters. The first replicate's filter consisted of a mixed cellulose ester membrane (0.45 μm pore size, 25 mm diameter, filtration area 176.6 mm^2) and had an analysed area/filter area ratio of 0.67% (resulting from 50 analysed vertically fields and 50 fields horizontally, magnification: 1000 X, total analysed area 0.012 mm^2), while the second replicate's filters was a silver membrane filter (0.8 μm pore size, 13 mm diameter, filtration area 19.6 mm^2) with an analysed area/filter area ratio of 5.54% (20 fields vertically, 20 fields horizontally, magnification: 500 X, total analysed area 0.027 mm^2. Procedural blanks were analysed the same way.

2.5. Chemical analyses of lubricants

Lubricant analyses were performed by solvent extraction and Gas-Chromatography detection (GC), according to Garrido-López et al. (2006). Briefly, one cap of each brand was sectioned by steel scissors in small pieces nearly of the same size of a HDPE sample used as positive control, consisting of small HPDE pellets containing 10% of behenamide. Samples were extracted with 2-propanol (Sigma Aldrich, Schnelldorf, Germany) in a soxhlet apparatus (FALC Instruments, Lurano, Italy). Samples were then concentrated by a Rotary Evaporator (Laborota 4000, Heidolph Instruments, Schwabach, Germany) until dryness and dissolved in 2 mL of the same solvent under 20 min of sonication. For the lubricant identification and quantification in caps, the GC and Mass Spectrometer Trace ISQ QD Single Quadrupole GC-MS (Thermo Fisher) was used. An aliquot of 1 μL was injected in Splitless Mode in a Zebron-5MS plus capillary column (60 m; 0.32 mm; 1 μm). Oven program started at 200 °C for 0 min, then 10 °C/min to 280 °C for 0, finally 10 °C/min to 340 °C for 30 min. Run time was 44 min. Helium was used as carrier gas at the flow rate at 1.2 mL/min. Inlet temperature, MS transfer line and the ion source was 300 °C. Ionization was obtained by electron impact at 70 eV and acquisition mode operated by full scan for selecting ions of interest and by SIM mode for quantification. The qualifier ions having m/z of 59, 72, 128, and 339 and those having m/z values of 59, 72, 126, and 337 were selected for behenamide and erucamide quantification. Behenamide and erucamide analytical standards were purchased by Sigma Aldrich (Schnelldorf, Germany) and dissolved in 2-propanol.

Analyses were performed by external calibration curves using peak area as independent variable; correction for recovery was applied. Each sample was injected twice, and the mean value was considered for quantification. Quality assurance (QA) and quality control (QC) were performed by procedural blanks, replicates analyses and recovery tests. No peaks were detected in blank and the positive control sample gives a recovery of 72%.

2.6. Statistical analyses

Statistically analysis was implemented on the particle concentration in bottled mineral water (particles per 250 mL sample volume) identified by SEM using the RStudio statistical software. Two-way ANOVA with $p < 0.05$ was applied to test for possible effects of treatment (mechanical stress) and bottle weight (brand). Dunnett's test with $p < 0.05$ was applied to test for differences between blanks and bottle water samples. Further statistical analysis was performed on particle dimensions of filtered bottle water and air blanks using the SPSS statistical software. Mann-Whitney test with $p < 0.05$ was applied to test for differences between particle sizes in water and blanks. Kruskal-Wallis tests with $p < 0.05$ were used to test for differences between particle sizes among treatments and brands.

3. Results

3.1. Microplastic on caps and bottlenecks

The opening/closing treatment showed a strong effect on cap material (Fig. 2). On caps opened just once (in order to perform the analysis), we observed no evident signs of deformation and no evident particle release. We detected only few single flakes of polymer half detached at the edge of the closing sectors. Since caps showed no signs of abrasions, it seemed very likely that these deformations derived from the production processes (injection molding). On caps opened/closed 10 times, loose particles were still not abundant, but we noted an increase in the effects of mechanical stress on cap structures. Interestingly, caps from Brand 2 bottles showed the worst condition with deep signs of abrasion and abundant material detached from the cap structure. Samples of bottle caps deriving from bottles opened/closed 100 times showed impressive signs of mechanical stress such as abrasions and deep grooves (Fig. 2). At higher magnification, the effects detected on caps after mechanical stress were even worse increasing the magnitude of damages and the number of released particles in the low dimensional range (Fig. 3). In detail we observed tears and widespread abrasions (Fig. 3A and B), torn up particles (Fig. 3C) and numerous detached particles even on bottleneck rings (Fig. 3D).

Among the three brands, caps of Brand 2 showed the worst state in both abrasion and detached particles. In order to confirm these results, caps and bottlenecks were prepared again on new bottles, and similar results were obtained. To quantify the effect of particle release from the three caps, all particles, along a vertical line from the cap edge to the cap bottom of the bottles opened/closed 100 times, were counted and measured.

Results of the particle density analysis of these cap samples confirmed major differences between brands, revealing caps from Brand 2 to release exceedingly more MPs than Brand 1 and 3 (Fig. 4A).

Extrapolating the HDPE particle density to the entire inner cap surface, we obtained a total particle number of 63,400, 1,225,500 and 333,800 for caps of Brand 1, 2 and 3, respectively. Of all three brands, detached MPs varied in size ranging from 0.54 to 39.9 μm. The majority of these MPs fell into the size category of 1 - <5 μm (64%), then in the size range of 0.5 - <1 (25%) μm, and finally those in the range 5 - <40 μm (11%). Hence, nearly 90% of released particles were <5 μm. However, caps from Brand 2 and 3 released relatively more smaller particles (0.5 - <1 μm) than from Brand 1 (Fig. 4B), though a correlation with cap weight could not be identified.

Fig. 5 shows the extent of mechanical stress to bottleneck samples. In bottles opened/closed 1 and 10 times, bottlenecks of the three brands did not show any evident sign of abrasion, and only after 100 times, signs of mechanical damage were observed. This goes in line with the known differences in the material hardness, with PET generally being harder than HDPE (average hardness of HDPE is 65 Shore D, whereas for PET is 85 Shore D according to (ASTM, 2015)). No free particles have been observed on the necks of 1-time-opened bottles, and very few have been found on those opened/closed 10 times. The picture changed in the samples from bottles opened/closed 100 times, showing many particles spread on their neck, near the edge of the bottle or attached to the closing rings (Fig. 5).

Since PET and HDPE displayed different EDS spectra, particles of these two materials could be easily distinguished from each other. On HDPE cap samples we randomly selected 10 particles per brand; 9 out of 10 (two brands) and 10 out of 10 (the third) analysed

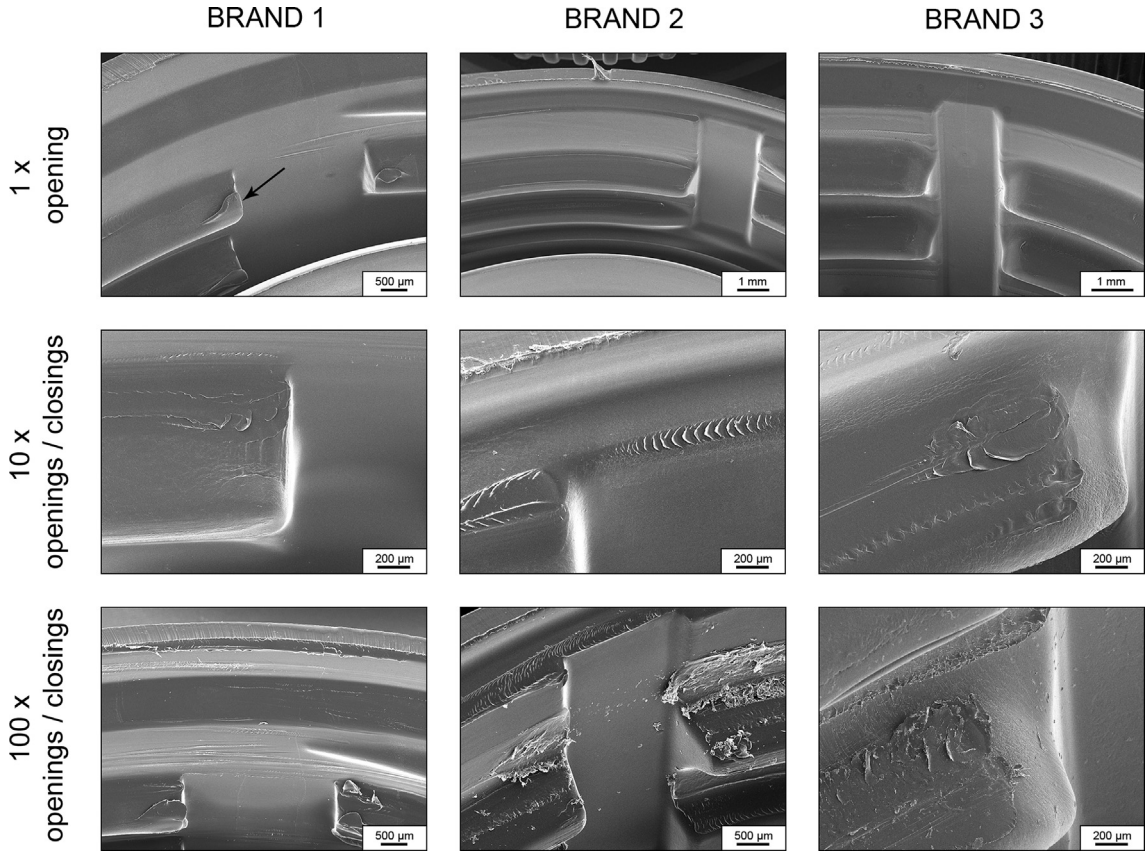

Fig. 2. SEM images of HDPE caps from the three considered brands after exposure to mechanical stress.

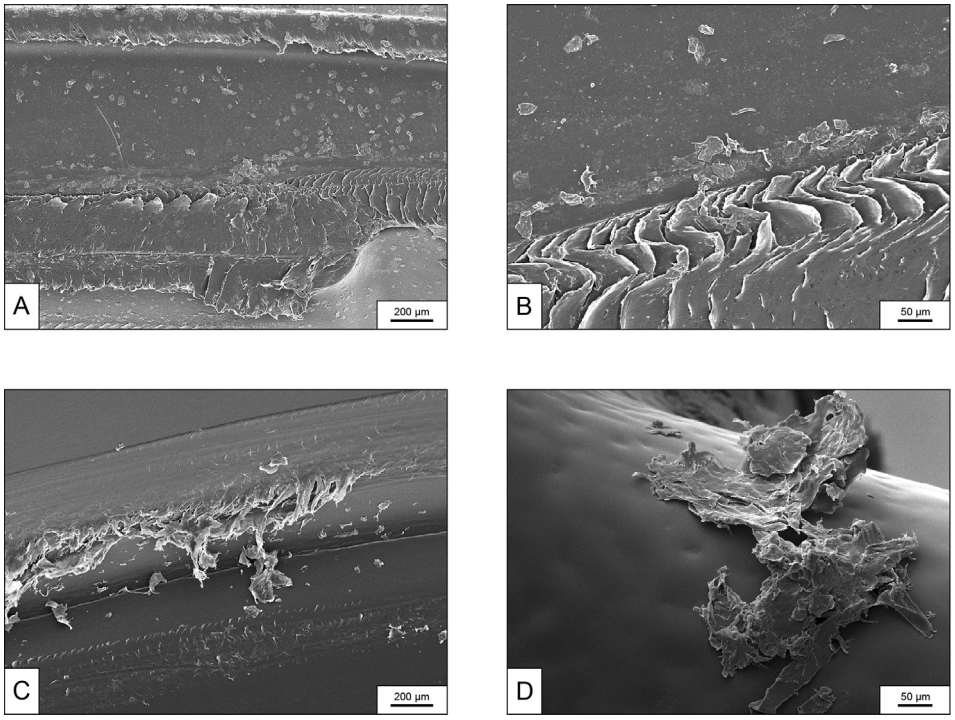

Fig. 3. SEM images showing the effects of repeated opening/closing treatments (100 x) on cap (A–C) and bottleneck(D).

particles consisted of 100% carbon, which is consistent with HDPE. This result clearly indicated that nearly all of them came from their respective caps and not from bottleneck which is made of PET (carbon and oxygen peaks in the spectra). The two not identified particles showed EDS spectra characterized mainly by carbon but having only traces of oxygen not enough to be consistent with PET composition. The obtained results go in line with the different hardness of PET and HDPE and indicated the cap as the weakest link of the system. An exemplary HDPE particle with its respective spectrum is shown in Fig. 6.

Results from GC/MS analyses showed that caps from Brand 1 bottles did not present peaks corresponding to the analysed lubricants, while caps from Brand 2 and Brand 3 bottles contained 1.0% and 0.08% of behenamide, respectively. Caps with the highest release of particles (Brand 2) contained the highest lubricant content (1% behenamide).

3.2. Microplastic on PET inner surface

Looking for a possible MP release from the bottle inner wall surface due to mechanical stress, bottle samples of the three brands were analysed by SEM. Morphological analyses of their respective inner walls revealed PET to be resistant towards the treatment procedure, without showing severe effects of mechanical damage. PET resulted as a polymer with a very ductile behavior: samples from no-treated-bottles and from bottles squeezed for 1 min did not show any differences in material morphology, and also bottles subjected to 10 min treatment showed no evidence of breaks or abrasions, some deformation lines excluded (Fig. 7). At our experimental conditions and at RT (21–22 °C) the viscoelastic nature of PET is not questioned and no release of wear particles was observed in the samples, independently from both the brand and treatment time.

3.3. Microplastic in bottled water

The comparison of particle numbers in water samples exposed to the three treatments on silver filters was compatible to the results obtained on cellulose filters. Against our assumptions, brands and treatments had no significant influence on particle concentration in water (two-way ANOVA: $F_{2,4} = 4.29$, $p = 0.10$ and $F_{2,4} = 6.10$, $p = 0.06$, respectively). The mean total particle number in water samples on silver filters was 980 ± 320 Standard Error (SE) per L. No significant differences existed between the total number of particles in blank and bottle water samples of the three treatments (Dunnett, $p = 0.23$, $p = 0.26$ and $p = 0.91$ for 0, 1 and 10 min, respectively). However, the particle size distribution between blanks and bottle water samples differed significantly (Mann-Whitney, $p < 0.001$) (Fig. 8A). In fact, the majority (almost 90%) of particles in procedural blanks were of small size (<5 µm), while in water samples about half of the particles were bigger (>5 µm) (Supporting Information S5). Examples of particles with different shapes found in our samples can be seen in Supporting Information S6. Comparison of particle sizes between the three treatment and the three brands showed no significant differences (Kruskal-Wallis, $\chi^2 = 1.2$; d.f. = 2; $p = 0.28$ and $\chi^2 = 2.5$; d.f. = 2; $p = 0.28$, respectively). These results confirmed the analyses on the total number of particles and on those ≥3 µm (Fig. 8B), which were those analysed for the elemental composition to discriminate MPs from other materials (two-way ANOVA: $F_{2,4} = 5.19$, $p = 0.08$ and $F_{2,4} = 3.70$, $p = 0.12$, for brands and treatments, respectively). The identification by elemental analysis of the number of MPs is more interesting than the total number of particles, even though the instrumental limit allowed us to consider only particle ≥3 µm.

Elemental analyses performed on 58 particles on cellulose filters revealed that only two particles (3.4%) had a C:O ratio corresponding to that of PET, 17 (29%) had a slightly different C:O ratio, thus could not be confirmed as PET, and the remaining 39 (69%) showed variable elemental compositions. The two PET particles derived: one from water of no-treatment bottle from Brand 3 (3.3 µm), and the other from water of the 10 min treatment bottle from Brand 2 (25.4 µm). On silver filters, out of 50 analysed particles, one particle showed an elemental composition of 100% carbon,

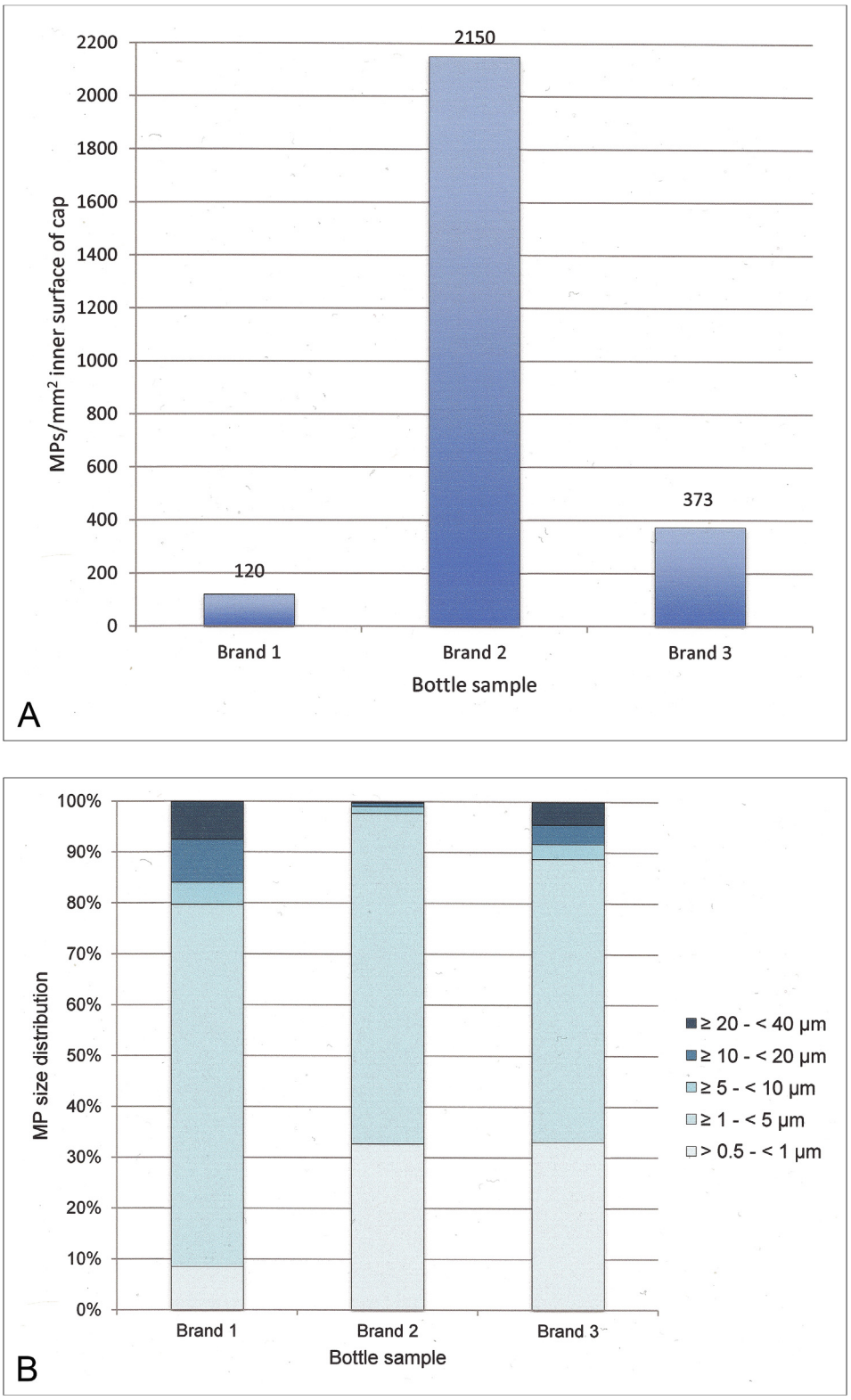

Fig. 4. (A) MP particle density on inner surface of HDPE caps (opened/closed 100 x) for the three water bottle brands. (B) Comparison of size distribution of MP particles between different brands.

consistent with the HPDE of the cap (Fig. 9A) and three with a C:O ratio corresponding to that of PET (Fig. 9B) reaching 8% of MPs on total particles. Among the other, 12 (24%) had a slightly different C:O ratio, and 34 (68%) showed a variable composition mainly with Si, Ca and Fe (Fig. 9C). Interestingly, the morphological features of the particle with 100% C (Fig. 9A) were very similar to those derived from cap abrasion (for comparison see Figs. 3C–D and 6). The particle consistent to HDPE (28 µm), and the three corresponding to

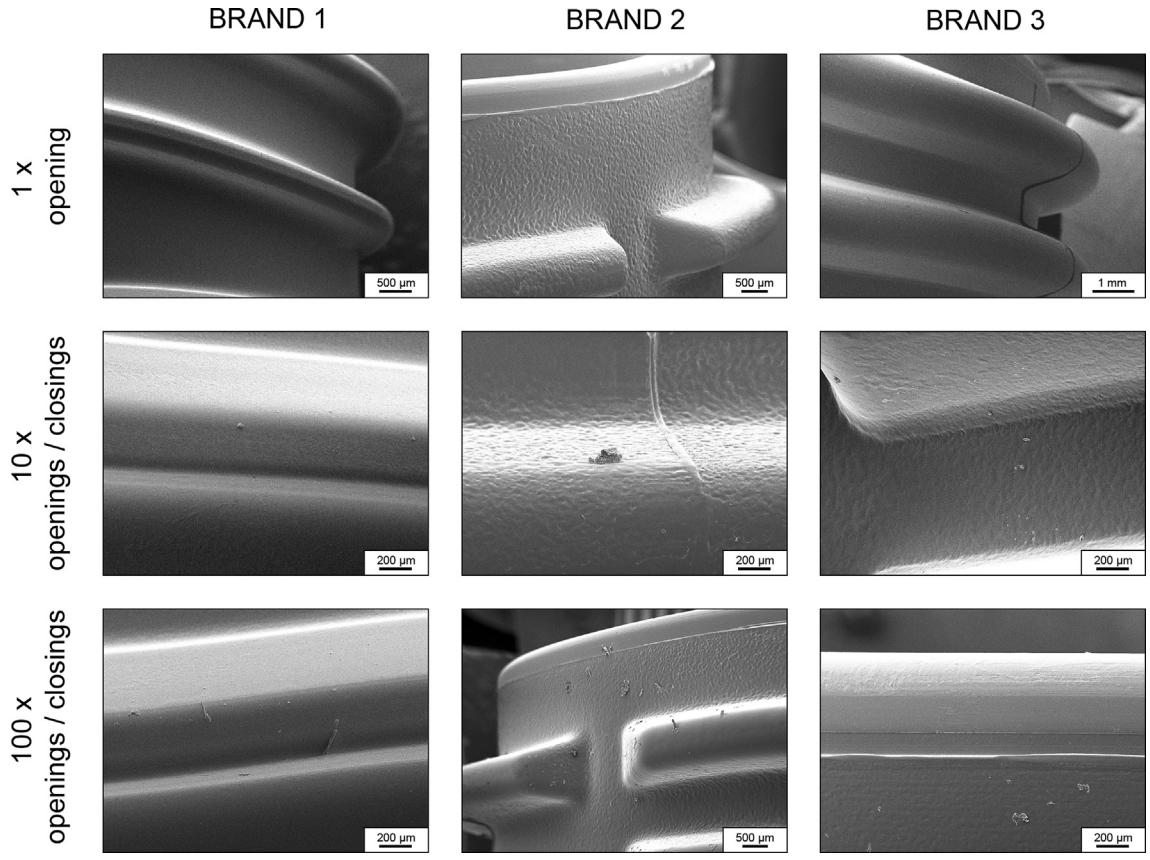

Fig. 5. SEM images of PET bottlenecks from bottle of the three considered brands after exposure to mechanical stress.

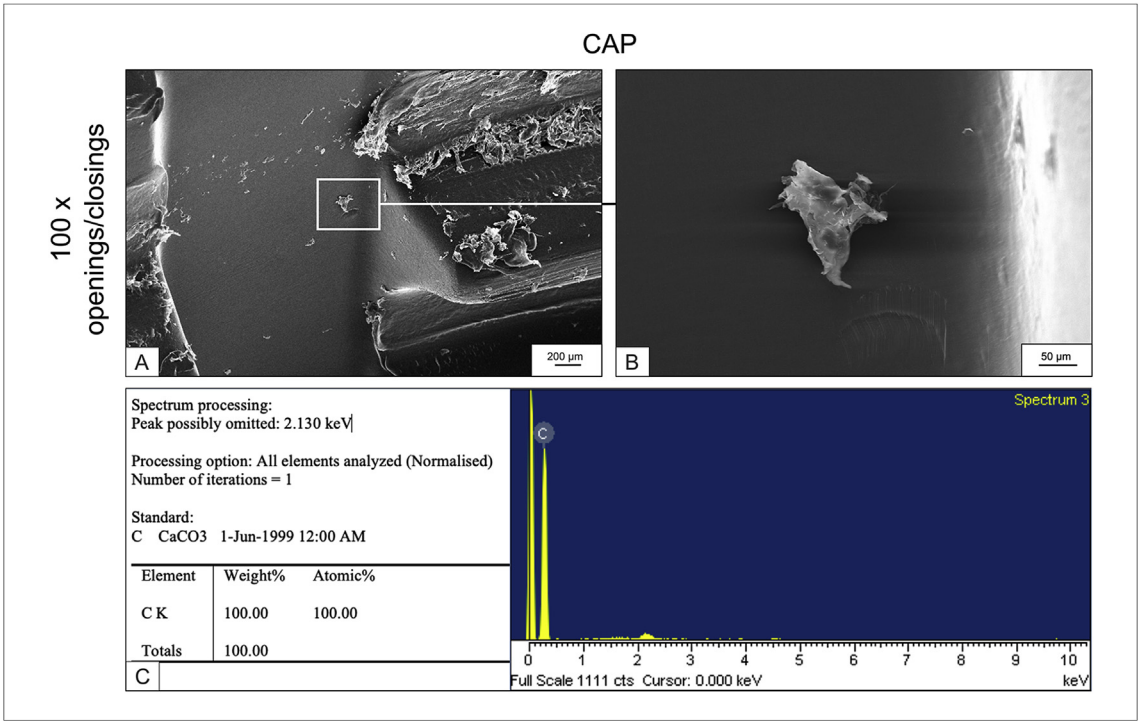

Fig. 6. (A + B) SEM images of HDPE fragments detached from cap after exposure to mechanical stress (100 x opened/closed). (C) EDS spectrum of particle B confirming HDPE material (after removal of the element Au, which derives from the gold cover). (For interpretation of the references to colour in this figure legend, the reader is referred to the Web version of this article.)

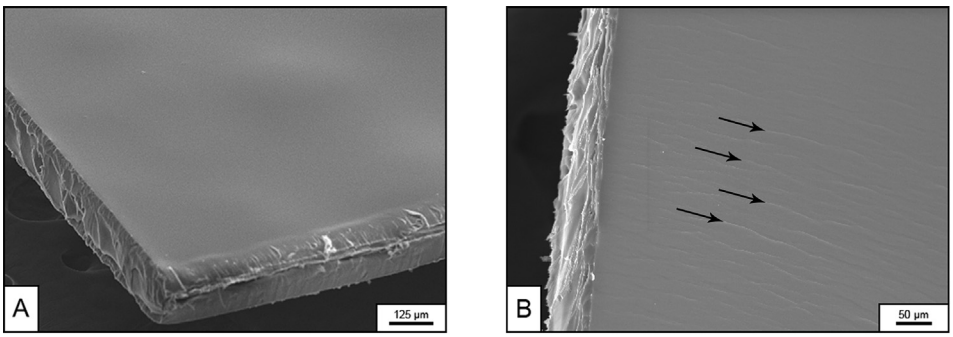

Fig. 7. SEM images of bottle inner wall samples. A: 0 min treatment (control); B: sample subjected to mechanical stress for 10 min with some deformation lines (arrows).

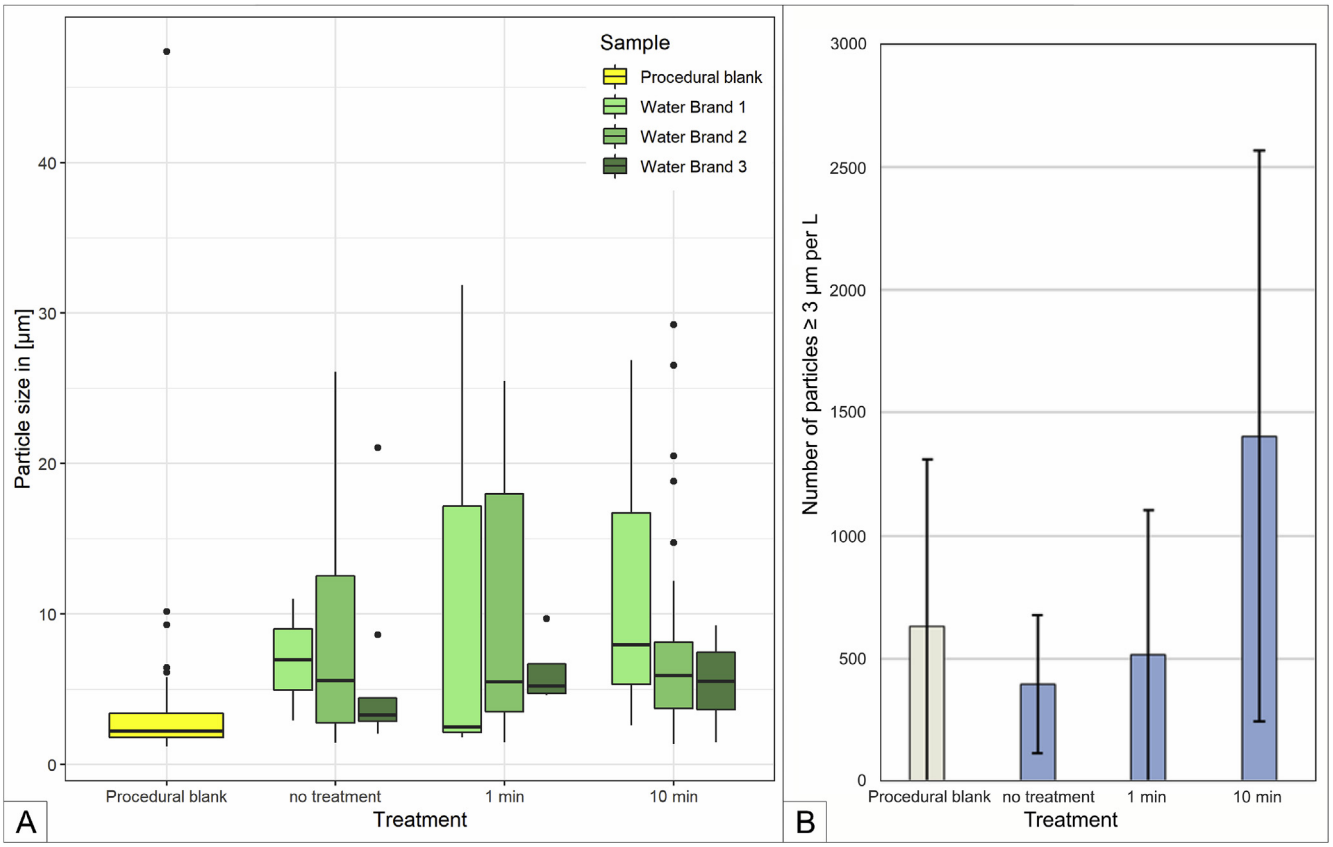

Fig. 8. (A) Size distribution of filtered particles of blank and water samples after treatment of bottles (squeezing/crushing), and of the different brands. (B) Mean number ± SD of particles per L in procedural blanks and water after 0, 1, and 10 min treatment.

PET composition (ranged between 22.0 and 23.2 µm) were detected in water of 10 min treatment bottle from Brand 3. No PET or polymer particle with 100% carbon in their spectra were detected in procedural blanks. Considering all the analysed water samples and particles identified as MPs, we can calculate a mean MP concentration of 148 ± 253 (SD) MP/L.

4. Discussion

4.1. Cap-bottleneck friction: a source of microplastics

Results from our analyses showed that particle release increased with extended mechanical stress on HDPE caps and PET bottlenecks. This was more the case for Brand 2 than for Brand 1 and 3, with caps from Brand 1 being least sensible to abrasion. This was confirmed by the quantitative analysis of particle density on caps opened/closed 100 times, revealing Brand 2 to release the most particles (and Brand 1 the least). Obviously, our data about HPDE particles on caps are extrapolations and they intended to show the potential amounts of MPs released by a single cap from a plastic bottle, as a consequence of mechanical stress. HDPE, being softer than PET, is the crucial component of plastic bottles. Differently from the existing studies on MP concentration in bottled water by Mason et al. (2018), Ossmann et al. (2018), Schymanski et al. (2018) and Zuccarello et al. (2019), our results were not obtained from water samples; they represent direct exposure source during drinking straight from the bottle.

The industrial approach to contain MP production is the use of lubricant incorporated as slip additive to the polymer surface to reduce friction of the material and therefore the torque on the cap

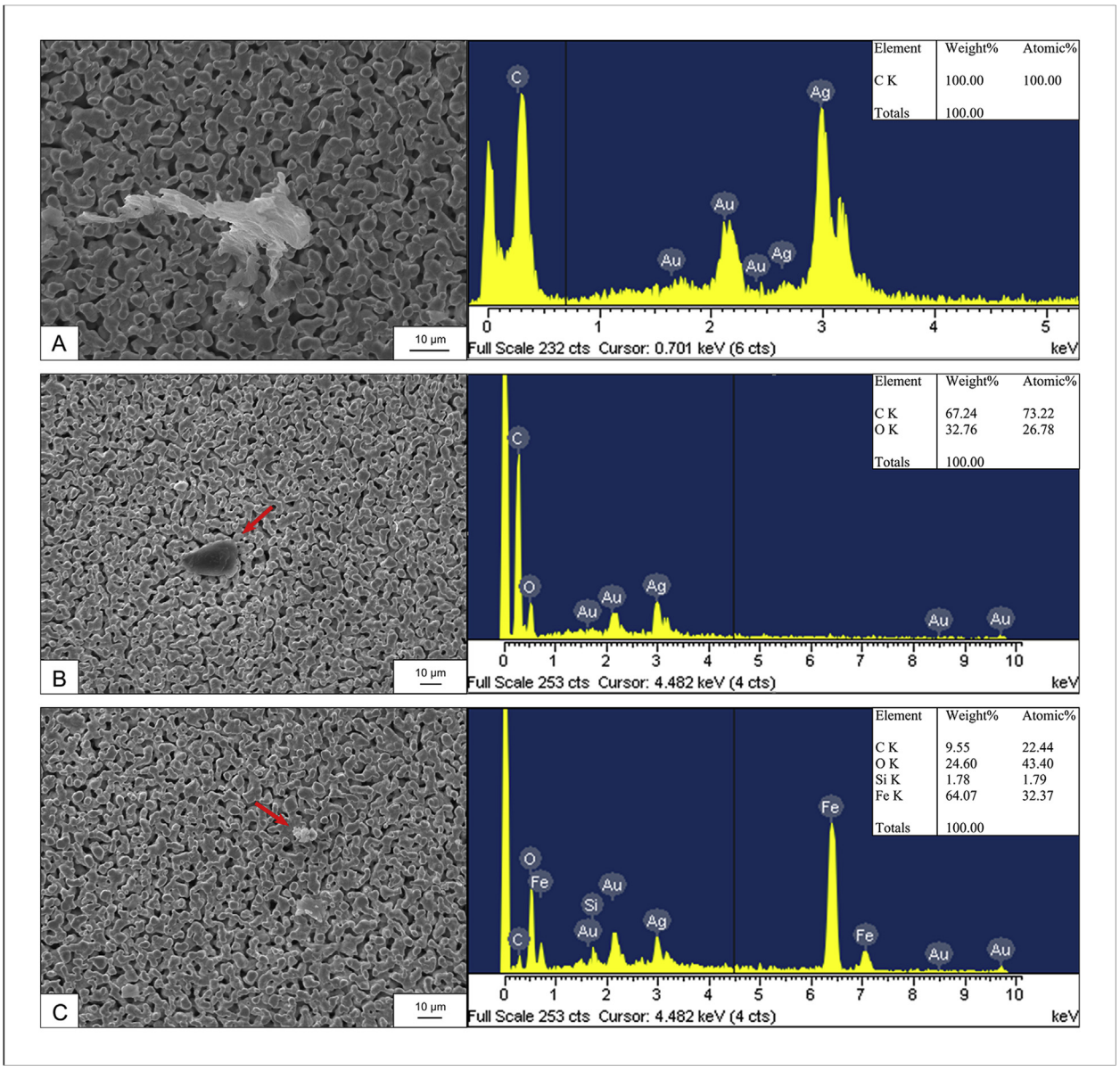

Fig. 9. SEM images and respective EDS spectra with elemental quantitative data of analysed particles from filtered water showing the particle diversity. (A) MP particle on silver filter with specific elemental composition of C = 100% indicating polymeric origin, such as HDPE. (B) MP particle on silver filter with specific elemental composition and C: O ratio corresponding to PET. (C) Exemplary non-polymeric particles on silver filter. Gold (Au) and Silver (Ag) were removed from the output listing as they derived from the gold-coating and the silver background of the filter. (For interpretation of the references to colour in this figure legend, the reader is referred to the Web version of this article.)

(Dulal et al., 2017). Amongst the common lubricants applied on HDPE caps, and listed as indirect additive for food contact substances (FDA, 2018), are oleamide, behenamide and erucamide (long chain primary alkylamides), the latter being the most commonly used. Lubricants show a different crystal structure and rheology and therefore differ in their effectivity (Ramírez et al., 2002). Further influence on their performance have the surface amounts, distribution and storage condition, such as temperature (Dulal et al., 2017; Pan et al., 2017). According to the European Union Commission Regulation No 10/2011 on plastic materials and articles intended to come into contact with food, the named additives have no specific migration limit (SML), which means they have a generic migration limit of 60 mg/kg of food. Particular caps with these additives shall not transfer their constituents to food simulants in quantities exceeding 10 mg of total constituents released per dm^2 of food contact surface (mg/dm^2) (EC, 2011a). Regarding toxicity, the potential risk of erucamide to human health is considered to be low (ECCC HC, 2018). No hazards were identified for behenamide (ECHA, 2019). However, studies investigating the health effects of oleamide are limited and read-across from erucamide are applied to fill the data gaps addressing the human health increasing the uncertainty for risk assessment to human health (ECCC HC, 2018). Since the information about the use of lubricant is not required by law, we performed additional GC/MS analyses on caps from the three brands trying to correlate the observed damages and particle release to a specific compound or dose. Our chemical analyses revealed very different lubricant contents in the three caps: they weren't detected in caps from Brand 1, while caps from Brand 2 and 3 contained 1.0% and 0.08% of behenamide, respectively. By these results, the extent of MP release was not related to the lubricant content, on the contrary the Brand with the higher release of MP showed the highest lubricant content

(Brand 2), while the Brand with the lowest release of MP did not present any lubricant (Brand 1), suggesting that other features than lubricant content should explain the extent of MP release.

The great difference existing in cap abrasion among the different brands with Brand 2 releasing more than 10 times higher than Brand 1, could be explained by the structural features of the cap-bottleneck system. The cap-neck friction and the subsequent release of MPs from Brand 2 could have been caused by the sequence of sectors of its bottleneck, visible in Fig. 5 (rather than a continuous ring as in Brand 1 and 3). This structural difference in bottleneck design is clearly an important element and could explain our results: the bottleneck structure divided by sectors as the one of Brand 2 can be the main reason of increased MP particle release in our samples.

It must be considered that our results derive from a series of 100 times opening/closing, which is normally hard to obtain with a 500 mL plastic bottle. Nonetheless, such a result can be achieved by the systematic reuse of the same bottle throughout a week, or even for longer period. The repeated refilling of the same PET bottle and mainly the reuse of its HDPE cap is certainly more sustainable, but indeed generates a greater number of MP particles, which leads to a higher MP exposure in the plastic bottle-users with potentially risks to human health. Welle and Franz (2018), who published a literature review on the existing studies on MPs in bottled mineral water, evaluated the risk for humans based on reported MP content and total mass transfer of small molecules like additives and oligomers, concluding that exposure estimations would not raise a safety concern for consumers. By our results, if plastic bottles are to be re-used, we recommend rinsing the bottleneck as well as the cap of the bottles to prevent accumulation of MPs on their surface.

Results from our analyses showed that most of the MP particles produced by repeated opening and closing series derived from the cap (HDPE) and stayed below 5 μm in size (about 80, 98 and 89% for Brand 1, 2 and 3, respectively; Fig. 4B), and that for Brand 2 and 3 bottles, about one third of the whole particles were below 1 μm (size class = 0.5–0.99 μm) confirming the very small nature of these MPs. Analogous to nonplastic nanomaterials, it is very likely that also for MPs size may play a pivotal role in their toxicity, with the smallest particles being the most dangerous. This has already been reported in mammals (Kubo et al., 1999). Literature about potential toxicity of MPs is constantly increasing in number, but data on the effects of MPs on living organisms are sometimes contradictory. In fact, while many studies have demonstrated that MP ingestion is able to induce sub-lethal adverse effects on different animals (Alomar et al., 2017; Blarer and Burkhardt-Holm, 2016; Lu et al., 2016), other studies have reported light or null effects (Imhof et al., 2017; Kaposi et al., 2014; Weber et al., 2018). Unfortunately, no information on the effects of ingested MPs in humans is available so far. Even though in human the intestinal absorption of MPs appears to be limited, the epithelium of the gut is not impenetrable to nanoplastics (NPs). Indeed, *in vivo* human data on NPs are not available and only PS has been used as model particle in mammalian *in vivo* and *in vitro* studies (Lusher et al., 2017). We were not able to detect NPs, which are smaller than 100 nm by definition (EC, 2011b), however, their possible toxicity, despite their relative low mass, is worth of further and more detailed studies. A very recent review (Eerkes-Medrano et al., 2019) underlined this issue, additionally reporting that bottled water had the highest number of MPs with respect to tap water, but with a considerably lower mass, due to their small size. Since all plastics contain reactive oxygen species (ROS), due to their polymerization and processing history (Wright and Kelly, 2017), MPs ingested via drinking water can produce oxidative stress, which may lead to chronic inflammation and tissue damage. Even by minimizing the possible MP uptake with the simplest one-time use of PET bottled water (one opening only), which did not produce an evident release of MPs in the cap-bottleneck area, the re-use of PET bottles and especially the repeated cap-bottleneck frictions can produce impressive MP numbers (up to millions of particles) and consequently a higher exposure risk.

4.2. Effects of mechanical stress on PET bottles

Results from our analyses of filtered water after 0, 1, and 10 min squeezing bottle test showed no significant differences among the samples neither considering the total particle number, nor the particles ≥3 μm. Accordingly, the EDS analysis confirmed only few particles to be of plastic origin and looking at the inner wall surfaces of the PET bottles subjected to continued crushing/squeezing test, no ultrastructural differences were observed by SEM even after 10 min of treatment, some minor deformation lines excluded (Fig. 7). The mechanical stress tested in this paper wanted to mime a normal bottle use; considering that such a stress can derive during drinking, carrying and by handling bottles especially when they are half empty, even 10 min treatment does not seem unrealistic.

The experimental set up was designed to primarily determine possible MP, i.e. particles from both PET bottle and PE cap, increase in water due to the treatments. Although MP identification via EDS is solely based on the elemental composition and C:O ratio, the risk of misinterpretation for PET particles is low due to the very clear C:O ratio and strong oxygen peak. On the contrary, particles on filters identified as HDPE could potentially derive from other polymers containing only carbon (and hydrogen), such as PP or PS. Anyway, SEM imaging is a powerful tool for material inspection: the analysis of the inner bottle surface, the morphological study of the bottle neck design and cap opening system, greatly help in identifying new MP generation and detachment sites, mainly in a study that aims at finding potential sources of MPs after the application of strong mechanical stress. Thus, SEM/EDS results were suitable for our purposes, even though limiting when polymers with no distinct element peaks, such as oxygen in PET and chlorine in PVC, need to be identified (Wang et al., 2017).

The presence of MPs in water from single-use PET bottled was already considered. Data from the few published papers reported inconsistent results, mainly due the use of non-standardized procedures in preparing and analysing the samples. Wiesheu et al. (2016) considering a bottled mineral water and using μ-Raman spectroscopy did not reported significant differences between the sample and the controls, both showing a high number of fibres in the size range between 1 and 5 μm. Schymanski et al. (2018) found 14 ± 14 MPs/L (≥5 μm) applying μ-Raman spectroscopy, while Ossmann et al. (2018), by the same methodology, identified 2649 ± 2857 MPs/L (≥1 μm), with more than 98% being ≤ 5 μm. Mason et al. (2018), applying the Nile Red tagging methodology, party combined with FTIR spectroscopy, reported that 93% of all tested single-use PET bottles showed signs of MP contamination with an average of 325 MPs/L (≥6.5 μm). More recently, Zuccarello et al. (2019) by SEM-EDS methodology found 5.42E+07 ± 1.95E+07 MPs/L bottled water (0.5–10 μm). Unfortunately, this paper does not describe the details for the MPs extraction and analytical method, referring to a patent for industrial invention registered to the Italian Ministry of Economic Development, which is not of public domain. Moreover, the reported concentrations refer to the general particle content and could not distinguish between plastic polymer, dust or other components. That might explain the exceedingly high number of detected “MPs”. Apart from this, they further found a correlation of water particle content and bottle plastic thickness (hard plastics cause the release of bigger fragments but in minor number), which could not be confirmed by our study.

Table 1
Comparison of the mean number of MPs/L in single-use PET bottles among studies.

	This study	Schymanski et al. (2018)	Ossmann et al. (2018)	Mason et al. (2018)	
Particle size detection (limit)	≥3 μm	≥5 μm	≥1.5 μm	≥6.5–100 μm	≥100 μm
Analytical method	(SEM/EDS)	(μ-Raman)	(μ-Raman)	Nile Red tagging	(FTIR)
Total MPs (Mean ± SD)	148 ± 253	14 ± 14	2649 ± 2857	325	10.4
MP mass concentration	1.71 μg/L	1.8 μg/L	0.1 μg/L	–	–

According to a recent comment on the study by Zuccarello et al. (2019) published by Ossmann et al. (2019), the results of the study are more than questionable. The authors not only criticize the lack of information about the methodology, but also highlight the need for good quality research in order to deliver reliable data for an adequate assessment. Therefore, we excluded the very high values by Zuccarello et al. (2019) from our analysis. In general, a comparison of MP content in bottled mineral water with results from the available studies is difficult due to the different experimental setup and targeted plastic polymers. Our results (148 ± 253 (SD) MPs/L) compared to those by the other studies for single-use PET bottles, Zuccarello's excluded, are summarized in Table 1; values were directly taken from the respective articles.

Differences in the number of MPs/L among published studies can be explained by considering the different size limit of detectable particle due to the applied technique, which varies within these studies, as increasing concentration values are correlated to decreasing particle size limit for polymer identification. Mason et al. (2018) was limited to a polymer identification of particles larger than 100 μm, hence the small number compared to our results. However, also MP concentration by Schymanski et al. (2018) and Ossmann et al. (2018) differed from ours, despite the particle size limits for polymer identification differed only slightly to ours. It gives proof to the findings by Ossmann et al. (2018), who found increasing number of MPs with decreasing particle size, with 98% of particles in single-use bottles being smaller than 5 μm.

As Ossmann et al. (2018) already stated, every extrapolation causes increasing uncertainty. Nevertheless, our results support the findings by Ossmann et al. (2018) and Schymanski et al. (2018), who report PET to be the predominant polymer type present in bottled mineral water. This contradicts the findings by Mason et al. (2018) who suspect caps to be the main source of pollution, as they mainly found PE particles in their water. Since the detected PET particles in the present study did not significantly increase with the treatment, it is likely that they were due to the wear of the plastic bottles before purchasing, as before Schymanski et al. (2018) suggested, or to the filling processes. It must be noted that the highest MP concentration was found in both treated and untreated samples, confirming that the applied mechanical treatment did not produce an evident effect on MP particle release. This indicates a reliable behavior of the plastic polymers used in the bottles selected for our test and confirms PET as an effective material capable to sustain repeated squeezing, without gross deteriorations, at least at RT.

Since the concentration in mass of microplastic per volume of beverage (in μg/L) has become an important parameter value for risk assessment (Welle and Franz, 2018), we calculated the concentration of MP particles from the number of particles and their sizes. Following Welle and Franz (2018), the calculation is presented in the Supporting Information (Table S1), and resulting values are given in Table 1. Data highlight the differences between the studies regarding particle sizes with Ossmann et al. (2018) having a much lower mass concentration than Schymanski et al. (2018), despite the much higher particle number. Our value (1.71 μg/L), is very near to that of Schymanski et al. (2018) (1.8 μg/L). Following Welle and Franz (2018) our exposure estimations would not raise a safety concern for consumers.

5. Conclusions

This study provides more data for exposure estimates to MPs of plastic bottled mineral water. We found PET bottlenecks and HDPE caps to present a serious source of MPs, especially following extended mechanical stress (opening and closing procedure). Interestingly, high differences in measured MP density on caps surface existed among brands, likely related to the structural design of the bottleneck. For Brand 1, 2 and 3 we measured 63,400, 1,225,500 and 333,800 HDPE particles on the inner cap surface, respectively, revealing Brand 2 to release the most MPs. We detected MPs also in drinking water, which, extrapolated to 1L, sum up to 148 ± 253 MPs/L. Differently from caps, MP occurrence in water samples was not significantly related neither to the applied treatments nor to different bottle types (brand) supporting the results of total particle counts, which were not significantly higher after treatment. Therefore, PET material of our tested brands was resistant towards mechanical stress (squeezing/crushing test). MPs in filtered water likely derived from contamination of the water before bottling or due to wear of the bottles before purchase.

SEM/EDS was suitable for our experimental set up as it provided high-resolution images of the plastic surfaces to reveal abrasion, quantify particle release and the detection of PET particles in filtered water. However, this technique reaches its limit when a differentiation of polymers showing only carbon in their EDS spectra is desired. The use of positive controls proved the functionality of the applied system, but blanks revealed the sensitivity of this kind of analysis towards external contamination.

According to these results, though being declared as food-safe, PET and HDPE used for food packaging exhibit deficiencies such as the release of MPs due to frequent use. Moreover, the observed differences in the extent of MP release of bottlenecks/caps between the bottle brands reveals a variety in the plastic behavior that should be considered to an optimization of the admission criteria for food contact substances.

Chances of MP ingestion by humans increase with frequent use of the same single-use plastic bottle, though only from the bottleneck-cap system. According to Welle and Franz (2018), MP content in water of previous studies with lower and higher MP content compared to our, is not considered a safety concern. However, there is a lack of information regarding the potential toxicity of plastic polymers to human health. Research has to be intensified considering the degradation of plastic material and the release potential of particles and additives, especially regarding plastics used for food packaging.

Funding

This research did not receive any specific grant from funding agencies in the public, commercial, or not-for-profit sectors.

Declaration of competing interest

The authors declare that they have no known competing financial interests or personal relationships that could have appeared to influence the work reported in this paper.

Acknowledgements

Authors wish to thank Dr. Miriam Ascagni from Unitech NOLIMITS, Imaging facility at the University of Milan, for supporting us with her ImageJ expertise, and Dr. Ermelinda Falletta for her help in chemical analyses for lubricant quantification in caps.

Appendix A. Supplementary data

Supplementary data to this article can be found online at https://doi.org/10.1016/j.watres.2019.115082.

References

Alomar, C., Sureda, A., Capo, X., Guijarro, B., Tejada, S., Deudero, S., 2017. Microplastic ingestion by *Mullus surmuletus* Linnaeus, 1758 fish and its potential for causing oxidative stress. Environ. Res. 159, 135–142. https://doi.org/10.1016/j.envres.2017.07.043.

ASTM Standard Test Method for Rockwell Hardness of Plastics and Electrical Insulating Materials, 2015. ASTM international, West Conshohocken, PA, p. 6. https://doi.org/10.1520/D0785-08R15.

Blarer, P., Burkhardt-Holm, P., 2016. Microplastics affect assimilation efficiency in the freshwater amphipod *Gammarus fossarum*. Environ. Sci. Pollut. Res. Int. 23 (23), 23522–23532. https://doi.org/10.1007/s11356-016-7584-2.

Bouwmeester, H., Hollman, P.C., Peters, R.J., 2015. Potential health impact of environmentally released micro- and nanoplastics in the human food production chain: experiences from nanotoxicology. Environ. Sci. Technol. 49 (15), 8932–8947. https://doi:10.1021/acs.est.5b01090.

Dulal, N., Shanks, R., Gengenbach, T., Gill, H., Chalmers, D., Adhikari, B., Pardo Martinez, I., 2017. Slip-additive migration, surface morphology, and performance on injection moulded high-density polyethylene closures. J. Colloid Interface Sci. 505, 537–545. https://doi.org/10.1016/j.jcis.2017.06.040.

EC, E.C., 2011a. Commission Regulation of 14 January 2011 on Plastic Materials and Articles Intended to Come into Contact with Food (10/2011/EU), pp. 1–89. http://data.europa.eu/eli/reg/2011/10/oj.

EC, E.C., 2011b. Commission Recommendation of 18 October 2011 on the Definition of Nanomaterial (2011/696/EU), pp. 38–40. https://eur-lex.europa.eu/eli/reco/2011/696/oj.

ECCC HC, E.a.C.C.C., Health Canada, 2018. Fatty Amides Group, Draft Screening Assessment, Government of Canada. Canada. https://www.canada.ca/en/environment-climate-change/services/evaluating-existing-substances/screening-assessment-fatty-amides.html.

ECHA, E.C.A., 2019. In: Union, E (Ed.), Docosonamide, Registration Dossier. https://echa.europa.eu/de/registration-dossier/-/registered-dossier/10893/1.

Eerkes-Medrano, D., Leslie, H.A., Quinn, B., 2019. Microplastics in drinking water: a review and assessment. Curr. Opin. Environ. Sci. Health 7, 69–75. https://doi.org/10.1016/j.coesh.2018.12.001.

FDA, 2018. In: Services U.S.D.o.H.H.a. (Ed.), List of Indirect Additives Used in Food Contact Substances. Silver Spring, USA. https://www.fda.gov/food/ingredientspackaginglabeling/packagingfcs/indirectadditives/default.htm.

Galloway, T.S., 2015. In: Bergmann, M., Gutow, L., Klages, M. (Eds.), Marine Anthropogenic Litter. Springer International Publishing, Cham, pp. 343–366. https://doi.org/10.1007/978-3-319-16510-3.

Garrido-López, A., Esquiu, V., Tena, M.T., 2006. Determination of oleamide and erucamide in polyethylene films by pressurised fluid extraction and gas chromatography. J. Chromatogr. A 1124, 51–56. https://doi.org/10.1016/j.chroma.2006.04.086.

Hammer, J., Kraak, M.H., Parsons, J.R., 2012. Plastics in the marine environment: the dark side of a modern gift. Rev. Environ. Contam. Toxicol. 220, 1–44. https://doi.org/10.1007/978-1-4614-3414-6_1.

Imhof, H.K., Rusek, J., Thiel, M., Wolinska, J., Laforsch, C., 2017. Do microplastic particles affect Daphnia magna at the morphological, life history and molecular level? PLoS One 12 (11), e0187590. https://doi.org/10.1371/journal.pone.0187590.

Kaposi, K.L., Mos, B., Kelaher, B.P., Dworjanyn, S.A., 2014. Ingestion of microplastic has limited impact on a marine larva. Environ. Sci. Technol. 48 (3), 1638–1645. https://doi.org/10.1021/es404295e.

Koelmans, A.A., Mohamed Nor, N.H., Hermsen, E., Kooi, M., Mintenig, S.M., De France, J., 2019. Microplastics in freshwaters and drinking water: critical review and assessment of data quality. Water Res. 155, 410–422. https://doi.org/10.1016/j.watres.2019.02.054.

Kubo, T., Sawada, K., Hirakawa, K., Shimizu, C., Takamatsu, T., Hirasawa, Y., 1999. Histiocyte reaction in rabbit femurs to UHMWPE, metal, and ceramic particles in different sizes. J. Biomed. Mater. Res. 45 (4), 363–369. https://doi.org/10.1002/(SICI)1097-4636(19990615)45:4%3c363::AID-JBM11%3e3.0.CO;2-3.

Lehner, R., Weder, C., Petri-Fink, A., Rothen-Rutishauser, B., 2019. Emergence of nanoplastic in the environment and possible impact on human health. Environ. Sci. Technol. 53 (4), 1748–1765. https://doi.org/10.1021/acs.est.8b05512.

Liebmann, B., Köppel, S., Königshofer, P., Bucsics, T., Reiberger, T., Schwabl, P., 2018. Assessment of Microplastic Concentrations in Human Stools - Final Results of a Prospective Study. Monte Verità, Ascona, Switzerland. https://doi.org/10.13140/RG.2.2.16638.02884.

Lithner, D., Larsson, A., Dave, G., 2011. Environmental and health hazard ranking and assessment of plastic polymers based on chemical composition. Sci. Total Environ. 409 (18), 3309–3324. https://doi.org/10.1016/j.scitotenv.2011.04.038.

Lu, Y., Zhang, Y., Deng, Y., Jiang, W., Zhao, Y., Geng, J., Ding, L., Ren, H., 2016. Uptake and accumulation of polystyrene microplastics in zebrafish (*Danio rerio*) and toxic effects in liver. Environ. Sci. Technol. 50 (7), 4054–4060. https://doi.org/10.1021/acs.est.6b00183.

Lusher, A.L., Welden, N.A., Sobral, P., Cole, M., 2017. Sampling, isolating and identifying microplastics ingested by fish and invertebrates. Anal. Methods 9 (9), 1346–1360. https://doi.org/10.1039/C6AY02415G.

Mason, S.A., Welch, V.G., Neratko, J., 2018. Synthetic polymer contamination in bottled water. Front Chem 6, 407. https://doi.org/10.3389/fchem.2018.00407.

Ossmann, B.E., Sarau, G., Holtmannspotter, H., Pischetsrieder, M., Christiansen, S.H., Dicke, W., 2018. Small-sized microplastics and pigmented particles in bottled mineral water. Water Res. 141, 307–316. https://doi.org/10.1016/j.watres.2018.05.027.

Ossmann, B.E., Schymanski, D., Ivleva, N.P., Fischer, D., Fischer, F., Dallmann, G., Welle, F., 2019. Comment on "exposure to microplastics (<10 μm) associated to plastic bottles mineral water consumption: the first quantitative study by Zuccarello et al. [Water Research 157 (2019) 365–371]". Water Res. 162, 516–517. https://doi.org/10.1016/j.watres.2019.06.032.

Pan, H., Devasahayam, S., Bandyopadhyay, S., 2017. Study of microstructure and fracture properties of blunt notched and sharp cracked high density polyethylene specimens. Sci. Rep. 7 (1), 6096. https://doi.org/10.1038/s41598-017-03884-6.

Ramírez, M.X., Hirt, D.E., Wright, L.L., 2002. AFM characterization of surface segregated erucamide and behenamide in linear low density polyethylene film. Nano Lett. 2 (1), 9–12. https://doi.org/10.1021/nl0155911.

Schirinzi, G.F., Perez-Pomeda, I., Sanchis, J., Rossini, C., Farre, M., Barcelo, D., 2017. Cytotoxic effects of commonly used nanomaterials and microplastics on cerebral and epithelial human cells. Environ. Res. 159, 579–587. https://doi.org/10.1016/j.envres.2017.08.043.

Schneider, C.A., Rasband, W.S., Eliceiri, K.W., 2012. NIH image to ImageJ: 25 Years of image analysis. Nat. Methods 9 (7), 671–675. https://doi.org/10.1038/nmeth.2089.

Schymanski, D., Goldbeck, C., Humpf, H.U., Furst, P., 2018. Analysis of microplastics in water by micro-Raman spectroscopy: release of plastic particles from different packaging into mineral water. Water Res. 129, 154–162. https://doi.org/10.1016/j.watres.2017.11.011.

UNEP, U.N.E.P., 2016. Marine Plastic Debris and Microplastics – Global Lessons and Research to Inspire Action and Guide Policy Change. http://hdl.handle.net/20.500.11822/7720.

Wang, Z.-M., Wagner, J., Ghosal, S., Bedi, G., Wall, S., 2017. SEM/EDS and optical microscopy analyses of microplastics in ocean trawl and fish guts. Sci. Total Environ. 603–604, 616–626. https://doi.org/10.1016/j.scitotenv.2017.06.047.

Waring, R.H., Harris, R.M., Mitchell, S.C., 2018. Plastic contamination of the food chain: a threat to human health? Maturitas 115, 64–68. https://doi.org/10.1016/j.maturitas.2018.06.010.

Weber, A., Scherer, C., Brennholt, N., Reifferscheid, G., Wagner, M., 2018. PET microplastics do not negatively affect the survival, development, metabolism and feeding activity of the freshwater invertebrate *Gammarus pulex*. Environ. Pollut. 234, 181–189. https://doi.org/10.1016/j.envpol.2017.11.014.

Welle, F., Franz, R., 2018. Microplastic in bottled natural mineral water - literature review and considerations on exposure and risk assessment. Food Addit. Contam. A 35 (12), 2482–2492. https://doi.org/10.1080/19440049.2018.1543957.

Wiesheu, A.C., Anger, P.M., Baumann, T., Niessner, R., Ivleva, N.P., 2016. Raman microspectroscopic analysis of fibers in beverages. Anal. Methods 8, 5722–5725. https://doi.org/10.1039/c6ay01184e.

Wright, S.L., Kelly, F.J., 2017. Plastic and human health: a micro issue? Environ. Sci. Technol. 51 (12), 6634–6647. https://doi.org/10.1021/acs.est.7b00423.

Zuccarello, P., Ferrante, M., Cristaldi, A., Copat, C., Grasso, A., Sangregorio, D., Fiore, M., Oliveri Conti, G., 2019. Exposure to microplastics (<10mum) associated to plastic bottles mineral water consumption: the first quantitative study. Water Res. 157, 365–371. https://doi.org/10.1016/j.watres.2019.03.091.

Supporting Information

"Does mechanical stress cause microplastic release from plastic water bottles?"

Graphics: Figure S1 – S6

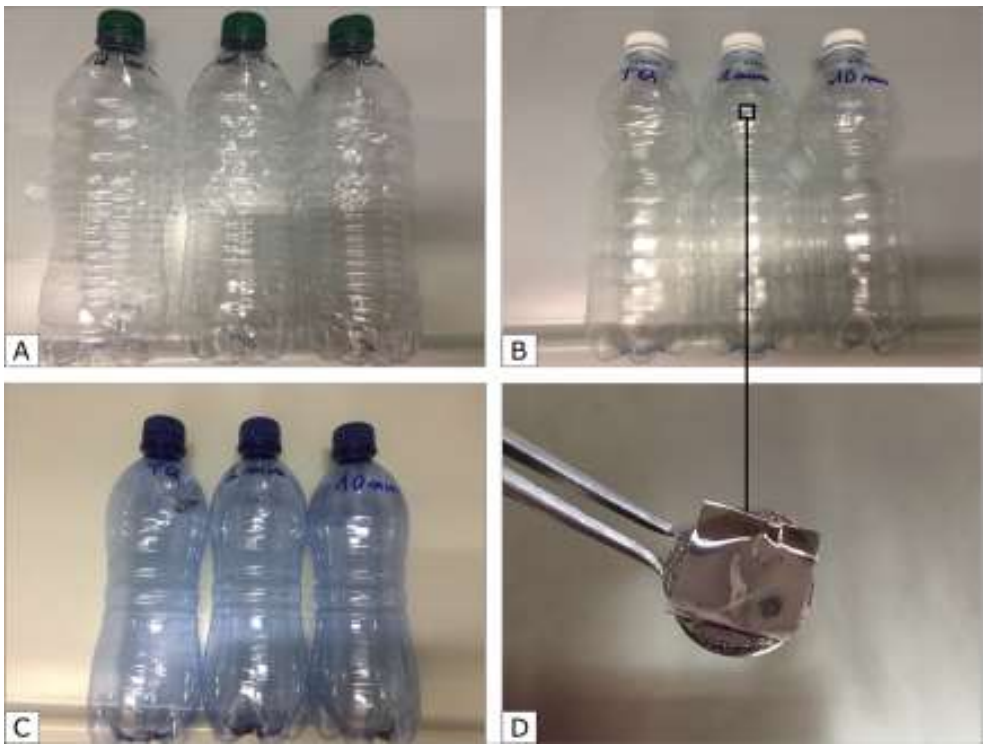

Figure S1. (A - C) Sampled PET single-use water bottles from three different brands (A: Brand 1 with 9.59 g, B: Brand 2 with 12.03 g, C: Brand 3 with 16.01 g) after the squeezing treatment (from left to right: no treatment, 1 min, 10 min) and after filtering the water. (D) One out of all nine removed parts of bottle inner wall mounted onto standard SEM mount and coated with a thin film of evaporated gold. The samples were morphologically analysed for effects of mechanical stress.

Figure S2. In-house manufactured glass filtration apparatus allowing to filter up to four samples simultaneously and valves to individually regulate vacuum. The setup consists of the following components; four open reservoir flasks that are mounted on top of four extension of a filtering head placed on top of a conical flask, which collects the sample liquids. Each of the four extensions has a porous plate on which the filter is seated and a closing valve below to individually regulate the vacuum. The tube of the vacuum pump is attached to an extended glass tube at the lower part of the filtering head. Metal clamps hold the reservoir flask and filtering head together and can be detached in order to remove the filter membranes.

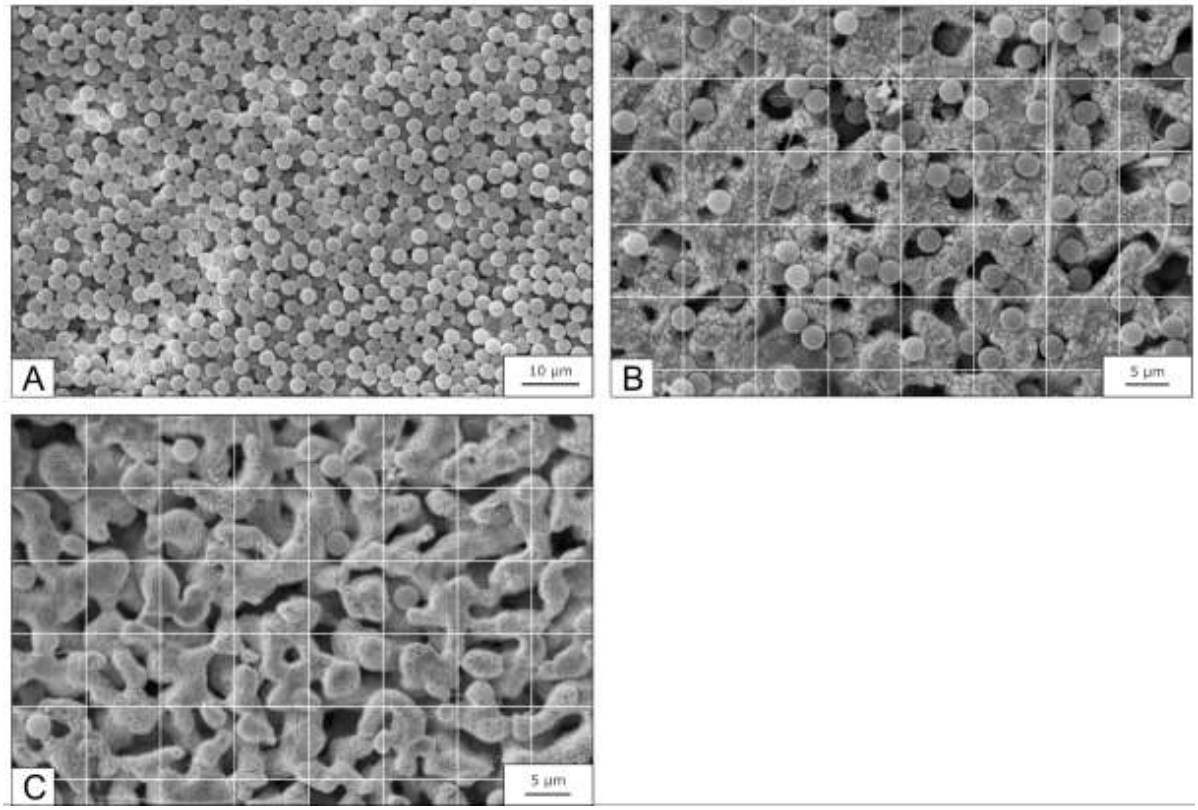

Figure S3. SEM images of control samples (polystyrene beads, 2.91 µm in size) on silver membrane filters (0.8 µm pore size). (A) First control sample: ~ 4,000,000 particles per 250 ml (magnification 5000), (B) second control sample: ~ 400,000 p/250 ml (magnification 1500), (C) third control sample: ~ 40,000 p/250 ml (magnification 1500).

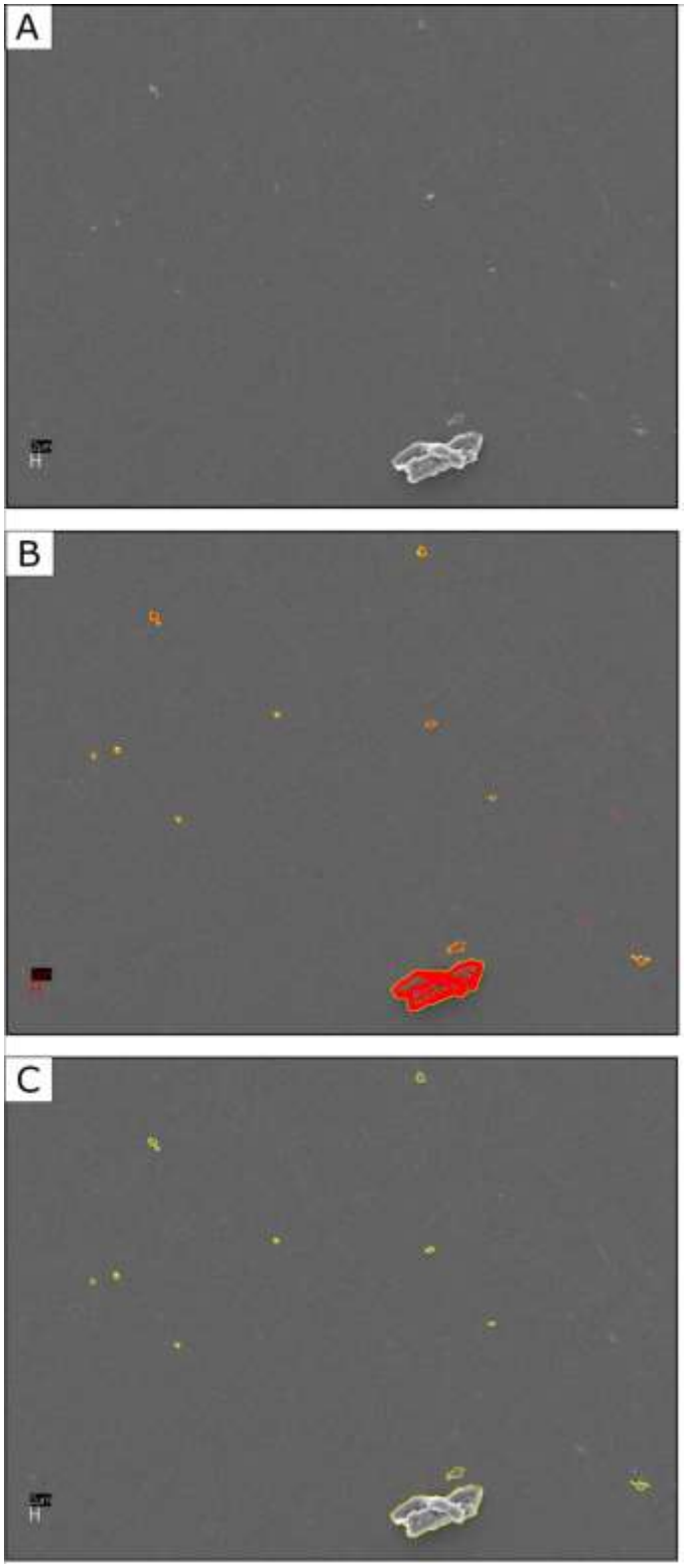

Figure S4. SEM images of MP particles on inner surface of cups (opened/closed 100 x) (A) recognized automatically by imaging software ImageJ (B) to calculate the area of detected particle (C).

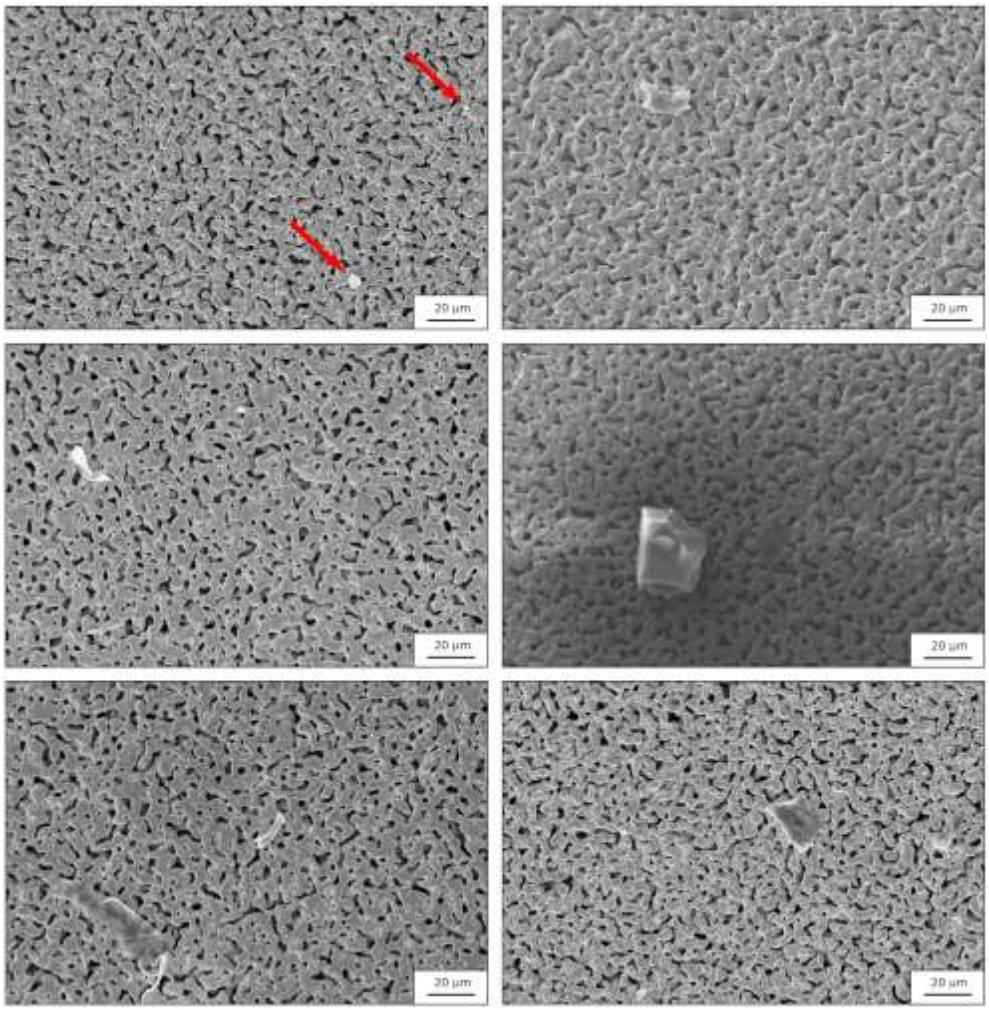

Figure S5. SEM images of selected irregular particles filtered from bottled mineral water on silver membrane filters showing the particle shape diversity.

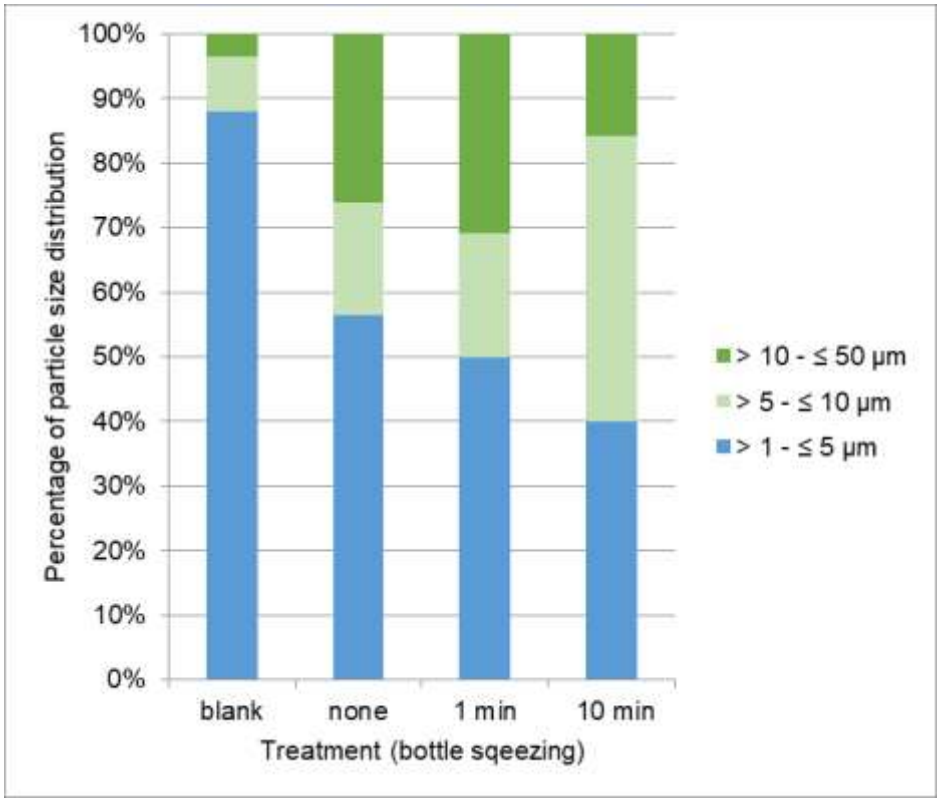

Figure S6. Percentage of particle size distribution of air blank and water samples after treatment of bottles (squeezing/crushing).

PAPER 4 – Detection and formation mechanism of secondary nanoplastic released from drinking water bottles

Anna Winkler, Francesco Fumagalli, Claudia Cella, Douglas Gilliland, Paolo Tremolada, Andrea Valsesia

Submitted to Water Research 2022

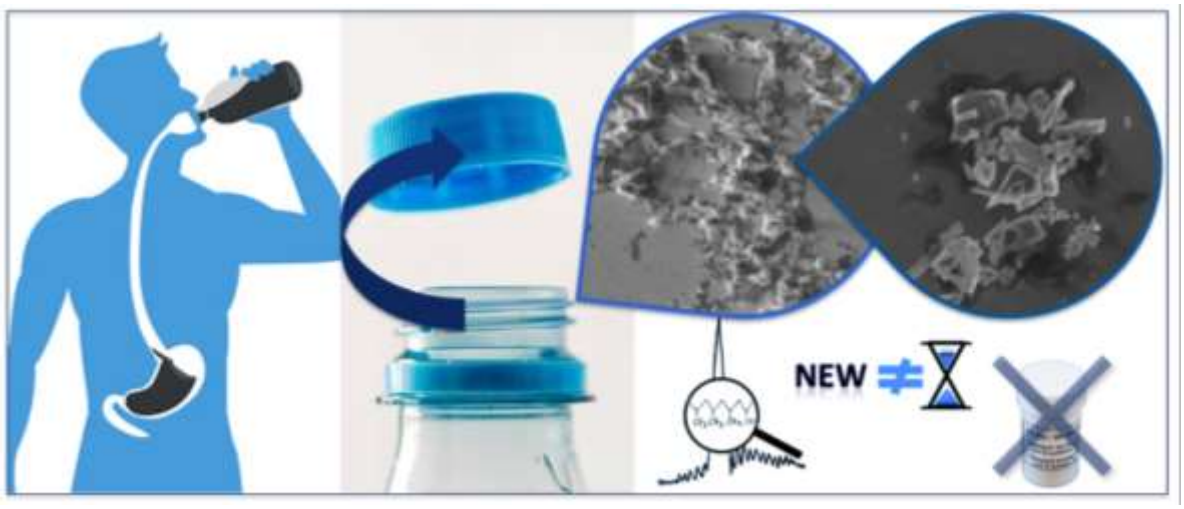

Detection and formation mechanisms of secondary nanoplastic released from drinking water bottles

Anna Winkler [a,ᵠ], Francesco Fumagalli [b,ᵠ], Claudia Cella [b], Douglas Gilliland [b], Paolo Tremolada [a], Andrea Valsesia [b,*]

[a] University of Milan, Department of Environmental Science and Policy, Milan, Italy.
[b] European Commission, Joint Research Center (JRC), Ispra, Italy.
[ᵠ] Equal contribution.
[*] Addresses for correspondence: Andrea Valsesia, European Commission, Joint Research Centre (JRC), Ispra, Italy. Email: andrea.valsesia@ec.europa.eu

Abstract

Since nanoplastics are currently considered potentially hazardous to the environment and human health, reliability of studies on nanoplastic exposure becomes crucial. However, analytical challenges limit our understanding of their formation and detection, thus hampering their biological interactions assessment. Here we provide a combined approach to quantitatively and qualitatively detect the release of nanoplastics in water matrix and, in particular, to measure direct exposure of consumers by simulated use of drinking water plastic bottles. We measured that the polyethylene sealing of the bottles released particles with a size distribution ranging from few hundreds nanometers up to about one micron and estimated a mass release in the order of few tenths of nanograms per opening/closing cycle. We observe that mechanical stress alters the physical-chemical characteristics of the generated secondary nanoplastics and degrades the material properties compared to the original bulk source, thus complicating their spectroscopic chemical identification. Our findings demonstrate that understanding material degradation processes is therefore crucial for identifying and quantifying nanoplastics in real samples. Moreover, methods allowing quantitative studies on the release of nanoplastic as a source of exposure are considered essential for proper assessment of their potential health hazards and to promote improvements in consumer products plastic packaging design.

Keywords: secondary nanoplastics, analytical methods, quantification methods, water bottles, single particle extinction and scattering, Raman spectroscopy.

Abbreviations: EPDM, ethylene-propylene-diene-monomer rubber; FTIR-ATR, Attenuated total reflection - Fourier-transform infrared spectroscopy; HDPE, High density polyethylene; LDPE, Low density polyethylene; mQ-H2O, Milli-Q ultrapure water; PE, Polyethylene; PET, Poly(ethylene terephthalate); MP, microplastics; NP, nanoplastics; PS, Polystyrene; SBR, styrene-butadiene rubber; SEM-EDX, Scanning Electron Microscopy - Energy Dispersive X-Ray Analysis; SPES, Single Particle Extinction and Scattering, XLPE, Cross-linked polyethylene; XPS, X-ray photoelectron spectroscopy; XRD, X-ray diffraction analysis

1 Introduction

Although the growing concern about plastic micro- (MP) and nanoparticles (NP) pervasive diffusion in the environment and human's food-chain, conclusive evidence of their potential health hazards is not yet available.[1,2] NP, defined in this work as secondary sub-micron objects resulting from fragmentation of plastic materials and exhibiting colloidal behaviour,[3] are the most difficult to detect but potentially the most harmful particles since they are small enough to interact at a cellular level. To date, a definitive statement on NP toxicity cannot be provided since it is agreed that insufficient scientific evidence is available about the level of exposure and their interaction with organisms.[4] This is not surprising considering how little is currently known about the physical-chemical properties of secondary nanoplastic debris. Depending on the measurement metric used and NP model characteristics,[3,5,6] toxicity experiments can lead to varying outcomes.[7] Despite these knowledge gaps, uptake of MP/NP via direct exposure from consumer goods is undisputed. Confirmed sources include both foods and beverages products,[8,9] such as bottled water[10,11] with focus on particulates originating from plastic packaging. Recently, a few studies have confirmed the release of MP/NP by food packaging, identifying different degradation pathways and unintentional sources of human consumption of secondary MP/NP. Mechanical stress to HDPE bottle screw caps, i.e., opening and closing a drinking water bottle, has been observed to release MP and identified as potential ingestion source through transfer via oral exposure[12,13]. Thermal stress from heat has also been confirmed to release MPs/NPs from food packaging, e.g. when brewing a teabags (consisting of nylon and PET)[14,15], cooking rice in PE cooking bags[15] or hot liquids in paper cups coated with PE films[16] and other plastic materials holding hot liquids[17,18]. Also thermal stress through freezing was has been verified to release MPs/NPs, as recently observed for ice-cube bags.[15] Contamination of MP/NP can also occur by simple contact of food product with the plastic packaging, as observed for, e.g. meat in extruded polystyrene trays[19] or transfer from plastic take-out containers[20]. Regulating bodies have thus begun discussing safety assessment actions for occurrence, analysis and toxicity of NPs in food and drinking water.[21]

While knowledge about MP detection is increasing, NP studies are still lagging behind since the development of comprehensive detection strategies proved challenging. Mass-spectroscopy based techniques can identify the presence of plastics in the nanogram range[22,23] but lack characterization capabilities of microscopic methods. While diffraction-limited spectroscopic identification/quantification techniques (e.g. μ-Raman) can in principle resolve sub-micron individual particles in laboratory conditions,[24] practical issues with matrix reduction and particle concentration from real samples greatly complicate the analysis.[25] Often, a multi-technique approach is needed to obtain the necessary information on chemical character, shape, size distribution, and concentration.[23,26] Moreover, physico-chemical mechanisms occurring during top-down formation of secondary NPs from larger particles are mainly responsible for the observed heterogeneity in their material properties, transfer pathways and reactivity.[27,28] Together with other stressors such as photodegradation and biodegradation, realistic degradation-induced modifications must be taken into account while developing reliable analytical detection methods since the use of overly simplified laboratory models may lead to non-representative conclusions.

In this study, we will describe a multi-technique analytical methodology for NP detection, identification and size distribution measurement as applied to the analysis of sub-micron particulate release from drinking water bottles under realistic use conditions. Furthermore, we identify and discuss NP physical-chemical properties modifications occurring during secondary formation pathways and their impact on particulate identification and quantification. Understanding the differences between secondary nano-objects and their primary macro sources can play a crucial role in designing effective biological interaction NP models and experiments.

2 Materials and methods

2.1 Study design

The release of MP/NP particles from PET-bottlenecks and HDPE cap material was determined after an opening and closing procedure to mimic the mechanical stress caused by using a bottle. Quantity, chemical and size range analyses of released particles were performed by Single Particle Extinction and Scattering (SPES), X-ray photoelectron spectroscopy (XPS), Scanning Electron Microscopy (SEM), μ-Raman spectroscopy, Fourier-transform infrared Attenuated total reflectance (FTIR-ATR) and μ-FTIR spectroscopy. Although all the methods are non-destructive, the analyses with SEM, XPS, μ-Raman and μ-FTIR require specific filters to provide optimal conditions for clear results, which made the use of a new set of prepared samples for these instruments necessary. The experimental process is described below.

2.2 Sample processing

For sampling material preparation, mineral water bottles (0.5 L) from local supermarkets were purchased, and the outer surface was cleaned with ethanol. The bottle itself consisted of transparent PET, and the cap was made of white HDPE material as indicated by the manufacturer and verified via FTIR-ATR measurements. To apply mechanical stress, one bottle was opened and closed 1, 10, and 50 times manually without fully removing the cap during each open-close cycle. The water content was previously released by cutting the bottle base with a cutter. When the bottle was first opened, the security ring detached from the cap and remained loose at the lower end of the bottleneck. To detach the MPs/NPs released from the PET bottleneck surface and HDPE cap that passed over to the bottleneck due to the treatment, the cap was removed. Particles were rinsed off the bottleneck by immersing it head down into a small glass beaker containing 15 mL Milli-Q ultrapure water (mQ-H_2O) so that only the bottleneck was entirely covered. The bottleneck was left in the solution for 3 minutes while gently agitating. For the analysis with SPES, the bottle was removed and the beaker transported to the instrument where the solution was directly analysed.

The same solutions were then used for μ-Raman and SEM analysis after two concentration steps. The concentration of the sample solution facilitates the analysis of volumes with low MP/NP concentration for spectroscopic and microscopic analyses by reducing the area of analysis to a small droplet on a suitable surface. The first concentration of the solutions was performed by applying an Amicon Ultra 25 mL Centrifugal Filter having a molecular weight cut-off of 100,000 kDa. The solution was centrifuged for 2 min. at max speed (4500 x g, swing-bucket rotor), leaving the residual sample in the top part of the Amicon unit. The sample reservoir contains the concentrate, of which 500 μL were collected using a pipette. The concentrate was transferred into an Amicon Ultra 0.5 mL Centrifugal Filter having a molecular

weight cut-off of 10,000 kDa. The sample was centrifuged for 2 min at max speed (21,130 × g, fixed angle), resulting in a concentrated solution of 25 µL. Of the final concentrate, 1 µL were taken with a pipette and spotted on silicon chips for Raman analysis. Another 1 µL were spotted on cleaned flat silicon chips for SEM analysis. Samples were dried before the analysis. In addition, the release of microplastic particles from the bottle material was tested by µ-FTIR spectroscopy. An additional bottle was opened/closed 50 times, and the bottleneck immersed in 0.1% sodium dodecyl sulfate (SDS) solution to aid hydrophobic particles recovery from the solution. However, since the analysis of one bottle opened/closed 50 times could identify only one PE particle, 390 µm in size (Figure S1), no further replicates were considered. For the sake of completeness, the method is described further below. Results and details of µ-FTIR analysis (of the detected PE micro- particle) are reported in the SI, Figure S1.

2.3 Quality control

Before proceeding with the experiments, it was necessary to verify that plastic particles potentially released on the bottleneck were indeed rinsed off from the bottle by immersion in mQ-H_2O for 3 minutes, without the use of additional solvents. Accordingly, SEM images (JEOL JSM-IT500) of the neck of two further bottles opened/closed 50 times were taken to count particles applying a semi-quantitative approach. One bottleneck before and one after the immersion was removed from the bottle body with a scalpel and mounted on aluminium stubs. For each bottleneck, three SEM images with a magnification of 50 X were taken on a vertical line from the top to the bottom edge of the bottleneck surface. The SEM images were processed to count detected microparticles on bottlenecks before and after the immersion in mQ-H_2O. Operating conditions were: accelerating voltage 20 kV, probe current 80 mA, and working distance 15.7–17.6 mm. The semi-quantitative analysis on the analysed surface area of the bottleneck revealed four particles (170–550 µm in size) before and no particles after the immersion of the bottle (Figure S2), confirming the successful removal of particles from the bottle into the water. EDS analysis of these particles resulted in an elemental composition of 100% carbon (Figure S3), which is consistent with HDPE and, therefore, suggesting particle derived from the cap material.

We included procedural lab blanks consisting of 15 µL mQ-H_2O, which underwent the same processes as the samples. The “blank” sample was placed in another beaker close to the soaking beaker for all the time needed to process the 50 times sample. Then it underwent the same processes. Moreover, pristine mQ-H_2O directly from the distributor was analysed by SPES for comparison.

Additionally, we cryomilled cap material (HDPE) of the same bottle brand as reference material for µ-Raman spectroscopy to simulate effects of mechanical stress (irregular particles rather than micro-and nanobeads). Cap material was cut into smaller pieces and placed in the sample holders (polycarbonate sample holder) of the cryomill (Cryomiller 6875 Freezer/Mill® Spex) together with NaCl to enhance grinding. Milling conditions were: 20 min cooling time, nine cycles of 2 min and 2 min rest, repeated four times. All glass wear and metal cutleries were cleaned with washing detergent and rinsed with fresh mQ-H_2O. Laboratory surfaces on which the preparations were performed were covered with a layer of aluminium foil. All persons wore cotton lab coats or non-synthetic clothes and washed their hands frequently.

2.4 Single particle extinction and scattering

For the determination of particle number and size distribution, single particle extinction and scattering analysis was performed using the CLASSIZER™ ONE (EOS S.r.l., Milan, Italy), equipped with a red light diode (λ = 640 nm, power < 50 mW). This light scattering method enables the analysis, classification and counting of single particles in fluids based on their optical properties. Briefly, particles passing the focal region of a light beam transmit and scatter light that can be collected onto a sensor placed in the far-field of the laser beam. This can give a measure of the complex amplitude of the forward scattered field via a self-reference interferometric scheme.[29,30] The scattered field amplitude depends on several important nanoparticles characteristics (i.e. size, refractive index (n) and shape) that can be analysed with the technique. In this work, we focus on the size distribution and particle concentration. The results are presented in a 2D histogram having as X- and Y-axis the complex scattered field components (*Re[S(0)]*, *Im[S(0)]*) and as Z-axis the concentration (counts·bin^{-1}·cm^{-3}) within each 2D-bin in the complex *S(0)* plane.[29] In the case of dielectric particles and under the assumption of spherical shape, both size and n can be simultaneously and unambiguously determined from the *S(0)* raw data thanks to the Mie scattering calculations. Even in the case of non-spherical particle shapes, and for particles aspect ratios (AR) lower than 2 – 3[31], the spherical approximation leads to a precision over the refractive index measurement better than 10%. Therefore, the evaluation of the numerical size distribution of the whole sample was obtained by applying the dielectric sphere model. The lower and upper detection limit for dielectric material such as polymers is 200 nm to 20 µm. The instrument was operated with a constant flow of 4 mL per minute. Total analysed volume varied from 66 to 78 mL, which was obtained by fluxing the sample multiple times to ensure a sufficient amount of detectable particles. Since the method is non-invasive and non-destructive, the suspension returned into the sample beaker and could be further used for µ-Raman and SEM investigation. In addition, by approaching the analysis with the Mean Field Approximation[32,33] and the Lorentz-Mie method, an average filling factor evaluation was performed to detect signs of agglomeration or indication for a shape similar to a ball of fibre or a porous particle. The average filling factor analysis reports the filling percentage inside the detected particle of the bulk expected material (HDPE or PET in our analysis). Analyses were performed by the software version ClassizerONE S1.4.34.

2.5 Micro-Raman Spectroscopy

Raman analysis was performed on the concentrated samples drop-casted onto the silicon chips. The samples on the chips were analysed using a WITec Confocal Raman Microscope (Witec, Ulm, Germany), equipped with a λ = 532 nm laser. The scan resolution was 200 nm and the integration time per pixel was 5 s. A 100× magnification object was used with numerical aperture of 1.25. Univariate analysis of the hyperspectral images was performed using the Witec instrument software (Witec Suite 5) by integration of the spectra corresponding to the spectral bands between 2800–3100 cm^{-1} assigned to the C - H stretching of polymers. Cosmic Rays Removal and baseline correction tools were applied to the spectra before univariate analysis. The lowest detection limit of single isolated nanoparticles for this instrument was 0.5 µm (using commercial PS beads, PolyScience Inc). The Raman spectra were fitted with an appropriate number of Voigt functions for each spectral band using a nonlinear, least-squares Levemberg-Marquardt regression method. Fitting parameters were peak centres, FWHM, areas for each peak and the common linear baseline. Peak positions were constrained ± 5 cm^{-1} using

literature references from HDPE. [34–37] The uncertainty of peak positions and areas were less than ± 0.5 cm^{-1} and ± 10%, respectively. Mass fractions of crystalline domains, *trans* and amorphous conformers were calculated according to the method originally suggested by Strobl et al. [38,39] and later adopted by several authors [40] describing PE using a three phases model (amorphous, orthorhombic crystalline and non-crystalline consecutive trans conformers, NCCT). In the method, the intensity of the $\tau(CH_2)$ twist vibration band around 1300 cm^{-1} is used as internal normalisation standard. The band intensity ratio with its components intensities 1298 cm^{-1} and 1305 cm^{-1} yields the *trans* and amorphous conformers' mass fractions. The reference band ratio with the 1416 cm^{-1} peak (interchain interactions from $\delta(CH_2)$ + $\omega(CH_2)$ vibrations) can then be used to differentiate the mass fraction contribution from the orthorhombic crystalline regions from the non-crystalline consecutive *trans* conformers ($\chi_{othorhombic} = \chi_{trans} - \chi_{NCCT}$). For comparison, reference spectra acquired on the bottles bulk materials are shown in Figure S4.

2.6 Scanning Electron Microscopy

Scanning electron microscopy (SEM) images of concentrated samples on silicon chips were recorded using a Thermofisher, FEI, NOVA 600i electron microscope operating at an acceleration of 2 kV and magnification of 65X at a working distance varying from 4 to 7 mm. Further high-resolution SEM images were acquired from different sample areas with varying magnifications (1000 –16000 X). EDS spectroscopy and mapping were carried out in a Nova 600i Nanolab (Thermofisher, Eindhoven, The Netherlands) equipped with a EDS system for elemental analysis (EDAX Inc, Mahwah, NJ, USA). The EDS system mounts an Octane Elect Plus x-rays detector. Typical EDS maps and spectra were acquired using Acceleration Voltage values between 10kV and 25 kV, with Take Off angle of 35° and Dwell Time of 200 ms.

2.7 X-ray photoelectron spectroscopy

XPS measurements were performed with an Axis Ultra spectrometer (Kratos, Manchester, UK), using a Kα Al monochromatic source (hv = 1486.6 eV) operating at 150 W and a X-ray spot size of 400 × 700 μm^2 in the hybrid mode. Large spot sizes allowed to obtain good *S/N* ratios in recorded spectra, even if they can introduce drawbacks related to possible substrate contribution and require suitable film deposition method. In order to overcome these issues, we deposited filtered particulate films by drop/casting, and we used Teflon strips as substrates. Sample preparation procedures established in literature were followed for solid [41] and nanoparticles [42] surfaces, respectively. The residual pressure of the analysis chamber during the analysis was less than 8×10^{-9} Torr. For each sample, both survey spectra (0 – 1150 eV, pass energy 80 eV) and high-resolution spectra (pass energy at 40 eV) were recorded. Surface charge was compensated by a magnetic charge compensation system, and the energy scale was calibrated by setting the C 1s hydrocarbon peak to 285.00 eV in binding energy.[43,44] The data were processed using Vision2 software (Kratos Analytical, UK), and the analysis of the XPS peaks was carried out using a commercial software package (CasaXPS v2.3.18PR1, Casa Software, Ltd., UK). Peak fitting was performed with no preliminary smoothing. Symmetric Gaussian–Lorentzian (70% Gaussian and 30% Lorentzian) product functions were used to approximate the line shapes of the fitting components after a 3-parameters Tougaard-type background subtraction. Concentrated samples were dispersed in mQ-H_2O and drop-casted on clean Teflon substrates. The use of Teflon substrate allows minimizing the uncertainties in the stoichiometric evaluation of the C content of the surface, mainly due to adventitious

hydrocarbon contamination. This is especially critical in case of low thicknesses of the analysed films. The high binding energy shift of electrons originating from C-F bonds and the precisely known Teflon stoichiometry allows separating with high confidence the substrate and sample contributions during the C 1s peak fitting. Accordingly, Teflon substrate contribution to the C 1s signal was not considered in the elemental quantification of the sample. For comparison, reference spectra acquired on the bottles bulk materials are shown in Figure S5.

2.8 Micro-FTIR Spectroscopy

For the preparation of the µ-FTIR analysis, the particles were removed from the bottleneck as described above. The solution was transferred into a standard vacuum-filtration apparatus and the beaker rinsed with 5 mL mQ-H_2O. The filter membrane was Whatman® Anodisc inorganic filter membrane (diam. 13 mm) with a nominal pore size of 0.1 µm. The membrane is composed of a high purity alumina porous matrix. After filtration, the membrane was placed in a clean, covered petri dish for drying. Micro-FTIR microscopy was performed using a Bruker Infrared Imaging Microscope. Since the surface of the filters is transparent for IR-radiation with wavenumbers above 1300 cm^{-1}, measurement of all particles > 10 µm (approximate detection limit for this instrument in our configuration) was carried out in transmission mode in a wavenumber range of 4000 – 1300 cm^{-1}. Transmission mode allowed for the determination of the particle, minimising the interference of a potential surface cover layer or soiling. The measurements were controlled by native Bruker OPUS8.5 software. For each experiment, either the full or, in the case of blanks, at least ¼ of the surface area of the filter was analysed. A total of 64 scans were taken for each spectrum, with a spectral resolution of 4 cm^{-1}. The IR absorbance was compared with spectra generated by reference material obtained from PET from bottlenecks and HDPE from bottle caps and with internal OPUS spectral library. For comparison, reference spectra acquired on the bottles bulk materials are shown in Figure S6. Both sides of the bottle body and screw cap were measured to expose eventual occurrence of oxidation due to weathering/ageing of the polymeric materials[41] in the bottle. ATR-FTIR analysis shows no differences between the two surfaces of the bottle components (see Figure S7).

2.9 Data analysis

Origin, CasaXPS and Microsoft Excel were used for data analysis. Origin and Inkscape were used for exporting data graphs.

3 Results and discussion

3.1 Morphological and chemical analysis

The release of MP/NP particles from commercial drinking water bottles was determined after several opening-closing cycles (1, 10, and 50 times) to mimic product (re)utilisation. The bottleneck-cap system (made of polyethylene terephthalate, PET, and polyethylene, PE, respectively, as stated by the manufacturer and verified via FTIR-ATR measurements) was rinsed with mQ-H_2O after opening/closing cycles to recover released particulate. Care was taken to ensure efficient recovery and to avoid contamination from external sources. Chemical and size distribution analyses of released particles were performed combining Scanning

Electron Microscopy (SEM), Single Particle Extinction and Scattering (SPES)[29], X-ray photoelectron spectroscopy (XPS), μ-Raman and μ-Fourier-transform infrared (FTIR) spectroscopy. For SPES, that allows outlining particle size distribution and concentration, and μ-FTIR measurements the rinsing water was analysed directly while for other techniques the solution was centrifugally filtered (at 10^4 kDa cut-off) and concentrated on a Si-chip surface. Qualitative SEM images analysis show that the amount of residual particulate recovered from the neck of water bottles after simulated use deviates from the procedural blank and increases with the number of opening/closing cycles (Figure 1b–d), indicating an accumulation of particles whose approximate size range was well below 5 μm (Figure 1e–h). SEM/EDS elemental composition analysis on recovered particles showed almost exclusively carbon with the measured *O/C* ratio being close to zero (Figure S2 and S3). This observation is compatible with common commodity thermoplastics such as PE (i.e. bottle cap material), PP, and PS, and with some synthetic elastomers compositions (e.g. SBR, styrene-butadiene rubber; EPDM, ethylene-propylene-diene-monomer rubber) but not with PET (i.e. bottle material). Chemical identification of sub-micron particles via EDS is complicated due to increasing interference from surface oxidation[45] and matrix contaminations.[25] Moreover, the size range of the observed residual particulate lies below the detection limit of μ-FTIR spectrometers,[46–48] as already observed in previous investigations on similar systems.[12]

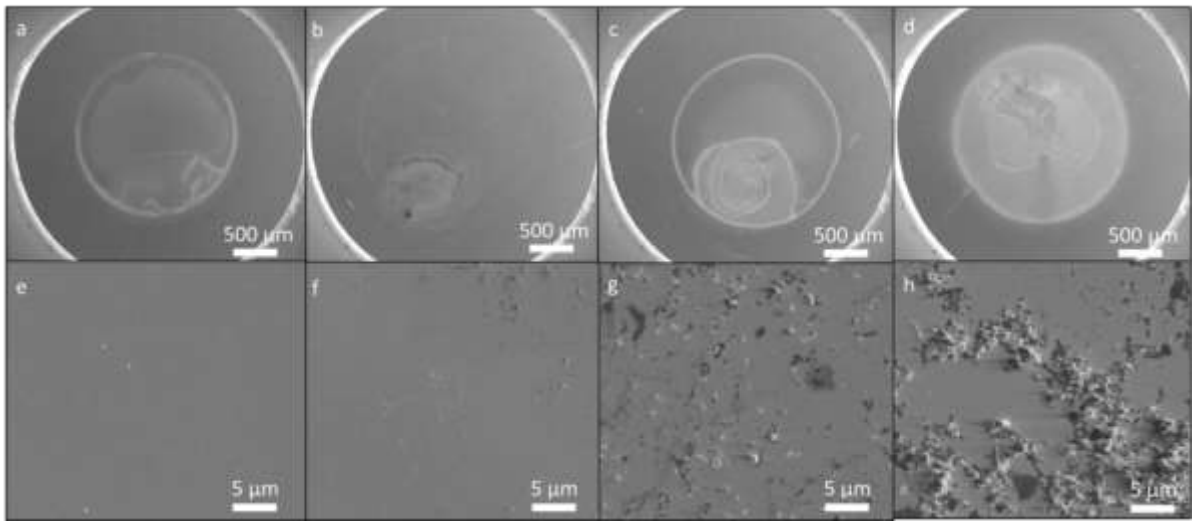

Figure 1. Microscopic analysis of the nanoparticulate released from water bottles. SEM images of concentrated particulates dried on silicon chips. Full droplet area (magnification 65X) from procedural blank (a) and drinking water bottles opened/closed 1, 10, and 50 times (b–d). (e–h) High-resolution SEM images of the particulate aggregated at the centre of the droplet footprints in a–d, respectively, magnification 16000X.

Accordingly, μ-FTIR analysis of the unfiltered rinsing water did not result in any statistically relevant PE or PET particle detection, even though some large PE objects were occasionally detected (Figure S1). An XPS study was conducted on both the recovered particulates in the nano-range and the cleaved HDPE cap in order to chemically identify the materials through their elemental composition and stoichiometric ratios (Figure 2, Table S1 and S2). In fact, in the HDPE spectrum (Figure 2c), the asymmetric line shape of the main *C-C*, *C-H* component can be used for chemical identification since it can be reliably fitted using the four symmetric *C-H* stretch vibrational components typical of PE.[49] However, the

nanoparticulate *O/C* elemental ratio exhibits a six-fold increase with respect to the cap material ($O/C_{HDPEcap}$ = [6.5 ± 1.8] %; O/C_{NP} = [35.7 ± 3.3] %), thus making the chemical identification based on stoichiometric ratios quite problematic. In addition, this increased surface oxidation (Figure 2e, Table S2) in the nanoparticle spectrum resulted in a large overlap between the *C-O* components and the high binding energy tail of the *C-C*, *C-H* component, effectively making a univocal deconvolution of vibrational *C-H* components not feasible.

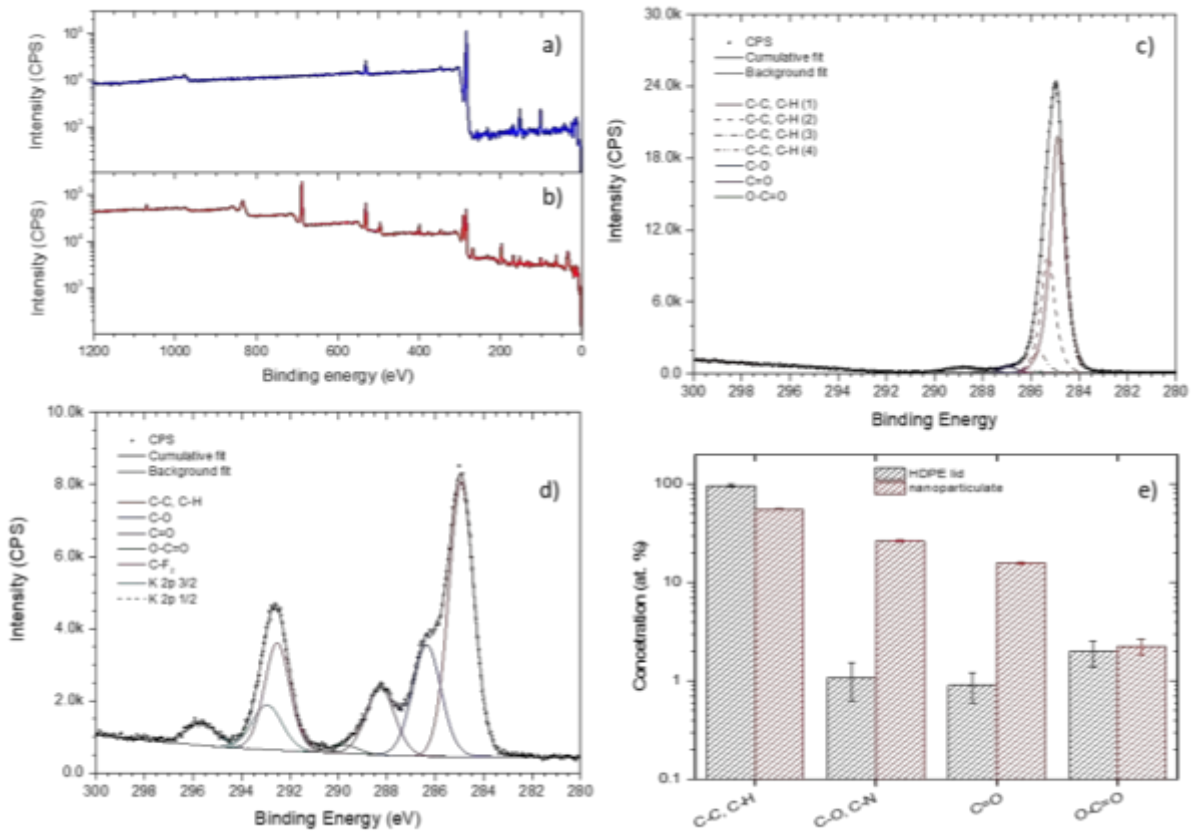

Figure 2. Chemical analysis of the released nanoparticulate surface. XPS survey spectra of (a) the HDPE cap surface (cleaved bulk material) and (b) the concentrated particulate recovered from bottleneck immersion in mQ-H_2O (50 opening/closing cycles). Concentrated particulates were drop-cast and dried onto clean Teflon substrates. (c) High-resolution C 1s spectra of the HDPE cap surface and associated individual peak contributions fitting (line shapes used are GL(80) for the C-H vibrational components[49] and GL(30) for the oxidized peaks). (d) High-resolution C 1s spectra of the concentrated particulate recovered from bottleneck immersion in mQ-H_2O (50 opening/closing cycles) (line shapes used are GL(30) for all peaks). (e) Quantification of carbon atom bonds from the deconvolution of the high-resolution C 1s peak envelope for both HDPE cap surface and recovered nanoparticulate (contributions from $[CF_2]_n$ substrate was subtracted). Values are also reported in Table S2.

3.2 Quantification and sizing

We analysed particle dispersions with Single Particle Extinction and Scattering (SPES).[29] A detailed description of the technique and an explanation of how to interpret data is given in the SI. The four panels in Figure 3 show SPES histograms for the procedural blank, consisting of mQ-H_2O undergoing the same manipulations as the bottle samples (Figure 3a), and the particle dispersions recovered after 1, 10, and 50 (Figure 3b-d) opening/closing cycles. SPES data for

unprocessed mQ-H_2O are shown in Figure S8. The scattering data-points cluster in two slightly separated areas which can be qualitatively separated into two distinct particle populations (green and blue circles in Figure 3c) with different size-distribution characteristics and different behaviour with respect to number of opening/closing cycles.

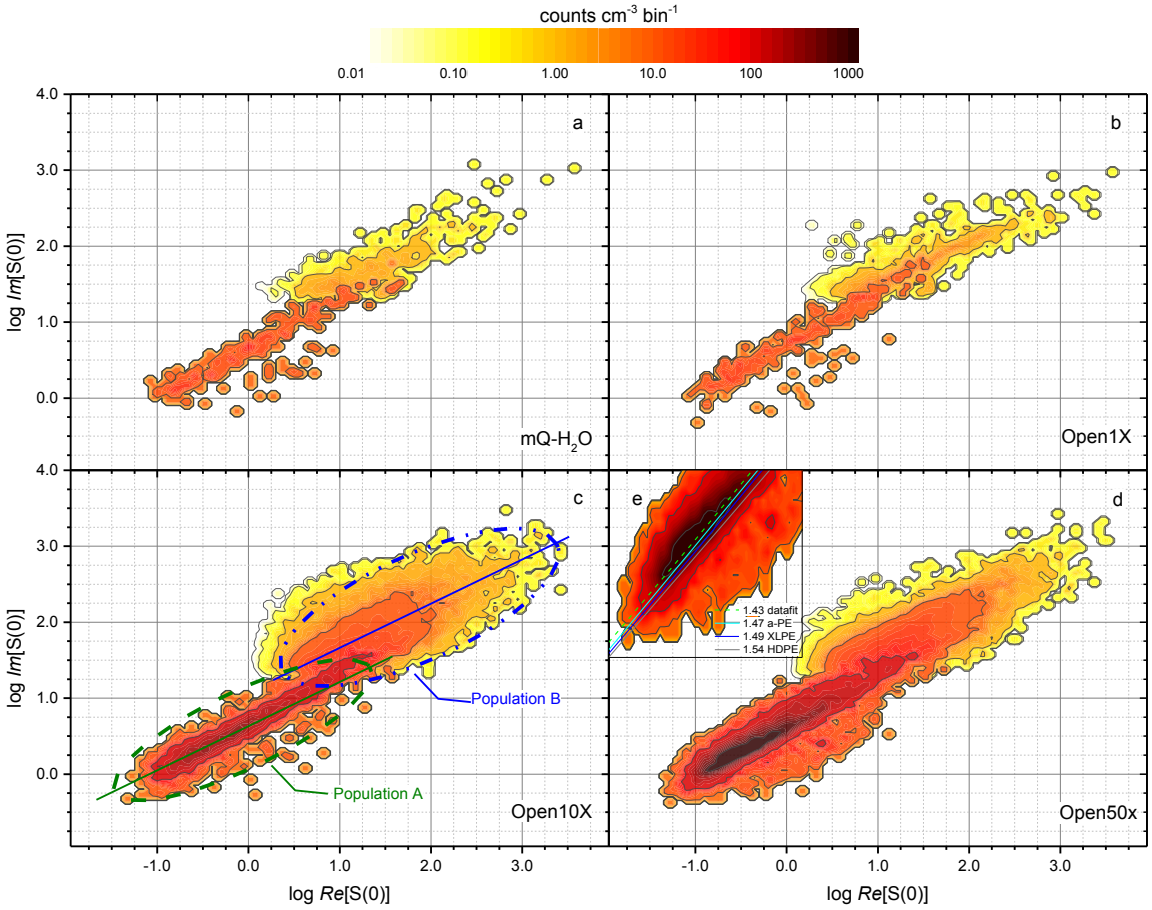

Figure 3. SPES analysis of the released nanoparticulate. Experimental SPES results obtained from (a) procedural blank and suspensions obtained from washing bottle(necks) opened 1, 10, and 50 times (b, c and d, respectively). (e) Effective refractive index derived from SPES data of samples compared with expected values from different forms of PE (amorphous PE, XLPE and HDPE). Two-dimensional (2D) plots (histograms) provide the raw data distribution of single particle scattered light fields amplitude in the complex plane *Re*[S(0)]-*Im*[S(0)]. Typically, the scattered field values depend on size, refractive index and shape of each particle.

The first group (Population-A), characterised by a high particle concentration, exhibits objects with typically sub-micron dimensions ($\bar{d}_A$ = [0.72 ± 0.09] µm with d_{FWHM_A} = [0.57 ± 0.05] µm, D_{90_A} =[1.04 ± 0.14] µm) and refractive index around n_A = [1.42 ± 0.01]. All size-distribution descriptors show little variance with the number of opening/closing cycles. In contrast, the second group of particles (Population-B), was present at lower concentrations with typical dimensions being in the low micron range ($\bar{d}_B$ = [2.13 ± 0.50] µm with d_{FWHM_B} = [1.90 ± 0.46] µm, D_{10_B} = [1.19 ± 0.32] µm) and n_B = [1.41 ± 0.04]. In this case, all descriptors show higher variance with increasing cycle number. The increasing integral counts of SPES histograms indicates that the total particle concentration in the suspensions also increases with the number of opening/closing cycles, as observed in the SEM pictures. However, the numbers

of recovered particles and its dependence on the number of cycles are different when considered separately for the two particle populations (see Figure S9). Particle counts in Population-A, $[N]_A$, is at least an order of magnitude higher than in Population B, $[N]_B$, for all the experiments.

Another important difference is that the total number of recovered particles increased roughly linearly ($r_{Pearson} = 0.98$; $R^2_{Adj.} = 0.94$) with the number of cycles for Population-A while it exhibits a plateau for Population-B (see Figure S9). This would suggest that the former could be linked to the opening-closing cycles while the latter may derive from environmental contamination occurring during manipulation. SPES analysis of mQ-H_2O used for particle recovery (Figure S8) reveals that a very small amount of particles with sizes in the low micron range is already present at this stage. A summary with the principal statistical descriptors characterising Population-A number-based particle size distribution is given in Table 1 for different opening-closing cycles and for the control experiments. The full table with all the statistical descriptors of both Population-A and Population-B particle distributions can be found in Table S3 in the Supporting Information section. The overall particle number-based distributions (absolute) as a function of the cycle number and their cumulative distributions (normalised) are shown in Figure 4. An effect caused by the eventual release of MPs/NPs through the detachment of the security ring from the cap during the first opening of the bottle was not observed. Moreover, the reported numbers of released NPs refer to those on the bottleneck, while it can be assumed that further NPs remained on the inner surface of caps as reported by Winkler et al.[12] for MPs/NPs in the size range of 0.54 to 39.9 μm.

Table 1. Particle size-distributions descriptors from SPES data fitting of Population-A nanoparticles. Absolute number of recovered particle [N] (ad.), refractive index, *n* (ad.), distribution mean, $\bar{d}$ (μm). When appropriate, standard deviations are indicated in parentheses. For [N] the relative error in total number of particle estimation is around 20%.

Population A	$[N]_A$ *ad.*	n_A *ad.*	$\bar{d}_A$ *μm*
mQ-H_2O	1.0E3	-- [c]	-- [c]
BLANK	11.8E4	1.43(0.04)	0.75
OPEN 1X	12.4E4	1.41(0.03)	0.82
OPEN 10X	13.5E5	1.43(0.04)	0.69
OPEN 50X	33.0E5	1.43(0.04)	0.64
Average[a]	n.a.[b]	1.42	0.72
St.Dev.[a]	n.a. [b]	0.01	0.09

a) Averages and standard deviations calculated only on OPEN 1x, 10x and 50x
b) Not applicable.

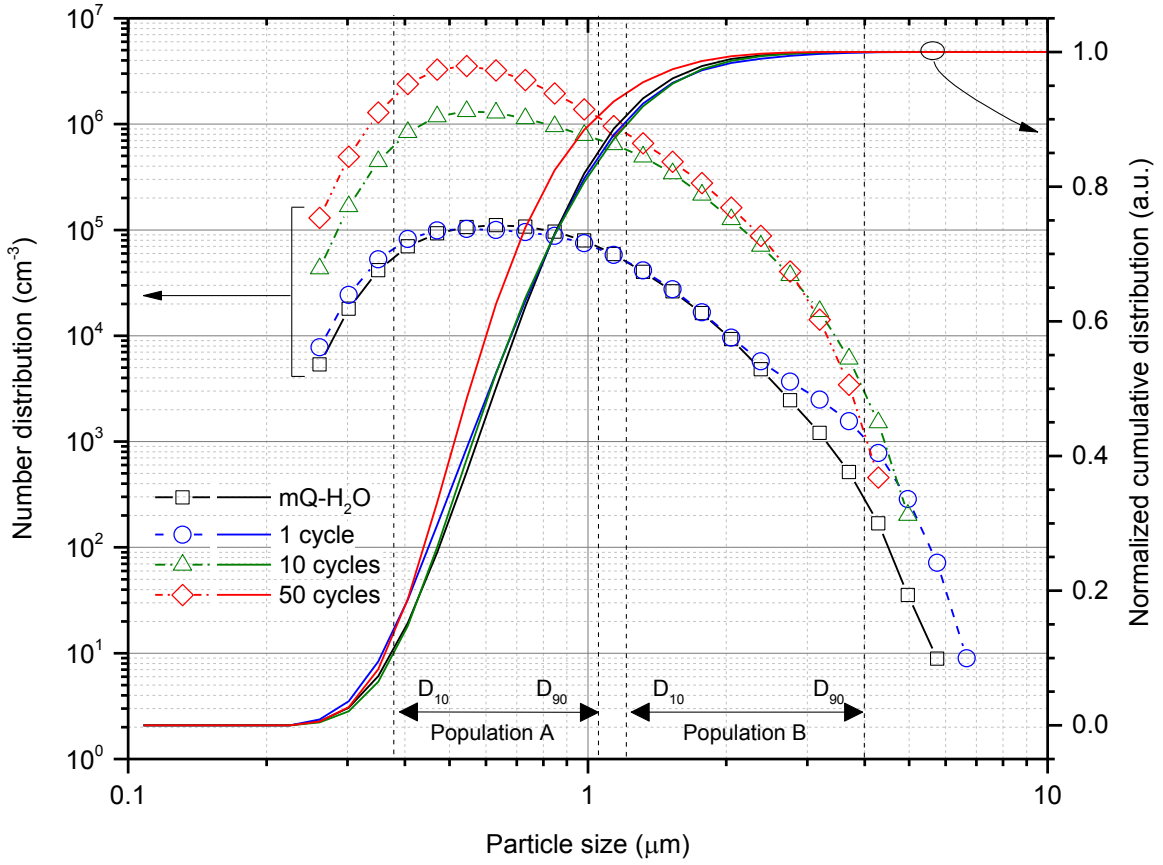

Figure 4. Quantitative description of the released nanoparticulate. Number-based particle size distribution (left axis) and normalised cumulative particle size distribution obtained from SPES experiments with mQ-H_2O (procedural blank) and suspensions obtained from washing bottle(necks) opened 1, 10, and 50 times. Dotted lines indicated the boundaries of Population-A and B particle distributions expressed in terms D_{10} and D_{90} as calculated from SPES histograms. The average volume analysed per sample was V=[15±0.3]mL.

To identify the likely source of the released particulate, the refractive index derived from SPES data was compared with HDPE and PET reference values. The best-fit between particle representative data-points belonging to Population-A and Mie scattering calculations (i.e. with constant-n contour lines in the (*Re[S(0)]*, *Im[S(0)]*) plane under the assumption of spherical shape) results in an average n_A = [1.42 ± 0.01] (inset, Figure 3e). This value does not substantially vary with the number of cycles. The measured n value lies in a range compatible with polymeric materials, but it is considerably smaller than the nominal values of the bottle components, PET (n_{PET} = 1.57) and HDPE (n_{HDPE} = 1.54). Under the working hypothesis that particles observed in Population-A originate mechanically during the opening/closing cycles from the bottleneck-cap system, we can identify at least three factors that may contribute to explaining the difference between observed and calculated refractive indices:

i) occurrence of non-isometric nanoparticles, whose $n_{effective}$ is lower than n_{bulk};

ii) occurrence of nanoparticle aggregates, whose $n_{effective}$ is the volume-average between n_{bulk} and n_{medium};

iii) phase variations occurring during nanoparticle formation during the opening/closing cycles (typically $n_{amorphous} < n_{crystallline}$, see Figure 3e).

As for hypothesis (i), it is often observed that the spherical-shape assumption is rarely met in environmental and/or non-model samples. The occurrence of complex shapes in particulate distribution has the effect of lowering the $n_{effective}$ value calculated from SPES data.[50] Assuming quasi-spherical, non-isometric particles with aspect-ratio < 3 (as can be hypothesised based on SEM images, Figure S10), the predicted $n_{effective}$ values[31] would result in $n_{effective\_PE} >$ 1.46 and $n_{effective\_PET} >$ 1.49. Support for hypothesis (ii) also derives from SEM analysis (Figure S10), where the granular appearance of the filtered particulate suggests that they may be composed of smaller sub-units. An analysis of the filling-factor (*ff*) can be made based on the mean-field approximation and the Lorentz-Mie method[32], assuming the empty volume of the particles is filled with the suspension medium (n_{H2O} = 1.33). To explain the experimentally observed n_A, particle conglomerates should have $ff_{\_PE}$ = [48.5 ± 19.1] % and $ff_{\_PET}$ = [42.6 ± 16.8] %, respectively. These calculations can be qualitatively compared to experimental data using theoretical *ff* values predicted for (relatively) monodisperse, randomly packed, isometric hard objects. Depending on the packing mechanism, a theoretical limiting *ff* ranging from 52% to 62% can be obtained. A slightly higher *ff* could be reached if an external energy source aids conglomerate formation.[51,52] Comparing these theoretical values with the experiments, we can conclude that the conglomerate's scenario is more likely to match the case of PE release. Hypothesis (iii) is made based on the observed amorphisation of semicrystalline polymers during mechanical fragmentation.[53] Optical properties of semicrystalline polymers are related to their structural characteristics, such as crystalline fraction (X_c), and the refractive index of crystalline domains is normally higher than that of amorphous regions according to their relative densities. Commercial PET presents X_c around 20 – 30% (determined by calorimetry[54]) and n_{PET} = 1.57; while in the HDPE bottle caps, an X_c = 80% was determined by X-ray diffraction (XRD) measurements[51] (Figure S11) and n_{HDPE} = 1.54. The refractive index of purely amorphous PET has been measured to be around $n_{amorph\text{-}PET}$ = 1.54;[55] while in different PE formulations the correlation between X_c and n is clear, e.g. n_{LDPE} = 1.51, $X_{c\_LDPE} \approx$ 50%; n_{XLPE} = 1.49, $X_{C\text{-}XLPE} \approx$ 40% and $n_{amorph-PE}$ = 1.47, $X_{c\_amorph\text{-}PE} \approx$ 0%. Some of these values have been used to calculate the constant-*n* lines in Figure 3e and compared to the data best-fit line for Population-A. The trend in particle concentrations and the three scenarios proposed in the previous paragraph are qualitatively consistent with the hypothesis that particulates in Population A originate from the PE cap system under the influence of the opening/closing cycles. Nonetheless, none of these effects alone can be invoked to unambiguously explain the discrepancy between the observed n_A value and n_{PE}, and univocal identification of the chemical nature of the nanoparticles based only on these observations is not possible.

3.3 Chemical identification

To unequivocally identify the particle's chemical nature, we further analyzed the particulate residue via μ-Raman spectroscopy. Figure 5a shows spectra in the group frequencies and characteristic CH_2-stretching regions measured on the nanoparticulates recovered after 1, 10, and 50 cycles. Particulate spectra are compared to the HDPE cap spectrum and literature[34–37] (Figure S12). Figure 5b–e shows surface maps displaying integrated Raman intensity in the spectral range between 1400 – 1500 cm^{-1}, a region characteristic of functional group vibrations $\delta(CH_2)$ and $\delta(CH_3)$ and compatible with both natural organic materials and carbon based polymeric materials. Both single-point Raman spectra and intensity maps support the SEM and SPES observations which indicate that the recovered particles in the submicron-size range increase in number with the number of opening/closing cycles and can be distinguished from those of procedural blanks. Particulate chemical identification based on standard automated spectral correlation operated using different commercial and home-built reference material libraries[56] did not show any reliable match with either the packaging materials (HDPE, PET), expected impurities (based on XPS analysis) or known contaminants from our preparation protocol. In general, spectra from recovered particulates show a marked intensity loss, high signal-to-noise (*S/N*) ratio and poorly defined, broad spectral features compared to the bulk material. This is due to reduced scattering material volume in the laser focal spot, reduced particle size, and inhomogeneous broadening effects (mainly due to morphological inhomogeneity in our sample). The Raman bands with the highest *S/N* were recorded for the 50 cycles sample, exhibiting also the highest particulate concentration. Raman bands from the samples appear in similar spectral regions where the HDPE cap also exhibits Raman bands, however, band head positions and individual peak shapes appear to be different between the bulk and the nanomaterials.

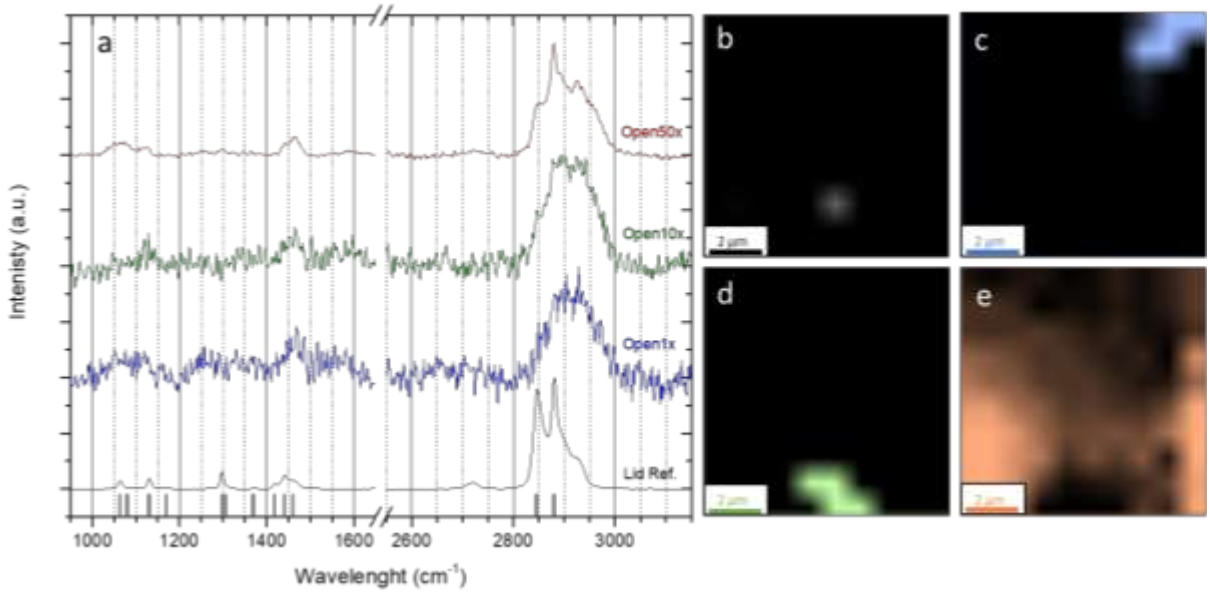

Figure 5. Chemical analysis of the released nanoparticulate. (a) Confocal Raman spectrum of the water bottle HDPE cap surface (black) and particulate recovered from water bottle opened/closed 1 (blue), 10 (green), and 50 (red) times. Data are shown in the group frequencies and CH_2-stretching distinct regions. Black vertical lines above the X-axis represent HDPE reference Raman peak centre positions taken from literature.[34–37] (b–e) Univariate Raman maps of the selected sample area (rim of the droplet) from

concentrated samples of procedural blanks and bottles opened/closed for 1, 10, and 50 cycles. The maps were generated by plotting integrated intensity in the spectral range at 1400–1500 cm^{-1}.

To gain insight into the chemical nature of the recovered nanofraction, we closely analysed the group frequencies region (1000 – 1550 cm^{-1}, Figure 6a-b) and the $\nu(CH_2)$ region (2775 – 3025 cm^{-1}, Figure 6d-f). The features of the spectra from recovered particulates (Figure 6a) were compared with model nanoparticulate obtained by cryomilling HDPE bottle caps (after resuspension in mQ-H_2O and filtration with a 1.2 µm cut-off filter, Figure 6b) and the HDPE cap spectra (Figure 6c). The cryomilled material was included to separate possible thermal effects in NP formation occurring during cycling. Raman band assignments for semicrystalline PE molecular vibrations are well established in the literature;[34–37] Table S4 summarises the Raman shifts, vibrational modes and structural phase assignments for all the individual peaks obtained from band envelopes deconvolution shown in Figure 6.

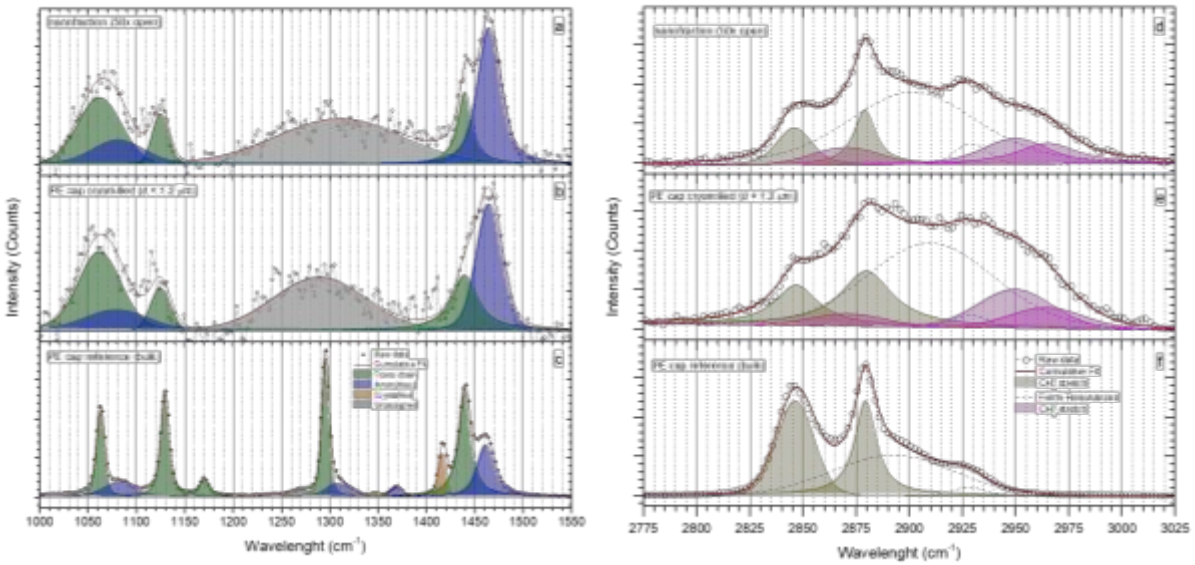

Figure 6. Chemical identification of the released nanoparticulate. Raman spectra and spectral features deconvolution in the 1000–1550 cm^{-1} group frequencies region for (a) the particulate recovered from washing the bottleneck (50 cycles), (b) for the filtered fraction from cryomilled PE cap material, and (c) PE cap bulk reference. Data are normalised to maximum intensity. Raman spectra and spectral features deconvolution in the 2775–3025 cm^{-1} CH_x stretch frequencies region for (d) the material recovered from cap washing opened 50 times, (e) the filtered fraction from cryomilled PE cap, and (f) the PE cap bulk material reference. Data are normalised to maximum intensity.

In Figure 6, the different peak phase assignments are colour-coded for ease of reference; orange is assigned to the orthorhombic crystalline phase, green for all non-crystalline consecutive *trans* (NCCT)[40] configurations and blue for amorphous domains. All peaks identified in the HDPE spectrum were identified and phase-assigned,[34–37] and the resulting crystallinity calculated[39] from experiments was found to be as follows: $X_{orthorhombic\_Raman}$ = [10.3 ± 0.5] %, (X_{amorph_Raman} = [18.3 ± 0.5] % and X_{NCCT_Raman} = [71.4 ± 0.5] %). This result agrees with the XRD measurements (see Figure S11, which give a compound crystalline fraction of $X_{orthorhombic+NCCT\_XRD}$ = [78.9 ± 0.5] % and an amorphous fraction of X_{amorph_XRD} =

[21.1 ± 0.5] % in agreement also with reference values for commercial HDPE.[57] For the two nanomaterials, the first band in the group frequencies region (Figure 6a–b) shows two peaks degrading towards higher wavenumbers and extends from 1000 to 1150 cm^{-1}. The second band is a broad, featureless peak centred around 1300 cm^{-1}, while the third band shows two components of increasing intensity and extends from 1400 to 1500 cm^{-1}. The fourth band (Figure 6d–e) is located at higher wavenumbers and extends from 2800 to 3000 cm^{-1}, showing several poorly resolved band heads. In literature, the fundamental Raman bands occurring in these regions have been confidently assigned to ν(C-C) from aliphatic chains, τ(CH_2) and δ(CH_2), respectively, for PE and several other polyolefins.[35,58–60]. Knowing the assignment of HDPE cap spectral features allows a detailed comparison with the spectra of both types of nanoparticulates. We note that the spectral features in Figure 6a–b can be confidently reconstructed using a subgroup of HDPE individual peaks keeping their Raman-shift fixed (but varying intensity and FWHM). The peaks observed in the nanoparticulate spectra belong either to the amorphous or *trans* conformations but not to the crystalline orthorhombic phase. In general, the following observations hold:

i) Raman-shifts for different peaks do not vary in all three analyzed materials. FWHM increases in all nanomaterials with respect to bulk HDPE.

ii) Nanoparticulate show decreased relative intensities of ν(C-C) and δ(CH_2) Raman bands components assigned to *trans* configurations.

iii) Nanoparticulate show increased relative intensities in the same spectral regions for peaks assigned to amorphous conformational components.

iv) Nanoparticulate show a decrease and broadening of the whole τ(CH_2) band.

v) The peak related to the orthorhombic crystalline phase (at 1416 cm^{-1}) is absent in the nanoparticulate.

Moreover, the spectrum of the recovered nanoparticulate qualitatively resembles spectra recorded for melt phase HDPE obtained during high-temperature recrystallisation.[61] Crystallinity evaluated from the two nanomaterial Raman spectra is zero due to the absence of the 1416 cm^{-1} peak, but control measurements via XRD were not possible due to the low amount of the recovered nanoparticulate and the cryomilled nanofraction remaining after filtration with the 1.2 μm cut-off filters. However, spectra taken on the unfractionated cryomilled particulates (without filtration steps, with a broad size distribution spanning up to several tens of μm) reveal a 40% increase of the amorphous PE fraction (see Figure S11). Raman results are consistent with the observed reduction in the measured refractive index for Population-A in the SPES histograms (Figure 2e), thus supporting a scenario in which nanoparticles are produced by mechanical action during opening/closing cycles and originate from the HDPE cap. These secondary nanomaterials may degrade and lose their crystalline character during formation, resulting in amorphous PE nanoparticles. The PE assignment of the unknown nanoparticulate, according to μ-Raman analysis, implying their origin from the bottle screw cap and not from the PET-made bottleneck is also supported by comparing Raman,

FTIR and EDX spectra of the recovered particulate with the corresponding reference spectra for the bulk materials shown in Figures S1, S3-S7, and Figure 2c.

The $\nu(CH_x)$ region (2800 – 3000 cm^{-1}) for the same three materials is treated separately (Figure 6d-f) as it provides a different kind of information. The reference HDPE cap spectrum exhibits the common band structure for this material.[35–37,62] The two narrow band heads can be assigned to the $\nu_s(CH_2)$ (2845 cm^{-1}) and $\nu_{as}(CH_2)$ (2880 cm^{-1}) modes. They contain contributions from amorphous and crystalline regions and have no definite phase assignment. The broad spectral features forming the high-wavenumber band tail arise due to Fermi resonances between the $\nu_s(CH_2)$ vibration at 2845 cm^{-1} and the $\delta(CH_2)$ at 1440 cm^{-1}.[35] These broad features carry most of the integrated band intensity, and their predicted Raman shifts are around 2900 cm^{-1} and 2930 cm^{-1}. [35] These contributions should not be confused with $\nu_{as}(CH_3)$ vibrations located at slightly higher wavenumbers (2952 and 2964 cm^{-1}). Highly-crystalline HDPE is normally characterized by long, linear hydrocarbon chains exhibiting high molecular weight and low branching (< 1%) resulting in a very low CH_3/CH_2 ratio, so methyl-terminations contributions are normally negligible for this polymer. Spectral analysis for the nanoparticulate reveals how typical PE $\nu(CH_2)$ vibrations band structure is also preserved in the two nanomaterials. Both $\nu_s(CH_2)$ and $\nu_{as}(CH_2)$ individual peaks are detected at the expected Raman-shift, [36] even though they appear broader and less intense. We also observe that their intensity ratio (I_{2845}/I_{2880}) is slightly decreased. However, interpretation is not straightforward due to the relative uncertainty introduced by evaluating the contribution of the broad underlying Fermi resonance bands. [35,37]

A marked difference between bulk and nanomaterials spectra is the appearance of an intense band tail at high wavenumbers with non-negligible intensity in the region 2930 – 2980 cm^{-1}. Raman intensity in this spectral region is normally not observed in common PE-based materials (e.g. HDPE [this study], LDPE [63] or XLPE (Figure S13), irrespective of their crystallinity degree and cross-linking. This band is fitted with two additional peaks (Figure 6d-e) centred at 2852 and 2964 cm^{-1}. Moreover, an additional component (2871 cm^{-1}) is observed between the two $\nu(CH_2)$ peaks. The observed Raman-shifts of these peaks match with the predicted shifts and relative intensities of methyl- terminations stretching modes in aliphatic chains.[35] More precisely, the assignments are $\nu_s(CH_3)$ (2871 cm^{-1}), in-plane $\nu_{as}(CH_3)$ (2852 cm^{-1}) and its out-of-plane counterpart (2964 cm^{-1}). These peaks indicate a marked increase in the number density of methyl terminations in the nanoparticulate sample compared to the cap material and could suggest the occurrence of PE linear chains scission events[64] induced by mechanical stresses acting during nanoparticle formation upon cycling. Not surprisingly, the nanomaterials $\nu(CH_x)$ band appearance is qualitatively similar to the spectral shape of the same region measured in short-chained polyolefins in the liquid state.[60] The similarity between the recovered nanoparticles spectra and the cryomilled sample supports the hypothesis that the main mechanisms responsible for nanoparticle formation and amorphization have a mechanical origin.

4 Conclusion

In conclusion, NP release from drinking water plastic bottles under simulated use was observed and characterised combining SEM, XPS, SPES and μ-Raman analysis. The combination of SPES and μ-Raman represent the minimal set of techniques necessary to apply the methodology for the quantification and identification of NP in simple matrices like drinking water. The size distribution of nanoparticles released from the packaging ranged from D_{10_A} = [0.38 ± 0.03] μm to D_{90_A} = [1.04 ± 0.14] μm, possibly extending to lower sizes below the SPES detection limit (200 nm). Nanoparticles were composed of amorphous PE, likely originating from HDPE caps via mechanical action during opening/closing cycles. From the SPES size distribution data and considering particle shape and fill-factor approximations, the total mass of amorphous PE in the form of nanoparticles released can be estimated not to exceed a few tenths of ng per cycle. This study shows that, in a realistic environment, stressors acting during the top-down formation of NPs may alter the physical-chemical characteristics of the nanoparticulate with respect to those of their original source bulk material, thus hindering their identification. We have found out that even mechanical stress alone acting during NP formation can degrade the materials even without the occurrence of other external stressors. Analytical detection methods development, understanding the physical-chemical processes occurring during secondary generation and the design of relevant NP models can be linked in a circular positive feedback loop. We have shown that the design of improved analytical schemes for secondary NP identification and quantification allows for further insights into material degradation/fragmentation processes. A deeper understanding of degradation mechanisms during secondary NP formation could then be used to design improved model NP materials that could be exploited for further developing analytical methods. Moreover, the effect of degradation/fragmentation pathways on physical-chemical properties of the NP should also be taken into account during the design of model engineered nanomaterials for use in studies about secondary NP fate, effects on human health, sampling and analysis.[3]

Author Contributions

The manuscript was written through contributions of all authors. All authors have given approval to the final version of the manuscript. ᵖ These authors contributed equally: Anna Winkler, Francesco Fumagalli. AW, CC and AV designed the study and prepared the samples. CC prepared and executed SPES experiments. AV executed Raman measurements. FF performed FTIR and XPS measurements; he also analysed, and interpreted SPES, Raman and XPS data. DG and PT supervised the overall work and contributed to the results discussion/manuscript drafting.

Funding Sources

This research was conducted under the framework of the JRC Research Infrastructure Access Agreement No. 335559/11 2019-1-RD–Nanobiotech, “Open access to JRC Research Infrastructures.” under the supervision of Dr. Pascal Colpo (EU-JRC Ispra, Unit F.2).

Acknowledgements

The authors acknowledge Dr. Giacomo Ceccone (EU-JRC Ispra, Unit F.2) for valuable discussions and technical help with XPS data fitting. Dr. Tiziano Sanvito (EOS S.r.l., Milano, Italy) is acknowledged for the fruitful discussion about SPES data interpretation.

References

(1) Mitrano, D. M.; Wick, P.; Nowack, B. Placing Nanoplastics in the Context of Global Plastic Pollution. *Nat. Nanotechnol.* **2021**, *16* (5), 491–500. https://doi.org/10.1038/s41565-021-00888-2.

(2) Lim, X. Z. Microplastics Are Everywhere - but Are They Harmful? *Nature* **2021**, *593* (7857), 22–25. https://doi.org/10.1038/D41586-021-01143-3.

(3) Gigault, J.; El Hadri, H.; Nguyen, B.; Grassl, B.; Rowenczyk, L.; Tufenkji, N.; Feng, S.; Wiesner, M. Nanoplastics Are Neither Microplastics nor Engineered Nanoparticles. *Nat. Nanotechnol.* **2021**, *16* (5), 501–507. https://doi.org/10.1038/s41565-021-00886-4.

(4) Zhang, R.; Silic, M. R.; Schaber, A.; Wasel, O.; Freeman, J. L.; Sepúlveda, M. S. Exposure Route Affects the Distribution and Toxicity of Polystyrene Nanoplastics in Zebrafish. *Sci. Total Environ.* **2020**, *724*, 138065. https://doi.org/10.1016/J.SCITOTENV.2020.138065.

(5) Lin, W.; Jiang, R.; Hu, S.; Xiao, X.; Wu, J.; Wei, S.; Xiong, Y.; Ouyang, G. Investigating the Toxicities of Different Functionalized Polystyrene Nanoplastics on Daphnia Magna. *Ecotoxicol. Environ. Saf.* **2019**, *180*, 509–516. https://doi.org/10.1016/J.ECOENV.2019.05.036.

(6) Blancho, F.; Davranche, M.; Fumagalli, F.; Ceccone, G.; Gigault, J. A Reliable Procedure to Obtain Environmentally Relevant Nanoplastic Proxies. *Environ. Sci. Nano* **2021**, *8* (11), 3211–3219. https://doi.org/10.1039/D1EN00395J.

(7) Kögel, T.; Bjorøy, Ø.; Toto, B.; Bienfait, A. M.; Sanden, M. Micro- and Nanoplastic Toxicity on Aquatic Life: Determining Factors. *Sci. Total Environ.* **2020**, *709*, 136050. https://doi.org/10.1016/J.SCITOTENV.2019.136050.

(8) Laborda, F.; Trujillo, C.; Lobinski, R. Analysis of Microplastics in Consumer Products by Single Particle-Inductively Coupled Plasma Mass Spectrometry Using the Carbon-13 Isotope. *Talanta* **2021**, *221*, 121486. https://doi.org/10.1016/J.TALANTA.2020.121486.

(9) Fadare, O. O.; Wan, B.; Guo, L. H.; Zhao, L. Microplastics from Consumer Plastic Food Containers: Are We Consuming It? *Chemosphere* **2020**, *253*, 126787. https://doi.org/10.1016/J.CHEMOSPHERE.2020.126787.

(10) Shruti, V. C.; Pérez-Guevara, F.; Elizalde-Martínez, I.; Kutralam-Muniasamy, G. Current Trends and Analytical Methods for Evaluation of Microplastics in Stormwater. *Trends Environ. Anal. Chem.* **2021**, *30*, e00123. https://doi.org/10.1016/J.TEAC.2021.E00123.

(11) Cox, K. D.; Covernton, G. A.; Davies, H. L.; Dower, J. F.; Juanes, F.; Dudas, S. E. Human Consumption of Microplastics. *Environ. Sci. Technol.* **2019**, *53* (12), 7068–7074. https://doi.org/10.1021/ACS.EST.9B01517.

(12) Hernandez, L. M.; Xu, E. G.; Larsson, H. C. E.; Tahara, R.; Maisuria, V. B.; Tufenkji, N. Plastic Teabags Release Billions of Microparticles and Nanoparticles into Tea. *Environ. Sci. Technol.* **2019**, *53* (21), 12300–12310. https://doi.org/10.1021/acs.est.9b02540.

(13) Winkler, A.; Santo, N.; Ortenzi, M. A.; Bolzoni, E.; Bacchetta, R.; Tremolada, P. Does Mechanical Stress Cause Microplastic Release from Plastic Water Bottles? *Water Res.* **2019**, *166*, 115082. https://doi.org/10.1016/J.WATRES.2019.115082.

(14) Weisser, J.; Beer, I.; Hufnagl, B.; Hofmann, T.; Lohninger, H.; Ivleva, N. P.; Glas, K. From the Well to the Bottle: Identifying Sources of Microplastics in Mineral Water. *Water 2021, Vol. 13, Page 841* **2021**, *13* (6), 841. https://doi.org/10.3390/W13060841.

(15) Allan, J.; Belz, S.; Hoeveler, A.; Hugas, M.; Okuda, H.; Patri, A.; Rauscher, H.; Silva, P.; Slikker, W.; B, S.-K.; Tong, W.; Anklam, E. Regulatory Landscape of Nanotechnology and Nanoplastics from a Global Perspective. *Regul. Toxicol. Pharmacol.* **2021**, *122*. https://doi.org/10.1016/J.YRTPH.2021.104885.

(16) Materić, D.; Kasper-Giebl, A.; Kau, D.; Anten, M.; Greilinger, M.; Ludewig, E.; Sebille, E. van; Röckmann, T.; Holzinger, R. Micro- and Nanoplastics in Alpine Snow: A New Method for Chemical Identification and (Semi)Quantification in the Nanogram Range. *Environ. Sci. Technol.* **2020**, *54* (4), 2353–2359. https://doi.org/10.1021/ACS.EST.9B07540.

(17) Ter Halle, A.; Jeanneau, L.; Martignac, M.; Jardé, E.; Pedrono, B.; Brach, L.; Gigault, J. Nanoplastic in the North Atlantic Subtropical Gyre. *Environ. Sci. Technol.* **2017**, *51* (23), 13689–13697. https://doi.org/10.1021/acs.est.7b03667.

(18) Gillibert, R.; Balakrishnan, G.; Deshoules, Q.; Tardivel, M.; Magazzù, A.; Donato, M. G.; Maragò, O. M.; Lamy De La Chapelle, M.; Colas, F.; Lagarde, F.; Gucciardi, P. G. Raman Tweezers for Small Microplastics and Nanoplastics Identification in Seawater. *Environ. Sci. Technol.* **2019**, *53* (15), 9003–9013. https://doi.org/10.1021/acs.est.9b03105.

(19) Valsesia, A.; Quarato, M.; Ponti, J.; Fumagalli, F.; Gilliland, D.; Colpo, P. Combining Microcavity Size Selection with Raman Microscopy for the Characterization of Nanoplastics in Complex Matrices. *Sci. Rep.* **2021**, *11* (1). https://doi.org/10.1038/s41598-020-79714-z.

(20) Schwaferts, C.; Niessner, R.; Elsner, M.; Ivleva, N. P. Methods for the Analysis of Submicrometer- and Nanoplastic Particles in the Environment. *TrAC - Trends in Analytical Chemistry*. Elsevier B.V. March 1, 2019, pp 52–65. https://doi.org/10.1016/j.trac.2018.12.014.

(21) Hamzah, M.; Khenfouch, M.; Rjeb, A.; Sayouri, S.; Houssaini, D. S.; Darhouri, M.; Srinivasu, V. V. Surface Chemistry Changes and Microstructure Evaluation of Low Density Nanocluster Polyethylene under Natural Weathering: A Spectroscopic

Investigation. In *Journal of Physics: Conference Series*; Institute of Physics Publishing, 2018; Vol. 984. https://doi.org/10.1088/1742-6596/984/1/012010.

(22) Liu, P.; Zhan, X.; Wu, X.; Li, J.; Wang, H.; Gao, S. Effect of Weathering on Environmental Behavior of Microplastics: Properties, Sorption and Potential Risks. *Chemosphere* **2020**, *242*. https://doi.org/10.1016/J.CHEMOSPHERE.2019.125193.

(23) Potenza, M. A. C.; Sanvito, T.; Pullia, A. Measuring the Complex Field Scattered by Single Submicron Particles. *AIP Adv.* **2015**, *5* (11), 117222. https://doi.org/10.1063/1.4935927.

(24) Gniadek, M.; Dąbrowska, A. The Marine Nano- and Microplastics Characterisation by SEM-EDX: The Potential of the Method in Comparison with Various Physical and Chemical Approaches. *Mar. Pollut. Bull.* **2019**, *148*, 210–216. https://doi.org/10.1016/J.MARPOLBUL.2019.07.067.

(25) Schymanski, D.; Goldbeck, C.; Humpf, H. U.; Fürst, P. Analysis of Microplastics in Water by Micro-Raman Spectroscopy: Release of Plastic Particles from Different Packaging into Mineral Water. *Water Res.* **2018**, *129*, 154–162. https://doi.org/10.1016/J.WATRES.2017.11.011.

(26) Facchetti, S. V.; La Spina, R.; Fumagalli, F.; Riccardi, N.; Gilliland, D.; Ponti, J. Detection of Metal-Doped Fluorescent Pvc Microplastics in Freshwater Mussels. *Nanomaterials* **2020**, *10* (12), 1–14. https://doi.org/10.3390/nano10122363.

(27) Galafassi, S.; Di Cesare, A.; Di Nardo, L.; Sabatino, R.; Valsesia, A.; Fumagalli, F.; G, C.; Volta, P. Microplastic Retention in Small and Medium Municipal Wastewater Treatment Plants and the Role of the Disinfection. *Environ. Sci. Pollut. Res. Int.* **2021**. https://doi.org/10.1007/S11356-021-16453-2.

(28) Beamson, G.; Clark, D. T.; Kendrick, J.; Briggs, D. *Observation of Vibrational Asymmetry in the High Resolution Monochromatized XPS of Hydrocarbon Polymers*; 1991.

(29) Potenza, M. A. C.; Albani, S.; Delmonte, B.; Villa, S.; Sanvito, T.; Paroli, B.; Pullia, A.; Baccolo, G.; Mahowald, N.; Maggi, V. Shape and Size Constraints on Dust Optical Properties from the Dome C Ice Core, Antarctica. *Sci. Rep.* **2016**, *6*. https://doi.org/10.1038/srep28162.

(30) Chyacutelek, P.; Grams, G. W.; Pinnick, R. G. Light Scattering by Irregular Randomly Oriented Particles. *Science* **1976**, *193* (4252), 480–482. https://doi.org/10.1126/SCIENCE.193.4252.480.

(31) Chýlek, P.; Wang, R. T.; Pinnick, R. G.; Srivastava, V. Scattering of Electromagnetic Waves by Composite Spherical Particles: Experiment and Effective Medium Approximations. *Appl. Opt. Vol. 27, Issue 12, pp. 2396-2404* **1988**, *27* (12), 2396–2404. https://doi.org/10.1364/AO.27.002396.

(32) Nava, G.; Fumagalli, F.; Gambino, S.; Farella, I.; Dell'Erba, G.; Beretta, D.; Divitini, G.; Ducati, C.; Caironi, M.; Cola, A.; Di Fonzo, F. Towards an Electronic Grade Nanoparticle-Assembled Silicon Thin Film by Ballistic Deposition at Room

Temperature: The Deposition Method, and Structural and Electronic Properties. *J. Mater. Chem. C* **2017**, *5* (15). https://doi.org/10.1039/C7TC00187H.

(33) Nava, G.; Fumagalli, F.; Fonzo, F. Di. Large Area Porous 1D Photonic Crystals Comprising Silicon Hierarchical Nanostructures Grown by Plasma-Assisted, Nanoparticle Jet Deposition. *Artic. Nanotechnol.* **2018**. https://doi.org/10.1088/1361-6528/aade21.

(34) Katiyar, N. K.; Biswas, K.; Tiwary, C. S. Cryomilling as Environmentally Friendly Synthesis Route to Prepare Nanomaterials. *https://doi.org/10.1080/09506608.2020.1825175* **2020**, *66* (7), 493–532. https://doi.org/10.1080/09506608.2020.1825175.

(35) Bach, C.; Dauchy, X.; Etienne, S. Characterization of Poly(Ethylene Terephthalate) Used in Commercial Bottled Water. In *IOP Conference Series: Materials Science and Engineering*; 2009; Vol. 5. https://doi.org/10.1088/1757-899X/5/1/012005.

(36) Iiyama, K.; Ishida, T.; Ono, Y.; Maruyama, T.; Yamagishi, T. Fabrication and Characterization of Amorphous Polyethylene Terephthalate Optical Waveguides. *IEEE Photonics Technol. Lett.* **2011**, *23* (5), 275–277. https://doi.org/10.1109/LPT.2010.2101058.

(37) Gaston, F.; Dupuy, N.; Marque, S. R. A.; Dorey, S. Evaluation of Multilayer Film Stability by Raman Spectroscopy after Gamma-Irradiation Sterilization Process. *Vib. Spectrosc.* **2018**, *96*, 52–59. https://doi.org/10.1016/J.VIBSPEC.2018.03.002.

(38) Snyder, R. G.; Hsu, S. L.; Krimm, S. Vibrational Spectra in the C□H Stretching Region and the Structure of the Polymethylene Chain. *Spectrochim. Acta Part A Mol. Spectrosc.* **1978**, *34* (4), 395–406. https://doi.org/10.1016/0584-8539(78)80167-6.

(39) Bentley, P. A.; Hendra, P. J. Polarised FT Raman Studies of an Ultra-High Modulus Polyethylene Rod. *Spectrochim. Acta Part A Mol. Biomol. Spectrosc.* **1995**, *51* (12), 2125–2131. https://doi.org/10.1016/0584-8539(95)01513-3.

(40) Zhang, D.; Shen, Y. R.; Somorjai, G. A. Studies of Surface Structures and Compositions of Polyethylene and Polypropylene by IR+visible Sum Frequency Vibrational Spectroscopy. *Chem. Phys. Lett.* **1997**, *281* (4–6), 394–400. https://doi.org/10.1016/S0009-2614(97)01311-0.

(41) Cowger, W.; Steinmetz, Z.; Gray, A.; Munno, K.; Lynch, J.; Hapich, H.; Primpke, S.; Frond, H. De; Rochman, C.; Herodotou, O. Microplastic Spectral Classification Needs an Open Source Community: Open Specy to the Rescue! *Anal. Chem.* **2021**, *93* (21), 7543–7548. https://doi.org/10.1021/ACS.ANALCHEM.1C00123.

(42) Migler, K. B.; Kotula, A. P.; Walker, A. R. H. Trans-Rich Structures in Early Stage Crystallization of Polyethylene. *Macromolecules* **2015**, *48* (13), 4555–4561. https://doi.org/10.1021/MA5025895.

(43) Rull, F.; Prieto, A. C.; Casado, J. M.; Sobron, F.; Edwards, H. G. M. *Estimation of Crystallinity in Polyethylene by Raman Spectroscopy*; 1993; Vol. 24.

(44) Bach, C.; Dauchy, X.; Etienne, S. Characterization of Poly(Ethylene Terephthalate) Used in Commercial Bottled Water. *IOP Conf. Ser. Mater. Sci. Eng.* **2009**, *5* (1). https://doi.org/10.1088/1757-899X/5/1/012005.

(45) Furukawa, T.; Sato, H.; Kita, Y.; Matsukawa, K.; Yamaguchi, H.; Ochiai, S.; Siesler, H. W.; Ozaki, Y. Molecular Structure, Crystallinity and Morphology of Polyethylene/ Polypropylene Blends Studied by Raman Mapping, Scanning Electron Microscopy, Wide Angle X-Ray Diffraction, and Differential Scanning Calorimetry. *Polym. J.* **2006**, *38* (11), 1127–1136. https://doi.org/10.1295/polymj.PJ2006056.

(46) Corsetti, S.; Rabl, T.; McGloin, D.; Kiefer, J. Intermediate Phases during Solid to Liquid Transitions in Long-Chain n-Alkanes. *Phys. Chem. Chem. Phys.* **2017**, *19* (21), 13941–13950. https://doi.org/10.1039/C7CP01468F.

(47) Tomba, J. P.; Silva, L. I.; Genga, M. G.; Galland, G. B.; Perez, C. J. Characterizing Chemical Composition of Polyolefin-Based Copolymers from Spectral Features in the C—H Stretching Region. *J. Raman Spectrosc.* **2019**, *50* (4), 576–586. https://doi.org/10.1002/JRS.5554.

(48) Jin, Y.; Kotula, A. P.; Snyder, C. R.; Hight Walker, A. R.; Migler, K. B.; Lee, Y. J. Raman Identification of Multiple Melting Peaks of Polyethylene. *Macromolecules* **2017**, *50* (16), 6174–6183. https://doi.org/10.1021/ACS.MACROMOL.7B01055.

(49) Howell, N. K.; Arteaga, G.; Nakai, S.; Li-Chan, E. C. Y. Raman Spectral Analysis in the C - H Stretching Region of Proteins and Amino Acids for Investigation of Hydrophobic Interactions. *J. Agric. Food Chem.* **1999**, *47* (3), 924–933. https://doi.org/10.1021/jf981074l.

(50) Portesi, C.; Visentin, D.; Durbiano, F.; Abete, M. C.; Rizzi, M.; Maurino, V.; Rossi, A. M. Development of a Rapid Micro-Raman Spectroscopy Approach for Detection of NIAS in LDPE Pellets and Extruded Films for Food Packaging Applications. *Polym. Test.* **2019**, *80*, 106098. https://doi.org/10.1016/J.POLYMERTESTING.2019.106098.

(51) Veitmann, M.; Jumeau, R.; Bourson, P.; Ferriol, M.; Lahure, F. Understanding and Control of High Temperature Oxidation Flaws of Low-Density Poly(Ethylene) with Raman Spectroscopy. *Int. J. Spectrosc.* **2014**, *2014*, 1–9. https://doi.org/10.1155/2014/194563.

(52) Villa, S.; Sanvito, T.; Paroli, B.; Pullia, A.; Delmonte, B.; Potenza, M. A. C. Measuring Shape and Size of Micrometric Particles from the Analysis of the Forward Scattered Field. *J. Appl. Phys.* **2016**, *119* (22). https://doi.org/10.1063/1.4953332.

(53) Bohren, C. F.; Huffman, D. R. Absorption and Scattering of Light by Small Particles. *Absorpt. Scatt. Light by Small Part.* **1998**. https://doi.org/10.1002/9783527618156.

(54) Strobl, G. R.; Hagedorn, W. Raman Spectroscopic Method for Determining the Crystallinity of Polyethylene. *J. Polym. Sci. Polym. Phys. Ed.* **1978**, *16* (7), 1181–1193. https://doi.org/10.1002/POL.1978.180160704.

(55) Bañuls-Ciscar, J.; Fumagalli, F.; Ruiz-Moreno, A.; Rossi, F.; Suraci, S. V.; Fabiani, D.; Ceccone, G. A Methodology to Investigate Heterogeneous Oxidation of Thermally Aged

Cross-Linked Polyethylene by ToF-SIMS. *Surf. Interface Anal.* **2020**, *52* (12), 1178–1184. https://doi.org/10.1002/sia.6848.

(56) Bennet, F.; Müller, A.; Radnik, J.; Hachenberger, Y.; Jungnickel, H.; Laux, P.; Luch, A.; Tentschert, J. Preparation of Nanoparticles for ToF-SIMS and XPS Analysis. *J. Vis. Exp.* **2020**, *163*.

(57) Baer, D. R.; Engelhard, M. H. XPS Analysis of Nanostructured Materials and Biological Surfaces. *J. Electron Spectros. Relat. Phenomena* **2010**, *178–179* (C), 415–432. https://doi.org/10.1016/j.elspec.2009.09.003.

(58) Shard, A. G. Practical Guides for X-Ray Photoelectron Spectroscopy: Quantitative XPS. *J. Vac. Sci. Technol. A* **2020**, *38* (4), 041201. https://doi.org/10.1116/1.5141395.

Supporting Information

"Detection and formation mechanisms of secondary nanoplastic released from drinking water bottles"

Data tables: Table S1 – S4

Graphics: Figure S1 – S13

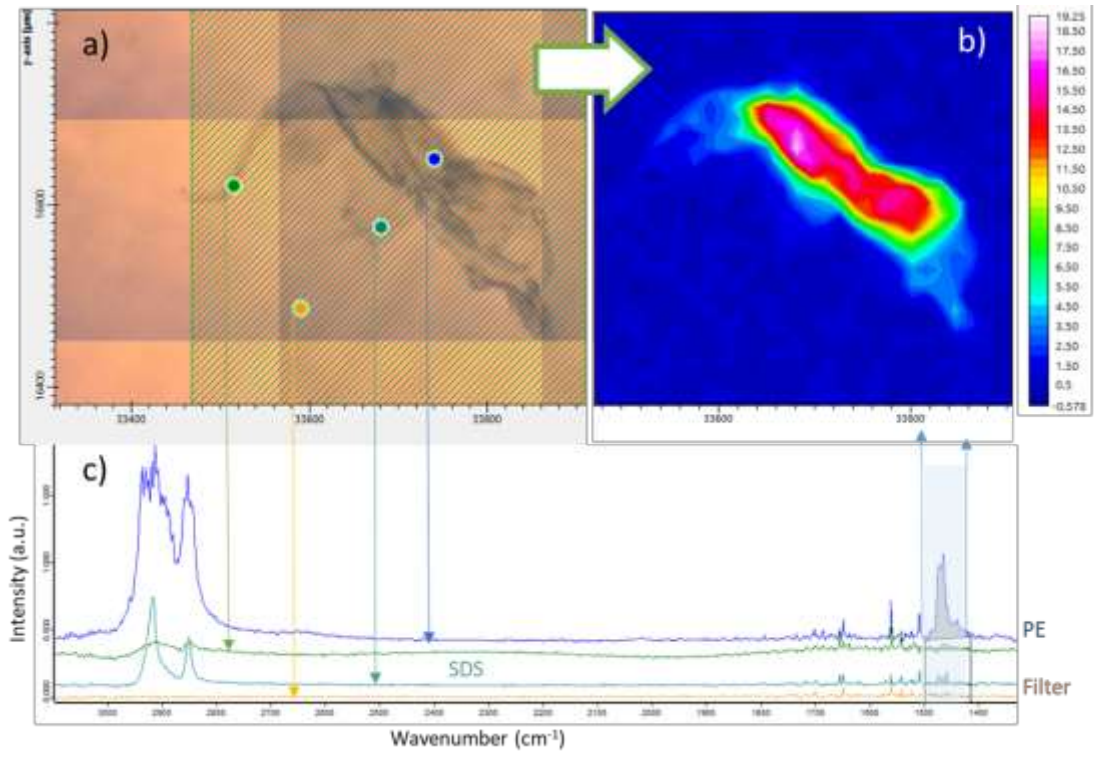

Figure S1. Optical image (a) selected spectra and FTIR chemical image (b) and full spectra form selected areas (c) of a microplastic PE fragment on an Anodisc filter (filtered solution with released particles from a bottle opened/closed 50 times). The μ-FTIR images were generated by choosing the band region of 1470–1405 cm^{-1} for integration. The colour-scale represents the intensity of the integrated band. All pictures have the same lateral dimensions as labelled in the X and Y axis in panel (a) and (c).

Full filters after filtration were imaged in reflection and potential region of interest were manually selected for subsequent spectroscopic analysis (see Figure S1a). On average, each replica filter presented a number of candidate objects between 30 and 100. Each object IR transmission spectrum was recorded and analysed. In triplicate filters analysis the most common spectral hit was assigned to polyamide (around 10% of the hits, know source of contamination in our laboratory) and to sodium dodecyl sulphate (SDS), an anionic surfactant used to aid hydrophobic particles recovery from the solution (see Figure S1b). In some cases, broadband unassigned spectra were recorded but reliable spectral match with the available libraries was not possible. In experiments using water recovered from cap washing (50x

openings) only one single, large plastic particle (390 µm in size) was detected and assigned to PE. The band centred at 1405–1470 cm^{-1} (CH_2 and CH_3 bending vibration) was used for chemical imaging of the PE particle (see Figure S1c).

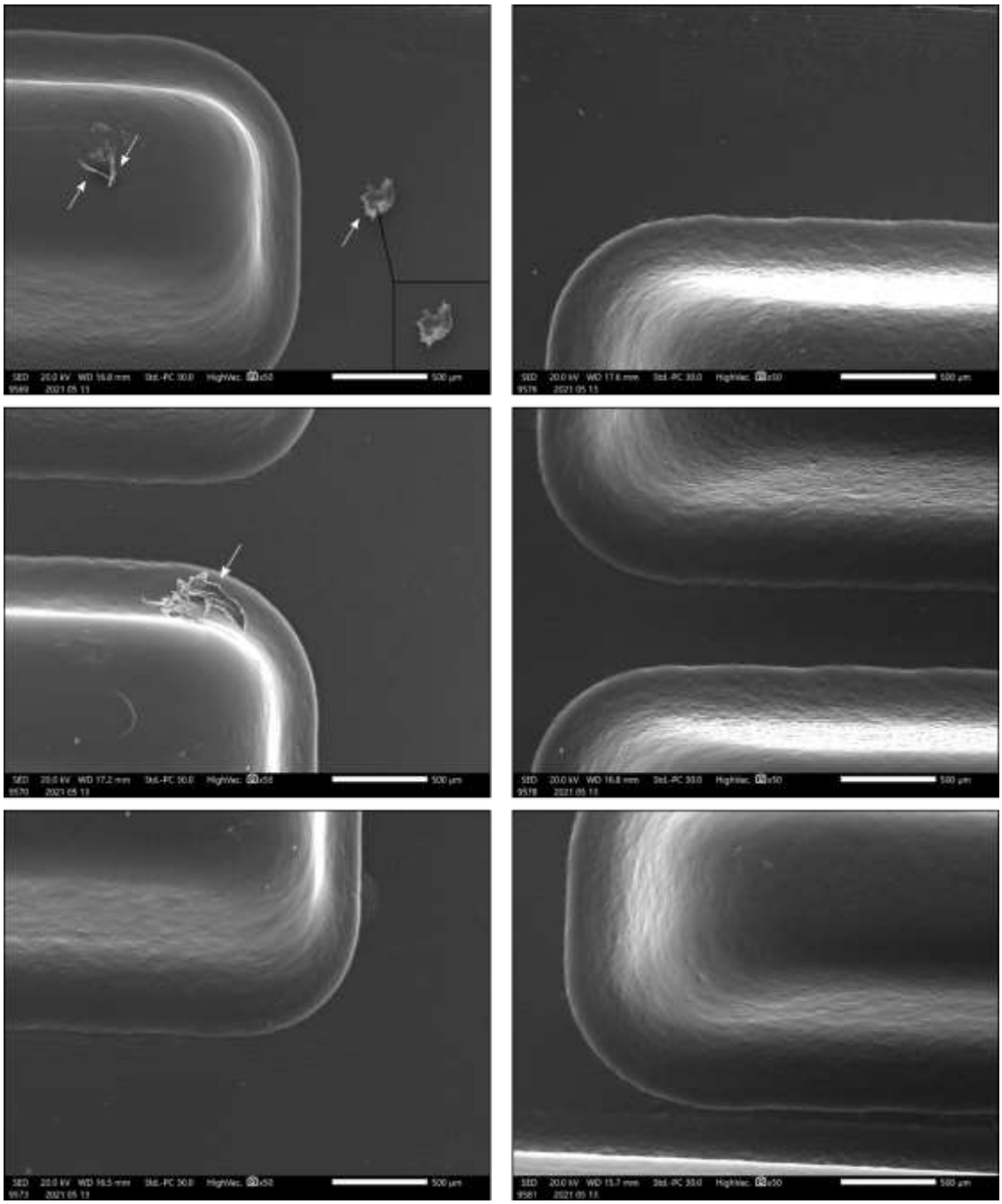

Figure S2. SEM images of bottlenecks (vertical line from top to bottom, magnification 50X) of two bottles opened/closed 50 times. Left panel: before immersion of the bottle in mQ-H_2O. Right panel: after immersion of the bottle in mQ-H_2O. Particles indicated with a white arrow were analysed by EDX (see Figure S3).

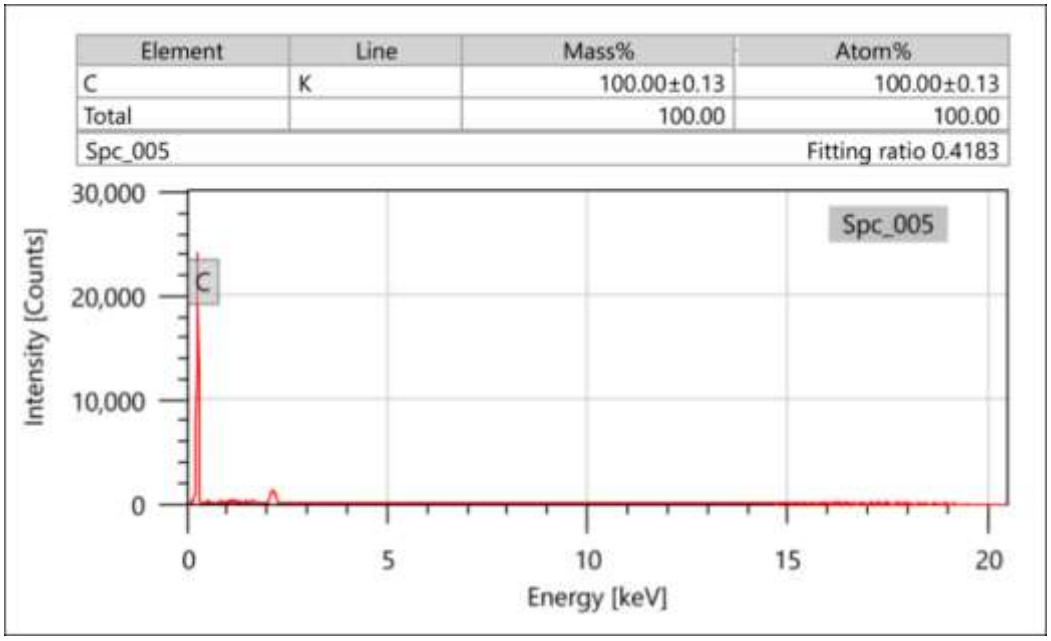

Figure S3. EDX spectrum representative for all particles on bottleneck (> 100 µm in size, indicated with white arrow in Figure S2), showing an elemental composition of 100% carbon, which is consistent with HDPE (cap material) and other common polymers compositions.

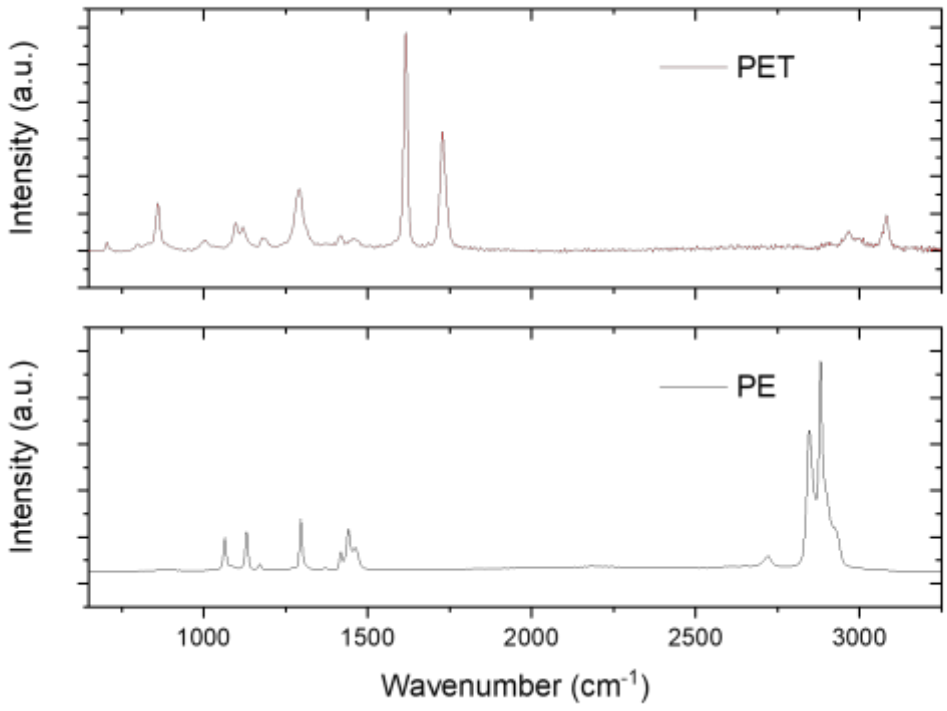

Figure S4. Raman reference spectra for the drinking water bottle bulk materials (upper panel, bottleneck assigned to PET; lower panel bottle screw cap assigned to PE).

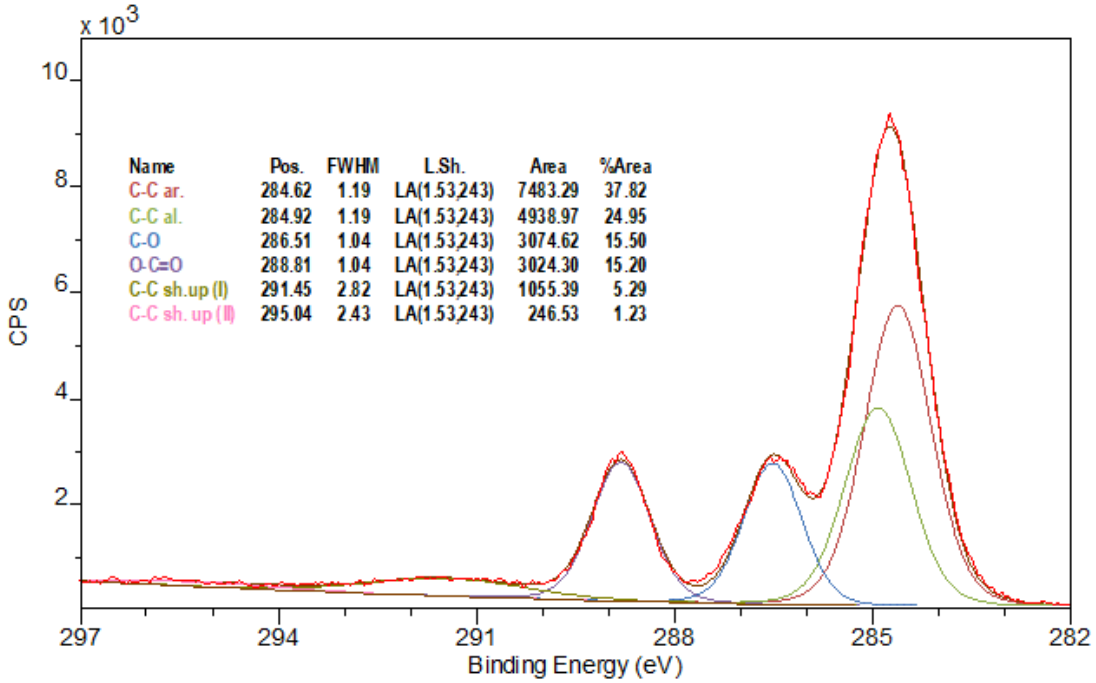

Figure S5. High-resolution reference spectrum (lower panel) of C 1s peak of bottle bulk material, with individual components deconvolution (bottleneck, assigned to PET). The corresponding reference spectra for the bottle screw cap (assigned to PE) is shown in Figure 2c in the main article.

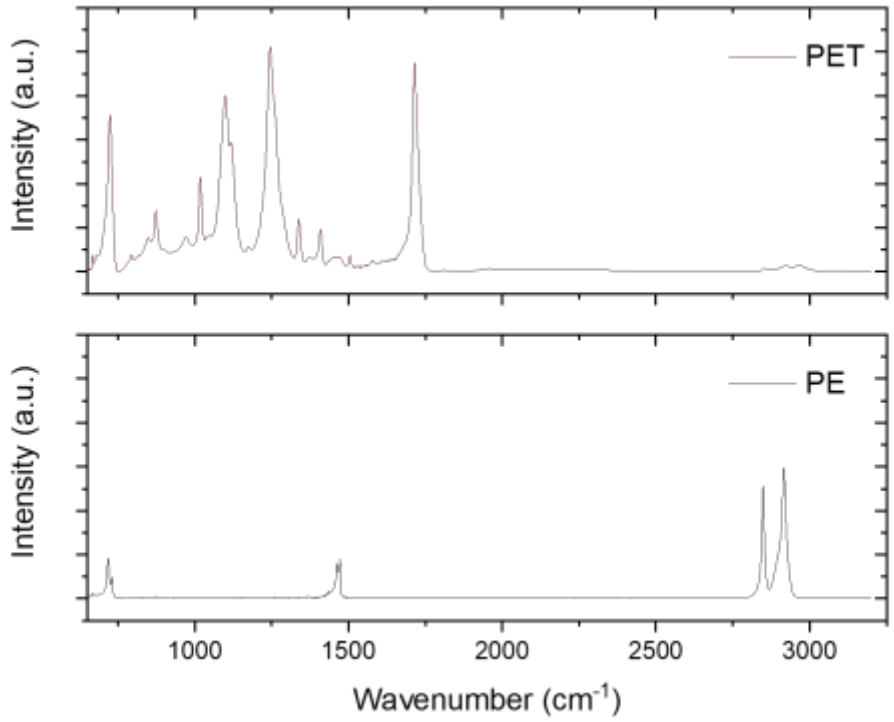

Figure S6. ATR-FTIR reference spectra for the drinking water bottle bulk materials (upper panel, bottle neck assigned to PET; lower panel bottle screw cap assigned to PE).

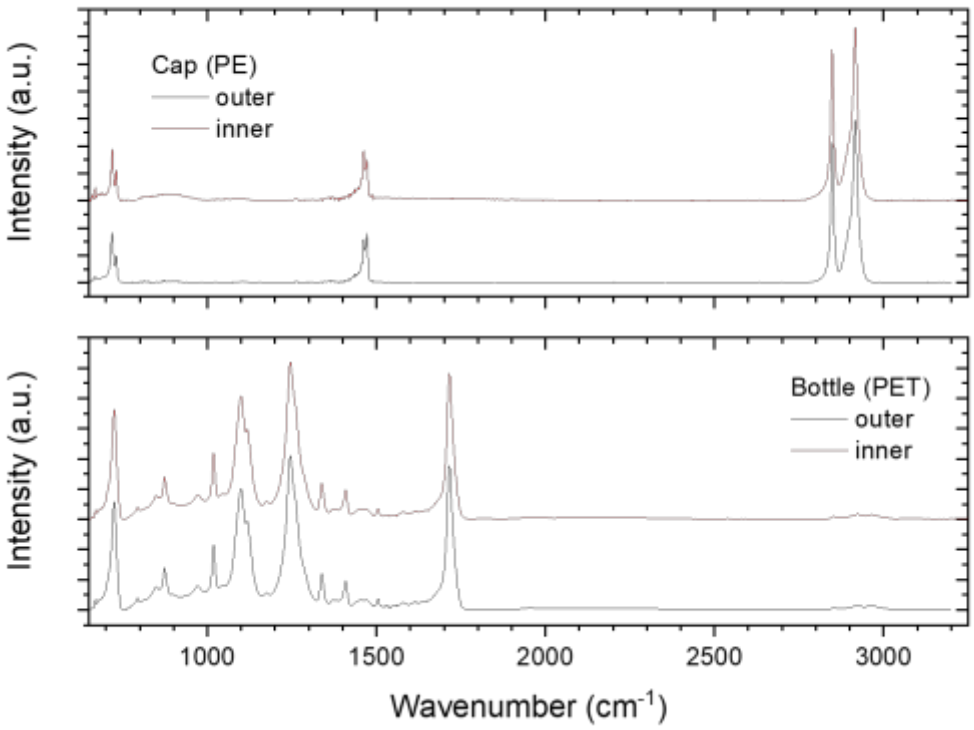

Figure S7. ATR-FTIR reference spectra for the drinking water bottle bulk materials comparing internal and external surfaces (lower panel, bottleneck assigned to PET; upper panel bottle screw cap assigned to PE).

Table S1. Surfaces atomic relative concentration (in percentage, %) table from XPS measurement of the HDPE cap and recovered nanoparticulate. Standard deviations indicated in brackets, concentrations are corrected after Teflon background subtraction.

	C1s (%)	*O1s* (%)	*N 1s* (%)	*Na 1s* (%)	*Ca 2p* (%)	*K 2p* (%)	*Cl 2p* (%)	*Si 2p* (%)
HDPE cap	**92.44 (2.1)**	**6.00 (1.52)**	--	--	--	--	--	**1.56 (0.51)**
Nanoparticulate	**62.14 (2.15)**	**22.23 (1.30)**	**5.10 (0.61)**	**1.50 (0.21)**	**3.06 (1.96)**	**2.71 (0.83)**	**2.09 (0.51)**	**1.17 (0.22)**

Bulk HDPE (Figure 2a) shows principally carbon (92.4±2.1)%, minor surface oxidation (6.0±1.5)% and traces of silicon (less than 2%, likely from siloxanes used as release agents in polymers production). The nanoparticulate spectrum (Figure 2b) exhibits a richer elemental composition: Carbon still dominates (62.1±2.1)%, Oxygen concentration increases (22.2±1.3)% and traces of Nitrogen, Potassium, Calcium, Sodium, Chlorine and Silicon were also detected (see Table S1). This increase can be attributed to the interplay between the

increased surface area and the interaction with the liquid environment, even if a contribution from airborne and/or manipulation contamination cannot be excluded.

Table S2. Surfaces carbon atom bonds relative concentration (in percentage, %) table from XPS measurement of the HDPE cap and recovered nanoparticulate. Standard deviations indicated in brackets, all vibrational contributions are summed in C-C, C-H contribution, individual C-O and C-N contributions are not resolved and are considered together, final concentrations are corrected after Teflon background subtraction.

	C-C, C-H *(%)*	***C-O, C-N*** *(%)*	***C=O*** *(%)*	***O-C=O*** *(%)*
HDPE cap	96.05 (2.89)	1.07 (0.44)	0.91 (0.32)	1.97 (0.56)
Nanoparticulate	55.66 (1.10)	26.25 (0.63)	15.83 (0.40)	2.26 (0.39)

A detailed analysis of high-resolution C 1s spectra (Figure 2c–d) revealed more details of the nanoparticle oxidation environment. C 1s peak envelope deconvolution for the bulk cap material allows to differentiate and quantify the small contributions (below 2%) from chemical shifts associated with different carbon-oxygen bonds (C-O, carbonyl and carboxyl, see details in Table S2).

Table S3. Particle size-distributions descriptors from SPES data fitting. Absolute number of recovered particle [N] (ad.), volumetric concentration *[c]* (cm^{-3}), refractive index, *n* (ad.), distribution mean, $\bar{d}$ (µm), distribution FWHM, d_{FWHM} (µm), distribution 10th percentile, D_{10} (µm) and distribution 90th percentile, D_{90} (µm). When appropriate, standard deviations are indicated in parentheses. For [N] the relative error in total number of particle estimation is around 20%.

Population A	$[N]_A$ *ad.*	$[c]_A$ cm^{-3}	n_A *ad.*	$\bar{d}_A$ *µm*	d_{FWHM_A} *µm*	D_{10_A} *µm*	D_{90_A} *µm*
mQ-H_2O	1.0E3	6.9E1	-- [c]	-- [c]	-- [c]	-- [c]	-- [c]
BLANK	11.8E4	7.9E3	1.43(0.04)	0.75	0.63	0.38	1.1
OPEN 1X	12.4E4	8.3E3	1.41(0.03)	0.82	0.63	0.42	1.2
OPEN 10X	13.5E5	9.0E4	1.43(0.04)	0.69	0.54	0.37	1.0
OPEN 50X	33.0E5	2.2E5	1.43(0.04)	0.64	0.54	0.36	0.92
Average[a]	n.a.[b]	n.a.[b]	1.42	0.72	0.57	0.38	1.04
St.Dev.[a]	n.a. [b]	n.a. [b]	0.01	0.09	0.05	0.03	0.14

Population B	$[N]_A$	$[c]_B$	n_B	$\bar{d}_B$	d_{FWHM_B}	D_{10_B}	D_{90_B}
	ad.	cm^{-3}	*ad.*	*µm*	*µm*	*µm*	*µm*
mQ-H_2O	1.8E3	1.2E2	1.37(0.05)	0.69	0.4	0.2	1.1
BLANK	6.4E3	4.3E2	1.42(0.03)	2.0	2.8	1.1	2.7
OPEN 1X	11.8E3	7.9E2	1.41(0.03)	2.2	1.8	1.2	3.1
OPEN 10X	13.0E4	8.7E3	1.37(0.03)	2.6	2.4	1.5	3.6
OPEN 50X	15.0E4	1.0E4	1.45(0.04)	1.6	1.5	0.87	2.2
Average[(a)]	n.a. [(b)]	n.a. [(b)]	1.41	2.13	1.90	1.19	2.97
St.Dev.[(a)]	n.a. [(b)]	n.a. [(b)]	0.04	0.50	0.46	0.32	0.71

a) Averages and standard deviations calculated only on OPEN 1x, 10x and 50x
b) Not applicable.
c) Validated particles count too low.

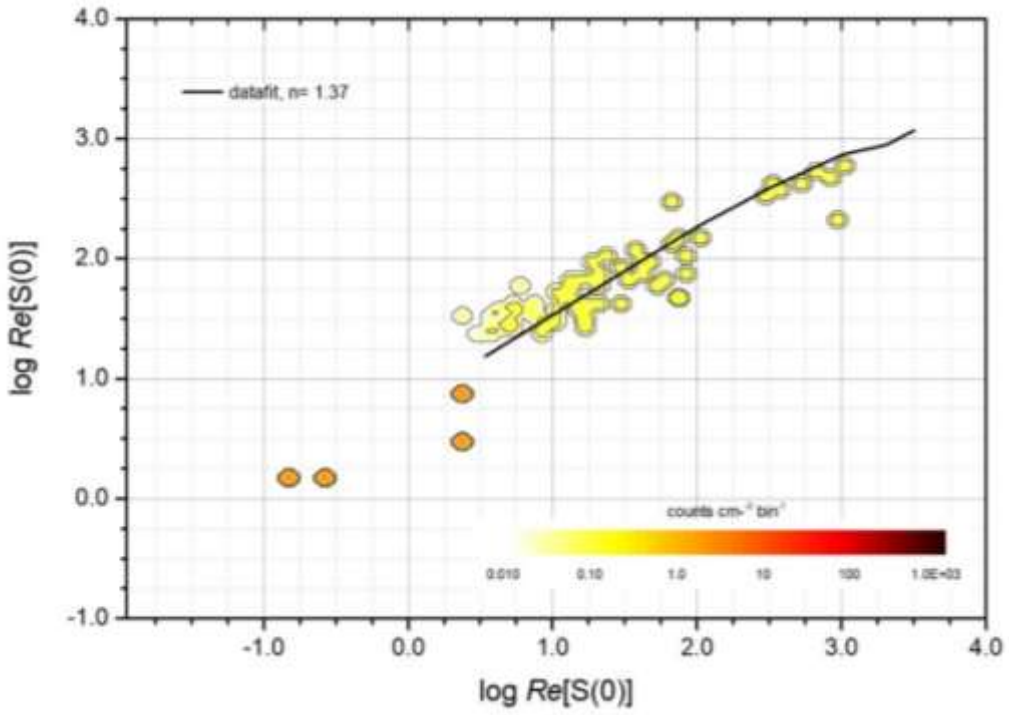

Figure S8. Experimental SPES results obtained with pristine mQ-H_2O.

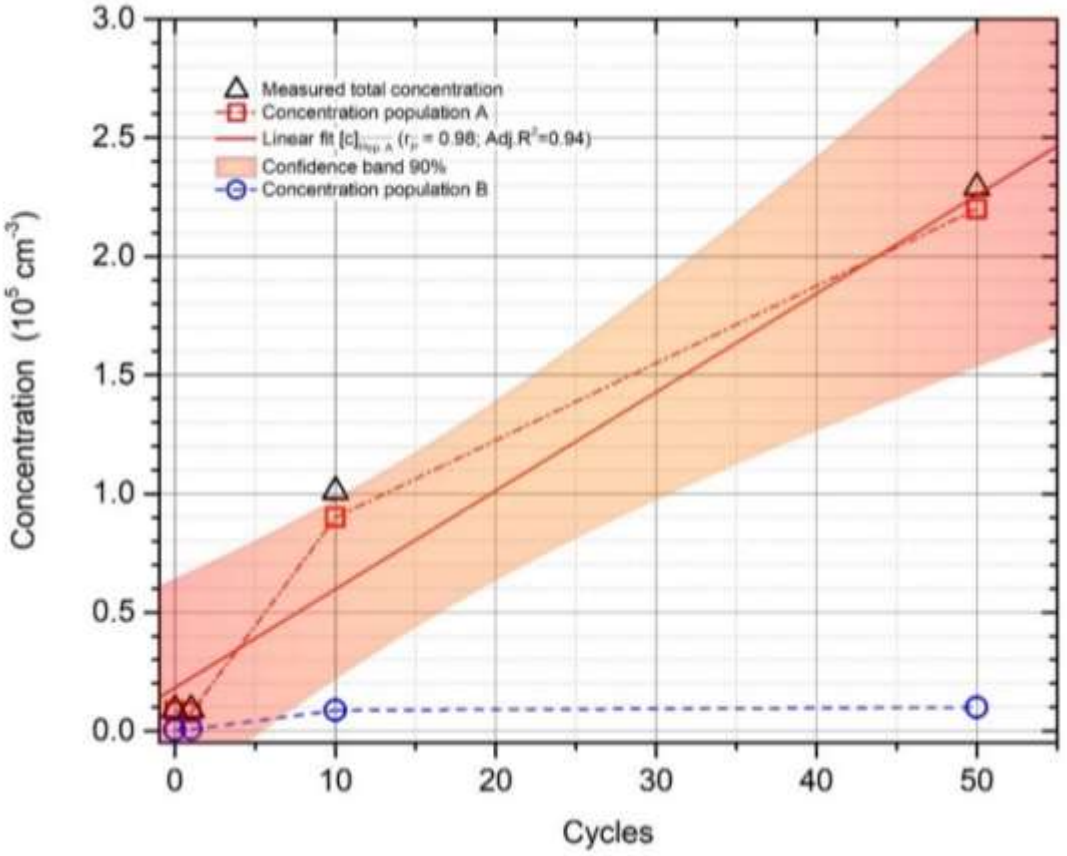

Figure S9. Absolute number of recovered nanoparticles obtained from SPES data plotted against number of opening/closing cycles.

Two factors are expected to contribute to micro/nanoparticulate collection and accumulation in the mQ-H_2O dispersion used to wash bottlenecks surfaces: i) collection of airborne aerosols from the lab environment and ii) accumulation of micro- or nanoplastic particles originating from the bottle materials due to the mechanical effects (e.g. stress, abrasion) occurring during the opening/closing action. These factors are expected to correlate positively with the ambient exposure time ("open" time of the cycle) and with the number of opening cycles, respectively. While the former collection pathway could contribute to the accumulation of a variety of nanomaterials, the latter is expected to generate mainly HDPE and/or PET particulate.

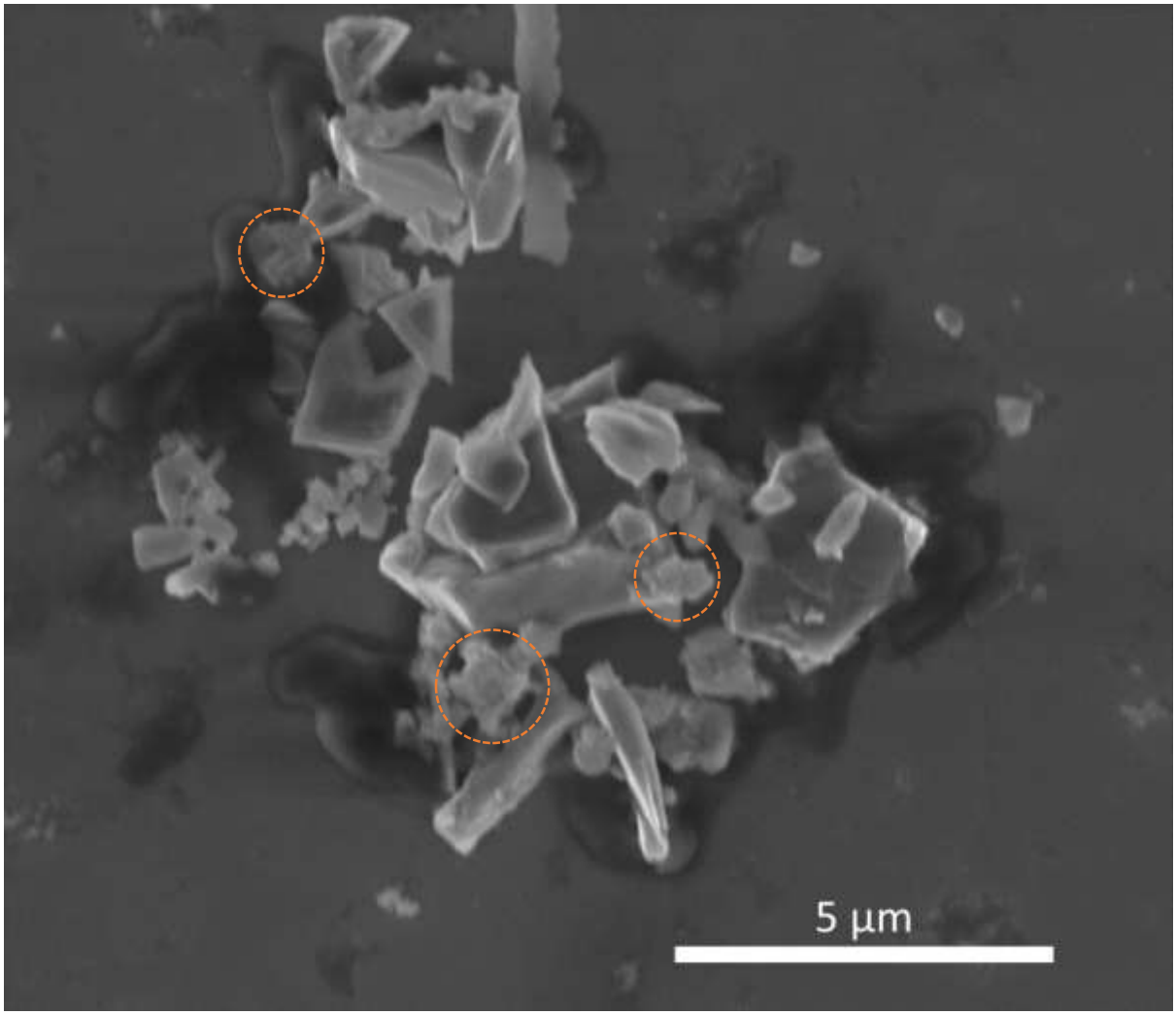

Figure S10. High-resolution SEM (magnification 16kX) of particles recovered from washing bottleneck opened/closed 50 times, showing non-spherical shapes and the presence of conglomerates (red circles).

We should also note here that the theoretical void fraction values depend non-trivially on the details of the shape of the particles,[1] especially in the case of highly anisotropic objects and from the size distribution dispersion but considering the characterisation data available for our particle distribution (see Figure 4) and high-resolution SEM images (see Figure S10), the isometric and monodisperse assumptions can be considered to hold in good approximation for a qualitative analysis.

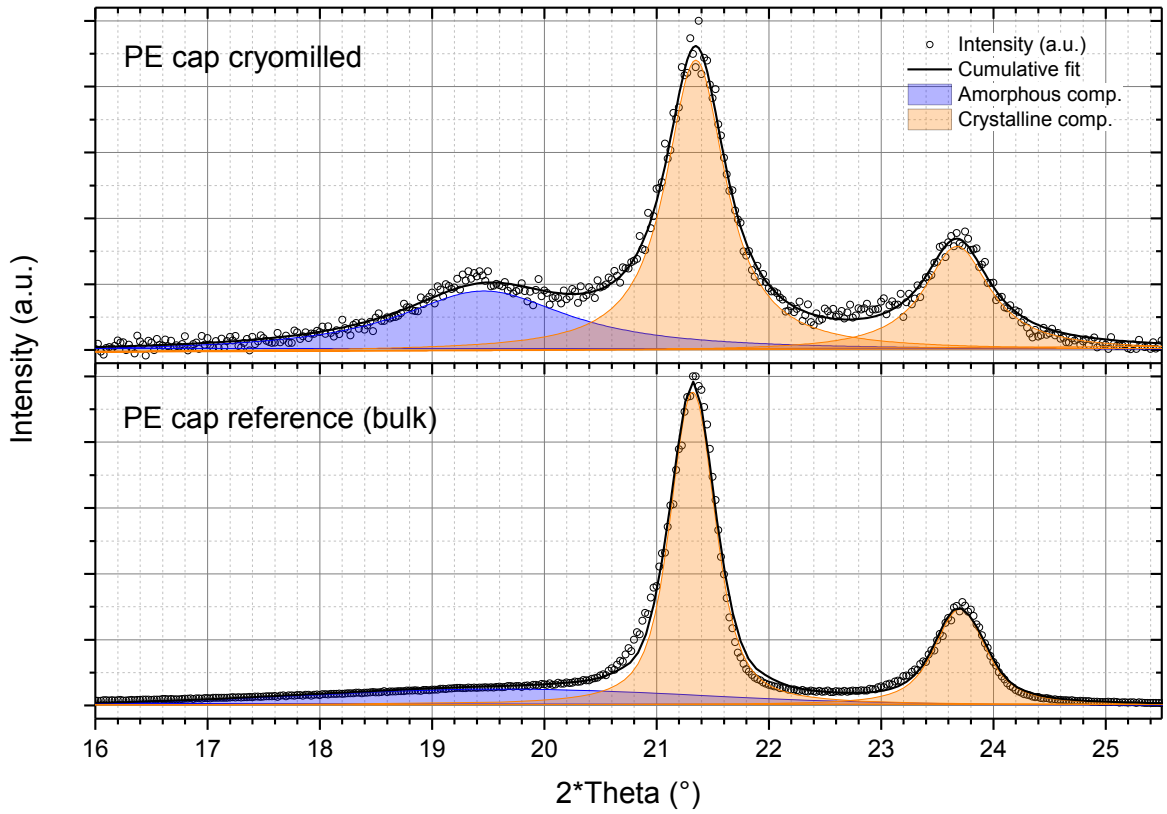

Figure S11. X-ray diffraction pattern in the region 16° < 2θ < 25° and peak deconvolution from cryomilled PE cap material (upper panel) and PE cap bulk reference material (lower panel).

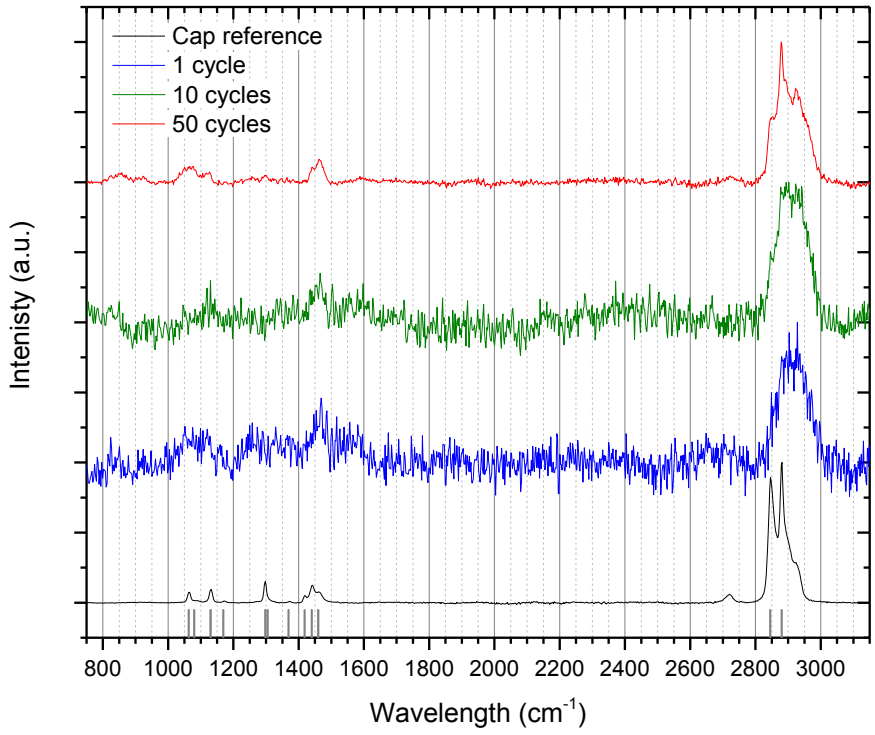

Figure S12. Confocal Raman spectrum of the water bottle HDPE cap surface (black) and particulate recovered from water bottle opened/closed 1 (blue), 10 (green), and 50 (red) times. Data are normalized to max intensity. Black vertical lines above the X-axis represent HDPE reference Raman peak centre positions taken from literature.[6–9]

Table S4. Vibrational modes and phase assignments of Raman bands of PE.

(*) ± 2 cm-1 depending on the reference.[2–5]

(**) Notation from Snyder et al.,[3]

Raman shift* / cm^{-1}	**Vibrational modes**	**Phase assignment**
1063	$\nu_{as.}$ (C-C) stretch	Trans chain
1080	ν (C-C) stretch	Amorphous
1130	$\nu_{s.}$ (C-C) stretch	Trans chain
1169	ρ (CH_2) rock	Trans chain
1270	Unassigned	--
1298	τ (CH_2) twist	Trans chain

1305	τ (CH_2) twist	Amorphous
1369	ω (CH_3) wag	Amorphous
1418	δ (CH_2) + ω (CH_2) bend + wag	Crystalline (orthorhombic)
1440	δ (CH_2) bend	Trans chain
1460	δ (CH_2) bend	Amorphous
2845	$\nu_{s.}$ (CH_2) stretch	Crystalline, Amorphous
2871	ν_s (CH_3) stretch	
2880	$\nu_{as.}$ (CH_2) stretch	Crystalline, Amorphous
2900	Fermi resonance $d(0)^+ \delta\delta^+(0)$ (**)	
2930	Fermi resonance $d(0)^+ \delta\delta^+(\pi)$ (**)	
2952	ν_{as} (CH_3) stretch (in-plane)	
2964	ν_{as} (CH_3) stretch (out-of-plane)	

In this sample (Figure 6), three peaks are observed in the C-C stretch region; a broad peak centred near 1080 cm^{-1} arising from amorphous conformations and two narrower components at 1060 and 1130 cm^{-1} assigned to antisymmetric and symmetric *trans* conformations (containing contributions from both orthorhombic crystalline and non-crystalline consecutive trans). The latter mesomorphic phase consists of locally aligned, *trans*-rich chain segments, and it is normally regarded as a pre-crystalline structure.[6] Just beside the C-C region, a small, sharp peak located at 1169 cm^{-1} is observed and assigned to the CH_2 rock vibration. This vibration is normally also assigned to *trans* conformations.[7] In the next region, typical of the CH_2 twist vibrations, two individual peaks can be isolated; a strong, sharp peak centred at 1298 cm^{-1} and attributed to *trans* conformations, and a broad, less intense peak appearing at 1305 cm^{-1} as a high wavenumber shoulder of the stronger peak and attributed to amorphous conformations. Computational results suggest that the sharp CH_2 twist peak could arise from the contribution of extended mesomorphic regions spanning 3 to 5 consecutive *trans* chains. Therefore, this band is normally used as an internal standard[8] for normalisation and crystallinity calculations. The third region includes CH_2 bend vibrations; it exhibits a complex band that can be deconvolved using three independent peaks. The first peak head at 1416 cm^{-1} is uniquely assigned to interchain interactions arising from bending and wagging vibrations in the orthorhombic unit cell of the polymer crystalline domains. The two peak heads appearing at higher wavenumbers belong instead to CH_2 bending modes and arise from *trans* conformations (at 1440 cm^{-1}) and amorphous domains (at 1460 cm^{-1}), respectively.

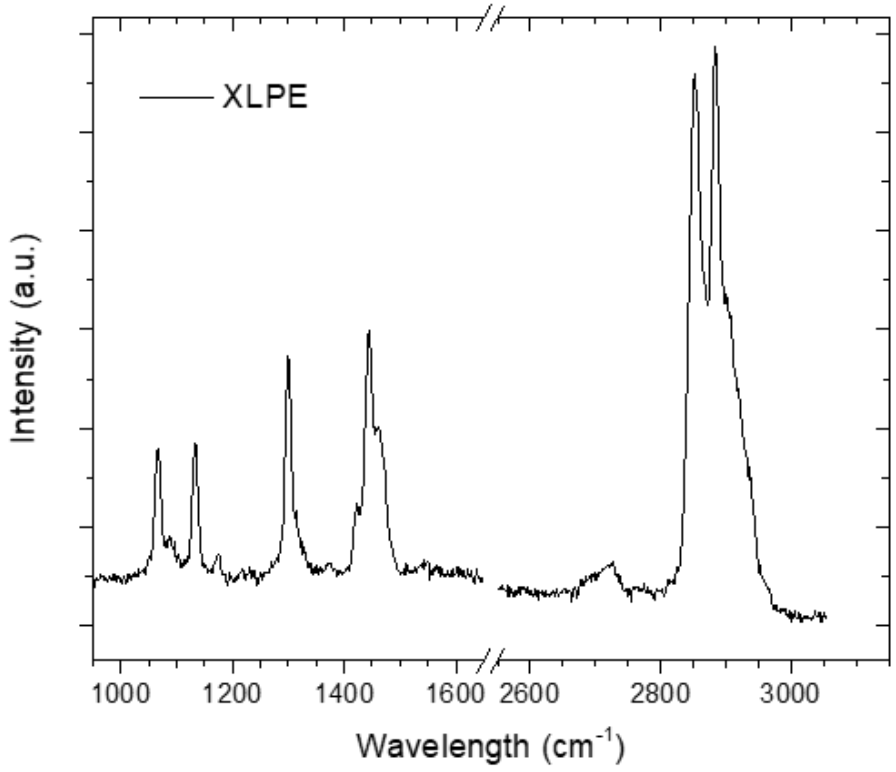

Figure S13. Confocal Raman spectrum of reference cross-linked polyethylene, XLPE (calculated crystallinity around 50%). Data are shown in the group frequencies and CH_2-stretching characteristic regions.

References

1. Donev, A. et al. Improving the Density of Jammed Disordered Packings Using Ellipsoids. Science (80). 303, 990–993 (2004).

2. Gaston, F., Dupuy, N., Marque, S. R. A. & Dorey, S. Evaluation of multilayer film stability by Raman spectroscopy after gamma-irradiation sterilization process. Vib. Spectrosc. 96, 52–59 (2018).

3. Snyder, R. G., Hsu, S. L. & Krimm, S. Vibrational spectra in the C□H stretching region and the structure of the polymethylene chain. Spectrochim. Acta Part A Mol. Spectrosc. 34, 395–406 (1978).

4. Bentley, P. A. & Hendra, P. J. Polarised FT Raman studies of an ultra-high modulus polyethylene rod. Spectrochim. Acta Part A Mol. Biomol. Spectrosc. 51, 2125–2131 (1995).

5. Zhang, D., Shen, Y. R. & Somorjai, G. A. Studies of surface structures and compositions of polyethylene and polypropylene by IR+visible sum frequency vibrational spectroscopy. Chem. Phys. Lett. 281, 394–400 (1997).

6. Migler, K. B., Kotula, A. P. & Walker, A. R. H. Trans-Rich Structures in Early Stage Crystallization of Polyethylene. Macromolecules 48, 4555–4561 (2015).

7. Furukawa, T. *et al.* Molecular structure, crystallinity and morphology of polyethylene/ polypropylene blends studied by Raman mapping, scanning electron microscopy, wide angle X-ray diffraction, and differential scanning calorimetry. *Polym. J.* **38**, 1127–1136 (2006).

8. Meier, R. J. Studying the length of trans conformational sequences in polyethylene using Raman spectroscopy: a computational study. *Polymer (Guildf).* **43**, 517–522 (2002).

PAPER 5 – Human airway organoids and microplastic fibers: a new exposure model for emerging contaminants

Anna Winkler, Alessandro Cherubini, Francesco Rusconi, Nadia Santo, Laura Madaschi, Pistoni Clelia, Giorgia Moschetti, Maria Lucia Sarnicola, Mariacristina Crosti, Lorenzo Rosso, Paolo Tremolada, Lorenza Lazzari, Renato Bacchetta

Environment International 2022

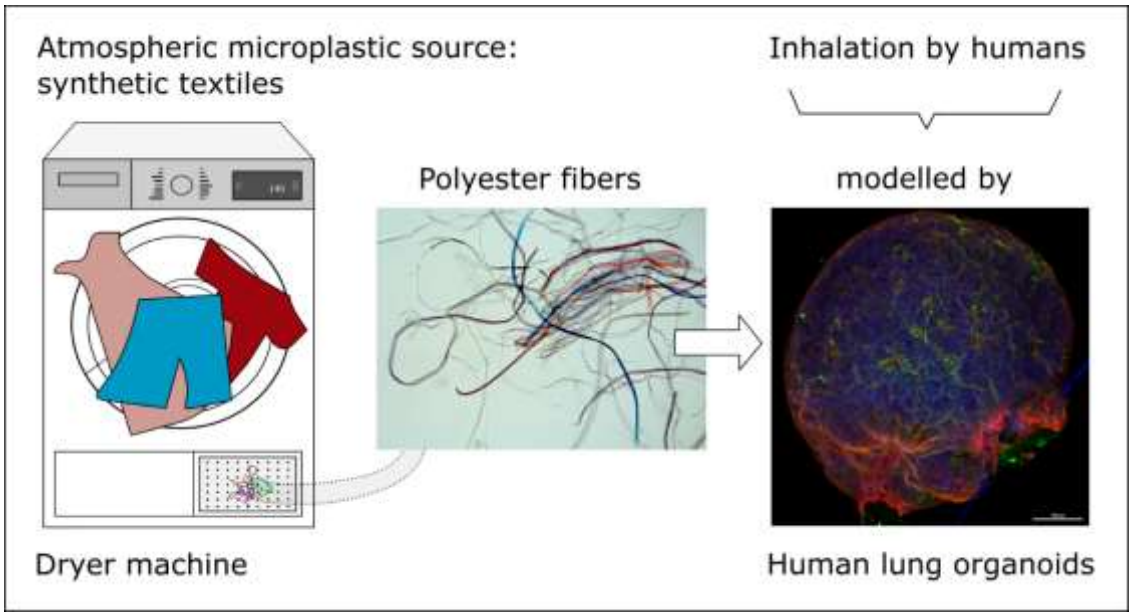

Environment International 163 (2022) 107200

Contents lists available at ScienceDirect

Environment International

journal homepage: www.elsevier.com/locate/envint

Full length article

Human airway organoids and microplastic fibers: A new exposure model for emerging contaminants

Anna Sophie Winkler [a], Alessandro Cherubini [c,1], Francesco Rusconi [c,1], Nadia Santo [b,1], Laura Madaschi [b,1], Clelia Pistoni [c], Giorgia Moschetti [d], Maria Lucia Sarnicola [d], Mariacristina Crosti [d], Lorenzo Rosso [e], Paolo Tremolada [a], Lorenza Lazzari [c,*], Renato Bacchetta [a,*]

[a] Department of Environmental Science and Policy, University of Milan, Via Celoria 26, 20133 Milan, Italy
[b] Unitech NOLIMITS, Imaging Facility, University of Milan, Via Golgi 19, 20133 Milan, Italy
[c] Laboratory of Regenerative Medicine - Cell Factory, Department of Transfusion Medicine and Hematology, Fondazione IRCCS Ca' Granda Ospedale Maggiore Policlinico, Via Francesco Sforza 35, 20122 Milan, Italy
[d] Istituto Nazionale Genetica Molecolare INGM 'Romeo ed Enrica Invernizzi', Via Francesco Sforza 35, 20122 Milan, Italy
[e] Department of Pathophysiology and Transplantation, University of Milan and Thoracic Surgery and Transplantation Unit, Fondazione IRCCS Ca Granda Ospedale Maggiore Policlinico, Via Francesco Sforza 35, 20122 Milan, Italy

ARTICLE INFO

Handling Editor: Adrian Covaci

Keywords:
Airway organoids
Airborne microplastic
Polyester fibers
Dryer machine

ABSTRACT

Three-dimensional (3D) structured organoids are the most advanced *in vitro* models for studying human health effects, but their application to evaluate the biological effects associated with microplastic exposure was neglected until now. Fibers from synthetic clothes and fabrics are a major source of airborne microplastics, and their release from dryer machines is poorly understood. We quantified and characterized the microplastic fibers (MPFs) released in the exhaust filter of a household dryer and tested their effects on airway organoids (1, 10, and 50 μg mL^{-1}) by optical microscopy, scanning electron microscopy (SEM), confocal microscopy and quantitative reverse transcription–polymerase chain reaction (qRT-PCR). While the presence of MPFs did not inhibit organoid growth, we observed a significant reduction of SCGB1A1 gene expression related to club cell functionality and a polarized cell growth along the fibers. The MPFs did not cause relevant inflammation or oxidative stress but were coated with a cellular layer, resulting in the inclusion of fibers in the organoid. This effect could have long-term implications regarding lung epithelial cells undergoing repair. This exposure study using human airway organoids proved suitability of the model for studying the effects of airborne microplastic contamination on humans and could form the basis for further research regarding the toxicological assessment of emerging contaminants such as micro- or nanoplastics.

1. Introduction

Atmospheric contamination through airborne particles and fibers is a long-existing and growing research topic of environmental pollution. Several epidemiological studies have already linked air pollution through ambient atmospheric particulate matter to many adverse human health effects, including respiratory illness, cardiovascular disease, and carcinogenic effects (Churg and Bauer, 2000; Loomis et al., 2013; Valavanidis et al., 2008). In addition to the well-known air pollutants such as combustion particles from fuel-burning emissions and other particulate organic matter and aerosols (Nel, 2005), microplastics (MPs) are now considered as emerging components of air pollution (Zhang et al., 2020).

The human health effects of MPs and nanoplastics (NPs) are usually

Abbreviations: ATR-FTIR, attenuated total reflection Fourier transform infrared spectroscopy; hAO, human airway organoid; hPO, human pancreas organoid; MP, microplastic; MPF, microplastic fiber; NP, nanoplastic; qRT-PCR, quantitative reverse transcription–polymerase chain reaction; SEM-EDS, scanning electron microscope - energy dispersive x-ray spectroscopy.

* Corresponding authors.
E-mail addresses: lorenza.lazzari@policlinico.mi.it (L. Lazzari), renato.bacchetta@unimi.it (R. Bacchetta).

[1] These authors contributed equally to this work.

https://doi.org/10.1016/j.envint.2022.107200
Received 16 October 2021; Received in revised form 1 March 2022; Accepted 21 March 2022
Available online 26 March 2022

deduced from *in vivo* exposure tests in animal models, i.e., mammalian or nonmammalian models such as mice, rats, *Xenopus laevis* (De Felice et al., 2018), and zebrafish (Bhagat et al., 2020), and from *in vitro* models such as human cell cultures. After exposure, i.e., inhalation or ingestion, MPs/NPs may pass through biological barriers, leading to translocation in the body tissue. The cell uptake, however, is size-dependent; it has been proven that cell internalization increases with decreasing particle size (Liu et al., 2021) with an assumed upper particle size limit for intracellular uptake of 10 μm (for polyethylene), (Bruinink et al. (2015)). Indeed, the transfer of MPs/NPs into human cells has been demonstrated using a variety of human cell lines, including epidermal cells (Triebskorn et al., 2019), lung epithelial cells (Lim et al., 2019; Schirinzi et al., 2017; Xu et al., 2019), endothelial cells (Barshtein et al., 2016), and intestinal cells (Cortés et al., 2020; Domenech et al., 2020). Human two-dimensional (2D) cell cultures are common *in vitro* models used to evaluate the biological effects associated with MP/NP exposure; however, these systems have some limitations such as an inaccurate representation of the *in vivo* tissue (Costa et al., 2016). Very recently, organoids, which are three-dimensional (3D) cellular structures generated from induced pluripotent stem cells, embryonic stem cells, or adult tissue-resident stem cells (Shamir and Ewald, 2014) have been shown to be a powerful tool to overcome the limits of 2D culture. Indeed, organoids, such as kidney (Takasato et al., 2016), brain (Lancaster et al., 2013), intestine (Sato et al., 2011), liver (Huch et al., 2015), pancreas (Dossena et al., 2020) and lung (Sachs et al., 2019) organoids, have recently emerged as attractive model systems that contain key aspects of *in vivo* tissue and organ complexity while being more experimentally manageable than model organisms. Moreover, these 3D structures have been recently applied in nanosafety research (Kämpfer et al., 2020) and modeling diseases such as cancer (Tuveson and Clevers, 2019).

MPs are ubiquitous in the environment (Prata et al., 2020a; 2020b). In the atmosphere, the largest proportion of the MPs consists of microplastic fibers (MPFs) derived from various sources, including synthetic clothes, textiles, and upholstery (Henry et al., 2019). Especially indoor, airborne MPF pollution arises from the wear and tear of clothing, carpets, and furniture (e.g., polyester, nylon, acrylic, and polyamide) (Akanyange et al., 2021), with synthetic clothing mostly made of polyethylene terephthalate (namely, polyester) as the largest source of airborne MPs (Dris et al., 2016). Furthermore, Dris et al. (2017) and Liu et al. (2019) have investigated and compared MPFs in indoor and outdoor air. They found that indoor air contains considerably higher amounts of natural and synthetic fibers than outdoor air and dust, with an indoor fiber concentration ranging from 1.0 to 60.0 fibers m^{-3} (Dris et al., 2017). Also Gaston et al. (2020) found that the interior air space (9.8 ± 7.3 fibers per m^{-3}) was significantly more enriched with MPFs relative to the outdoor space outdoors. As Rist et al. (2018) already pointed out, airborne MPF from synthetic clothes represent an important contribution to the total MP exposure pathways, especially considering that people spend most of their lifetime indoors (Akanyange et al., 2021). Recent studies also have demonstrated that a major pathway for MPFs is the atmosphere, through which they can reach very remote areas such as glaciers (Ambrosini et al., 2019), the Arctic region (Bergmann et al., 2017; Lusher et al., 2015), and Antarctica (Reed et al., 2018; Waller et al., 2017).

MPFs can be released into the wastewater through the washing of synthetic textiles and clothes, as demonstrated previously in several studies (Browne et al., 2011; De Falco et al., 2019). In addition to the washing process, the drying of synthetic textiles with a household clothes dryer further emits MPFs into the atmosphere via the exhaust air. However, the air contamination caused by the drying of synthetic clothes and fabrics is still poorly understood. Recently, O'Brien et al. (2020) have reported and quantified for the first time the amount of MPFs released from a clothes dryer into the ambient air. The issue was further addressed by Kapp and Miller (2020) who studied the spatial distribution of MPFs emitted from the vent of a clothes dryer directly into the environment.

Human inhalation of atmospheric MPFs has been demonstrated *in vivo* (human lung biopsies) by Pauly et al. (1998) and Pimentel et al. (1975). The deposition of MPs, however, depends on the properties and lung anatomy (Churg and Bauer, 2000; Lippmann et al., 1980). Currently, it is well known that humans in certain exposure scenarios, such as industrial workers, are particularly susceptible to pulmonary diseases caused by airborne synthetic fibers (Goldberg and Thériault, 1994; Mastrangelo et al., 2002). In the attempt to estimate the human inhalation of indoor airborne MPs, Vianello et al. (2019) set up a mannequin simulating the human metabolic rate and breathing (male person with light activity). The simulated human exposure revealed an average inhaled concentration of 9.3 ± 5.8 MPs m^{-3} (or 272 MPs per day), corresponding to the value of indoor airborne fibers reported by Dris et al. (2017) (median value of 5.4 fibers m^{-3}) and Gaston et al. (2020) (mean value of 9.8 ± 7.3 fibers m^{-3}) – disregarding the problem of comparing the results of studies using different analytical techniques.

The available data or information providing evidence of the negative human health effects of inhaled MPFs are still rare and insufficient (Prata, 2018). To date, the human exposure risk still remains unclear, and the consequences of MPF exposure are not yet well understood (Prata et al., 2020a; 2020b). Accordingly, there is an increasing demand for interdisciplinary research between environmental and human health sciences (Dris et al., 2017). In this study, we propose the application of the innovative human organoid model for human exposure tests for MPs/NPs and other particulate contaminants. Considering the described exposure risk for humans to airborne MPs, the use of the human lung airway as an organoid model in this study is an innovative experimental approach.

Importantly, exposure tests should apply environmentally relevant MP properties (Prata et al., 2020a; 2020b), such as fibrous or aged MPs. Therefore, to test the effects of airborne MPFs on human airway organoids (hAOs), polyester fibers emitted from the drying process of synthetic clothes and fabrics were collected and used as a test contaminant. The specific aims of this paper were as follows: i) to characterize the release of MPFs in the exhaust filter of a household dryer machine; ii) to analyze the effect of these environmentally relevant MPFs on hAOs as a possible target of airborne contamination from synthetic clothes; iii) to characterize the established hAOs; and iv) to evaluate the use of human organoid models to assess the effects of pollutants to humans.

2. Material and methods

2.1. hAO isolation and culture

The herein applied hAOs were generated from tissue-resident adult stem cells. Healthy human lung tissues (airway space) were obtained from the Thoracic Surgery and Lung Transplant Unit, IRCCS Ca' Granda Ospedale Maggiore Policlinico, Milan, Italy. The use of human specimens was approved by the Institutional Review Board (CE 0001977). Young patients underwent minimal invasive wedge lung resection for spontaneous pneumothorax.

For the processing of solid lung tissue, the biopsies (0.5–1 cm^3) were minced in small pieces and rinsed with wash medium (Dulbecco's modified Eagle medium, DMEM) supplemented with 1% fetal bovine serum, 1% penicillin/streptomycin and 1 × Glutamax (see Table S1 for the source and ID numbers of all reagents used). Fragments were digested in wash medium containing 0.125 mg mL^{-1} collagenase I, 0.125 mg mL^{-1} dispase II, and 0.1 mg mL^{-1} DNase I for 90 min at 37 °C. The digestion was stopped by adding cold wash medium, and the suspension was filtered through a 70-μm cell strainer and then spun for 5 min at 400*g*. In case of visible red pellets, erythrocytes were lysed in 5 mL of red blood cell lysis buffer for 15 min at room temperature before the addition of wash medium and centrifugation at 400*g*. The cell pellet was mixed with Matrigel, and 40 μL of Matrigel-cell suspension was allowed to solidify on prewarmed nontissue culture 24-well plates for 20–30 min. After complete Matrigel solidification, culture medium

containing AdDMEM/F12 supplemented with 10 mM Hepes, 1 × penicillin/streptomycin, 1 × Glutamax, 1% B27, 1.25 mM N-acetylcysteine, 25 ng mL^{-1} FGF7, 500 ng mL^{-1} RSPO1, 100 ng mL^{-1} FGF10, 100 ng mL^{-1} Noggin, 5 mM nicotinamide, 500 nM A83.01, and 500 nM SB202190 was added. For establishment of the organoids, the culture medium was supplemented with 10 μM Rock inhibitor Y27632 during the first three days. The culture medium was changed every 3–4 days. After 10–14 days, the organoids were removed from the Matrigel, mechanically dissociated into small fragments, and then split 1:4–1:6 in fresh Matrigel, enabling the formation of new organoids. All cell cultures were routinely tested for mycoplasma contamination by quantitative reverse transcription–polymerase chain reaction (qRT-PCR).

2.2. hAO characterization

Total RNA from organoids was isolated using TRIzol reagent, according to the manufacturer's instructions. The RNA concentration and purity were verified using a NanoDrop ND-100 spectrophotometer (NanoDrop Technologies). For the qRT-PCR assay, cDNA was synthesised from 200 ng of total RNA with SuperScript IV VILO. The cDNA was diluted 10-fold, and 1 μL of the sample was used as a template for qRT-PCR analysis with SYBR Select Master Mix on a CFX96 thermal cycler (Bio-Rad). The relative expression levels of the specific target genes, taken from an airway organoid milestone paper (Sachs et al., 2019), were determined using the $\Delta\Delta C_t$ method and normalized to the geometric mean of the ACTB and TBP mRNA levels using the primers listed in Table S2.

To characterize the hAO, gene expression analysis by qRT-PCR was performed after 10–14 days of standard culture and again after MPF exposure to investigate possible changes in the lung cell compartments: Claudin 1 (CLDN1) for lung epithelium, Keratin 5 (KRT5) for basal cells, NK2 Homeobox 1 (NKX2.1) for lung cell marker, Nephrocystin 1 (NPHP1) and Dynein Axonemal Heavy Chain 5 (DNAH5) for ciliated cells, Secretoglobin Family 1A member 1 (SCGB1A1) for club cells, Surfactant protein A1 (SFTPA1) and Surfactant protein C (SFTPC) for Alveolar Type 2 (AT2) cells. All primers were reported in Table S2.

2.3. Sampling and characterization of MPFs from a dryer machine

To generate environmentally relevant MPFs for the human organoid exposure experiment, polyester fibers emitted from the drying of synthetic clothes and fabrics were collected. Specifically, one polyester t-shirt, six sweatshirts, and two blankets of different colors (dry weight: 5427 g) were washed in a washing machine and subsequently dried in a common domestic tumble dryer. The dryer filter was previously cleaned by a vacuum cleaner, and all fibers derived from the first drying cycle were discarded. The same items were then washed again, and the synthetic fibers from the filtered exhaust air of the tumble dryer were collected (Figure S1), wrapped in aluminum foil, and transported to the laboratory for subsequent analyses.

The MPFs were first morphologically analyzed with a Leica EZ4D stereomicroscope and then with a Leica DMRA2 light microscope equipped with a Leica DC300 F digital camera. The size distribution, detailed morphology, and the elemental composition (C:O ratio) of the fibers were studied with a Zeiss LEO 1430 scanning electron microscope (SEM) coupled with a Centaurus detector for energy dispersive x-ray spectroscopy (EDS) analysis. A subsample of MPFs was mounted onto standard SEM stubs and gold-coated. For the size distribution analysis, thirty SEM images (magnification × 50) were taken. The length (n = 450) and width (n = 450) of MPFs was measured with the imaging software ImageJ. The width of the irregular fibers (e.g. flat fibers) was measured at their smallest and largest width in equal numbers. The elemental analysis was performed using Oxford Instruments INCA version 4.04 software (Abingdon, UK). The operating conditions were as follows: accelerating voltage, 20 kV; probe current, 360 pA; and working distance, 15.0 mm.

To further characterize the material, attenuated total reflection Fourier transform infrared spectroscopy (ATR-FTIR) on bulk polyester fabrics was performed using a Perkin Elmer FTIR Spectrometer Spectrum One and a Perkin Elmer Universal ATR Sampling Accessory consisting of a diamond crystal. Measurements were carried out in a wavenumber range of 4000–650 cm^{-1} with a spectral resolution of 4 cm^{-1}.

2.4. MPF exposure to hAOs

The MPFs collected from the filter of the dryer machine were resuspended at a final concentration of 500 μg mL^{-1} in AdDMEM/F12 supplemented with 10 mM Hepes, 1 × penicillin/streptomycin, and 1 × Glutamax; then the sample was sonicated at a high intensity (3 × 5 min) using a Bioruptor sonicator (Diagenode). To obtain organoid-MPF co-cultures, the hAOs were split as described above, and then the organoid fragments were embedded in Matrigel drops and mixed with MPFs at a ratio of 70% Matrigel with organoids and 30% culture medium containing the MPFs, at different concentrations (1, 10, and 50 μg mL^{-1}). Differently from Watson et al. (2016), who used inverted monolayers to assure that polypropylene nanoplastics contacted the cell surfaces, the here performed fragmentation allowed the outer as well as the inner cell surface of the organoid to have contact with the MPF. Moreover, to improve the exposure, we removed the organoids from the Matrigel, allowing them to grew in culture suspension. So far, the organoids showed an apical-out polarity as previously reported (Co et al., 2019), improving their barrier function against external stimuli. Upon solidification of the Matrigel, the organoid-MPF coculture was supplemented again with the culture medium containing the MPFs at the respective concentrations. After ten days, the organoids reached maturation (ca. 200–300 μm in diameter). At this point, in order to improve the interaction between the organoids and MPFs, the hAOs were carefully removed from the Matrigel and cultured in suspension with only culture medium containing the MPFs at the same concentrations for 1 week with gentle agitation. An organoid coculture was cultivated under the same conditions without MPF exposure as a control. After exposure, the airway organoid-MPF cocultures were collected for gene expression analysis and fixed for confocal microscopy and SEM analysis, as described below.

2.5. SEM analysis

To study the effects of MPFs on organoid growth, the control and exposed samples were fixed in a mixture of 4% paraformaldehyde and 2% glutaraldehyde in 0.1 M sodium cacodylate-buffered solution at pH 7.4. After several washes in the same buffer, the samples were post-fixed in 1% OsO_4 for 1.5 h at 4 °C and then dehydrated in a graded ethanol series. As a final step, the organoids were treated with hexamethyldisilazane for complete chemical dehydration. All samples were mounted onto standard aluminum stubs, gold sputtered, and analyzed under a Zeiss LEO 1430 SEM at 20 kV.

2.6. Immunofluorescence staining and confocal microscopy

For confocal microscopy analysis, the organoids were washed with 0.01 M phosphate-buffered saline, pH 7.4 (PBS) and fixed for 15 min in 4% paraformaldehyde, incubated in 0.05 M NH_4Cl in PBS for 30 min, permeabilized for 15 min in PBS containing 1% bovine serum albumin (BSA) and 0.2% Triton X-100, and blocked for 30 min in 1% BSA. The organoids were incubated overnight at 4 °C with a mouse monoclonal antibody against α-tubulin diluted in 0.1% BSA/PBS. The samples were then rinsed in PBS and incubated for 3 h at room temperature with rhodamine phalloidin (cytoskeleton) and the secondary Alexa Fluor 488-conjugated goat anti-mouse antibody. After several washes with PBS, the organoids were finally incubated for 5 min at room temperature with the DNA dye Hoechst 33342 (1:5000). At the end of the staining

procedure, the organoids were washed with PBS (3 × 5 min), mounted in 1:2 PBS/glycerol, and observed under a Nikon A1 confocal microscope.

For the images in Fig. 1 showing the immunofluorescent sections of the hAOs, the organoids were fixed 2 °C in PBS containing 0.2% Triton X-100, 5% BSA, 2% FBS and 5% goat serum. For the staining, the organoids were incubated O/N at 4 °C with the specific primary antibody in PBS containing 0.2% Triton X-100, 3% BSA and 3% FBS. After

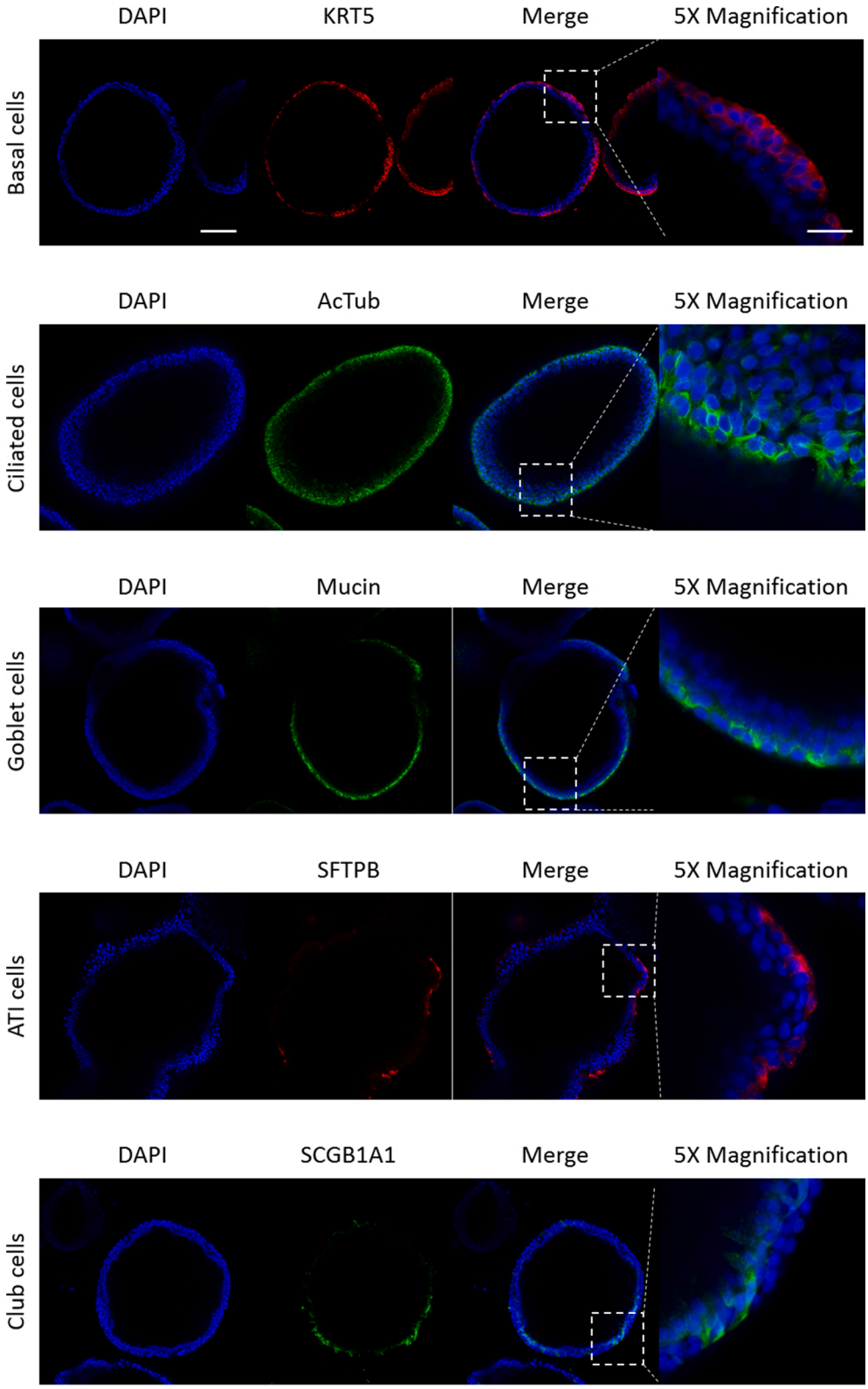

Fig. 1. Organoids recapitulate human airway counterpart. Immunofluorescent sections of human airway organoids (hAOs) showing markers for basal cells (KRT5), ciliated cells (acetylated α-tubulin), goblet cells (Mucin), ATI cells (SFTPB) and club cells (SCGB1A1). Nuclei were counterstained in blue. Scale bars: 100 μm, 25 μm (inset × 5 magnification). (For interpretation of the references to color in this figure legend, the reader is referred to the web version of this article.)

five washes with PBS containing 0.05% Triton X-100, the organoids were incubated O/N at 4 °C with specific conjugated secondary antibodies. Finally, nuclei were stained O/N at 4 °C with DAPI. Images were acquired using a Leica TCS SP8 confocal microscope (Leica, Wetzlar, Germany) with HC Pl fluotar APO 20x/0.55 objective.

2.7. Inflammatory cytokine, oxidative stress and obesogenic evaluation

To investigate the possible changes in the inflammatory cytokine expression in hAOs after MPF exposure, gene expression analysis by qRT-PCR was performed as described above at the end of the coculture with the highest MPF concentration using the primers listed in Table S2. Considering that the exposure of MPFs could induce oxidative stress in human tissues (Hu and Palić, 2020), we analyzed the expression of genes involved in oxidative stress pathways reported in relation to MPF exposure, including superoxide dismutase family genes (SOD1 and SOD2), glutathione detox-related genes (GSTA1 and GPX1), catalase (CAT), and ROS-controlling genes (NOX2, COX1, and ND1). In addition, the capacity of our 3D structures to respond to standard inflammatory stimuli was evaluated after treatment with poly(I:C) (50 μg mL^{-1}) or Staphylococcal enterotoxin B (SEB, 2 μg mL^{-1}) as a positive control.

To investigate a possible contribution of MPF to obesogenic effects (Kannan and Vimalkumar, 2021), gene expression analysis by qRT-PCR was performed as previously described. We analyzed the following genes involved in the adipogenic pathway: peroxisome proliferator-activated receptor gamma (PPARγ), a transcription factor that induces the adipogenic gene expression program during development, promotes adipose remodeling, and regulates the functions of adipocytes in lipid storage, adipokine secretion, and energy homeostasis, and its associated adiponectin.

For the ELISA analysis, organoids supernatant was collected and centrifuged at 300 × g for 5 min. Interleukin-6 concentration was determined using ultra-sensitive ELISA kit (Immunotools, Germany) according to the manufacturer's instructions.

For the flow cytometry analysis, hAOs were collected and washed with PBS and centrifuged for 10 min at 300 × g. Then, cells were dissociated by trypsinization using Trypsin with EDTA for 30 min to obtain a single-cell suspension. The samples were stained using 1:200 MitoSOX red mitochondrial superoxide indicator (Table S1), and incubated for 20 min in the dark at room temperature (RT). Finally, the samples were suspended in PBS and analysed using the FACSCanto II cytometer with FACSDiva analysis software (BD).

2.8. Organoid volume measurement

To determine the volume of hAOs, bright-field images were acquired with a Nikon Eclipse TS100 microscope equipped with a digital camera (Nikon Instrument Europe) at the end of the MPF exposure. hAOs (n = 10 fields) were analyzed at × 4 magnification. At least three independent experiments were analyzed. Organoid volumes were calculated in ImageJ software using the following formula: $4/3\,\pi\,r^3$, where "r" was the mean of the longest diameter and the shortest diameter of the spheroid divided by two.

2.9. MTT test

The hAOs (control groups and MPFs-treated groups) were seeded as previously described and at the end of the MPFs exposure they were collected and used for the MTT assay as described below. First, hAOs were washed with PBS to remove all the culture medium and successively seeded into non-tissue culture 24-well plates with a phenol red free DMEM high glucose medium containing the MTT substrate. After a 2 h incubation at 37 °C the medium was replaced with a 96% ethanol and all the samples were incubated for 1 h at 37 °C in dark. Finally, all the ethanol containing the product of MTT reaction was collected and its absorbance was detected using a spectrophotometer (TECAN, GENios plus) at 570 nm.

2.10. Data analysis

For statistical analysis of the gene expression data, a two-way analysis of variance followed by Bonferroni's multiple comparison test ($\alpha = 0.05$) was performed. The metabolic activity was tested by *t*-test analysis followed by Kolmogorov-Smirnov correction. Photoshop was used to export the image graphs.

3. Results

3.1. hAO isolation and characterization

The hAOs were generated starting from biopsies of healthy lung donors. When embedded in Matrigel, lung cells were organized in a polarized pseudostratified epithelium with a central hollow lumen, resulting positive for basal (KRT5), ciliated (AC-TUB), goblet (Mucin), ATI (SFTPB) and club (SCGB1A1) cell markers, supporting their airway identity (Fig. 1). Gene expression analysis showed that the hAO lines derived from three different donors have similar gene expression profiles recapitulating all cell types of airway tissue (compared to human pancreas organoids as a control), supporting the reproducibility of our culture methods (Figure S2).

The organoids were analyzed by optical microscopy, confocal 3D construction, and SEM imaging. The normal organoids (control group) exhibited a spherical shape with a typical diameter of 200–300 μm and an inner cavity (Fig. 2A–B). Confocal 3D reconstruction confirmed that the cells were well differentiated, showing the presence of ciliated cells and nonciliated cells, including club cells (identified by the presence of microvilli), that were irregularly distributed on the surface and corresponding to their *in vivo* position (Fig. 2C–E). Immunofluorescence experiments with the actin cytoskeleton marker revealed the different shapes and dimensions of the cells containing nuclei, which were visible in the surface section (Fig. 2C–E) and transverse plane (Fig. 2D). Moreover, the inner surface of the organoids established a differentiated cell structure, including ciliated cells facing the organoid cavity, as demonstrated in Fig. 2D. The presence of cilia at the inner surface of the organoids could be explained by the rotating motion of the organoid cavity, which can be seen in a video recording of the organoids (Video S1). Finally, high-resolution SEM imaging of the organoid surface showed the same irregularly shaped ciliated and nonciliated cells, displaying the dimensions of the cilia and microvilli (Fig. 2F).

3.2. MPFs in the air filter of a dryer machine

The total weight of the MPFs removed from the air filter of a dryer machine was 2.3 g (Figure S1), which was released from 5.4 kg of 100% polyester fabrics. The procedure was repeated once again with the same fabrics (rewashing and redrying), and the release of MPFs was 2.5 g (0.44 g ± 0.014 of dry MPFs kg^{-1} dry fabric, 1 SD, $n = 2$). Optical microscopy experiments demonstrated fibers of different colors, reflecting the color mixture of the dried materials (Fig. 3A–B). For a more detailed analysis, SEM (Fig. 3C–E) revealed that the MPFs varied in size and morphology. The fiber length was on average 700 ± 400 μm (1 SD, $n = 450$, min 68 μm, max 3,638 μm). The size distribution analysis (Fig. 3F) showed that the majority of fibers were in the range of 200–800 μm (68.5 %). Only 5.6 % of MPFs were smaller than 200 μm, and 0.4 % larger than 2,200 μm. Interestingly, the shape of these MPFs differed at the transverse surface; no MPFs had a round profile along the entire length, but they exhibited a varying profile from flat and twisted to tattered (Fig. 3C–E). Flat MPFs exhibited maximum widths of 25 μm along their widest dimension and a minimum height of 1 μm along their thinnest dimension. The fiber width was on average 10 ± 5 μm (1 SD, $n = 450$). Furthermore, we observed that some fibers showed a rough surface, where small pieces of < 10 μm flaked off from the fiber (Fig. 3D)

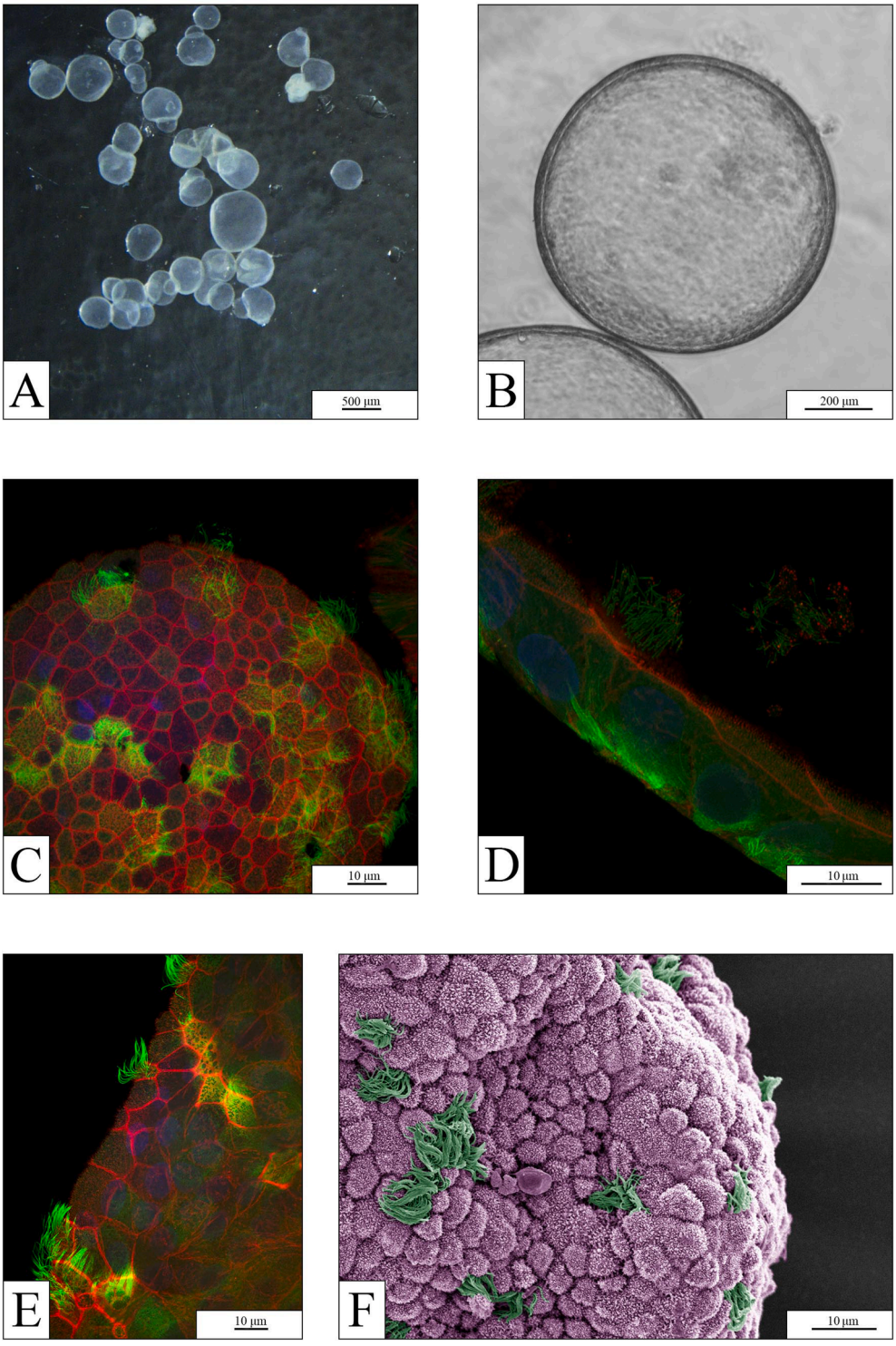

Fig. 2. Characterization of human airway organoids (control group, $n = 3$). (A) Stereo microscopy image and (B) optical microscopy image of organoids. (C–E) Immunofluorescence imaging of the organoid surface and the transverse section generated by confocal microscopy showing the cellular organization with a cytoskeletal marker (anti-acetylated tubulin; green) and counterstaining of the actin cytoskeleton (phalloidin 565; red) and nuclei (Hoechst 33342; blue). (F) Pseudo-colored SEM image of the organoid's surface showing irregularly shaped multiciliated (green) and nonciliated cells with microvilli (purple). (For interpretation of the references to color in this figure legend, the reader is referred to the web version of this article.)

or a chapped ending was revealed (Fig. 3E), which could lead to the release of very small MPs from the fibers.

Although very speculative, we estimated the number of fibers released by the drying process by considering the average dimensions of the fibers and their uncertainties (SE of the mean). From the mean measured dimensions of collected fibers and the propagation of their errors, we determined a fiber volume of $V_{fiber} = 7.0 \times 10^{-5} \pm 5.2 \times 10^{-6}$ mm^3 $fiber^{-1}$ ($\pm\delta V_{fiber}$) and an average mass of a fiber of $M_{fiber} = 9.6 \times 10^{-5} \pm 7.2 \times 10^{-6}$ mg $fiber^{-1}$ ($\pm\delta M_{fiber}$), assuming that the density of polyester is 1.38 mg mm^{-3} and that the density's variability was negligible in comparison to that of the fiber volume. According to these data, 2.3 g of polyester fibers collected in the filter of a dryer machine should contain $23 \times 10^6 \pm 1.7 \times 10^6$ fibers. Given the large SD of measured fiber length and width and the resulting large uncertainty of the fiber volume and mass, the calculated values (number of fibers) also had large variability. Nevertheless, the estimate provides an order of magnitude for the number of fibers that could be released from the drying of synthetic fabrics.

Elemental analysis of single fibers isolated from the dryer lint showed a C:O ratio of 74:26, which corresponds to that of polyester (see

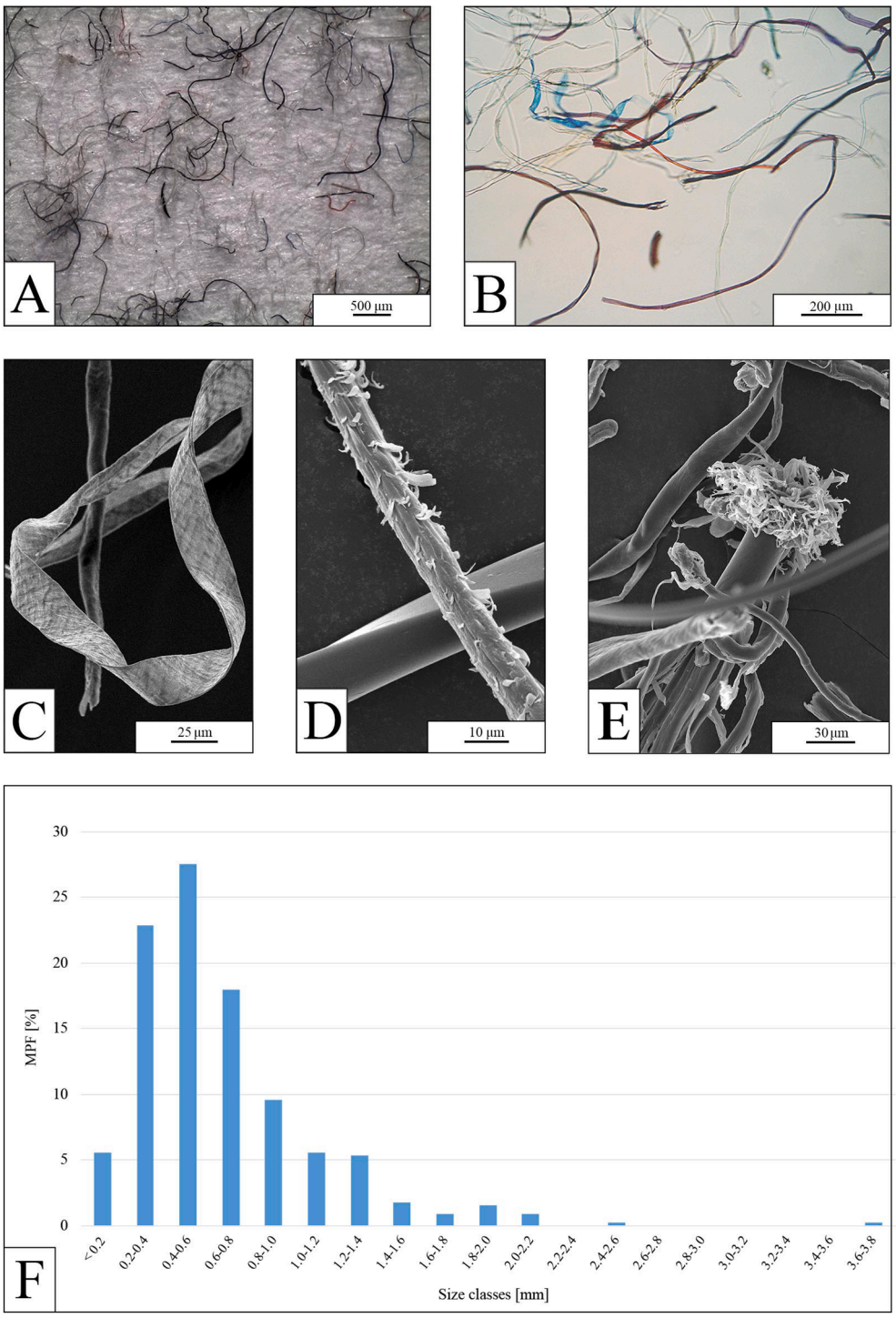

Fig. 3. Synthetic fibers obtained from the air filter of a dryer machine. (A–B) Optical microscopy images demonstrating MPFs of different sizes and colors. (C–E) SEM images of MPFs at different magnifications showing varying morphologies. (F) Size distribution analysis of $n = 450$ MPFs, number percentages are grouped in 200 µm size classes.

Figure S3 for the EDS spectrum). The ATR-FTIR spectrum of all original bulk fabrics used for the drying showed all characteristic absorbance peaks of polyester (Figure S4, ATR-FTIR spectrum of PET from a plastic water bottle as reference).

3.3. hAOs exposed to MPFs

The hAOs exposed to MPFs were affected by all concentrations of MPFs. Based on the average mass of a fiber and the suspension volume in the exposure wells (0.5 mL), we estimate the number concentrations of MPFs which were added to the organoid cultures to be 5 ± 1, 52 ± 4, and 259 ± 19 MPFs well^{-1}. Optical microscopy, confocal 3D construction, and SEM image analyses revealed that the organoids exposed to MPFs were not inhibited in their growth and did not exhibit any cellular abnormalities compared to the control group, independent of the MPF concentration (Fig. 4A–F). Most organoids did not interact with the fibers, or only to a small extent, and maintained their radial (almost spherical) architecture (Fig. 4D–F).

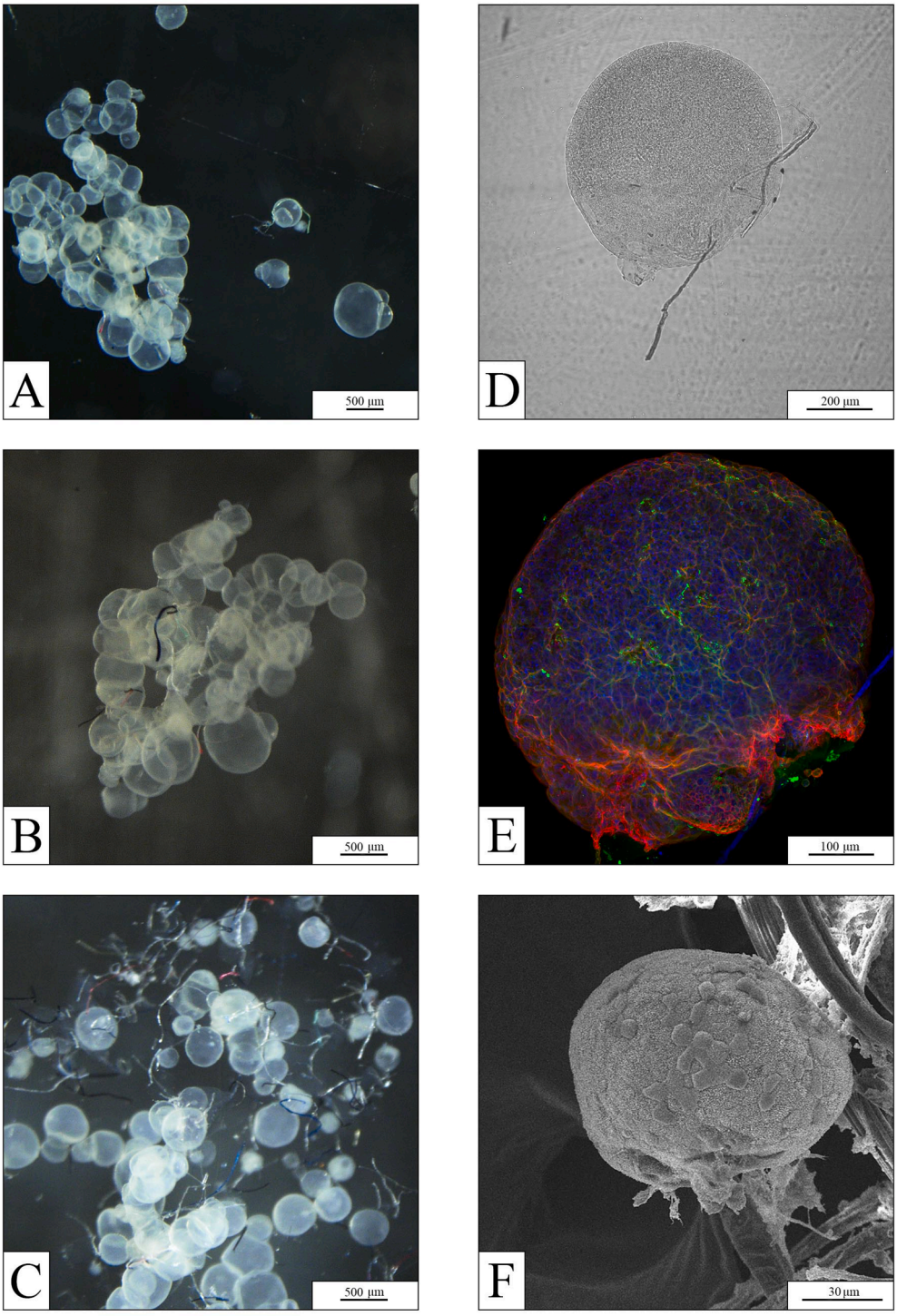

Fig. 4. MPFs interact with hAOs in coculture. (A–C) Stereo microscopy images of organoids in suspension with MPFs at increasing concentrations (top to bottom: 1, 10, and 50 µg mL^{-1}). (D) Phase contrast image and (E) immunolabeled 3D reconstruction of the same organoid (MPF concentration: 10 µg mL^{-1}) showing the interaction between the organoid and a fiber. The organoid was stained for cytoskeletal proteins: microtubules (anti-acetylated tubulin; green), F-actin (phalloidin 565; red), and nuclei (Hoechst 33342; blue). Also visible in blue is a synthetic fiber. (F) SEM image of an organoid (MPF concentration: 50 µg mL^{-1}) in contact with a fiber, demonstrating a spherical body and a differentiated cell structure. All analyses were performed at least three times. (For interpretation of the references to color in this figure legend, the reader is referred to the web version of this article.)

Fluorescence staining of the surface (Fig. 5A–B) and transverse (Fig. 5C) sections of the organoids as well as high-resolution SEM images (Fig. 5D–H) showed the same cellular structure as the controls, including ciliated and nonciliated cells, even when the organoids were in contact with MPFs. The notable observation was a higher density of polarization of the cytoskeleton near the fiber contact site, visible as an intensification of the red color in Fig. 5B. Owing to an organoid that had broken apart (likely during the transfer of the dehydrated organoid onto the aluminum stub), we were able to take SEM images of the inner surface of the organoids and could observe the same cellular differentiation (multiciliated and nonciliated cells) as the outer surface (Fig. 5E). Rather than depending on the MPF concentration, the observed effects varied with the degree of MPF-organoid contact, which presumably depended on the development phase of the organoids. The organoids that made contact with fibers during maturation grew around the fibers (Fig. 5F–H). No assumptions could be made on a size-dependent effect of the MPFs as the experimental setup did not account for this. All effects are attributed to the size ranges mentioned before.

Interestingly, the organoids closely bonded to an MPF formed an organoid-fiber interlacement or fully encompassed the MPF. We further observed that some organoids grew polarized around the fibers. For example, Fig. 6A–G shows cell growth along the length of a fiber. The

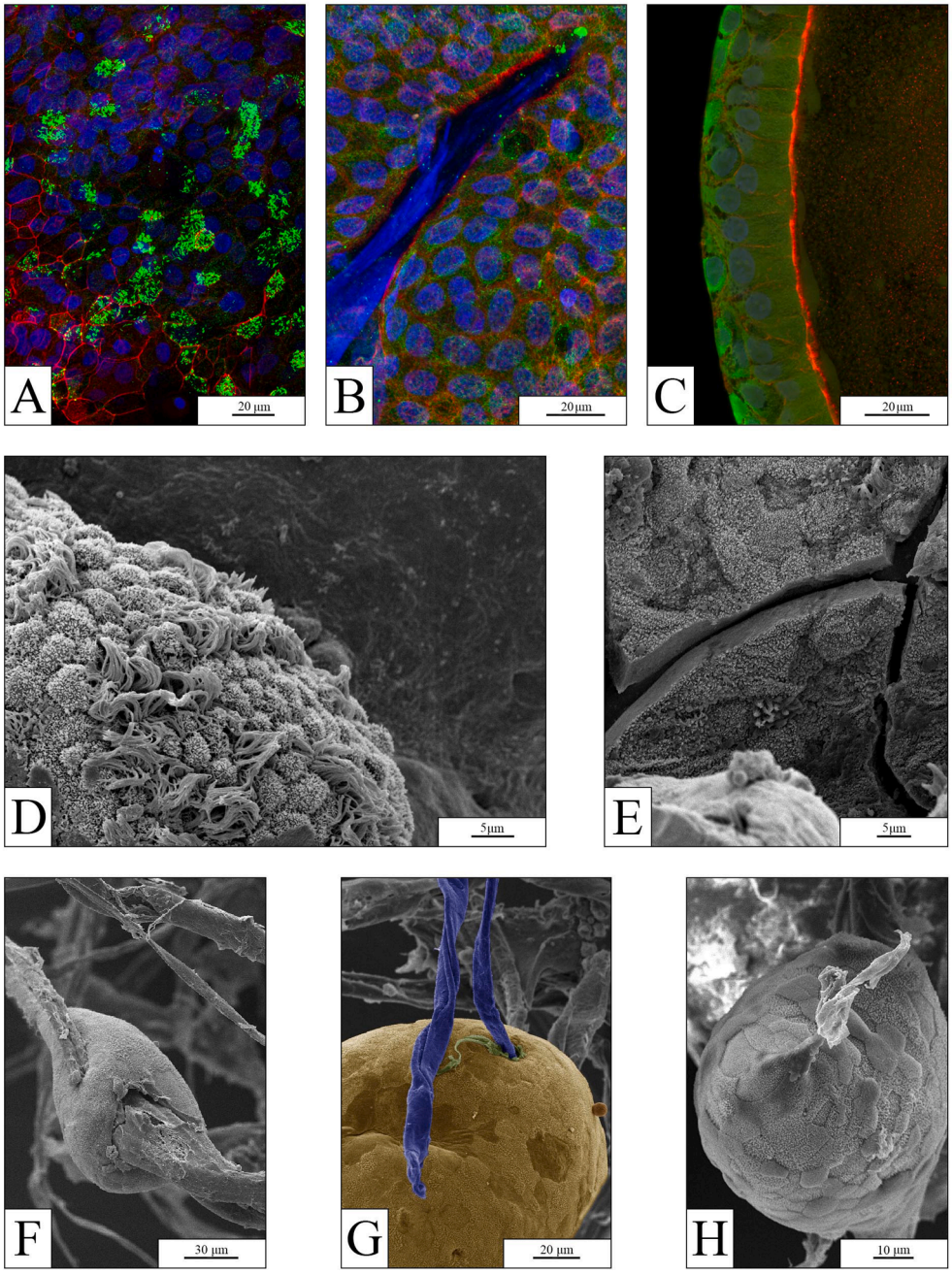

Fig. 5. hAOs growth around the fibers. (A–B) Surface and (C) transverse sections of an immunolabeled organoid (MPF concentration: 50 µg mL^{-1}) showing the cell organization. The organoid was stained to show ciliated cells (anti-acetylated tubulin; green), F-actin cytoskeleton (phalloidin 565; red), and nuclei (Hoechst 33342; blue). Also visible in blue is a synthetic fiber. (D) SEM image of an organoid's outer surface showing ciliated and nonciliated cells (MPF concentration: 10 µg mL^{-1}). (E) SEM image of the inner surface of an organoid that had broken apart, demonstrating cell differentiation facing the organoid's cavity (MPF concentration: 10 µg mL^{-1}). (F–H) SEM images of organoids (MPF concentration: 50 µg mL^{-1}) demonstrating a differentiated cell structure and integration of a fiber into the organoid; the image in panel G is partially pseudo-colored for better visualization (cell tissue, yellow; fiber, blue). All analyses were performed at least three times. (For interpretation of the references to color in this figure legend, the reader is referred to the web version of this article.)

organoids seemingly surrounded the fibers by developing netlike extensions of cells (clearly visible in Fig. 6D–F), resulting in a full internalization of the MPFs. While the cells of the organoid body growing along the length of a fiber exhibited a differentiated structure (Fig. 6A–B), the thin cell extension covering the surface of a fiber exiting the organoid body (Fig. 6D–F) was rather smooth and uniform. These observations of cells covering a fiber with a thin layer stands in contrast to the images depicted in Fig. 5F–H showing that cells did not cover the fibers once they left the organoid. We also noticed that organoids in suspension with MPFs can be damaged by fibers piercing the cell tissue (Fig. 6C).

3.4. Effect of MPF on hAOs

To verify that the lung heritage of hAOs was not affected by their exposure to MPFs, we performed gene expression analysis of the typical epithelial lung markers NKX2.1 and CLDN1 as well as the specific airway lung markers SFTPA1 and SFTPC (AT2 cells), SCGB1A1 (club cells), NPHP1 and DNAH5 (ciliated cells), and KRT5 (basal cells); all these genes were slightly reduced even if not at a statistically significant level except for the SCBG1A1 that was significantly less expressed (Fig. 7A). In addition, no difference in the expression of epithelial to mesenchymal transition markers was observed (Fig. 7B).

Regarding the possible obesogenic effects associated to MPF exposure as recently suggested by Kannan and Vimalkumar (2021), we observed a slight increase in hAO volume relevance after MPF treatment. However, this tendency was not significant as also showed by gene expression analysis of genes involved in the adipogenic pathway (Fig. 7C–D). MTT viability test showed no significant differences between the control group and the MPFs treated group of hAO (Figure S5A).

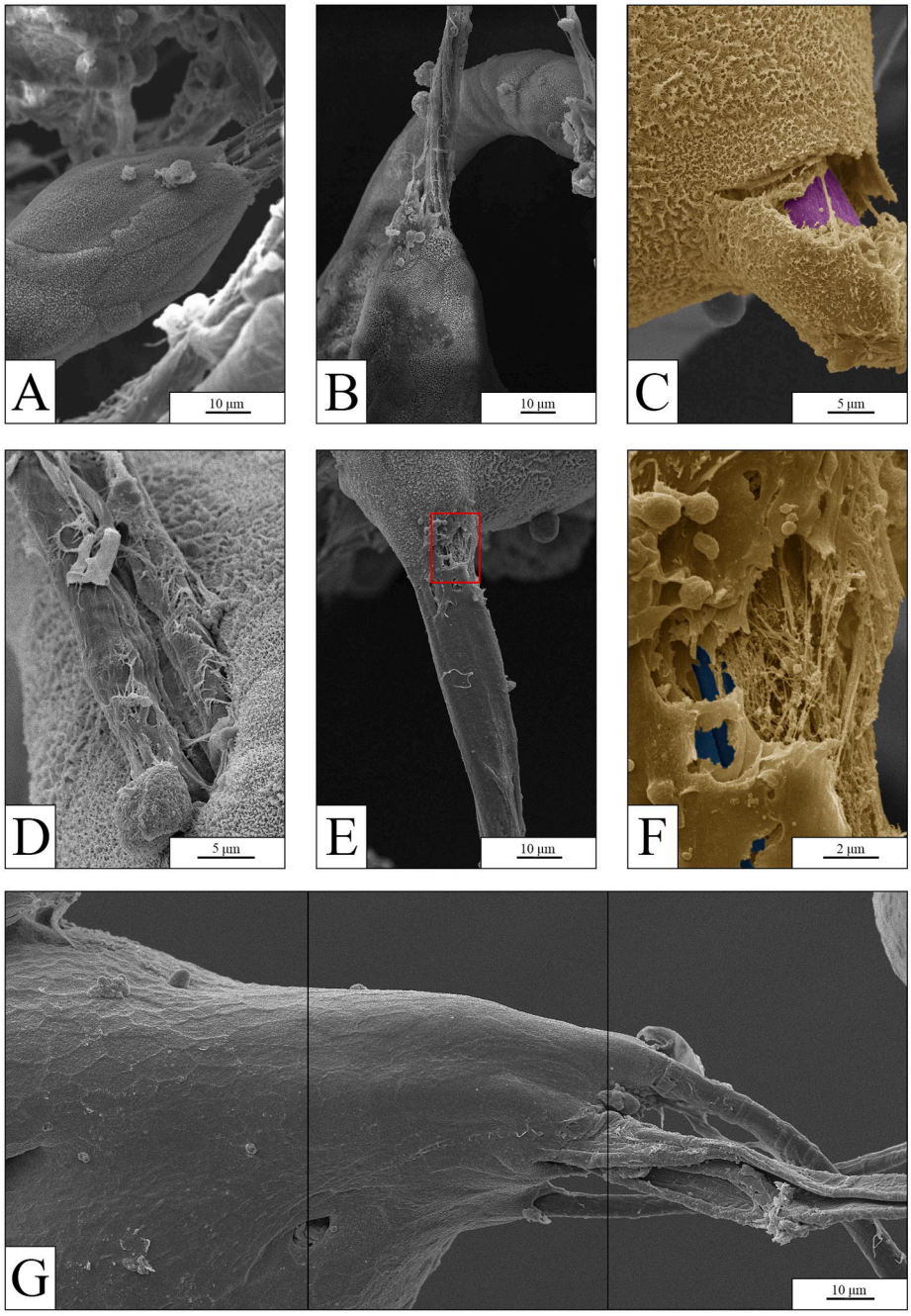

Fig. 6. SEM images of hAOs exposed to MPFs. Partially pseudo-colored for better visualization (cell tissue, yellow; fibers, purple/blue). (A–B) Oriented cell growth of organoids along the length of a fiber; the cell structure and partially coated fibers are shown (MPF concentration: 10 µg mL^{-1}). (C) Complete internalization of a fiber inside an organoid (MPF concentration: 50 µg mL^{-1}). (D) Net-like extension of cells growing on a fiber. (E and its magnification F) Thin cell extension covering the surface of a fiber exiting the organoid body (MPF concentration: 50 µg mL^{-1}). (G) Merged image of three continuous images showing the polarized growth of organoids with the length of multiple fibers (MPF concentration: 50 µg mL^{-1}). All analyses were performed at least three times. (For interpretation of the references to color in this figure legend, the reader is referred to the web version of this article.)

3.5. *Inflammation and oxidative stress evaluation*

To investigate possible changes in the expression of inflammatory cytokines and oxidative stress-related genes, gene expression analysis of hAOs was performed at the end of their coculture with the highest MPF concentration. The results revealed no significant differences in the gene expression of cytokines or oxidative stress-related genes (Fig. 8A–B), while GSTA1 and COX1 showed a slight increase in hAOs exposed to MPFs in relation to the control hAOs (Fig. 8B). In contrast, an increase of inflammatory markers was observed after xenobiotic stimuli, as observed in other organoid models (Aguilar et al., 2021, Jose et al., 2020) (Fig. 8A). Focusing on the protein level, IL 6 was not observed in the medium of hAOs treated with microplastics, while an increase amount of this cytokine was detected after xenobiotic treatment (Figure S5B). Regarding the mitochondrial oxidative stress, hAOs exposed to MPFs and to poly(I:C) showed a similar trend of oxidative stress, as also observed in 2D cell culture and animal model (Dong et al., 2020; Ruenraroengsak and Tetley, 2015; Umamaheswari et al., 2021) but only with the positive control the level of mitochondrial superoxide was statistically significant versus the non-treated hAOs (Figure S5C).

4. Discussion

The first objective of the present study was to set up an innovative *in vitro* model based on the use of 3D structures that could adequately represent the native lung, where emerging atmospheric contaminants such as synthetic materials could have adverse human health effects. And secondly, we wanted to use this model to investigate the potential effects of polyester fibers isolated from a dryer machine on human lung biology, most of all after the recent evidences showing that even the

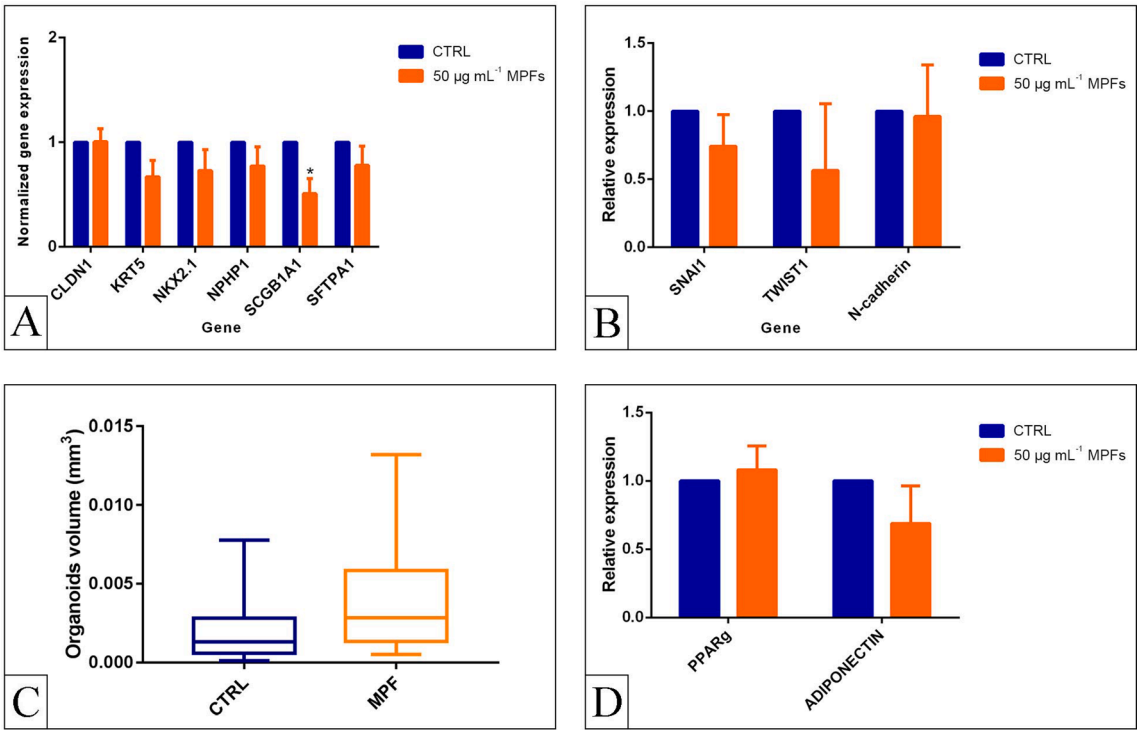

Fig. 7. hAOs were not affected by MPFs. Control organoids compared to organoids exposed to MPFs (MPF concentration: 50 µg mL^{-1}) for selected target genes: (A) general epithelial lung markers and specific airway markers, (B) epithelial to mesenchymal transition markers, (C) organoid volume calculated measuring their long and short diameter ($n = 3$). (D) qRT-PCR analysis of the control organoids compared to organoids exposed to MPFs (MPF concentration: 50 µg mL^{-1}) for adipogenic target genes. Data in panel A, B, D are shown as means ± S.E.M. ($n = 4$), statistical analysis was performed by two-way ANOVA followed by Bonferroni correction; * $P < 0.05$. Data in panel C are shown as box and whisker plot; the line within the box marks the median, the boundaries of the boxes the 25 and 75 percentiles, and the whisker limits delineate the minimum and the maximum value after outlier removal.

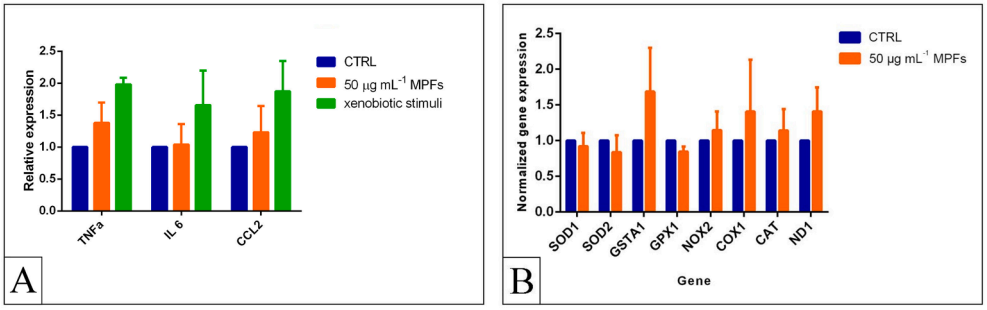

Fig. 8. qRT-PCR analysis for inflammation and oxidative stress evaluation. Control organoids compared to organoids exposed to MPFs (MPF concentration: 50 µg mL^{-1}) for selected target genes: (A) Inflammatory cytokines compared to the response of positive control organoids to standard inflammatory stimuli, and (B) oxidative stress-related genes. Data are shown as means ± S.E.M. ($n = 4$), statistical analysis was performed by two-way ANOVA followed by Bonferroni correction.

emissions of MPFs from mechanical drying are found in the air, particularly indoor air (O'Brien et al., 2020).

It is becoming increasingly clear that the 3D cell culture is a more accurate way to represent human tissue outside the body and simulate conditions in a living organism. Standard 2D cell cultures (monolayers), with cells often all at the same stage, cannot accurately represent how cells grow or how they are affected by disease and injury (Jensen and Teng, 2020). In this context, organoids have been recently exploited to overcome the limitations of 2D cell culture systems. Due to their capacity to self-organize into minimal biological units and thus potentially recapitulate the functionality and complexity of the tissue of origin, they have emerged as powerful models for studying human development and disease (Fatehullah et al., 2016). Although airway organoids do not yet recapitulate all of the complex structures and cellular interactions associated with the different regions of the lung (e.g., trachea, bronchi, bronchioles, alveoli and all mesenchymal and vascular compartments), they contain the specific cell types present in the epithelium of the original organ. Therefore, they can be applied for basic and translational research (Barkauskas et al., 2017). We showed that lung-specific cell types, including basal, AT2, and ciliated cells, are represented in our human airway organoids (Fig. 5A).

To date organoids derived from different sources have been used to successfully study specific diseases (Dutta et al., 2017; Mellin and Boddey, 2020) and to screen new drugs (Broutier et al., 2017). Already some studies have been published to support how these three-dimensional structures provide a new opportunity to mimic human organ development, morphology and physiology in a similar manner as *in vivo* models (Lancaster et al., 2013; Schutgens and Clevers, 2020). In this panorama, human lung organoids have been used to mimic a response to inflammatory stimuli (Jose et al., 2020) and to study the

pathophysiology of *Cryptosporidium* infection (Heo et al., 2018). The compatibility of this system for the toxicological assessment has been recently reported by Truskey (2018) and by Kuratnik and Giardina (2013).

This study presents an attempt to use human airway organoids for the assessment of the effects of MPFs. Although plastics are inert materials, in recent years several studies have described health risks for humans through the many routes of MPF exposure. Not least, the recent increased use of synthetic masks due to the COVID-19 pandemic exacerbated for example the route of inhalation. Despite the existing knowledge about MPs, less is known regarding the MPF particulate toxicity effects in a short- and long-term exposure and still many mechanisms have to be elucidated regarding their impact on human health.

Synthetic textiles have been identified and extensively described as one of the major sources of MPFs in wastewater (Browne et al., 2011; De Falco et al., 2019). The current research is the first to report the amount and features of MPFs released from synthetic fabrics in a dryer machine, addressing potential atmospheric contamination. In fact, a recent paper by O'Brien et al. (2020) has shown that the use of dryer machines causes an increase of the MPF concentration in the ambient air; however, they did not measure the total amount of MPFs released by the drying process. Washing and drying textiles in household machines present two possible MPF emission pathways: one being through the wastewater (residual water in textiles after the centrifugation cycle of the washing machine), and one being via the air passing by an integrated air filter. The former goes directly into domestic wastewater without filters. Here, we focused on the air pathway; MPFs released by textiles and forced by a strong air flux into the air exhaust are retained by the air filter and then specifically collected at the end of each drying cycle. Considering the evidence reported by O'Brien et al. (2020), the air filter does not remove all MPFs coming from the dryer machine. Thus, the total amount of MPFs released in the air flux can be even higher. FTIR analysis showed clean spectra for bulk fabric confirming polyester material (Figure S4).

Based on a review of studies regarding atmospheric MPs, Prata et al. (2020a; 2020b) calculated that a person's lungs could be exposed to 26–130 airborne MPs a day. This estimation is slightly lower than the average inhaled concentration of 272 MPs per day determined by Vianello et al. (2019). The effects of MPs on human health have been previously tested only using a variety of 2D cell lines (Dong et al., 2020; Hwang et al., 2019; Palaniappan et al., 2021; Schirinzi et al., 2017). The observed effects were very diverse and depended on the properties of the particle (e.g., size and polymer), the duration and concentration of exposure (6-12-24-48 h), and the tested cell lines. In particular, tests representing the human lung should use MPs in size and shape that have been shown to be present in the air. Since a substantial portion of airborne environmental MPs consists mostly of MPFs between 200 and 600 μm (Dris et al., 2016; Henry et al., 2019) and fibers greater than 250 μm have been found in human lungs (Pauly et al., 1998), the MPFs applied in the current study (51% having sizes between 200 and 600 μm) represent an environmentally relevant and realistic test material.

Our experimental MPF concentrations (with an estimated 518 MPFs mL^{-1}, corresponding to 50 μg mL^{-1}) are in agreement with previously published studies on 2D methodology (Dong et al., 2020; Hwang et al., 2019). Moreover, in the hAO exposure volume of 0.5 mL (single well volume where organoids were incubated), the mass and estimated number of MPFs were 0.5 μg and 5 MPFs, 5 μg and 52 MPFs, and 25 μg and 259 MPFs, for the three concentrations, respectively. For the purpose of this experiment, which was to determine the effect on hAOs once in contact with the fibers, we focused on the direct points of contact rather than on the overall fitness of the hAOs in the well (e.g. a counting of intact hAOs per well). Indeed, the first step of most of the inhaled particles, including MPFs is the deposition by impaction (Vianello et al., 2019). Therefore, this organoid-MPF contact situation triggered the interaction between fibers and lung epithelium once fibers reach the inner lung tissues, independently from their concentrations in the air.

Our findings show that after an MPF exposure of 17 days, only a slight non-statistically significant increase in the expression of the inflammatory markers both at molecular and protein level was observed. Potential toxic effects attributable to MPs observed in exposed animal models include impairment of adipogenesis and lipid metabolism (Kannan and Vimalkumar, 2021; Lu et al., 2018). Therefore, we investigated two crucial key regulators of metabolism, PPARγ and adiponectin (Astapova and Leff, 2012), but no statistically significant changes were observed. Organoid volumes at the end of the MPF exposure showed a slight but still evident increase (Fig. 7C). Overall, no clear obesity-promoting effect can be determined after our MPF exposure.

The airway epithelium is the first barrier of the host defense system in the respiratory tract. An adequate and balanced cell composition guarantees an optimal epithelial structure and functionality. In respiratory diseases, this balance may be altered. In our experiments, we observed a change in this cellular balance but most relevant is that SCGB1A1 was found to be significantly reduced. This club cell secretory protein is mainly expressed by nonciliated respiratory epithelial cells and has demonstrated potent anti-inflammatory, anti-tumor, and antitoxicant functions (Broeckaert and Bernard, 2000; Lakind et al., 2007). SCGB1A1 has frequently been used as a biomarker to monitor lung injury caused by various diseases or environmental exposures. Its decrease has been consistently observed to associate with airway inflammatory diseases (Broeckaert et al., 2006; Zhu et al., 2019).

Confocal microscopy and SEM images did not provide any evidence of organoid cell growth inhibition. This observation was not completely surprising, as the field of biomaterials is increasingly demonstrating how plastic can be applied as an inert scaffold to support cell growth for human tissue engineering without altering the biological features (Jubeli et al., 2019). Although the biocompatibility of several plastic materials has already been demonstrated (the hAO themselves grew inside plastic wells made of polystyrene, control included), polyester fibers can contain additives that can be added to textiles in order to impart desirable physical, chemical, and biological (i.e., antimicrobial, color) properties (Chu et al., 2021; Sait et al., 2021). Since additives are typically not covalently bonded to the polymer matrix and can therefore leach, they are considered more harmful than the polymer itself, inducing several effects such as endocrine disruption, immunotoxicity (Tang et al., 2020), genotoxicity and developmental toxicity (Zhao et al., 2020). Our results did not show significant inflammation- or oxidative stress-induced effects of polyester MPFs on hAO development, suggesting that additives, whenever they were present, did not cause adverse effects. However, any further conclusions about long-term effects cannot be drawn with this model.

One of the most relevant results related to MPF exposure was the polarization of the cell growth along the fibers such that the organoid was induced to envelop the encountered fibers by a cellular layer. This behavior was clearly observed in different cases and at different MPF concentrations, indicating that it should be carefully considered a possible adverse effect of MPFs. This effect is particularly alarming if we consider repair processes that could follow MPF inhalation, as it is known that fibers can be retained in the lungs.

If we compare our 3D *in vitro* experimental approach with the already published 2D experimental strategies, we have to underline that our system has been exposed to MPFs for a longer period of time, 17 days versus 6–24 h (Dong et al., 2020; Hwang et al., 2019; Palaniappan et al., 2021; Schirinzi et al., 2017). The longer exposure time could explain the slight differences observed where our hAO had enough time to adapt to the MP environment. The presented data, which combine morphological approaches with molecular/biochemical techniques, were suitable to characterize the MPFs-hAO interactions from a complementary perspective; while confocal and electron microscopy were able to evaluate the overall results on organoid morphology and architecture also at cellular level, the added toxicological markers analyzed three specific toxicological pathways in more detail: inflammation, oxidative stress, and obesogenic response. However, further insights are needed to

complete the toxicological analysis of MPFs. A more detailed analysis could include a co-localization analysis of MPF, changes in specific cell markers, levels of key enzymes which control the anti-oxidative balance, such as superoxide dismutase (SOD), or the contents of other oxidative stress marker, such as malondialdehyde (MDA). These methodologies are suggestions for further evaluation of the effects of airborne pollutants such as MPFs on humans and to further test the proposed human exposure model.

5. Conclusion

In the present study, we employed a 3D *in vitro* model representing a normal lung to test the effects of inhaled and deposited MPFs. Based on the findings of this study, the presence of nonbiodegradable fibers during the repair phase of a damaged lung epithelium may lead to their inclusion in the repaired tissue with unknown effects on long term perspective. Moreover, we observed a significant reduction of SCGB1A1 gene expression, which has frequently been used as a biomarker to monitor lung injury. Having thoroughly described the cell composition of the hAOs used for the first time via gene expression and microscopic analyses, this work contributes to the development of urgently needed human models for assessing the impact of particulate matter pollutants. We conclude that hAOs are suitable for testing MPs and other airborne contaminants, including NPs, to determine the potential risks of atmospheric particles in developing adverse pulmonary effects, but further testing is needed to yield valuable insights using this model and complete the analysis of the effects of inhaled MPFs.

6. Author Information

Lorenza Lazzari is co-last author for the human organoids. Renato Bacchetta is co-last-author for microplastic and microscopy analyses.

Funding

This research did not receive any specific grant from funding agencies in the public, commercial, or not-for-profit sectors.

CRediT authorship contribution statement

Anna Sophie Winkler: Formal analysis, Writing – original draft, Writing – review & editing, Visualization. **Alessandro Cherubini:** Formal analysis, Investigation, Writing – review & editing. **Francesco Rusconi:** Formal analysis, Investigation, Writing – review & editing. **Nadia Santo:** Investigation. **Laura Madaschi:** Investigation. **Clelia Pistoni:** Investigation. **Giorgia Moschetti:** Investigation. **Maria Lucia Sarnicola:** Investigation. **Mariacristina Crosti:** Investigation. **Lorenzo Rosso:** Investigation. **Paolo Tremolada:** Conceptualization, Methodology, Formal analysis, Resources, Writing – review & editing. **Lorenza Lazzari:** Writing – review & editing, Methodology, Resources, Investigation, Supervision. **Renato Bacchetta:** Conceptualization, Methodology, Investigation, Resources, Writing – review & editing, Visualization, Supervision.

Declaration of Competing Interest

The authors declare that they have no known competing financial interests or personal relationships that could have appeared to influence the work reported in this paper.

Acknowledgements

We appreciated Dr. Elena Pini from the Department of Pharmaceutical Sciences at the University of Milan for performing the FTIR analyses. The authors would like to thank Dr. Angela Ronchi for her inspiration.

Appendix A. Supplementary material

Supplementary data to this article can be found online at https://doi.org/10.1016/j.envint.2022.107200.

References

Aguilar, C., Alves da Silva, M., Saraiva, M., Neyazi, M., Olsson, I.A.S., Bartfeld, S., 2021. Organoids as host models for infection biology – a review of methods. Exp. Mol. Med. 53 (10), 1471–1482. https://doi.org/10.1038/s12276-021-00629-4.

Akanyange, S.N., Lyu, X., Zhao, X., Li, X., Zhang, Y., Crittenden, J.C., Anning, C., Chen, T., Jiang, T., Zhao, H., 2021. Does microplastic really represent a threat? A review of the atmospheric contamination sources and potential impacts. Sci. Total Environ. 777, 146020. https://doi.org/10.1016/j.scitotenv.2021.146020.

Ambrosini, R., Azzoni, R.S., Pittino, F., Diolaiuti, G., Franzetti, A., Parolini, M., 2019. First evidence of microplastic contamination in the supraglacial debris of an alpine glacier. Environ. Pollut. 253, 297–301. https://doi.org/10.1016/j.envpol.2019.07.005.

Astapova, O., Leff, T., 2012. Adiponectin and PPARγ, in: Vitamins & Hormones. Elsevier, pp. 143–162. https://doi.org/10.1016/B978-0-12-398313-8.00006-3.

Barkauskas, C.E., Chung, M.-I., Fioret, B., Gao, X., Katsura, H., Hogan, B.L.M., 2017. Lung organoids: current uses and future promise. Development 144, 986–997. https://doi.org/10.1242/dev.140103.

Barshtein, G., Livshits, L., Shvartsman, L.D., Shlomai, N.O., Yedgar, S., Arbell, D., 2016. Polystyrene nanoparticles activate erythrocyte aggregation and adhesion to endothelial cells. Cell Biochem. Biophys. 74 (1), 19–27. https://doi.org/10.1007/s12013-015-0705-6.

Bergmann, M., Wirzberger, V., Krumpen, T., Lorenz, C., Primpke, S., Tekman, M.B., Gerdts, G., 2017. High Quantities of microplastic in arctic deep-sea sediments from the HAUSGARTEN observatory. Environ. Sci. Technol. 51 (19), 11000–11010. https://doi.org/10.1021/acs.est.7b0333110.1021/acs.est.7b03331.s001.

Bhagat, J., Zang, L., Nishimura, N., Shimada, Y., 2020. Zebrafish: an emerging model to study microplastic and nanoplastic toxicity. Sci. Total Environ. 728, 138707. https://doi.org/10.1016/j.scitotenv.2020.138707.

Broeckaert, Bernard, 2000. Clara cell secretory protein (CC16): characteristics and perspectives as lung peripheral biomarker: Clara cell secretory protein. Clin. Exp. Allergy 30 (4), 469–475. https://doi.org/10.1046/j.1365-2222.2000.00760.x.

Broeckaert, F., Clippe, A., Knoops, B., Hermans, C., Bernard, A., 2006. Clara cell secretory protein (CC16): features as a peripheral lung biomarker. Ann. N. Y. Acad. Sci. 923, 68–77. https://doi.org/10.1111/j.1749-6632.2000.tb05520.x.

Broutier, L., Mastrogiovanni, G., Verstegen, M.MA., Francies, H.E., Gavarró, L.M., Bradshaw, C.R., Allen, G.E., Arnes-Benito, R., Sidorova, O., Gaspersz, M.P., Georgakopoulos, N., Koo, B.-K., Dietmann, S., Davies, S.E., Praseedom, R.K., Lieshout, R., IJzermans, J.N.M., Wigmore, S.J., Saeb-Parsy, K., Garnett, M.J., van der Laan, L.JW., Huch, M., 2017. Human primary liver cancer-derived organoid cultures for disease modeling and drug screening. Nat. Med. 23 (12), 1424–1435. https://doi.org/10.1038/nm.4438.

Browne, M.A., Crump, P., Niven, S.J., Teuten, E., Tonkin, A., Galloway, T.S., Thompson, R.C., 2011. Accumulation of microplastic on shorelines wordwide: sources and sinks. Environ. Sci. Technol. 9175–9179 https://doi.org/10.1021/es201811s.

Bruinink, A., Wang, J., Wick, P., 2015. Effect of particle agglomeration in nanotoxicology. Arch. Toxicol. 89 (5), 659–675. https://doi.org/10.1007/s00204-015-1460-6.

Chu, J., Hu, X., Kong, L., Wang, N., Zhang, S., He, M., Ouyang, W., Liu, X., Lin, C., 2021. Dynamic flow and pollution of antimony from polyethylene terephthalate (PET) fibers in China. Sci. Total Environ. 771, 144643. https://doi.org/10.1016/j.scitotenv.2020.144643.

Churg, A., Bauer, M., 2000. Ambient atmospheric particles in the airways of human lungs. Ultrastruct. Pathol. 24, 353–361. https://doi.org/10.1080/019131200750060014.

Co, J.Y., Margalef-Català, M., Li, X., Mah, A.T., Kuo, C.J., Monack, D.M., Amieva, M.R., 2019. Controlling epithelial polarity: a human enteroid model for host-pathogen interactions. Cell Rep. 26 (9), 2509–2520.e4. https://doi.org/10.1016/j.celrep.2019.01.108.

Cortés, C., Domenech, J., Salazar, M., Pastor, S., Marcos, R., Hernández, A., 2020. Nanoplastics as a potential environmental health factor: effects of polystyrene nanoparticles on human intestinal epithelial Caco-2 cells. Environ. Sci. Nano 7 (1), 272–285. https://doi.org/10.1039/C9EN00523D.

Costa, E.C., Moreira, A.F., de Melo-Diogo, D., Gaspar, V.M., Carvalho, M.P., Correia, I.J., 2016. 3D tumor spheroids: an overview on the tools and techniques used for their analysis. Biotechnol. Adv. 34 (8), 1427–1441. https://doi.org/10.1016/j.biotechadv.2016.11.002.

De Falco, F., Di Pace, E., Cocca, M., Avella, M., 2019. The contribution of washing processes of synthetic clothes to microplastic pollution. Sci. Rep. 9, 6633. https://doi.org/10.1038/s41598-019-43023-x.

De Felice, B., Bacchetta, R., Santo, N., Tremolada, P., Parolini, M., 2018. Polystyrene microplastics did not affect body growth and swimming activity in Xenopus laevis tadpoles. Environ. Sci. Pollut. Res. 25 (34), 34644–34651. https://doi.org/10.1007/s11356-018-3408-x.

Domenech, J., Hernández, A., Rubio, L., Marcos, R., Cortés, C., 2020. Interactions of polystyrene nanoplastics with in vitro models of the human intestinal barrier. Arch. Toxicol. 94 (9), 2997–3012. https://doi.org/10.1007/s00204-020-02805-3.

Dong, C.-D., Chen, C.-W., Chen, Y.-C., Chen, H.-H., Lee, J.-S., Lin, C.-H., 2020. Polystyrene microplastic particles: in vitro pulmonary toxicity assessment. J. Hazard. Mater. 385, 121575. https://doi.org/10.1016/j.jhazmat.2019.121575.

Dossena, M., Piras, R., Cherubini, A., Barilani, M., Dugnani, E., Salanitro, F., Moreth, T., Pampaloni, F., Piemonti, L., Lazzari, L., 2020. Standardized GMP-compliant scalable production of human pancreas organoids. Stem Cell Res. Ther. 11, 94. https://doi.org/10.1186/s13287-020-1585-2.

Dris, R., Gasperi, J., Mirande, C., Mandin, C., Guerrouache, M., Langlois, V., Tassin, B., 2017. A first overview of textile fibers, including microplastics, in indoor and outdoor environments. Environ. Pollut. 221, 453–458. https://doi.org/10.1016/j.envpol.2016.12.013.

Dris, R., Gasperi, J., Saad, M., Mirande, C., Tassin, B., 2016. Synthetic fibers in atmospheric fallout: A source of microplastics in the environment? Mar. Pollut. Bull. 104 (1-2), 290–293. https://doi.org/10.1016/j.marpolbul.2016.01.006.

Dutta, D., Heo, I., Clevers, H., 2017. Disease modeling in stem cell-derived 3D organoid systems. Trends Mol. Med. 23 (5), 393–410. https://doi.org/10.1016/j.molmed.2017.02.007.

Fatehullah, A., Tan, S.H., Barker, N., 2016. Organoids as an in vitro model of human development and disease. Nat. Cell Biol. 18 (3), 246–254. https://doi.org/10.1038/ncb3312.

Gaston, E., Woo, M., Steele, C., Sukumaran, S., Anderson, S., 2020. Microplastics differ between indoor and outdoor air masses: insights from multiple microscopy methodologies. Appl. Spectrosc. 74 (9), 1079–1098.

Goldberg, M.S., Thériault, G., 1994. Retrospective cohort study of workers of a synthetic textiles plant in Quebec: I. General mortality. Am. J. Ind. Med. 25 (6), 889–907. https://doi.org/10.1002/ajim.4700250612.

Henry, B., Laitala, K., Klepp, I.G., 2019. Microfibres from apparel and home textiles: prospects for including microplastics in environmental sustainability assessment. Sci. Total Environ. 652, 483–494. https://doi.org/10.1016/j.scitotenv.2018.10.166.

Heo, I., Dutta, D., Schaefer, D.A., Iakobachvili, N., Artegiani, B., Sachs, N., Boonekamp, K.E., Bowden, G., Hendrickx, A.P.A., Willems, R.J.L., Peters, P.J., Riggs, M.W., O'Connor, R., Clevers, H., 2018. Modelling cryptosporidium infection in human small intestinal and lung organoids. Nat. Microbiol. 3 (7), 814–823. https://doi.org/10.1038/s41564-018-0177-8.

Hu, M., Palić, D., 2020. Micro- and nano-plastics activation of oxidative and inflammatory adverse outcome pathways. Redox Biol. 37, 101620. https://doi.org/10.1016/j.redox.2020.101620.

Huch, M., Gehart, H., van Boxtel, R., Hamer, K., Blokzijl, F., Verstegen, M.A., Ellis, E., van Wenum, M., Fuchs, S., de Ligt, J., van de Wetering, M., Sasaki, N., Boers, S., Kemperman, H., de Jonge, J., Ijzermans, J.M., Nieuwenhuis, E.S., Hoekstra, R., Strom, S., Vries, R.G., van der Laan, L.W., Cuppen, E., Clevers, H., 2015. Long-term culture of genome-stable bipotent stem cells from adult human liver. Cell 160 (1-2), 299–312. https://doi.org/10.1016/j.cell.2014.11.050.

Hwang, J., Choi, D., Han, S., Choi, J., Hong, J., 2019. An assessment of the toxicity of polypropylene microplastics in human derived cells. Sci. Total Environ. 684, 657–669. https://doi.org/10.1016/j.scitotenv.2019.05.071.

Jensen, C., Teng, Y., 2020. Is it time to start transitioning from 2D to 3D cell culture? Front. Mol. Biosci. 7, 33. https://doi.org/10.3389/fmolb.2020.00033.

Jose, S.S., De Zuani, M., Tidu, F., Hortová Kohoutková, M., Pazzagli, L., Forte, G., Spaccapelo, R., Zelante, T., Frič, J., 2020. Comparison of two human organoid models of lung and intestinal inflammation reveals toll-like receptor signalling activation and monocyte recruitment. Clin. Transl. Immunol. 9 (5) https://doi.org/10.1002/cti2.v9.510.1002/cti2.1131.

Jubeli, E., Khzam, A., Yagoubi, N., 2019. Cells integration onto scaffolds prepared from polyester based polymers – importance of polymer thermal properties in addition to hydrophilicity. Int. J. Polym. Mater. Polym. Biomater. 68 (17), 1068–1077. https://doi.org/10.1080/00914037.2018.1525549.

Kämpfer, A.A.M., Busch, M., Schins, R.P.F., 2020. Advanced *in vitro* testing strategies and models of the intestine for nanosafety research. Chem. Res. Toxicol. 33 (5), 1163–1178. https://doi.org/10.1021/acs.chemrestox.0c00079.

Kannan, K., Vimalkumar, K., 2021. A review of human exposure to microplastics and insights into microplastics as obesogens. Front. Endocrinol. 12, 724989 https://doi.org/10.3389/fendo.2021.724989.

Kapp, K.J., Miller, R.Z., Mukherjee, A., 2020. Electric clothes dryers: an underestimated source of microfiber pollution. PLoS ONE 15 (10), e0239165. https://doi.org/10.1371/journal.pone.0239165.

Kuratnik, A., Giardina, C., 2013. Intestinal organoids as tissue surrogates for toxicological and pharmacological studies. Biochem. Pharmacol. 85 (12), 1721–1726. https://doi.org/10.1016/j.bcp.2013.04.016.

Lakind, J.S., Holgate, S.T., Ownby, D.R., Mansur, A.H., Helms, P.J., Pyatt, D., Hays, S.M., 2007. A critical review of the use of Clara cell secretory protein (CC16) as a biomarker of acute or chronic pulmonary effects. Biomarkers 12 (5), 445–467. https://doi.org/10.1080/13547500701359327.

Lancaster, M.A., Renner, M., Martin, C.-A., Wenzel, D., Bicknell, L.S., Hurles, M.E., Homfray, T., Penninger, J.M., Jackson, A.P., Knoblich, J.A., 2013. Cerebral organoids model human brain development and microcephaly. Nature 501 (7467), 373–379. https://doi.org/10.1038/nature12517.

Lim, S.L., Ng, C.T., Zou, L.i., Lu, Y., Chen, J., Bay, B.H., Shen, H.-M., Ong, C.N., 2019. Targeted metabolomics reveals differential biological effects of nanoplastics and nanoZnO in human lung cells. Nanotoxicology 13 (8), 1117–1132. https://doi.org/10.1080/17435390.2019.1640913.

Lippmann, M., Yeates, D.B., Albert, R.E., 1980. Deposition, retention, and clearance of inhaled particles. Occup. Environ. Med. 37 (4), 337–362. https://doi.org/10.1136/oem.37.4.337.

Liu, C., Li, J., Zhang, Y., Wang, L., Deng, J., Gao, Y., Yu, L., Zhang, J., Sun, H., 2019. Widespread distribution of PET and PC microplastics in dust in urban China and their estimated human exposure. Environ. Int. 128, 116–124. https://doi.org/10.1016/j.envint.2019.04.024.

Liu, L., Xu, K., Zhang, B., Ye, Y., Zhang, Q., Jiang, W., 2021. Cellular internalization and release of polystyrene microplastics and nanoplastics. Sci. Total Environ. 779, 146523. https://doi.org/10.1016/j.scitotenv.2021.146523.

Loomis, D., Grosse, Y., Lauby-Secretan, B., Ghissassi, F.E., Bouvard, V., Benbrahim-Tallaa, L., Guha, N., Baan, R., Mattock, H., Straif, K., 2013. The carcinogenicity of outdoor air pollution. Lancet Oncol. 14 (13), 1262–1263. https://doi.org/10.1016/S1470-2045(13)70487-X.

Lu, L., Wan, Z., Luo, T., Fu, Z., Jin, Y., 2018. Polystyrene microplastics induce gut microbiota dysbiosis and hepatic lipid metabolism disorder in mice. Sci. Total Environ. 631–632, 449–458. https://doi.org/10.1016/j.scitotenv.2018.03.051.

Lusher, A.L., Tirelli, V., O'Connor, I., Officer, R., 2015. Microplastics in arctic polar waters: the first reported values of particles in surface and sub-surface samples. Sci. Rep. 5, 14947. https://doi.org/10.1038/srep14947.

Mastrangelo, G., Fedeli, U., Fadda, E., Milan, G., Lange, J.H., 2002. Epidemiologic evidence of cancer risk in textile industry workers: a review and update. Toxicol. Ind. Health 18 (4), 171–181. https://doi.org/10.1191/0748233702th139rr.

Mellin, R., Boddey, J.A., 2020. Organoids for liver stage malaria research. Trends Parasitol. 36 (2), 158–169. https://doi.org/10.1016/j.pt.2019.12.003.

Nel, A., 2005. Air pollution-related illness: effects of particles. Science 308 (5723), 804–806.

O'Brien, S., Okoffo, E.D., O'Brien, J.W., Ribeiro, F., Wang, X., Wright, S.L., Samanipour, S., Rauert, C., Toapanta, T.Y.A., Albarracin, R., Thomas, K.V., 2020. Airborne emissions of microplastic fibres from domestic laundry dryers. Sci. Total Environ. 747, 141175. https://doi.org/10.1016/j.scitotenv.2020.141175.

Palaniappan, S., Sadacharan, C.M., Rostama, B., 2022. Polystyrene and polyethylene microplastics decrease cell viability and dysregulate inflammatory and oxidative stress markers of MDCK and L929 cells in vitro. Expo Health 14 (1), 75–85. https://doi.org/10.1007/s12403-021-00419-3.

Pauly, J.L., Stegmeier, S.J., Allaart, H.A., Cheney, R.T., Zhang, P.J., Mayer, A.G., Streck, R.J., 1998. Inhaled cellulosic and plastic fibers found in human lung tissue. Can. Epidemiol. Prev. Biomark. 7, 419–428.

Pimentel, J.C., Avila, R., Lourenco, A.G., 1975. Respiratory disease caused by synthetic fibres: a new occupational disease. Thorax 30 (2), 204–219. https://doi.org/10.1136/thx.30.2.204.

Prata, J.C., 2018. Airborne microplastics: consequences to human health? Environ. Pollut. 234, 115–126. https://doi.org/10.1016/j.envpol.2017.11.043.

Prata, J.C., Castro, J.L., da Costa, J.P., Cerqueira, M., Duarte, A.C., Rocha-Santos, T., 2020a. In: Handbook of Microplastics in the Environment. Springer International Publishing, Cham, pp. 1–25. https://doi.org/10.1007/978-3-030-10618-8_37-1.

Prata, J.C., da Costa, J.P., Lopes, I., Duarte, A.C., Rocha-Santos, T., 2020b. Environmental exposure to microplastics: an overview on possible human health effects. Sci. Total Environ. 702, 134455. https://doi.org/10.1016/j.scitotenv.2019.134455.

Reed, S., Clark, M., Thompson, R., Hughes, K.A., 2018. Microplastics in marine sediments near Rothera Research Station. Antarctica. Mar. Pollut. Bull. 133, 460–463. https://doi.org/10.1016/j.marpolbul.2018.05.068.

Rist, S., Carney Almroth, B., Hartmann, N.B., Karlsson, T.M., 2018. A critical perspective on early communications concerning human health aspects of microplastics. Sci. Total Environ. 626, 720–726. https://doi.org/10.1016/j.scitotenv.2018.01.092.

Ruenraroengsak, P., Tetley, T.D., 2015. Differential bioreactivity of neutral, cationic and anionic polystyrene nanoparticles with cells from the human alveolar compartment: robust response of alveolar type 1 epithelial cells. Part. Fibre Toxicol. 12, 19. https://doi.org/10.1186/s12989-015-0091-7.

Sachs, N., Papaspyropoulos, A., Zomer-van Ommen, D.D., Heo, I., Böttinger, L., Klay, D., Weeber, F., Huelsz-Prince, G., Iakobachvili, N., Amatngalim, G.D., de Ligt, J., van Hoeck, A., Proost, N., Viveen, M.C., Lyubimova, A., Teeven, L., Derakhshan, S., Korving, J., Begthel, H., Dekkers, J.F., Kumawat, K., Ramos, E., van Oosterhout, M. F., Offerhaus, G.J., Wiener, D.J., Olimpio, E.P., Dijkstra, K.K., Smit, E.F., van der Linden, M., Jaksani, S., van de Ven, M., Jonkers, J., Rios, A.C., Voest, E.E., van Moorsel, C.H., van der Ent, C.K., Cuppen, E., van Oudenaarden, A., Coenjaerts, F.E., Meyaard, L., Bont, L.J., Peters, P.J., Tans, S.J., van Zon, J.S., Boj, S.F., Vries, R.G., Beekman, J.M., Clevers, H., 2019. Long-term expanding human airway organoids for disease modeling. EMBO J. 38 https://doi.org/10.15252/embj.2018100300.

Sait, S.T.L., Sørensen, L., Kubowicz, S., Vike-Jonas, K., Gonzalez, S.V., Asimakopoulos, A. G., Booth, A.M., 2021. Microplastic fibres from synthetic textiles: Environmental degradation and additive chemical content. Environ. Pollut. 268, 115745. https://doi.org/10.1016/j.envpol.2020.115745.

Sato, T., Stange, D.E., Ferrante, M., Vries, R.G.J., van Es, J.H., van den Brink, S., van Houdt, W.J., Pronk, A., van Gorp, J., Siersema, P.D., Clevers, H., 2011. Long-term expansion of epithelial organoids from human colon, adenoma, adenocarcinoma, and Barrett's epithelium. Gastroenterology 141 (5), 1762–1772. https://doi.org/10.1053/j.gastro.2011.07.050.

Schirinzi, G.F., Pérez-Pomeda, I., Sanchís, J., Rossini, C., Farré, M., Barceló, D., 2017. Cytotoxic effects of commonly used nanomaterials and microplastics on cerebral and epithelial human cells. Environ. Res. 159, 579–587. https://doi.org/10.1016/j.envres.2017.08.043.

Schutgens, F., Clevers, H., 2020. Human organoids: tools for understanding biology and treating diseases. Annu. Rev. Pathol. 15 (1), 211–234. https://doi.org/10.1146/annurev-pathmechdis-012419-032611.

Shamir, E.R., Ewald, A.J., 2014. Three-dimensional organotypic culture: experimental models of mammalian biology and disease. Nat. Rev. Mol. Cell Biol. 15 (10), 647–664. https://doi.org/10.1038/nrm3873.

Takasato, M., Er, P.X., Chiu, H.S., Little, M.H., 2016. Generation of kidney organoids from human pluripotent stem cells. Nat. Protoc. 11 (9), 1681–1692. https://doi.org/10.1038/nprot.2016.098.

Tang, Y.u., Zhou, W., Sun, S., Du, X., Han, Y.u., Shi, W., Liu, G., 2020. Immunotoxicity and neurotoxicity of bisphenol A and microplastics alone or in combination to a bivalve species. Tegillarca granosa. Environ. Pollut. 265, 115115. https://doi.org/10.1016/j.envpol.2020.115115.

Triebskorn, R., Braunbeck, T., Grummt, T., Hanslik, L., Huppertsberg, S., Jekel, M., Knepper, T.P., Krais, S., Müller, Y.K., Pittroff, M., Ruhl, A.S., Schmieg, H., Schür, C., Strobel, C., Wagner, M., Zumbülte, N., Köhler, H.-R., 2019. Relevance of nano- and microplastics for freshwater ecosystems: a critical review. TrAC, Trends Anal. Chem. 110, 375–392. https://doi.org/10.1016/j.trac.2018.11.023.

Truskey, G.A., 2018. Human microphysiological systems and organoids as in vitro models for toxicological studies. Front. Public Health 6, 185. https://doi.org/10.3389/fpubh.2018.00185.

Tuveson, D., Clevers, H., 2019. Cancer modeling meets human organoid technology. Science 364 (6444), 952–955.

Umamaheswari, S., Priyadarshinee, S., Kadirvelu, K., Ramesh, M., 2021. Polystyrene microplastics induce apoptosis via ROS-mediated p53 signaling pathway in zebrafish. Chem. Biol. Interact. 345, 109550. https://doi.org/10.1016/j.cbi.2021.109550.

Valavanidis, Athanasios, Fiotakis, Konstantinos, Vlachogianni, Thomais, 2008. Airborne particulate matter and human health: toxicological assessment and importance of size and composition of particles for oxidative damage and carcinogenic mechanisms. J. Environ. Sci. Health Part C 26 (4), 339–362. https://doi.org/10.1080/10590500802494538.

Vianello, A., Jensen, R.L., Liu, L., Vollertsen, J., 2019. Simulating human exposure to indoor airborne microplastics using a breathing thermal manikin. Sci. Rep. 9, 8670. https://doi.org/10.1038/s41598-019-45054-w.

Waller, C.L., Griffiths, H.J., Waluda, C.M., Thorpe, S.E., Loaiza, I., Moreno, B., Pacherres, C.O., Hughes, K.A., 2017. Microplastics in the Antarctic marine system: an emerging area of research. Sci. Total Environ. 598, 220–227. https://doi.org/10.1016/j.scitotenv.2017.03.283.

Watson, C.Y., DeLoid, G.M., Pal, A., Demokritou, P., 2016. Buoyant nanoparticles: implications for nano-biointeractions in cellular studies. Small 12 (23), 3172–3180. https://doi.org/10.1002/smll.201600314.

Xu, M., Halimu, G., Zhang, Q., Song, Y., Fu, X., Li, Y., Li, Y., Zhang, H., 2019. Internalization and toxicity: a preliminary study of effects of nanoplastic particles on human lung epithelial cell. Sci. Total Environ. 694, 133794. https://doi.org/10.1016/j.scitotenv.2019.133794.

Zhang, Y., Kang, S., Allen, S., Allen, D., Gao, T., Sillanpää, M., 2020. Atmospheric microplastics: a review on current status and perspectives. Earth-Sci. Rev. 203, 103118. https://doi.org/10.1016/j.earscirev.2020.103118.

Zhao, H.-J., Xu, J.-K., Yan, Z.-H., Ren, H.-Q., Zhang, Y., 2020. Microplastics enhance the developmental toxicity of synthetic phenolic antioxidants by disturbing the thyroid function and metabolism in developing zebrafish. Environ. Int. 140, 105750. https://doi.org/10.1016/j.envint.2020.105750.

Zhu, L., An, L., Ran, D.i., Lizarraga, R., Bondy, C., Zhou, X.u., Harper, R.W., Liao, S.-Y., Chen, Y., 2019. The club cell marker SCGB1A1 downstream of FOXA2 is reduced in asthma. Am. J. Respir. Cell Mol. Biol. 60 (6), 695–704. https://doi.org/10.1165/rcmb.2018-0199OC.

Supporting Information

"Human airway organoids and microplastic fibers: a new exposure model for emerging contaminants"

Data tables: Table S1 – S2

Graphics: Figure S1 – S5

Other Supplementary Material for this manuscript includes the following:

Video S1 (available at https://github.com/AnnaSophieWinkler/Human_airway_organoids)

Table S1. Utilized reagents.

Reagent	**Source**	**Identifier or catalogue number**
Antibodies		
Anti-acetylated Tubulin	Sigma-Aldrich	T7451
Anti-Human MUC1 Glycoprotein	StemCell Technologies Inc	01423
Recombinant Anti-Cytokeratin 5 antibody	abcam	ab75869
Anti Uteroglobin/SCGB1A1/CC10 (E-11)	Santacruz	sc-365992
Anti-Pro + Mature Surfactant Protein B antibody	abcam	ab40876
Goat anti-mouse igG Alexa Fluor Plus 488	Invitrogen	A32723
Goat anti-rabbit igG Alexa Fluor Plus 647	Invitrogen	A32733
Reagents and chemicals		
A83.01	Tocris	2939
AdDMEM/F12	Gibco	12634034
B27	Gibco	1750444
Bovine serum albumin (BSA)	Sigma-Aldrich	A9647
Collagenase I	Sigma-Aldrich	C9407
Dispase II	Life Technologies	17105-041
DMEM	Euroclone	ECB7501L
DMEM high glucose	Sigma-Aldrich	D1145
DNase I	Sigma-Aldrich	DN25
EDTA	Sigma-Aldrich	E7889
FBS	Invitrogen	10270106
FGF10	Peprotech	100-26
FGF7	Peprotech	100-19

Reagent	Source	Identifier or catalogue number
Glutamax	Gibco	35050061
Glutaraldehyde	EMS	16316
Hepes	Gibco	15630056
Hexamethyldisilazane	Sigma-Aldrich	440191
Hoechst 33342	Invitrogen	H3570
Matrigel	Corning	356231
MitoSOX red	Life technologies	M36008
MTT substrate	Sigma-Aldrich	M5655
N-Acetylcysteine	Sigma-Aldrich	A9165
Nicotinamide	Sigma-Aldrich	N0636
Noggin	Peprotech	120-10C
Osmium tetroxide (OsO_4)	Ted Pella	18463
Paraformaldehyde	Sigma-Aldrich	158127
Penicillin/Streptomycin	Gibco	15140122
Phalloidin-Atto 565	Sigma-Aldrich	94072
Phosphate-buffered saline (PBS)	Sigma-Life Science	P4417
Red blood cell lysis buffer	BD Pharm Lyse	555899
Rock inhibitor Y27632	Peprotech	1293823
RSPO1	Peprotech	120-38
SB202190	Sigma-Aldrich	S7067
Staphylococcal enterotoxin B (SEB)	Sigma-Aldrich	S4881
Sodium cacodylate	Sigma-Life Science	C4945
SuperScript IV VILO	Thermo Fisher Scientific	11756500
SYBR Select Master Mix	Thermo Fisher Scientific	4472937
Triton X-100	Sigma-Aldrich	X100
Trypsin NB Cell Culture Grade, 0.05% solution with EDTA	SERVA	37297
Reagents and chemicals		
TRIzol reagent	Thermo Fisher Scientific	15596-026

Table S2. Genes, forward (FWD) and reverse (REV) sequences of primers and their functions used in qRT-PCR analysis.

Gene	Name	Primer	Sequence	Function
SOD1	Superoxide Dismutase 1	FWD	CACTGGTGGTCCATGAAAAAGC	antioxidant enzyme
		REV	ACACCACAAGCCAAACGACT	
SOD2	Superoxide Dismutase 2	FWD	GCTCCCCGCGCTTTCTTA	antioxidant enzyme
		REV	GCTGGTGCCGCACACT	
GSTA1	Glutathione S-Transferase Alpha 1	FWD	GCAGCTGGAGTAGAGTTTGAAGAG	detoxification of electrophilic compounds
		REV	TCAGGTGGACATACGGGCA	
GPX1	Glutathione Peroxidase 1	FWD	AGAGTCTGGCTACTCTCTCGTT	detoxification of hydrogen peroxide
		REV	CCGGGATTTTGCCCTCCAT	
NOX2	NADPH oxidase 2	FWD	CATTATCCCAGTTGGGCCGT	maintain a healthy level of ROS
		REV	GTCTCAGGCCAATCACTTTGC	
COX1	Cytochrome c oxidase I	FWD	ATACCAAACGCCCCTCTTCG	preventing oxidative stress
		REV	TGTTGAGGTTGCGGTCTGTT	
CAT	Catalase	FWD	TTGCCACAGGAAAGTACCCC	catalysis of hydrogen peroxide
		REV	TGAGGCCAAACCTTGGTGAG	
ND1	NADH-ubiquinone oxidoreductase chain 1	FWD	ACGCCATAAAACTCTTCACCAAAG	ROS level regulation
		REV	TAGTAGAAGAGCGATGGTGAGAGCTA	
TNF-a	Tumor necrosis factor-alpha	FWD	GCCCATGTTGTAGCAAACCC	Inflammatory response
		REV	TATCTCTCAGCTCCACGCCA	
IL-6	Interleukin 6	FWD	GCCCAGCTATGAACTCCTTCT	Inflammatory response
		REV	GCAAGTCTCCTCATTGAATCCAG	
CCL2	Chemokine ligand 2	FWD	CATGAAAGTCTCTGCCGCCC	Monocytes and neutrophil activation
		REV	GGGCATTGATTGCATCTGGCTG	
CLDN1	Claudin 1	FWD	TTACTGCCCCCAGAGGATGA	Lung epithelium
		REV	TGCAACGTCGTTACGAGTCA	
KRT5	Keratin 5	FWD	GCATCACCGTTCCTGGGTAA	Basal cells marker
		REV	GACACACTTGACTGGCGAGA	
NKX2.1	NK2 Homeobox 1	FWD	ACCAAGCGCATCCAATCTCA	Lung marker
		REV	CAGAGCCATGTCAGCACAGA	
NPHP1	Nephrocystin 1	FWD	CAGAGCCACATGGCAACCTA	Ciliated cells marker
		REV	ACCCAGCCACAGCTTAACTC	
SCGB1A1	Secretoglobin Family 1A member 1	FWD	TCCTCCACCATGAAACTCGC	Club cells marker
		REV	AGGAGGGTTTCGATGACACG	
SFTPA1	Surfactant protein A1	FWD	CAGACGGGACCCCTGTAAAC	AT2 cells marker
		REV	CCTGTCATTCCACTGCCCAT	
SFTPC	Surfactant protein C	FWD	ATGGATGTGGGCAGCAAAGA	

		REV	CAGCAGGGAATGCCAAATCG	AT2 cells marker
DNAH5	Dynein Axonemal Heavy Chain 5	FWD	AGAGGCCATTCGCAAACGTA	Ciliated cells marker
		REV	CCCGGAAAATGGGCAAACTG	
PRSS1	Serine protease 1	FWD	AAGTGTGAAGCCTCCTACCC	Trypsinogen secretion
		REV	GGTGTAGACTCCAGGCTTGT	
PRSS3	Serine protease 3	FWD	CTCACCTGCCGTCATCAATG	Trypsinogen secretion
		REV	TTACACTCAGCCTGGGTCAG	
SNAI1	Snail family transcriptional repressor 1	FWD	TACAGCGAGCTGCAGGACT	Control of EMT during tumor progreassion
		REV	ATCTCCGGAGGTGGGATG	
TWIST1	Twist family BHLH transcription factor 1	FWD	GGAGTCCGCAGTCTTACGAG	Key transcription factor in EMT
		REV	TCTGGAGGACCTGGTAGAGG	
N-cadherin	N-cadherin gene	FWD	GGTGGAGGAGAAGAAGACCAG	EMT marker gene
		REV	GGCATCAGGCTCCACAGT	
PPARg	Peroxisome proliferator-activated receptor gamma	FWD	CATTCCATTCACAAGAACAGAT	Adipogenesis marker
		REV	GGCTTATTGTAGAGCTGAGT	
ADIPONECTIN	Adiponectin	FWD	TTCCATACCAGAGGGGCTCA	Adopogenesis marker
		REV	CCCTTGAGTCGTGGTTTCCT	
ACTB	beta actin	FWD	CACGATGGAGGGGAAGACGG	Cell structure
		REV	CGCCGCCAGCTCACCATG	
TBP	TATA-box binding protein	FWD	GCCACGCCAGCTTCGGAGAG	Transcription
		REV	CCGCAGCAAACCGCTTGGGA	
HPRT1	Hypoxanthine Phosphoribosyltransferase 1	FWD	CTGGCGTCGTGATTAGTG	Nucleotide-metabolism
		REV	CACACAGAGGGCTACAATG	

Figure S7. Polyester fibers collected from the filtered exhaust air after the drying of synthetic clothes and fabrics.

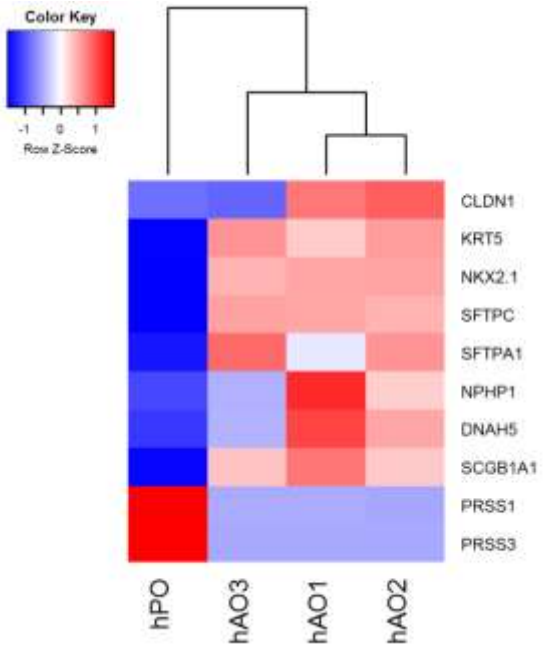

Figure S2. Gene expression heatmap of human airway organoids (hAOs). Organoids were generated from the biopsies of three healthy lung donors (hAO1–3) and a human pancreas organoid (hPO) for comparison. PRSS1 and PRSS3 are genes associated with the trypsinogen secretion in pancreas and used as negative control.

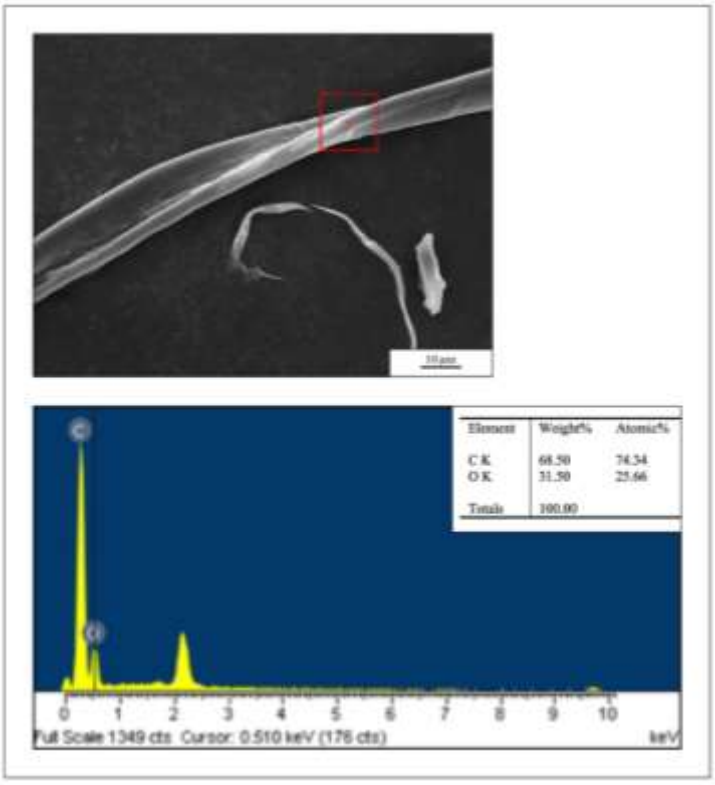

Figure S3. EDS spectrum of a polyester fiber from synthetic fabrics.

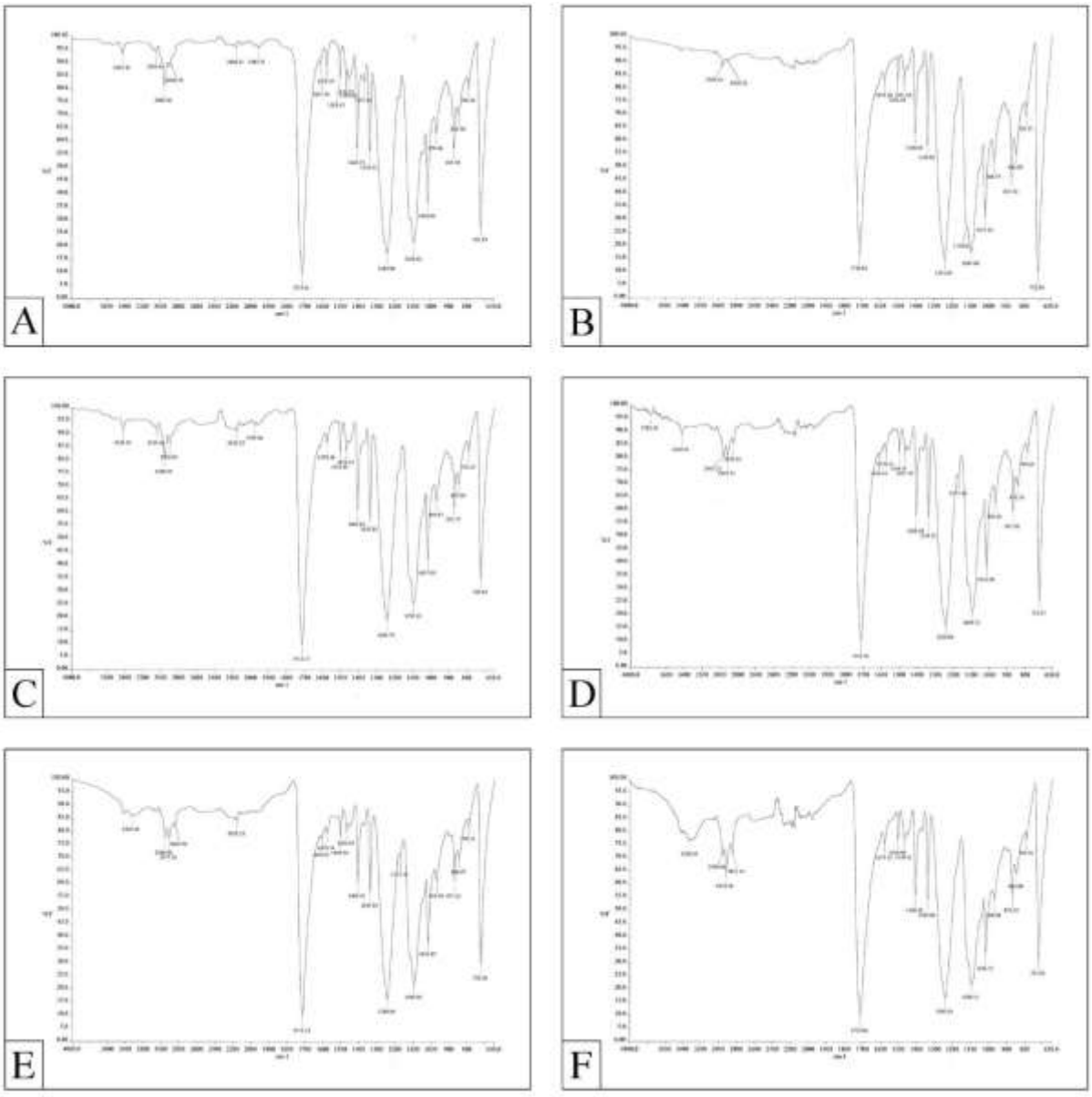

Figure S4. ATR-FTIR spectrum of all original bulk fabrics used for the drying compared to PET from a plastic water bottle as reference; (A) PET bottle, (B) Blanket, (C) T-shirt (D) Fleece Jacket, (E) Fleece Jacket2, (F) Fleece Jacket3.

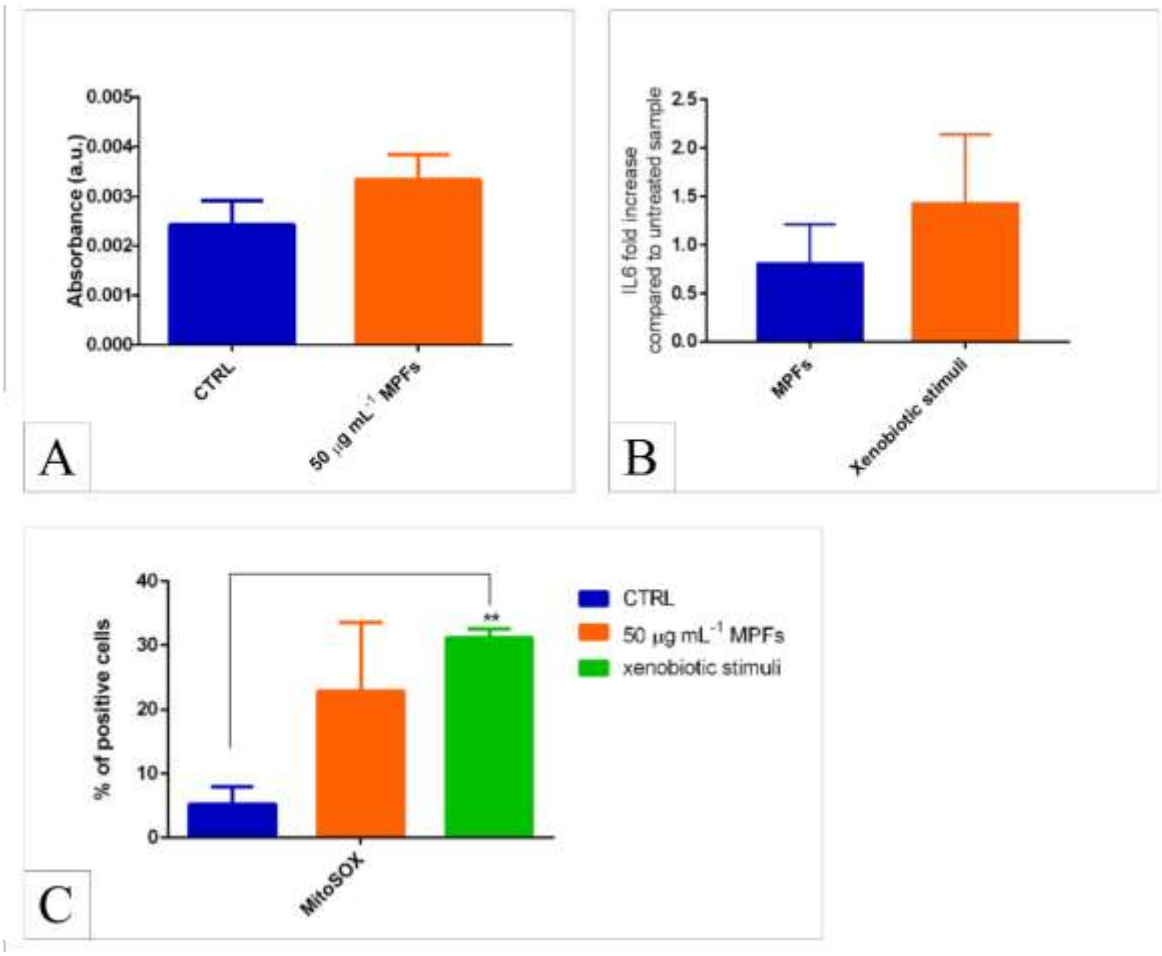

Figure S5. (A) MTT viability test of hAO; control group (n = 3; in orange) against MPFs treated group (n = 3; in blue). Data were presented as % of metabolic activity (control group set at 100%); data were normalized considering the number of organoids per well. (B) ELISA test of hAO supernatant: MPFs treated group (n = 3; in blue) and xenobiotic stimulated group (n = 3; in orange). Data were reported as fold increase of IL6 compared to untreated group. (C) MitoSOX flow cytometric analysis of hAO; control group (n = 3; in blue) against MPFs treated group (n = 3; in orange) and stimulated group (n = 3; in green). Data in panel A are shown as means ± Standard Deviation (n = 3), statistical analysis was performed by t-test analysis followed by Kolmogorov-Smirnov correction. Data in panel B are shown as means ± S.E.M. (n = 3). Data in panel C are shown as means ± S.E.M. (n = 3), statistical analysis was performed by two-way ANOVA followed by Bonferroni correction; ** P <0.01.

CHAPTER III – Conclusions

This thesis demonstrated the presence and fate of microplastics in a freshwater ecosystem and in bottled drinking water, showed that micro- and nanoplastics can be generated by opening plastic water bottles, and how secondary nanoplastics can be modified in their physical-chemical properties. Finally, a new model for human risk assessment of atmospheric plastic particles was presented.

The freshwater ecosystem investigations show the incidence of microplastics in all four analysed abiotic (surface water and sediment) and biotic (the wels catfish *Silurus glanis* and the caddisfly Hydropsychidae from the order Trichoptera) matrices simultaneously sampled at the Ticino River, as well as plastic ingestion of an avian freshwater species (*Alcedo atthis*). The results of this project demonstrated a high complexity of the distribution of microplastics along the river, evidenced by the absence of correlation of concentration in the biota to that in water and sediment and along the river (including pellets of the kingfisher). This finding was unexpected considering that higher microplastic concentrations are usually correlated to anthropogenic activity (here effluents of WWTPs) which increases towards the lower end of the river. In addition, the observed differences in microplastic from sediment and water samples in regard to size and shape indicate a considerable influence of other environmental factors such as e.g. biofouling in driving the environmental fate of microplastics. The overall results evidence that a single matrix alone cannot accurately represent the microplastic pollution level because the environmental features of sampling sites (flow velocity) are able to drive microplastic loads towards a specific matrix, especially in complex river systems such as those characterised by high natural conditions. In consequence, future studies need to perform multiple-matrix monitoring to assess microplastic pollution of a freshwater ecosystem - once common procedures for sampling and detection have agreed on. Moreover, the spatial variability and the opposing microplastic concentrations in water and sediment further indicates a strong role of the pronounced hydrodynamic conditions of the Ticino River, where microplastics can be deposited, retained and resuspended. The then calculated annual load to the Po River of 3.40×10^{11} microplastics demonstrated the order of magnitude of the microplastic load to the surface water network and the dimension of the potential load of microplastic from the freshwater network to the sea. This impressive but realistic value should encourage stricter monitoring and control of microplastic loads in aquatic ecosystems.

In the context of micro- and nanoplastic impacts on humans, information on plastic particle contamination of drinking water and exposure pathways of particles from food packaging is most valuable. This thesis' work as shown the release of micro- as well as nanoplastic particles from drinking water plastic bottles (single-use) under simulated use. While the PET material of the tested bottles (body and bottleneck) was resistant towards mechanical stress, the bottle lid made of HDPE was identified as source of the formation of plastic particles, which were also detected on bottlenecks, and therefore, available for human exposure via ingestion. Particularly the results regarding nanoplastics release are of interest to human exposure studies considering that smaller particles (few micrometer and nanometer range) are thought to be more hazardous. This work furthermore suggests that the release of micro- and nanoplastic particles from plastic packaging material, which also depended on the bottle brand, should be taken into account when designing new sustainable plastic strategies or principles guiding the revision of packaging, also regarding life cycle assessments.

By coupling different techniques, namely high resolution SEM, XPS, SPES and μRaman analysis, and applying concentration steps, this work presents a suitable approach for quantifying and identifying nanoplastics in simple matrices like drinking water, and by that, a design of improved analytical schemes for secondary nanoplastics. Moreover, it has been observed that mechanical stress alone can chemically modify plastic materials (here PE) even without the occurrence of other external stressors. The gained knowledge of physical-chemical modifications of secondary nanoplastics with respect to those of their original source bulk material explains the known challenges associated with their identification and deepens the understanding of degradation mechanisms during secondary nanoplastics formation, which is urgently needed for environmental nanoplastic sampling, effect and analysis studies.

Evaluating the effects of micro- and nanoplastics in humans is crucial for determining their risk potential. According to the World Health Organization,[70] quality-assured toxicological data are needed on the most common forms of plastic particles relevant for human health risk assessment. Having employed a 3D *in vitro* model representing a normal lung to test the effects of inhaled and deposited microplastic fibres, this thesis contributes to the development of urgently needed, reliable human models for assessing the impact of airborne particulate matter pollutants such as micro- and nanoplastics. Moreover, the developing of more reliable *in-vitro* toxicological models could contribute to overcome animal model needs which should be reduced and even avoided as much as possible, according to EU legislation. The cell composition of the used human airway organoids was thoroughly described for via gene expression and microscopic analyses. Based on the findings, it has been suspected that atmospheric microplastics can cause adverse effects on developing lungs, but further testing is needed to yield valuable insights using this model and complete the analysis of the effects of inhaled microplastics. The development of human airway organoids is of particular urgency since air is assumed to be the main source of micro- and nanoplastics uptake by humans.[56] Considering the benefits of 3D cell models presented in this thesis and following new developments, improvement and understanding, researchers currently working on micro-and nanoplastic effects on humans should seriously consider 3D cell culturing options.

With future plastic waste reduction through circular systems (e.g. reuse, recycling) and innovation in the design of plastic products (e.g. synthetic clothes releasing fewer fibres, biodegradable plastics), the microplastic emissions might reduce as well. However, plastic leakages will further occur, and the plastic present in the environment will steadily break down into micro- and nanoplastics that continue to threaten organisms and humans. For this reason, the quest on micro- and nanoplastic measurement and effects will continue until the body of evidence will be substantially improved.

BIBLIOGRAPHY

1. MacLeod M, Arp HPH, Tekman MB, Jahnke A. The global threat from plastic pollution. *Science*. 2021; 373(6550):61-65. doi:10.1126/science.abg5433

2. Borrelle SB, Ringma J, Law KL, et al. Predicted growth in plastic waste exceeds efforts to mitigate plastic pollution. *Science*. 2020; 369(6510):1515-1518. doi:10.1126/science.aba3656

3. Lebreton L, Slat B, Ferrari F, et al. Evidence that the Great Pacific Garbage Patch is rapidly accumulating plastic. *Sci Rep*. 2018; 8(1):4666. doi:10.1038/s41598-018-22939-w

4. Bergmann M, Gutow L, Klages M, eds. *Marine Anthropogenic Litter*. Springer International Publishing; 2015. doi:10.1007/978-3-319-16510-3

5. Galgani F, Pham CK, Claro F, Consoli P. Marine animal forests as useful indicators of entanglement by marine litter. *Mar Pollut Bull*. 2018; 135:735-738. doi:10.1016/j.marpolbul.2018.08.004

6. Hartmann NB, Hüffer T, Thompson RC, et al. Are We Speaking the Same Language? Recommendations for a Definition and Categorization Framework for Plastic Debris. *Environ Sci Technol*. Published online January 17, 2019. doi:10.1021/acs.est.8b05297

7. Smith M, Love DC, Rochman CM, Neff RA. Microplastics in Seafood and the Implications for Human Health. *Curr Environ Health Rep*. 2018; 5(3):375-386. doi:10.1007/s40572-018-0206-z

8. Kontrick AV. Microplastics and Human Health: Our Great Future to Think About Now. *J Med Toxicol*. 2018; 14(2):117-119. doi:10.1007/s13181-018-0661-9

9. Lehner R, Weder C, Petri-Fink A, Rothen-Rutishauser B. Emergence of Nanoplastic in the Environment and Possible Impact on Human Health. *Environ Sci Technol*. 2019; 53(4):1748-1765. doi:10.1021/acs.est.8b05512

10. Prata JC, Castro JL, da Costa JP, Cerqueira M, Duarte AC, Rocha-Santos T. Airborne Microplastics. In: Rocha-Santos T, Costa M, Mouneyrac C, eds. *Handbook of Microplastics in the Environment*. Springer International Publishing; 2020:1-25. doi:10.1007/978-3-030-10618-8_37-1

11. Duan J, Bolan N, Li Y, et al. Weathering of microplastics and interaction with other coexisting constituents in terrestrial and aquatic environments. *Water Res*. 2021; 196:117011. doi:10.1016/j.watres.2021.117011

12. Mitrano DM, Wick P, Nowack B. Placing nanoplastics in the context of global plastic pollution. *Nat Nanotechnol*. 2021; 16(5):491-500. doi:10.1038/s41565-021-00888-2

13. Frias JPGL, Nash R. Microplastics: Finding a consensus on the definition. *Mar Pollut Bull*. 2019; 138:145-147. doi:10.1016/j.marpolbul.2018.11.022

14. Rochman CM, Brookson C, Bikker J, et al. Rethinking microplastics as a diverse contaminant suite. *Environ Toxicol Chem*. 2019; 38(4):703-711. doi:10.1002/etc.4371

15. Mitrano DM, Wohlleben W. Microplastic regulation should be more precise to incentivize both innovation and environmental safety. *Nat Commun*. 2020; 11(1):5324. doi:10.1038/s41467-020-19069-1

16. ECHA. Microplastics - ECHA. European Chemical Agency. Published 2021. Accessed December 14, 2021. https://echa.europa.eu/hot-topics/microplastics

17. Napper IE, Thompson RC. Release of synthetic microplastic plastic fibres from domestic washing machines: Effects of fabric type and washing conditions. *Mar Pollut Bull*. 2016; 112(1):39-45. doi:10.1016/j.marpolbul.2016.09.025

18. Kole PJ, Löhr AJ, Van Belleghem FGAJ, Ragas AMJ. Wear and Tear of Tyres: A Stealthy Source of Microplastics in the Environment. *Int J Environ Res Public Health*. 2017; 14(10):1265. doi:10.3390/ijerph14101265

19. Schymanski D, Goldbeck C, Humpf HU, Fürst P. Analysis of microplastics in water by micro-Raman spectroscopy: Release of plastic particles from different packaging into mineral water. *Water Res*. 2018; 129:154-162. doi:10.1016/j.watres.2017.11.011

20. Ambrosini R, Azzoni RS, Pittino F, Diolaiuti G, Franzetti A, Parolini M. First evidence of microplastic contamination in the supraglacial debris of an alpine glacier. *Environ Pollut*. 2019; 253:297-301. doi:10.1016/j.envpol.2019.07.005

21. Bergmann M, Wirzberger V, Krumpen T, et al. High Quantities of Microplastic in Arctic Deep-Sea Sediments from the HAUSGARTEN Observatory. *Environ Sci Technol*. 2017; 51(19):11000-11010. doi:10.1021/acs.est.7b03331

22. Lusher AL, Tirelli V, O'Connor I, Officer R. Microplastics in Arctic polar waters: the first reported values of particles in surface and sub-surface samples. *Sci Rep*. 2015; 5(1):14947. doi:10.1038/srep14947

23. Munari C, Infantini V, Scoponi M, Rastelli E, Corinaldesi C, Mistri M. Microplastics in the sediments of Terra Nova Bay (Ross Sea, Antarctica). *Mar Pollut Bull*. 2017; 122(1):161-165. doi:10.1016/j.marpolbul.2017.06.039

24. Waller CL, Griffiths HJ, Waluda CM, et al. Microplastics in the Antarctic marine system: An emerging area of research. *Sci Total Environ*. 2017; 598:220-227. doi:10.1016/j.scitotenv.2017.03.283

25. Napper IE, Davies BFR, Clifford H, et al. Reaching New Heights in Plastic Pollution—Preliminary Findings of Microplastics on Mount Everest. *One Earth*. 2020; 3(5):621-630. doi:10.1016/j.oneear.2020.10.020

26. Pohl F, Eggenhuisen JT, Kane IA, Clare MA. Transport and Burial of Microplastics in Deep-Marine Sediments by Turbidity Currents. *Environ Sci Technol*. 2020; 54(7):4180-4189. doi:10.1021/acs.est.9b07527

27. Andrady AL. Microplastics in the marine environment. *Mar Pollut Bull*. 2011; (62):1596-1605. doi:10.1016/j.marpolbul.2011.05.030

28. Mani T, Hauk A, Walter U, Burkhardt-Holm P. Microplastics profile along the Rhine River. *Sci Rep*. 2016; 5(1). doi:10.1038/srep17988

29. Dris R, Gasperi J, Tassin B. Sources and Fate of Microplastics in Urban Areas: A Focus on Paris Megacity. In: Wagner M, Lambert S, eds. *Freshwater Microplastics*. Vol 58. Springer International Publishing; 2018:69-83. doi:10.1007/978-3-319-61615-5_4

30. Mintenig SM, Kooi M, Erich MW, et al. A systems approach to understand microplastic occurrence and variability in Dutch riverine surface waters. *Water Res*. 2020; 176:115723. doi:10.1016/j.watres.2020.115723

31. Rodrigues MO, Abrantes N, Gonçalves FJM, Nogueira H, Marques JC, Gonçalves AMM. Spatial and temporal distribution of microplastics in water and sediments of a freshwater system (Antuã River, Portugal). *Sci Total Environ*. 2018; 633:1549-1559. doi:10.1016/j.scitotenv.2018.03.233

32. Klein S, Worch E, Knepper TP. Occurrence and Spatial Distribution of Microplastics in River Shore Sediments of the Rhine-Main Area in Germany. *Environ Sci Technol*. 2015; 49(10):6070-6076. doi:10.1021/acs.est.5b00492

33. Horton AA, Svendsen C, Williams RJ, Spurgeon DJ, Lahive E. Large microplastic particles in sediments of tributaries of the River Thames, UK – Abundance, sources and methods for effective quantification. *Mar Pollut Bull*. 2017; 114(1):218-226. doi:10.1016/j.marpolbul.2016.09.004

34. Roch S, Walter T, Ittner LD, Friedrich C, Brinker A. A systematic study of the microplastic burden in freshwater fishes of south-western Germany - Are we searching at the right scale? *Sci Total Environ*. 2019; 689:1001-1011. doi:10.1016/j.scitotenv.2019.06.404

35. Wang S, Zhang C, Pan Z, et al. Microplastics in wild freshwater fish of different feeding habits from Beijiang and Pearl River Delta regions, south China. *Chemosphere*. 2020; 258:127345. doi:10.1016/j.chemosphere.2020.127345

36. Xu X, Wong CY, Tam NFY, Lo HS, Cheung SG. Microplastics in invertebrates on soft shores in Hong Kong: Influence of habitat, taxa and feeding mode. *Sci Total Environ*. 2020; 715:136999. doi:10.1016/j.scitotenv.2020.136999

37. Sfriso AA, Tomio Y, Rosso B, et al. Microplastic accumulation in benthic invertebrates in Terra Nova Bay (Ross Sea, Antarctica). *Environ Int*. 2020; 137:105587. doi:10.1016/j.envint.2020.105587

38. Smiroldo G, Balestrieri A, Pini E, Tremolada P. Anthropogenically altered trophic webs: alien catfish and microplastics in the diet of Eurasian otters. *Mammal Res*. 2019; 64(2):165-174. doi:10.1007/s13364-018-00412-3

39. Lu HC, Ziajahromi S, Neale PA, Leusch FDL. A systematic review of freshwater microplastics in water and sediments: Recommendations for harmonisation to enhance future study comparisons. *Sci Total Environ*. 2021; 781:146693. doi:10.1016/j.scitotenv.2021.146693

40. Schmidt C, Kumar R, Yang S, Büttner O. Microplastic particle emission from wastewater treatment plant effluents into river networks in Germany: Loads, spatial patterns of concentrations and potential toxicity. *Sci Total Environ*. 2020; 737:139544. doi:10.1016/j.scitotenv.2020.139544

41. Xia W, Rao Q, Deng X, Chen J, Xie P. Rainfall is a significant environmental factor of microplastic pollution in inland waters. *Sci Total Environ*. 2020; 732:139065. doi:10.1016/j.scitotenv.2020.139065

42. Dris R, Gasperi J, Saad M, Mirande C, Tassin B. Synthetic fibers in atmospheric fallout: A source of microplastics in the environment? *Mar Pollut Bull*. 2016; 104(1-2):290-293. doi:10.1016/j.marpolbul.2016.01.006

43. Plastics Europe. *Plastics - The Facts 2020; an Analysis of European Plastics Production, Demand and Waste Data*.; 2020. https://plasticseurope.org/wp-content/uploads/2021/09/Plastics_the_facts-WEB-2020_versionJun21_final.pdf

44. Koelmans AA, Mohamed Nor NH, Hermsen E, Kooi M, Mintenig SM, De France J. Microplastics in freshwaters and drinking water: Critical review and assessment of data quality. *Water Res*. 2019; 155:410-422. doi:10.1016/j.watres.2019.02.054

45. Stock F, Kochleus C, Bänsch-Baltruschat B, Brennholt N, Reifferscheid G. Sampling techniques and preparation methods for microplastic analyses in the aquatic environment – a review. *TrAC Trends Anal Chem*. Published online January 2019. doi:10.1016/j.trac.2019.01.014

46. Prata JC, da Costa JP, Duarte AC, Rocha-Santos T. Methods for sampling and detection of microplastics in water and sediment: A critical review. *TrAC Trends Anal Chem*. 2019; 110:150-159. doi:10.1016/j.trac.2018.10.029

47. Tian Z, Zhao H, Peter KT, et al. A ubiquitous tire rubber–derived chemical induces acute mortality in coho salmon. *Science*. 2021; 371(6525):185-189. doi:10.1126/science.abd6951

48. Zimmermann L, Göttlich S, Oehlmann J, Wagner M, Völker C. What are the drivers of microplastic toxicity? Comparing the toxicity of plastic chemicals and particles to Daphnia magna. *Environ Pollut*. 2020; 267:115392. doi:10.1016/j.envpol.2020.115392

49. Lithner D, Larsson A, Dave G. Environmental and health hazard ranking and assessment of plastic polymers based on chemical composition. *Sci Total Environ*. 2011; (409 (18)):3309-3324. doi:10.1016/j.scitotenv.2011.04.038

50. Bakir A, O'Connor IA, Rowland SJ, Hendriks AJ, Thompson RC. Relative importance of microplastics as a pathway for the transfer of hydrophobic organic chemicals to marine life. *Environ Pollut*. 2016; (219):56-65. doi:10.1016/j.envpol.2016.09.046

51. Diepens NJ, Koelmans AA. Accumulation of Plastic Debris and Associated Contaminants in Aquatic Food Webs. *Environ Sci Technol*. 2018; 52(15):8510-8520. doi:10.1021/acs.est.8b02515

52. Tang S, Lin L, Wang X, Feng A, Yu A. Pb(II) uptake onto nylon microplastics: Interaction mechanism and adsorption performance. *J Hazard Mater*. 2020; 386:121960. doi:10.1016/j.jhazmat.2019.121960

53. Wang J, Peng J, Tan Z, et al. Microplastics in the surface sediments from the Beijiang River littoral zone: Composition, abundance, surface textures and interaction with heavy metals. *Chemosphere*. 2017; 171:248-258. doi:10.1016/j.chemosphere.2016.12.074

54. Wright SL, Rowe D, Thompson RC, Galloway TS. Microplastic ingestion decreases energy reserves in marine worms. *Curr Biol*. 2013; 23(23):R1031-R1033. doi:10.1016/j.cub.2013.10.068

55. Rebelein A, Int-Veen I, Kammann U, Scharsack JP. Microplastic fibers — Underestimated threat to aquatic organisms? *Sci Total Environ*. 2021; 777:146045. doi:10.1016/j.scitotenv.2021.146045

56. Ivleva NP. Chemical Analysis of Microplastics and Nanoplastics: Challenges, Advanced Methods, and Perspectives. *Chem Rev*. 2021; 121(19):11886-11936. doi:10.1021/acs.chemrev.1c00178

57. Triebskorn R, Braunbeck T, Grummt T, et al. Relevance of nano- and microplastics for freshwater ecosystems: A critical review. *TrAC Trends Anal Chem*. 2019; 110:375-392. doi:10.1016/j.trac.2018.11.023

58. Gigault J, Halle A ter, Baudrimont M, et al. Current opinion: What is a nanoplastic? *Environ Pollut*. 2018; 235:1030-1034. doi:10.1016/j.envpol.2018.01.024

59. Gigault J, El Hadri H, Nguyen B, et al. Nanoplastics are neither microplastics nor engineered nanoparticles. *Nat Nanotechnol*. 2021; 16(5):501-507. doi:10.1038/s41565-021-00886-4

60. Yee MSL, Hii LW, Looi CK, et al. Impact of Microplastics and Nanoplastics on Human Health. *Nanomaterials*. 2021; 11(2):496. doi:10.3390/nano11020496

61. Magrì D, Sánchez-Moreno P, Caputo G, et al. Laser Ablation as a Versatile Tool To Mimic Polyethylene Terephthalate Nanoplastic Pollutants: Characterization and Toxicology Assessment. *ACS Nano*. 2018; 12(8):7690-7700. doi:10.1021/acsnano.8b01331

62. Nguyen B, Claveau-Mallet D, Hernandez LM, Xu EG, Farner JM, Tufenkji N. Separation and Analysis of Microplastics and Nanoplastics in Complex Environmental Samples. *Acc Chem Res*. 2019; 52(4):858-866. doi:10.1021/acs.accounts.8b00602

63. Blancho F, Davranche M, Fumagalli F, Ceccone G, Gigault J. A reliable procedure to obtain environmentally relevant nanoplastic proxies. *Environ Sci Nano*. 2021; 8(11):3211-3219. doi:10.1039/D1EN00395J

64. Lin W, Jiang R, Hu S, et al. Investigating the toxicities of different functionalized polystyrene nanoplastics on Daphnia magna. *Ecotoxicol Environ Saf*. 2019; 180:509-516. doi:10.1016/j.ecoenv.2019.05.036

65. Kögel T, Bjorøy Ø, Toto B, Bienfait AM, Sanden M. Micro- and nanoplastic toxicity on aquatic life: Determining factors. *Sci Total Environ*. 2020; 709:136050. doi:10.1016/j.scitotenv.2019.136050

66. Lusher AL, Hurley R, Arp HPH, et al. Moving forward in microplastic research: A Norwegian perspective. *Environ Int*. 2021; 157:106794. doi:10.1016/j.envint.2021.106794

67. Oßmann BE, Sarau G, Holtmannspötter H, Pischetsrieder M, Christiansen SH, Dicke W. Small-sized microplastics and pigmented particles in bottled mineral water. *Water Res*. 2018; 141:307-316. doi:10.1016/j.watres.2018.05.027

68. De-la-Torre GE. Microplastics: an emerging threat to food security and human health. *J Food Sci Technol*. 2020; 57(5):1601-1608. doi:10.1007/s13197-019-04138-1

69. Schwabl P, Köppel S, Königshofer P, et al. Detection of Various Microplastics in Human Stool. *Ann Intern Med*. 2019; 171(7):453-457. doi:10.7326/M19-0618

70. World Health Organization. *Microplastics in Drinking-Water*.; 2019. Accessed December 15, 2021. https://www.who.int/water_sanitation_health/publications/information-sheet190822.pdf

71. Hernandez LM, Xu EG, Larsson HCE, Tahara R, Maisuria VB, Tufenkji N. Plastic Teabags Release Billions of Microparticles and Nanoparticles into Tea. *Environ Sci Technol*. 2019; 53(21):12300-12310. doi:10.1021/acs.est.9b02540

72. Fadare OO, Wan B, Guo LH, Zhao L. Microplastics from consumer plastic food containers: Are we consuming it? *Chemosphere*. 2020; 253:126787. doi:10.1016/j.chemosphere.2020.126787

73. Pauly JL, Stegmeier SJ, Allaart HA, et al. Inhaled cellulosic and plastic fibers found in human lung tissue. *Cancer Epidemiol Biomark Prev Publ Am Assoc Cancer Res Cosponsored Am Soc Prev Oncol*. 1998; 7(5):419-428.

74. Pimentel JC, Avila R, Lourenço AG. Respiratory disease caused by synthetic fibres: a new occupational disease. *Thorax*. 1975; 30(2):204-219. doi:10.1136/thx.30.2.204

75. Prata JC. Airborne microplastics: Consequences to human health? *Environ Pollut*. 2018; 234:115-126. doi:10.1016/j.envpol.2017.11.043

76. Brahney J, Hallerud M, Heim E, Hahnenberger M, Sukumaran S. Plastic rain in protected areas of the United States. *Science*. 2020; 368(6496):1257-1260. doi:10.1126/science.aaz5819

77. Zhang Y, Kang S, Allen S, Allen D, Gao T, Sillanpää M. Atmospheric microplastics: A review on current status and perspectives. *Earth-Sci Rev*. 2020; 203:103118. doi:10.1016/j.earscirev.2020.103118

78. Wang C, Zhao J, Xing B. Environmental source, fate, and toxicity of microplastics. *J Hazard Mater*. 2021; 407:124357. doi:10.1016/j.jhazmat.2020.124357

79. Dris R, Gasperi J, Mirande C, et al. A first overview of textile fibers, including microplastics, in indoor and outdoor environments. *Environ Pollut*. 2017; 221:453-458. doi:10.1016/j.envpol.2016.12.013

80. Jin Y, Lu L, Tu W, Luo T, Fu Z. Impacts of polystyrene microplastic on the gut barrier, microbiota and metabolism of mice. *Sci Total Environ*. 2019; 649:308-317. doi:10.1016/j.scitotenv.2018.08.353

81. Eyles J, Alpar HO, Field WN, Lewis DA, Keswick M. The Transfer of Polystyrene Microspheres from the Gastrointestinal Tract to the Circulation after Oral Administration in the Rat. *J Pharm Pharmacol*. 1995; 47(7):561-565. doi:10.1111/j.2042-7158.1995.tb06714.x

82. De Felice B, Bacchetta R, Santo N, Tremolada P, Parolini M. Polystyrene microplastics did not affect body growth and swimming activity in Xenopus laevis tadpoles. *Environ Sci Pollut Res*. 2018; 25(34):34644-34651. doi:10.1007/s11356-018-3408-x

83. Bhagat J, Zang L, Nishimura N, Shimada Y. Zebrafish: An emerging model to study microplastic and nanoplastic toxicity. *Sci Total Environ*. 2020; 728:138707. doi:10.1016/j.scitotenv.2020.138707

84. Schirinzi GF, Pérez-Pomeda I, Sanchís J, Rossini C, Farré M, Barceló D. Cytotoxic effects of commonly used nanomaterials and microplastics on cerebral and epithelial human cells. *Environ Res*. 2017; 159:579-587. doi:10.1016/j.envres.2017.08.043

85. Liu L, Xu K, Zhang B, Ye Y, Zhang Q, Jiang W. Cellular internalization and release of polystyrene microplastics and nanoplastics. *Sci Total Environ*. 2021; 779:146523. doi:10.1016/j.scitotenv.2021.146523

86. Lim SL, Ng CT, Zou L, et al. Targeted metabolomics reveals differential biological effects of nanoplastics and nanoZnO in human lung cells. *Nanotoxicology*. 2019; 13(8):1117-1132. doi:10.1080/17435390.2019.1640913

87. Xu M, Halimu G, Zhang Q, et al. Internalization and toxicity: A preliminary study of effects of nanoplastic particles on human lung epithelial cell. *Sci Total Environ*. 2019; 694:133794. doi:10.1016/j.scitotenv.2019.133794

88. Barshtein G, Livshits L, Shvartsman LD, Shlomai NO, Yedgar S, Arbell D. Polystyrene Nanoparticles Activate Erythrocyte Aggregation and Adhesion to Endothelial Cells. *Cell Biochem Biophys*. 2016; 74(1):19-27. doi:10.1007/s12013-015-0705-6

89. Cortés C, Domenech J, Salazar M, Pastor S, Marcos R, Hernández A. Nanoplastics as a potential environmental health factor: effects of polystyrene nanoparticles on human intestinal epithelial Caco-2 cells. *Environ Sci Nano*. 2020; 7(1):272-285. doi:10.1039/C9EN00523D

90. Domenech J, Hernández A, Rubio L, Marcos R, Cortés C. Interactions of polystyrene nanoplastics with in vitro models of the human intestinal barrier. *Arch Toxicol*. 2020; 94(9):2997-3012. doi:10.1007/s00204-020-02805-3

91. Costa EC, Moreira AF, de Melo-Diogo D, Gaspar VM, Carvalho MP, Correia IJ. 3D tumor spheroids: an overview on the tools and techniques used for their analysis. *Biotechnol Adv*. 2016; 34(8):1427-1441. doi:10.1016/j.biotechadv.2016.11.002

92. Fischbach C, Chen R, Matsumoto T, et al. Engineering tumors with 3D scaffolds. *Nat Methods*. 2007; 4(10):855-860. doi:10.1038/nmeth1085

93. Kapałczyńska M, Kolenda T, Przybyła W, et al. 2D and 3D cell cultures – a comparison of different types of cancer cell cultures. *Arch Med Sci AMS*. 2018; 14(4):910-919. doi:10.5114/aoms.2016.63743

94. Shamir ER, Ewald AJ. Three-dimensional organotypic culture: experimental models of mammalian biology and disease. *Nat Rev Mol Cell Biol*. 2014; 15(10):647-664. doi:10.1038/nrm3873

95. Gaston F, Dupuy N, Marque SRA, Dorey S. Evaluation of multilayer film stability by Raman spectroscopy after gamma-irradiation sterilization process. *Vib Spectrosc*. 2018; 96:52-59. doi:10.1016/J.VIBSPEC.2018.03.002

96. Snyder RG, Hsu SL, Krimm S. Vibrational spectra in the C□H stretching region and the structure of the polymethylene chain. *Spectrochim Acta Part Mol Spectrosc*. 1978; 34(4):395-406. doi:10.1016/0584-8539(78)80167-6

97. Bentley PA, Hendra PJ. Polarised FT Raman studies of an ultra-high modulus polyethylene rod. *Spectrochim Acta A Mol Biomol Spectrosc*. 1995; 51(12):2125-2131. doi:10.1016/0584-8539(95)01513-3

98. Zhang D, Shen YR, Somorjai GA. Studies of surface structures and compositions of polyethylene and polypropylene by IR+visible sum frequency vibrational spectroscopy. *Chem Phys Lett*. 1997; 281(4-6):394-400. doi:10.1016/S0009-2614(97)01311-0

99. Migler KB, Kotula AP, Walker ARH. Trans-Rich Structures in Early Stage Crystallization of Polyethylene. *Macromolecules*. 2015; 48(13):4555-4561. doi:10.1021/MA5025895

100. Furukawa T, Sato H, Kita Y, et al. Molecular structure, crystallinity and morphology of polyethylene/ polypropylene blends studied by Raman mapping, scanning electron microscopy, wide angle X-ray diffraction, and differential scanning calorimetry. *Polym J*. 2006; 38(11):1127-1136. doi:10.1295/polymj.PJ2006056

101. Meier RJ. Studying the length of trans conformational sequences in polyethylene using Raman spectroscopy: a computational study. *Polymer*. 2002; 43(2):517-522. doi:10.1016/S0032-3861(01)00416-5

102. Donev A, Cisse I, Sachs D, et al. Improving the Density of Jammed Disordered Packings Using Ellipsoids. *Science*. 2004; 303(5660):990-993. doi:10.1126/SCIENCE.1093010

APPENDIX A – List of other publications and congress contributions

Other publications

PAPER 6 – **Anna Winkler**, Nadia Santo, Paolo Tremolada, Marco Parolini, Valerio Pasini, Marco Aldo Ortenzi, Renato Bacchetta (2019). Microplastic Release from Plastic Bottles - Comparison of Two Analytical Methodologies (SEM-EDX and μ-FTIR). In: Cocca M. et al. (eds) Proceedings of the 2nd International Conference on Microplastic Pollution in the Mediterranean Sea. ICMPMS 2019. Springer Water. Springer, Cham. https://doi.org/10.1007/978-3-030-45909-3_40

PAPER 7 – Alessandro Nessi, Alessandro Balestrieri, **Anna Winkler**, Andrea Guglielmo Casoni, Paolo Tremolada (2021). Kingfisher (*Alcedo atthis*) diet and prey selection as assessed by the analysis of pellets collected under resting sites (River Ticino, north Italy). Aquatic Ecology, volume 55, 135–147. https://doi.org/10.1007/s10452-020-09817-2

PAPER 8 – Renato Bacchetta, **Anna Winkler**, Nadia Santo, Paolo Tremolada (2021). The Toxicity of Polyester Fibers in *Xenopus laevis*. Water, volume 13, 3446. https://doi.org/10.3390/w13233446

PAPER 9 – Alessandro Balestrieri, **Anna Winkler,** Giovanni Scribano, Andrea Gazzola, Giuditta Lasctrico, Alice Grioni, Daniele Pelliteri-Rosa, Paolo Tremolada (2022). Differential effects of microplastic exposure in anuran tadpoles: a still underrated threat to amphibian conservation? Environmental Pollution, volume 303, 119137. https://doi.org/10.1016/j.envpol.2022.119137

PAPER 10 – Alessandro Nessi, **Anna Winkler**, Luca Ghezzi, Alessandro Balestrieri, Paolo Tremolada, Francesco Saliu (2022). Monitoring microplastics in terrestrial ecosystems: a case study using barn owl (*Tyto alba*) pellets. Submitted to Environmental Pollution.

Congress contributions

TALK 1 – *Following the Fate of Microplastic along the Ticino River, Italy*. Atti del XV Incontro dei giovani ricercatori in ecologia e scienze dei sistemi acquatici, Cuneo, Italy, 8th – 10th May 2019.

TALK 2 – *Spatial distribution of microplastic in surface water, sediment and biota along a river*. SETAC Europe 30th Annual Meeting, SciCon, 3rd – 7th May 2020.

TALK 3 – *Effects of polyester microfibers released from a domestic dryer machine on human lung organoids and Xenopus laevis*. MICRO 2020, 23rd – 27th November 2020.

TALK 4 – *Lung Organoids and Microplastic Fibres: A New Exposure Model for Emerging Contaminants*. SETAC Europe 31st Annual Meeting, 3rd – 6th May 2021.

TALK 5 – *Following the fate of microplastic along the Ticino river*. XXV Congresso A.I.O.L. 30th June 2021.

POSTER 1 – *Mechanical stress causes microplastic release from PET mineral water bottles*. SETAC Europe 29th Annual Meeting, Helsinki, Finland, 26th – 30th May 2019.

POSTER 2 – *Following the fate of microplastic along the Ticino River, Italy.* International Conference on Microplastic Pollution in the Mediterranean Sea, Capri, Italy, 15th – 18th September 2019.

POSTER 3 – *Microplastic release from plastic bottles – Comparison of two analytical methodologies (SEM-EDX and μ-FTIR)*. International Conference on Microplastic Pollution in the Mediterranean Sea, Capri, Italy, 15th – 18th September 2019.

APPENDIX B – Popular publications, educational activities and achievements

Popular publications

PUBLICATION 1 – Alessandro Nessi, Alessandro Balestrieri, **Anna Winkler**, Paolo Tremolada (2020). Il martin pescatore (*Alcedo atthis*) nella valle del Ticino: distribuzione, dieta e microplastiche. Published by "Ente di gestione delle aree protette del Ticino e del Lago Maggiore" and "Parco lombardo della Valle del Ticino". https://ente.parcoticino.it/pubblicazioni/il-martin-pescatore-alcedo-atthis-nella-valle-del-ticino-distribuzione-dieta-microplastiche/

PUBLICATION 2 – Paolo Tremolada, **Anna Winkler**, Andrea Masseroni (2021). Pericolo microplastiche nel Ticino. Published by "Piemonte parchi". http://www.piemonteparchi.it/cms/index.php/ambiente/divulgazione/item/4400-pericolo-microplastiche-nel-ticino

PUBLICATION 3 – Elisa Allodi, **Anna Winkler**, Alessandro Balestrieri, Paolo Tremolada (2022). Microplastiche nel Ticino: dal fiume all'uomo. Published by "Piemonte parchi".
http://www.piemonteparchi.it/cms/index.php/ambiente/divulgazione/item/5029-microplastiche-nel-ticino-dal-fiume-all-uomo

Teaching Activity

COURSE 1 – *Approaches to the Study of Ecological Systems*; holding lessons (2 h) "Microplastic in the Environment (Project Planning)" in 2020 and 2021

COURSE 2 – *Ecologia*; holding a lesson (2 h) about "Microplastics" in 2021

COURSE 3 – *Ecologia Quantitativa*; tutorial activity (12 h) for the practical sessions on the use of the software RStudio

COURSE 4 – *Scientific Writing*; holding lessons (6 h) on "Automated bibliography (Zotero and Mendeley)" for course I and II organized by Centro Italiano Studi Ornitologici and Journal AVOCETTA in 2021

External Seminars

SEMINAR 1 – *Microplastic detection in freshwater ecosystems and drinking water;* Seminario Limnologico, CNR Istituto di Ricerca sulle Acque, Verbania, Italy, November 2019

SEMINAR 2 – *Microplastic in the environment*; Rotary Club Frankfurt International, September 2020

Achievements

AWARD – *Premio Prof. Nicola Saino 2020* for best published article issued by the University of Milan for the paper "Does mechanical stress cause microplastic release from plastic water bottles?" published in Water Research, 2019

CALL – Winning of the *Open Access to JRC Research Infrastructures Call* by the European Commission 2019: Nanobiotechnology